PUBLISHER:

Address of Publisher & Editor's Office:

GDAŃSK UNIVERSITY
OF TECHNOLOGY
Faculty
of Ocean Engineering
& Ship Technology

ul. Narutowicza 11/12
80-233 Gdańsk, POLAND
tel.: +48 58 347 13 66
fax: +48 58 341 13 66
e-mail: office.pmr@pg.gda.pl

Account number:
BANK ZACHODNI WBK S.A.
I Oddział w Gdańsku
41 1090 1098 0000 0000 0901 5569

Editorial Staff:

Jacek Rudnicki Editor in Chief

Przemysław Wierzchowski Scientific Editor

Jan Michalski Editor for review matters

Aleksander Kniat Editor for international relations

Kazimierz Kempa Technical Editor

Piotr Bzura Managing Editor

Cezary Spigarski Computer Design

Domestic price:
single issue: 25 zł

Prices for abroad:
single issue:
- in Europe EURO 15
- overseas USD 20

ISSN 1233-2585

POLISH MARITIME RESEARCH

in internet

www.bg.pg.gda.pl/pmr/pmr.php

POLISH MARITIME RESEARCH

No 1 (81) 2014 Vol 21

CONTENTS

Editorial

POLISH MARITIME RESEARCH is a scientific journal of worldwide circulation. The journal appears as a quarterly four times a year. The first issue of it was published in September 1994. Its main aim is to present original, innovative scientific ideas and Research & Development achievements in the field of :

Engineering, **Computing & Technology**, **Mechanical Engineering**,

which could find applications in the broad domain of maritime economy. Hence there are published papers which concern methods of the designing, manufacturing and operating processes of such technical objects and devices as : ships, port equipment, ocean engineering units, underwater vehicles and equipment as well as harbour facilities, with accounting for marine environment protection.
The Editors of POLISH MARITIME RESEARCH make also efforts to present problems dealing with education of engineers and scientific and teaching personnel. As a rule, the basic papers are supplemented by information on conferences , important scientific events as well as cooperation in carrying out international scientific research projects.

Scientific Board

POLISH MARITIME RESEARCH 1(81) 2014 Vol 21; pp. 3-8
10.2478/pomr-2014-0001

Modified pid control design for roll fin actuator of nonlinear modelling of the fishing boat

Fuat Alarçin, Assoc. Prof.,
Hakan Demirel, Assistant,
M. Ertugrul Su, Assistant,
Ahmet Yurtseven, Assistant,
Yildiz Technical University, Turkey

ABSTRACT

This study aims to reduce roll motion of a fishing boat which arises from disturbing hydrodynamic effects by means of fin roll stabilizer. It is assured that roll motion with nonlinear damping and restoring moment coefficients are down to the desired level through classical PID and modified PID algorithms. At the time of sailing, stability, a very important concept, was examined using Lyapunov direct method taking initial conditions into consideration, and it was noted that the system was generally stable. In addition, NACA 0015 model was used for the fin roll stabilizer, and flow analysis was carried out with Computational Fluid Dynamics (CFD) method. In the simulation results, when the same gains were used, modified PID controller algorithms were relatively more effective compared to PID in the fin roll stabilizer system.

Keywords: stability analyses; nonlinear roll motion; modified PID; CFD

INTRODUCTION

Ships remain a research subject for researchers as they lack fundamentals about stability despite meeting the requirements of current laws. Roll motion is one of the most significant ship motions due to stability. Many publications concerning the ship roll motion were presented in literature [2, 5].

Solimon and Thompson [17] used Runga-Kutta method for analyze the nonlinear differential equation of roll motion. Haddara and Wang [7] examined the controllability and maneuvering performance of conventional surface ships using neural networks technique to predict the hydrodynamic parameters of the ship. Taylan [21] studied impact of nonlinear terms in ship rolling motion. Surendran and Reddy [18] revealed solution of differential equation of roll motion considering the nonlinearities in both the restoring moment and the damping moment using Matlab for a Ro-Ro ship. Karakaş et al. [12] analyzed nonlinear roll motion via a controller based on Lyapunov Direct Method in beam seas.

Safety of voyage has to be assured against the disrupting hydrodynamic effects of passengers as well as cargos, and amplitude has to be at an acceptable level. Therefore, a number of applications such as fin roll stabilizers and U-tube have been used in literature [3, 16, 9].

There are many control methods which could be used to reduce roll motion. Surendran et al. [19] used active fins to minimize roll motion of a ship by means of the PID controller. Guan and Zhang [6] offered nonlinear fin roll control originated from integrator backstepping associated with nonlinear damping term. They simplified the standard nonlinear backstepping algorithm in use of the Close-loop Gain Shaping Algorithm (CGSA). It was expressed that roll amplitude was reduced of around 90% comparing with uncontrolled result in the same simulation conditions. Ghassemi et al. [4] referred to neural network-PID controller for roll fin stabilizer.

In this study, roll amplitude of a ship under the wave effect has been ensured to be at stable zone using the hydraulic fin roll stabilizer system based on the 3rd level nonlinear damping effect and modeling 5th level restoring moment coefficient. These coefficients of the rolling motion equation of the fishing vessel in waves were obtained using theoretical methods. Stability analysis was conducted using Lyapunov method. It is provided with a Matlab code to solve a second order differential equation with constant coefficients using Matlab in-built solver ODE45. In addition, Classical PID and Modified PID controller results demonstrate the effectiveness of the Modified PID controller.

SHIP ROLL MOTION MATHEMATICAL MODEL

Because of different environmental conditions, ship motions have not the same amplitude and acceleration so reducing degrees of freedom makes it easy to find a solution. Components that make up the physical model and mathematical model of single degree of freedom ship roll motion are generated from

Taylan's [20] and Surendran's [19] previous studies and they are expressed on the basis of the following assumptions:

- ship is symmetric in the direction of port side and starboard side,
- all the other degrees of freedom of ship have been neglected,
- ship has been regarded as rigid body.

Considering some simplifications, the following nonlinear expression for the roll equation is obtained:

$$(I + J)\ddot{\emptyset} + B_1\dot{\emptyset} + B_2\dot{\emptyset}|\dot{\emptyset}| + B_3\dot{\emptyset}^3 +$$

$$+\Delta(c_1\emptyset + c_3\emptyset^3 + c_5\emptyset^5 + c_7\emptyset^7) = \quad (1)$$

$$= {\omega_e}^2 \propto_m I\cos(\omega_e t) - M_f$$

Where I is the mass moment of inertia for roll and J is added mass moment of inertia for roll. B_1, B_2, B_3, symbolize roll damping coefficients, c_1, c_3, c_5 and c_7 are expressed as restoring force coefficients. Ø, $\dot{Ø}$, $\ddot{Ø}$ represent angle, angular velocity and angular acceleration of roll motion respectively. Δ means the weight displacement of the ship, ω_e means wave encountering frequency, α_m means the maximum wave slope, M_f means the control moment of active fins.

Inertia value has an important effect with regards to nonlinear roll motion. This value has been expressed as below based on weight displacement of ship, breadth and the vertical distance of the center of gravity [19].

$$(I + J) = \frac{\Delta}{12g}(B^2 + 4KG^2) \quad (2)$$

The roll damping coefficients are considered as skin friction of the hull, eddy shedding from the hull, free surface waves, lift effect damping and bilge keel damping. Theoretical and semi-empirical methods have been used to utilize the roll damping by Ikeda and Himeno [11], Ikeda [10]. A non-dimensional damping coefficient for different ship types is expressed as follows.

$$B_1 = \frac{2a\sqrt{(I+J)\Delta GM}}{\pi} \quad (3)$$

$$B_2 = \frac{3}{4}b(I + J) \quad (4)$$

$$B_3 = 0.7B_2 \quad (5)$$

These coefficients, given a and b in Tab. 1 [6], are directly related to a linear damping coefficients B_1 and a non-linear damping coefficient, B_2 represents quadratic drag and B_3 is cubic [2].

Tab. 1. *The non-dimensional damping coefficients for three different types of the ship*

Types of the ship	a	b
Passenger ship	0.05	0.0125
Cargo ship	0.03	0.0155
Fishing ship	0.1	0.0140

The curve for righting arm has been represented by the polynomial.

$$M(\emptyset) = c_1\emptyset + c_3\emptyset^3 + c_5\emptyset^5 + c_7\emptyset^7 + \cdots$$

where: $c_1 > 0$, $c_3 < 0$, $c_5 > 0$ and $c_7 < 0$ for a damaged vessel but $c_7 = 0$ for an intact vessel. The roll restoring moment coefficients are defined by Taylan [21].

$$c_1 = \frac{d(GZ)}{d\emptyset} = GM \quad (6)$$

$$c_3 = \frac{4}{\emptyset_v^4}(3A_{\emptyset_v} - GM\emptyset_v^2) \quad (7)$$

$$c_5 = -\frac{3}{\emptyset_v^6}(4A_{\emptyset_v} - GM\emptyset_v^2) \quad (8)$$

$Ø_v$ means vanishing angle of stability, $A_{Ø_v}$ means area under the GZ curve up to angle of vanishing stability, GM represents the distance between the position of metacenter and the vertical center of gravity of the vessel. Depending on the above-referred coefficients, numerical calculations were performed for a fishing boat, whose body plan is given Fig. 1.

The righting arm curve of fishing boat is represented as graphical on Fig. 2. From this figure, it can be seen that lift develops in an approximately linear manner with an increasing angle of attack. The area under the curve is an indication a safety voyage against capsizing moments.

Because of the effects of high wave frequency, ship sailing on the sea generates undesired roll motion. The wave moment (M_w) and the encounter frequency of the wave (ω_e) can be calculated as follow;

$$M_w : {\omega_e}^2 \propto_m I\cos(\omega_e t)$$
$$\omega_e = \omega_w - \frac{\omega_w^2}{g}V\cos(\mu_w) \quad (9)$$

ω_w represents the wave frequency, α_m represents the maximum wave slope, μ_w represents the wave encounter angle of the ship. It can be seen that wave excitation will depend many different factors.

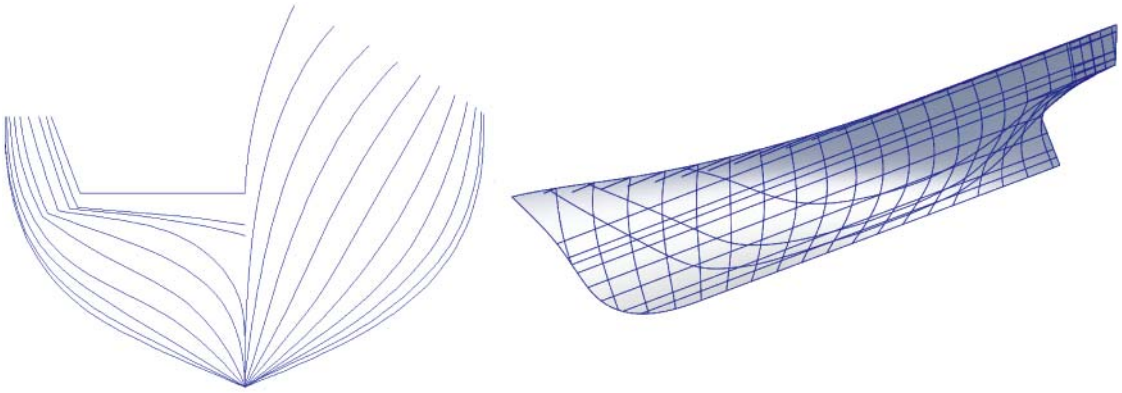

Fig. 1. *Body plan of the fishing boat*

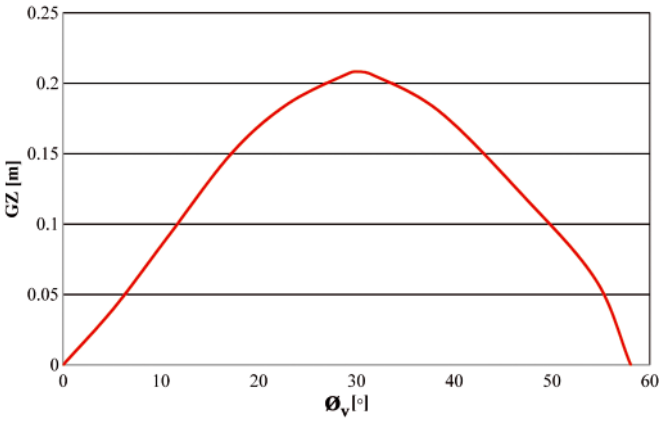

Fig. 2. Righting arm curve of fishing boat

STABILITY ANALYSIS VIA LYAPUNOV'S DIRECT METHOD

Stability analysis is a crucial subject for fishing boat. External forces like current weather and fishing conditions effect position of ship adversely. Fishing boat must have positive stability for safety voyage and fishing. Lyapunov's Direct Method was used for stability analyses by Ozkan [15]. This is a very robust and feasible method because it does not require any knowledge about the specific solutions of the equations. By using state variables of equation (1), the state space model of the ship can be written as:

$$\dot{\emptyset} = \dot{\emptyset}_1 = \emptyset_2$$

$$\dot{\emptyset}_2 = -(\omega_0{}^2\emptyset_1 + m_3\emptyset_1^3 + m_5\emptyset_1^5 + m_7\emptyset_1^7) + \quad (10)$$

$$-(b_1\emptyset_2 - b_2\emptyset_2|\emptyset_2| + b_3\emptyset_2^3)$$

Lyapunov function V(x) satisfying:

- $V(x) > 0$ positive definite and $V(0) = 0$
- $dV(\vec{x})/dt \leq 0$
- $V(x) \rightarrow \infty$ as $\|x\| \rightarrow \infty$

Lyapunov second method will be used to test for the system stability.

$$\dot{V}(x) = -\emptyset_2^2(b_1 + b_2|\emptyset_2| + b_3\emptyset_2^2) < 0 \quad (13)$$

$$V(x) = \omega_0^2\frac{\emptyset_1^2}{2} + m_3\frac{\emptyset_1^4}{4} + m_5\frac{\emptyset_1^6}{6} + \frac{\emptyset_2^2}{2} \quad (14)$$

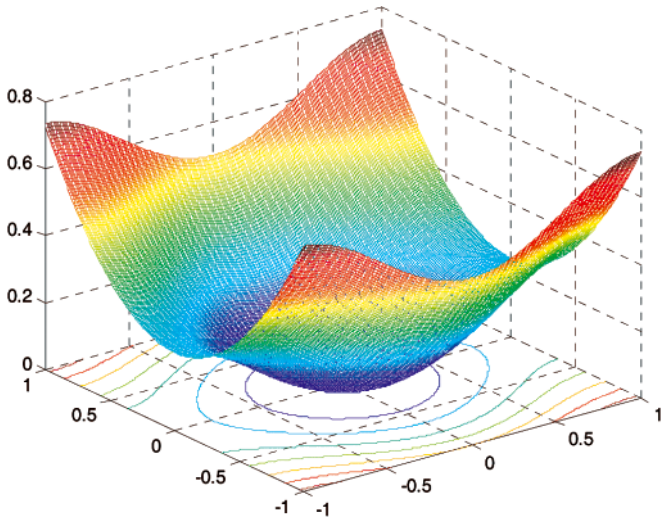

Fig. 3. Lyapunov function graphic

FIN ROLL CONTROL DESIGN

In this present work the fin-stabilizer consisted of two identical non-rectangular hydrofoils of a low aspect ratio, symmetrically placed on both sides of vessel. The motion of a ship can be affected by fins actuators that impart forces and moments. Actuators play a very important role within the control system structure. When the roll fin stabilizers attack to the fluid, it can be seen that the surface of fins lifting force caused by the rotation and angle of attack. The lift force and the lift in non-dimensional form is as in the following form [16]:

$$L = \frac{1}{2}\rho V A_F C_L \quad (15)$$

$$C_L = \frac{L}{0.5\rho V^2 A_F} \quad (16)$$

$$\dot{V}(t) = \frac{dV(\vec{x})}{dt} = \nabla V^T\dot{\vec{x}}$$

$$\frac{dV}{dt} = \propto_{11}\emptyset_1\emptyset_2 + \propto_{12}\emptyset_2 - \propto_{21}\omega_0^2\emptyset_1^2 - \propto_{21} m_3\emptyset_1^4 - \propto_{21} m_5\emptyset_1^6 - \propto_{21} m_7\emptyset_1^8 - \propto_{21} b_1\emptyset_1\emptyset_2 \quad (11)$$
$$- \propto_{21} b_2|\emptyset_2|\emptyset_1\emptyset_2 - b_3 \propto_{21}\emptyset_1\emptyset_2^3 - \propto_{22}\omega_0^2\emptyset_1\emptyset_2 - \propto_{22} m_3\emptyset_1^3\emptyset_2$$
$$- \propto_{22} m_5\emptyset_1^5\emptyset_2 - \propto_{22} b_1\emptyset_2^2 - \propto_{22} b_2|\emptyset_2|\emptyset_2^2 - \propto_{22} b_3\emptyset_2^4$$

If symmetric coefficients accept equal to zero, derivative of the Lyapunov function is negative; the conditions for asymptotic stability are found to be:

$$\frac{dV}{dt} = \emptyset_1\emptyset_2(\propto_{22}\omega_0^2 + m_3 \propto_{22}\emptyset_1^2 + m_5 \propto_{22}\emptyset_1^4 - \propto_{22}\omega_0^2) - \propto_{22} b_1\emptyset_2^2 - \propto_{22} m_3\emptyset_1^3\emptyset_2$$
$$- \propto_{22} m_5\emptyset_1^5\emptyset_2 - \propto_{22} b_2|\emptyset_2|\emptyset_2^2 - \propto_{22} b_3\emptyset_2^4 \quad (12)$$
$$\propto_{11} = \propto_{22}\omega_0^2 + m_3 \propto_{22}\emptyset_1^2 + m_5 \propto_{22}\emptyset_1^4$$

Lyapunov function is obtained depending on the non-linear roll damping coefficient. If this value is smaller than zero, non-linear roll motion can be said to be stable. Lyapunov function graphic for the system is given in the Fig. 3.

Where L lifting force (N); ρ density of fluid (t/m³); A_F fins area (m²); C_L fins lift coefficient (lift coefficient/rad); V the ship speed (m/s).General formulas of fin roll stabilizer are expressed as the following equations.

$$M_F \rho V^2 A_F C_L l_F \left(\alpha_f + \frac{\dot{\emptyset}}{V} l_F\right) \quad (17)$$

Where M_F, fin roll stabilizer moment; l_F the fins force arm; α angle attack.The result of hydrodynamic lift coefficient in function of attack angle of fin and roll angle of ship are presented in Fig. 4.

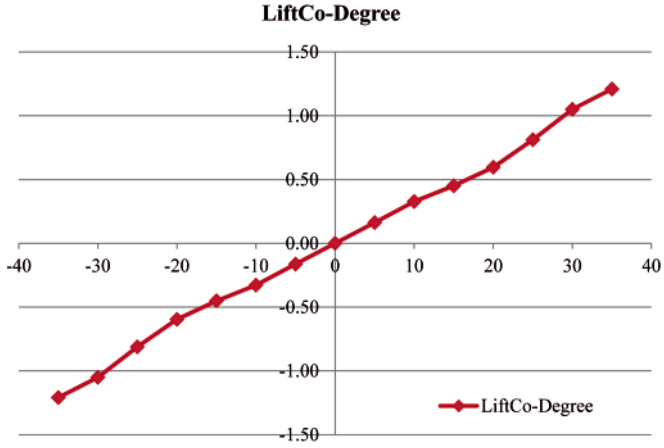

Fig. 4. *Lift coefficient*

Simulation was performed via 8 Parallel Processor and 24 GB of RAM hardware configuration. Fin was modeled in CFD package Star CCM +. Preprocessing, running and finishing parts were integrated in the program. At the time of Preprocessing, Trimmer, Surface Remesher and Prism Layer Masher solution mesh properties were actualized concurrently. Mesh created consisted of 970000 cells and 2900000 faces. A sample case of free surface shape around fin is presented Fig. 5.

We conceived only a magnitude constraint for the mechanical angle of the fins of 20°. Segregated flow, reynolds averaged Navier Stokes and k-ε turbulence model were used as solver to process of running. Convergence conditions are nearly 1E-5 (10^{-5}). Running is performed in parallel with 8 cores. In conclusion, the velocity and pressure gradients are obtained; the lift force coefficient was expressed by means of the model.

Modified pid controller

The classiccal PID controllers are the simplest form of controllers, and have being widely used satisfactorily in the field of process control systems. As seen in Fig. 6, it has basic and comprehensible structure. The classiccal PID controller of a plant is shown in Fig. 6 [14].

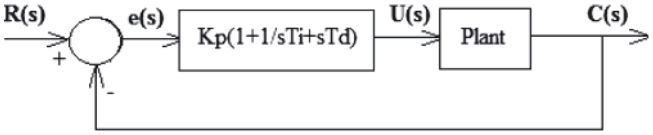

Fig. 6. *Classiccal PID controller of a plant*

R(s) and C(s) indicate input and output signal, respectively. K_p is proportional gain. T_i and T_d are integral and derivative time constant, respectively. U(s) is the manipulated signal. e(s) is differential signal between input and output signal. In time domain transfer function of classiccal PID controller is given below:

$$G_{pid}(t) = K_p \left[e(t) + \frac{1}{T_i}\int e(t)dt + T_d \frac{de(t)}{dt}\right] \quad (18)$$

where: K_p indicates proportional gain of controller. $T_i = K_p/K_i$, $T_d = K_d/K_p$ and e is the error between the reference and the output system, T_i is the intregral time, T_d is derivative time. The Laplace transform of the equation (18) is expressed in (19)

$$G_{pid}(s) = \left(K_p + \frac{K_i}{s} + sK_d\right) \quad (19)$$

K_i and K_d are integral and derivative gains, respectively. The easy implementation and clear control principle of this controller makes it popular in many applications [22, 23, 24, 8].

But they have some disadvantages that they may not provide optimum result, and can not keep desired result in some situations. So as to deal with this issue and have optimal control classiccal PID controller can be modified. While integral part stays remained, proportional and derivative action move to the feedback path so that any change of reference input signal may not being involved in the manipulated signal. The model of closed loop system with Modified PID is shown in Fig. 7.

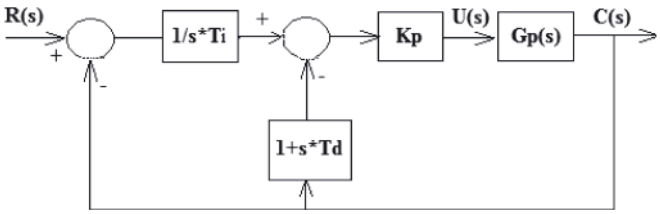

Fig. 7. *The model of closed loop system with modified PID controller*

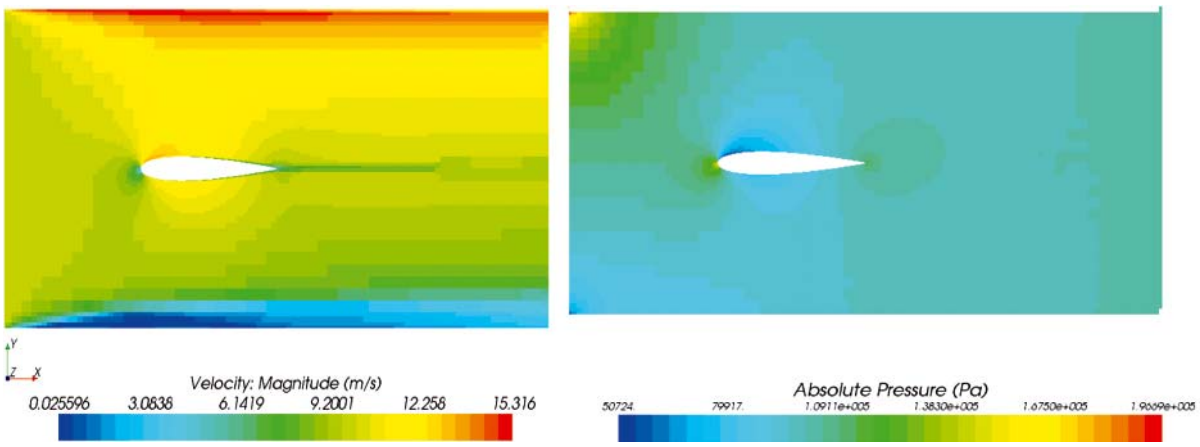

Fig. 5. *Velocity and pressure gradient cross section (attack angle + 20°)*

The modified PID controller signal is demonstrated as follow:

$$U(s) = Kp\frac{1}{sTi}R(s) - Kp(1 + \frac{1}{sTi} + sTd) \quad (20)$$

Prettier form of controller can be given as follow:

$$U(s) = \frac{Kp * R(s) - sTi * Kp - Kp - s^2TiTd * Kp}{sTi} \quad (21)$$

Transfer function of closed loop system with modified PID controller is given below:

$$\frac{C(s)}{R(s)} = \left(\frac{1}{sTi}\right)\frac{KpGp(s)}{1 + KpGp(s)\left(1 + \frac{1}{sTi} + sTd\right)} \quad (22)$$

After one more step transfer function can be obtained:

$$\frac{C(s)}{R(s)} = \frac{KpGp(s)}{s^2KpGp(s)TdTi + sKpGp(s)Ti + 2KpGp(s)} \quad (23)$$

As seen in above equation the system with Modified PID controller has no zeros. Its advantages are to prevent earlier peak and higher overshoot. The proposed Modified PID controller can prevent this negative effect as well as can ameliorate system response in comparison with classiccal PID.

SIMULATION

Among 13 different fishing boats with different block coefficient examined in both loaded and unloaded conditions, the model in the table below was taken as a basic one [1]. These fishing boats have same length, breadth, depth and draught but cross-sectional forms are different. In this case, a stability characteristic varies with block coefficient from geometric characteristics. Our model and fishing boat and the fin (NACA 0015) particulars are showed in Tab. 2.

Tab. 2. *The fishing boat and the fin (NACA 0015) particulars*

Principal Particulars	Parameter
Length between perpendiculars (L_{BP})	20 m
Breadth (B)	5.714 m
Depth (D)	3.2 m
Draught (T)	2.285 m
Displacement (∇)	119.34 m^3
Transverse metacentric height (GM)	0.57 m
Vertical center of gravity (KG)	2.4 m
Block coefficient (C_B)	0.457
Service speed (V)	10 kn
Fins area (A_F)	2.5 m^2
Fins lift coefficient (C_L)	0.59
Vanishing angle of stability ($Ø_v$)	58°

The simulation results for fin roll stabilizer system show roll angle and roll velocity in Fig. 8 and Fig. 9, respectively. Comparisons of the control performance are made between Classical PID and the MPID controllers.

The classical PID controller has given good result in considering of roll angle oscillation values. Nevertheless it still appears a steady error on time. On the other hand MPID halves the oscillation and error. Also in 10 seconds it prevents higher peak, which means avoid from higher roll angle.

The modified PID control response of the fin roll stabilizer is better than PID control as shown in Fig. 9. Although classical PID model has given almost same response such as the uncontrolled model, MPID model has ameliorated the fin roll velocity in range of -0.9 and 0.9.

Non-dimensional damping coefficients ($b_1 = 0.069$, $b_2 = 0.01$, $b_3 = 0.007$) and restoring moment coefficients ($m_1 = 1.204$, $m_3 = -1.8$, $m_5 = 0.61$, $m_7 = 0$) for fishing boat were calculated by empirical formulas. K_p, K_i and K_d control values were obtained by trial method. The values of PID gains $K_p = 0.2145$, $K_d = 1.2288$, $K_i = 2.89$ were ensured good roll reduction.

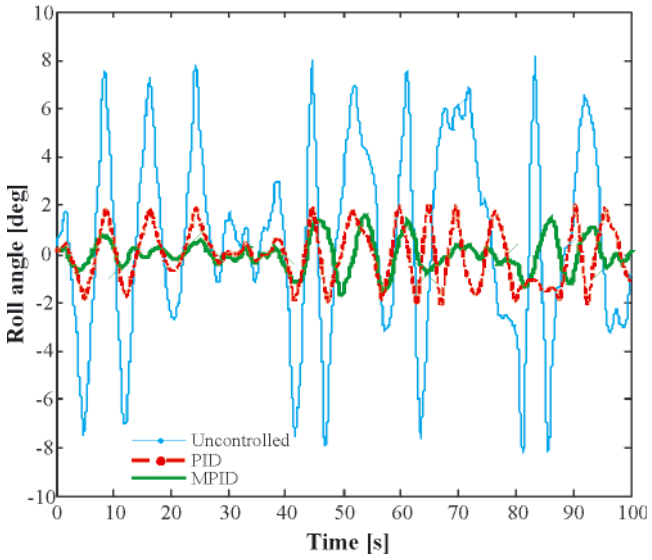

Fig. 8. *Comparison of roll angle response*

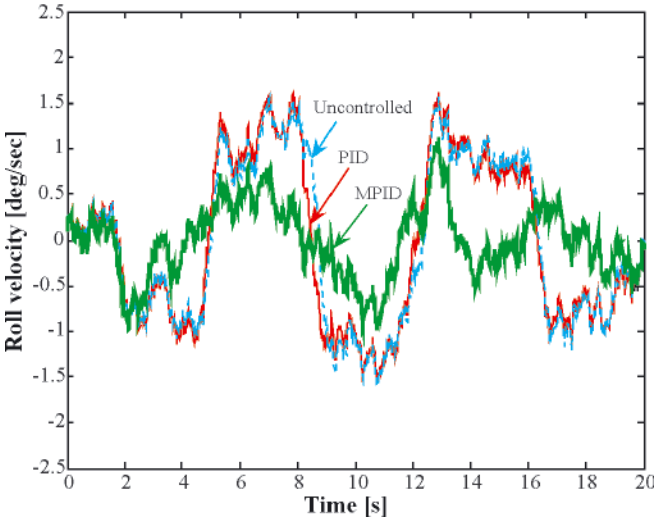

Fig. 9. *Comparison of roll velocity response*

In order to make fair comparison the step responses of two controllers with same gains are plotted in Fig. 10. Although PID has no early peak and nearly overshoots, MPID keeps stabilizing faster than Classical PID. Its early peak does not affect plant in a bad way. They give the almost same solution in settling time. Gains are calculated from the three terms of the process.

The comparison of the two controllers is presented in Tab. 3, which shows roll angle and roll velocity. The settling time for

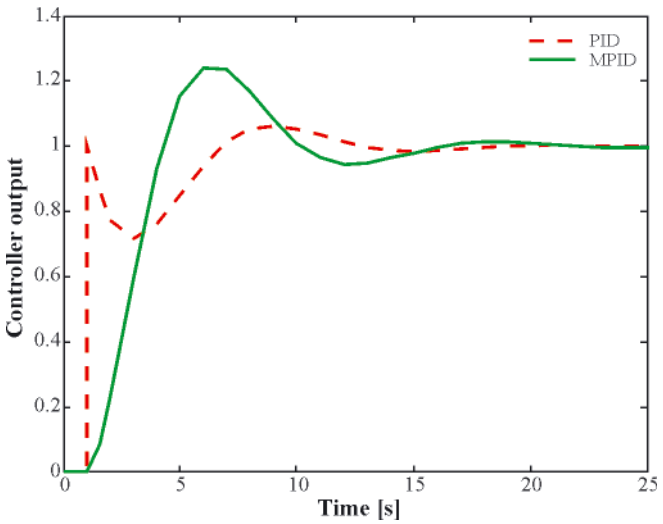

Fig. 10. *Step responses of PID and MPID*

uncontrolled is longer compared to the time for settlement of MPID.

Tab. 3. *Performance Comparisons*

Controller	Max. roll angle [deg]	Max. roll velocity [deg/s]
Uncontrolled	7.5°	1.5
PID	2°	1.3
MPID	1°	0.8

Roll reduction ratio (R_r) is used as the criteria for the roll reduction performance [13].

$$R_r = M_{fn} - M_{fs} \tag{24}$$

Where R_r is rolling magnification, in case of actuation of the fins and rolling magnification M_{fn} in case of non-actuation of the fins can be use.

RESULTS

This paper presents mathematical modeling and control of nonlinear roll motion with fin stabilizer system. The nonlinear terms which takes restoring and damping moment coefficients are calculated by empirical equations. The stability of nonlinear rolling motion of fishing boat is analyzed by Lyapunov direct method. During the simulation, it was assumed that the control gains are accepted same values for PID and MPID algorithms. From the simulation results, it can be observed that MPID controller shows significant improvement in roll magnitude around 86.6%. MPID controller performance had 13.3% greater than PID as shown in Tab. 3.

BIBLIOGRAPHY

1. Aydın M. and Akyıldız H.: *Assessment of the Intact Stability Characteristics of the Fishing Boats Suitable for Turkish Water*. ITU publications Vol. 4, No.6, 2005.
2. Dalzell J.F.: *A Note on the Form of Ship Roll Damping*, Journal of Ship Research, Vol. 22, 1978.
3. Fossen T.I.: *Guidance and Control of Ocean Vehicles*, John Wiley&Sons, 1994.
4. Ghassemi H., Dadmarzi F.H., Ghadimi P., Ommani B.: *Neural Network-PID Controller for Roll Fin Stabilizer*. Polish Maritime Research 2(65) Vol. 17, 2010.
5. *Grim O., Roll schwingungen, Stabilitat und Sicherheit in Seegang*, Schiffstechnik, 1952.
6. Guan W., Zhang X. K.: *Concise Robust Fin Roll Stabilizer Design Based on Integrator Backstepping and CGSA,* IEEE, 1/10, 2010.
7. Haddara M. and Wang Y.: *Parametric Identification of Maneuvering Models for Ships*, Int. Shipbuild. Programs, 445, pp. 5-27, 1999.
8. Hagiwara T., Yamada K., Ando Y., Murakamı I., Aoyama S., Matsuura S.: *A Design Method For Modified PID Control Systems For Multiple-Input, multiple-Output Plants To Attenuate Unknown Disturbances,* World Automation Congress. 2010.
9. Holden C. and Fossen T. I.: *A Nonlinear 7-DOF Model for U-Tanks of Arbitrary Shape*, *Ocean Engineering* 45, pp. 22–37, 2012.
10. Ikeda Y., *Prediction Methods of Roll Damping of Ships and their Application to Determine Optimum Stabilization Devices*, Proc, 6th Int. Workshop on stability, 2002.
11. Ikeda Y., HimenoY., Tanaka N.: *New York A Prediction Method for Ship Roll Damping*, Report No. 00405 of the Department of Naval Architecture, University of Osaka Prefecture, 1978.
12. Karakas Ş.C., Uçer E., Pesman E.: *Control Design of Fin Roll Stabilization in Beam Seas Based on Lyapunov's Direct Method*, Polish Maritime Research 2 (73), Vol. 19, 2012.
13. Kawazoe T., Nishikido S., Wada Y.: *Effect of Fin Area and Control Methods on Reduction of Roll Motion with Fin Stabilizer*, Bulletin of the M.E.S.J, Vol.22.No.1, 1994.
14. Ogata K.: *Modern Control Engineering*, Prentice-Hall, 4th Edition, New Jersey, 1990.
15. Ozkan I.R.: *Lyapunov's Direct Method for Stability Analysis of Ships*' ITU, PhD dissertation,1977.
16. Perez T., Goodwin G.C.: *Constrained predictive Control of Ship Fin Stabilizers to Prevent Dynamic Stall*, Control Engineering Practice 16, pp. 482–494, 2008.
17. Soliman M., and Thompson J.M.T.: *Transient and Steady State Analysis of Capsize Phenomena*, Applied Ocean Research, 13, pp. 82-92, 1991.
18. Surendran, S., Venkata Ramana Reddy, R., *Roll dynamics of a Ro-Ro ship,* International ship building progress, Vol. 49, No.4 pp. 301-320, 2002.
19. Surendran S., Lee S.K., Kim S.Y.: *Studies on an Algorithm to Control the Roll Motion Using Active Fins*, Ocean Engineering 34, pp. 542–551, 2007.
20. Taylan M.: *Solution of the Nonlinear Roll Model by a Generalized Asymptotic Method*, Ocean Engineering, Vol.26, pp. 1169-1181, 1999.
21. Taylan M.: *The Effect of Nonlinear Damping and Restoring in Ship Rolling,* Ocean Engineering, Vol.27, pp. 921-932, 2000.
22. Visioli A.: *Modified anti-windup Scheme for PID Controllers*. IEE Proc.-Cont. Theory App., 150, No 1. 2003.
23. Yamada K., Matsushima N. and Hagiwara T.: *A Design Method for Modified PID Controllers for Stable Plants and Their Application*. ECTI Transactions on Electrical Eng., Electronics and Communications Vol. 5, No. 1, 2007.
24. Concepción A. Monje, Blas M. Vinagre, Vicente Feliu, YangQuan Chen, *Tuning and auto-tuning of fractional order controllers for industry applications*, Control Engineering Practice, Volume 16, Issue 7, pp. 798-812, July 2008.

CONTACT WITH THE AUTHORS

Fuat Alarçin, Assoc. Prof.,
e-mail: alarcin@yildiz.edu.tr
Hakan Demirel, Assistant,
e-mail: demirelh@yildiz.edu.tr
M. Ertugrul Su, Assistant,
e-mail: mesu@yildiz.edu.tr
Ahmet Yurtseven, Assistant,
e-mail: ahmety@yildiz.edu.tr
Faculty of Naval Architecture and Maritime,
Yıldız Technical University,
Barbaros Bulvari Besiktas Istanbul TURKEY 34349

POLISH MARITIME RESEARCH 1(81) 2014 Vol 21; pp. 9-13
10.2478/pomr-2014-0002

Application of theory of semi-Markov processes to determining distribution of probabilistic process of marine accidents resulting from collision of ships

Jerzy Girtler, Prof.,
Gdansk University of Technology, Poland

ABSTRACT

In this paper is presented possible application of the theory of semi-Markov processes to elaborating an eight-state model of the process of occurrence of serviceability state and unserviceability states of sea-going ships making critical manoeuvres during their entering and leaving the ports. In the analysis it was taken into account that sea-going ships are in service for a very long time t ($t \to \infty$). The model was elaborated to determine the probability (P_0) of correct execution of critical manoeuvres during ship's entering and leaving the port as well as the probabilities P_j(j = 1, 2, 3, ..., 7) of incorrect execution of critical manoeuvres by a ship, that leads to marine accidents. It was assumed that such accidents result from: ship's grounding on port approaching fairway, collision with a ship on port approching fairway, collision with a pierhead during passing through port entrance, collision with a hydrotechnical structure during ship's passing through port channels, collision with a port quay during coming alongside it and collision with a ship already moored to the quay. The probability (P_0) was assumed a measure of safe execution of a critical manoeuvre. The probability characterizes possibility of avoiding any collision during ship's entering and leaving the port. The probability $P_a = 1 - P_0$ was assumed a measure of occurrence of a collsion and - consequently - marine accident. The probability P_a was interpreted as a sum of the probabilities P_j(j = 1, 2, 3, ..., 7) of occurrence of all the selected events. In summing up the paper, attention was drawn to its merits which - in opinion of this author - are crucial for research on real process of accidents during entering the port and leaving it by sea-going ship in difficult navigation conditions.

Key words: critical manoeuvre; port; probability; semi-Markov process; sea-going ship

PRELIMINARY REMARKS

In maritime shipping the increasing of safety of port manoeuvres associated with ship's entering the port, passing through port channels, and especially with coming alongside the quay and hauling off, is systematically pursued [1, 4, 5, 14]. Difficult hydrometeorological conditions result in that the ships sometimes cause collisions. They result from ship's grouding or collision with other ship on port approaching fairway, collision with pierhead or wavebreaker during passing through port entrance, collision with hydrotechnical structure during passing through port channels, collision with port's quay or other ship lain already along quay, during coming alongside the quay and mooring. Therefore the manoeuvres are called critical [1]. Risk of such collisions can be lowered by using tugs to bring ships in the port and next berth them and moor to quay as well as to haul out them from ports. However their use increases operational costs of ships and results in decrease of their profitability. Hence a question arises when to engage towing services is necessary as it is known that the biggest risk of the mentioned collisions takes place in difficult ship traffic conditions, and because such conditions it is easy to make the following errors [1, 4, 5, 10, 14, 15]:

- underestimating destructive action of sea currents and tides and hydrometeorological conditions,
- unprecise identification of ship propulsion and manoeuvrability qualities in a given ship traffic conditions,
- neglecting (disrespecting) importance of restricted visibility,
- not taking into account current values of speed and direction of wind, its gusts and direction changes.

Without any doubts the most convincing factor which informs on necessity of making use of towing services is the probability of collision occurrence in given traffic conditions during entering the port by ship and executing critical manoeuvres within it. The problem of determining such probability can be characterized in an analytical way by using the theory of semi-Markov processes. The theory is useful for determining occurrence probabilities of events possible to happen during execution of critical manoeuvres by ship

entering the port, moving inside it as well as leaving the port. This makes it necessary to elaborate a model of process of accidents resulting from execution of such manoeuvres.

MODEL OF PROCESS OF ACCIDENTS RESULTING FROM COLLISIONS OF SHIPS ENTERING THE PORT OR LEAVING IT

As assumed in the model, the most important events resulting in marine accidents are the following [1, 4, 5]: z_1 – grouding on port approaching fairway, z_2 – collision with other ship on port approaching fairway, z_3 – collision with pierhead during passing through port entrance, z_4 – collision with wavebreaker during passing through port entrance, z_5 – collision with hydrotechnical structure during passing through port channels, z_6 – collision with port's quay during coming alongside it, z_7 – ship's collision with other ship lain already along quay - during coming alongside the quay. Each of the events results in ship's damage which involves the ship into unserviceability state [4, 6, 7, 9]. Change of the state into serviceability one requires the ship to be renewed by doing an appropriate repair. On completion of the repair the ship regains its operational qualities lost as a result of the collision, that is equivalent to occurrence of the event z_0 which means recovering the state of serviceability by the ship. Successive occurrence of the mentioned states $z_i \in Z$ (i = 1, 2, …, 7) forms the process of marine accidents. Occurrence of every marine accident $z_i \in Z$ results in arising the unserviceability state $s_i \in S^*$ (i = 1, 2, …, 7). Removal of ship's damages due to the mentioned collisions results in occurring the serviceability state of the ship, s_0. The states can be called the reliability ones as the states $s_i \in S$ result from ship's damages (in this case due to collisions) whereas the state s_0 takes place as a result of ship's renewal. Obviously, the next collision can happen only when the ship is renewed after occurrence of the former collision. Therefore the model of the process of changes of the mentioned reliability states can be considered the semi-Markov process $\{W(t): t \geq 0\}$ with the set of states $S = \{s_i\}$; i = 0, 1, 2, …, 7. Changes of the mentioned states si (i = 0, 1, 2, …, 7) occur in the successive instants t_n ($n \in N$), and in the instant $t_0 = 0$ the ship is in the state s_0. The state s_0 lasts til the instant of ship's damage resulting from occurrence of any collision. And, the states s_i (i = 1, 2, …, 7) last until the ship is renewed. Changes of the states s_i into the states s_j (i, j = 0, 1, 2, 3; $i \neq j$) occur with the probability p_{ij} after the running time T_{ij} which is a random variable. In order to account for the situation in the phase of ship's service it is necessary to describe - in a probabilistic way - its process of accidents due to collisions with taking into account occurrence probabilities of the mentioned states s_i(i = 0, 1, 2, …, 7) possible to occur in the particular instants $t_0, t_1,..., t_{n1}, t_n$ of ship's service time [2, 3, 13]. Therefore the following set of classes of ship's reliability states can be distinguished:

$$s_i \in S \ (i = 0, 1, 2, \ldots, 7) \tag{1}$$

and interpreted as follows:

- s_0 – serviceability state,
- s_1 – ship's unserviceability state resulting from its grounding on port approaching fairway,
- s_2 – ship's unserviceability state resulting from its collision with other ship on port approaching fairway,
- s_3 – ship's unserviceability state resulting from its collision with pierhead during ship's passing through port entrance,
- s_4 – ship's unserviceability state resulting from its collision with wavebreaker during ship's passing through port entrance,
- s_5 – ship's unserviceability state resulting from its collision with a hydrotechnical structure during ship's passing through port channels,
- s_6 – ship's unserviceability state resulting from its collision with a port quay during coming alongside it,
- s_7 – ship's unserviceability state resulting from its collision with other ship already moored at a port quay - during coming alongside the quay,

It can be assumed that the ship state, s_i, existing in the instant t_{n+1} as well as the time interval of lasting the state which has happened in the instant t_n depends only on the state which has occurred in the instant t_{n1}, and not on the states which have happened in the instants $t_0, t_1,..., t_{n2}$ as well as not on their lasting time intervals. The assumption is obvious as there is no reletionship between collisions (hence the states $s_i \in S^*$ are independent events). And, the state s_0 depends only on a given state s_i and not on the state s_{i-1} directly preceding the state s_i. Therefore it can be assumed that the process $\{W(t): t \geq 0\}$ is semi-Markovian [5, 6, 8, 12].

The initial distribution of the process is as follows:

$$P\{W(0) = s_i\} = \begin{cases} 1 & \text{for} \quad i = 0 \\ 0 & \text{for} \quad i = 1,\ 2,\ 3,\ ...,\ 7 \end{cases} \tag{2}$$

and, the functional matrix is of the following form:

$$\mathbf{Q(t)} = \begin{bmatrix} 0 & Q_{01}(t) & Q_{02}(t) & Q_{03}(t) & Q_{04}(t) & Q_{05}(t) & Q_{06}(t) & Q_{07}(t) \\ Q_{10}(t) & 0 & 0 & 0 & 0 & 0 & 0 & 0 \\ Q_{20}(t) & 0 & 0 & 0 & 0 & 0 & 0 & 0 \\ Q_{30}(t) & 0 & 0 & 0 & 0 & 0 & 0 & 0 \\ Q_{40}(t) & 0 & 0 & 0 & 0 & 0 & 0 & 0 \\ Q_{50}(t) & 0 & 0 & 0 & 0 & 0 & 0 & 0 \\ Q_{60}(t) & 0 & 0 & 0 & 0 & 0 & 0 & 0 \\ Q_{70}(t) & 0 & 0 & 0 & 0 & 0 & 0 & 0 \end{bmatrix} \tag{3}$$

The graph of changes of the process, resulting from the functional matrix (3), is presented in Fig. 1.

The functional matrix **Q(t)** constitutes the model of changes of the reliability states $s_i \in S$(i = 0, 1, 2, …, 7) of ship. The non-zero elements Qij(t) of the matrix Q(t) depend on the distributions of random variables which are the time intervals of lasting the process $\{W(t): t \geq 0\}$ in the states s_i S(i = 0, 1, 2, …, 7). The elements of the functional matrix Q(t) are the probabilities of transition of the mentioned process from the state s_i to the state s_j ($s_i, s_j \in S$) during the time not greater than t, which are determined as follows:

$$Q_{ij}(t) = P\{W(\tau_{n+1}) = s_j, \quad \tau_{n+1} - \tau_n < t | W(\tau_n) = s_i\} = p_{ij}F_{ij}(t) \tag{4}$$

where:

p_{ij} – probability of one-step transition of uniform Markov chain;

$p_{ij} = P\{W(\tau_{n+1}) = s_j | W(\tau_n) = s_i = \lim_{t\to\infty} Q_{ij}(t)$;

$F_{ij}(t)$ – cumulative distribution function of the random variable T_{ij} which shows lasting time of the state s_i of the process $\{W(t): t \geq 0\}$ provided that the next state of the process will be the state s_j.

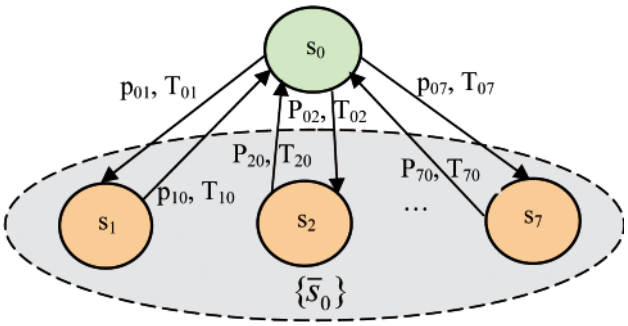

Fig. 1. *The graph of changes of the states of the process {W(t): t ∈ T}: s_0 – serviceability state of a ship, $\{\bar{s}_0\}$ – set of ship's unserviceability states (due to collisions) $\{\bar{s}_0\} = \{s_1, s_2, ..., s_7\}$, $s_i \in S(i = 1, 2, ..., 7)$ – unserviceability states, p_{ij} – probabilities of changes of the state s_i into the state s_j, T_{ij} – lasting time of the state s_i under condition that the next will be the state s_j (i, j = 0, 1, 2, ..., 7; i ≠ j)*

As results from the functional matrix **Q(t)** (3), the matrix **P** of the probabilities of transition of Markov chain inserted in the process, is as follows [4, 5, 6]:

$$\mathbf{P} = \begin{bmatrix} 0 & p_{01} & p_{02} & p_{03} & p_{04} & p_{05} & p_{06} & p_{07} \\ 1 & 0 & 0 & 0 & 0 & 0 & 0 & 0 \\ 1 & 0 & 0 & 0 & 0 & 0 & 0 & 0 \\ 1 & 0 & 0 & 0 & 0 & 0 & 0 & 0 \\ 1 & 0 & 0 & 0 & 0 & 0 & 0 & 0 \\ 1 & 0 & 0 & 0 & 0 & 0 & 0 & 0 \\ 1 & 0 & 0 & 0 & 0 & 0 & 0 & 0 \\ 1 & 0 & 0 & 0 & 0 & 0 & 0 & 0 \end{bmatrix} \tag{5}$$

In the process $\{W(t): t \geq 0\}$ the random variables T_{ij} are of definite, positive expected values. Therefore its limiting distribution [4, 5, 6, 11]:

$$P_j = \lim_{t\to\infty} P_{ij}(t) = \lim_{t\to\infty} P\{W(t) = s_j\} \tag{6}$$

$$s_j \in S(j = 0, 1, 2, \ldots, 7)$$

has the following form:

$$P_j = \frac{\pi_j E(T_j)}{\sum_{k=0}^{7} \pi_k E(T_k)} \tag{7}$$

The probabillities $\pi_j(j = 0, 1, 2, 3, \ldots, 7)$ in the formula (7) are the limiting probabilities of the Markov chain inserted in the process $\{W(t): t \geq 0\}$. And, $E(T_j)$ and $E(T_k)$ are expected values of the random variables T_j and T_k, respectively, which show lasting time of ship in the states s_j and s_k, respectively, independently of which state of it will occur later [6, 11].

In order to determine the limiting distribution (7) it is necessary to solve the set of equations which contain the mentioned limiting probabilities $\pi_j(j = 0, 1, 2,..., 7)$ of the Markov chain inserted in the process $\{W(t): t \geq 0\}$ as well as the matrix P of probabilities of transition from the state s_i to the state s_j, determined by the formula (5). The set is a system of the following form:

$$\left.\begin{aligned} &[\pi_0,\pi_1,\pi_2,\pi_3,\pi_4,\pi_5\pi,\pi_6,\pi_7] = [\pi_0,\pi_1,\pi_2,\pi_3,\pi_4,\pi_5,\pi_6,\pi_7] \cdot \mathbf{P} \\ &\sum_{k=0}^{7} \pi_k = 1 \end{aligned}\right\} \tag{8}$$

As a result of solving the set of equations (8) it is possible – by making use of the formula (7) – to obtain the following relations:

$$\left.\begin{aligned} &P_0 = \frac{E(T_0)}{E(T_0) + \sum_{k=0}^{7} p_{0k}E(T_k)}, \quad P_1 = \frac{p_{01}E(T_1)}{E(T_0) + \sum_{k=0}^{7} p_{0k}E(T_k)}, \quad P_2 = \frac{p_{02}E(T_2)}{E(T_0) + \sum_{k=0}^{7} p_{0k}E(T_k)} \\ &P_3 = \frac{p_{03}E(T_3)}{E(T_0) + \sum_{k=0}^{7} p_{0k}E(T_k)}, \quad P_4 = \frac{p_{04}E(T_4)}{E(T_0) + \sum_{k=0}^{7} p_{0k}E(T_k)}, \quad P_5 = \frac{p_{05}E(T_5)}{E(T_0) + \sum_{k=0}^{7} p_{0k}E(T_k)} \\ &P_6 = \frac{p_{06}E(T_6)}{E(T_0) + \sum_{k=0}^{7} p_{0k}E(T_k)}, \quad P_7 = \frac{p_{07}E(T_7)}{E(T_0) + \sum_{k=0}^{7} p_{0k}E(T_k)} \end{aligned}\right\} \tag{9}$$

The probability P_0 is the limiting probability that during a longer service time (theoretically at $t \to \infty$) sea-going ship which executes critical manoeuvres, is in the state s_0. Hence the probability determines correct execution of critical manoeuvres during which the ship does not suffer any collision and consequently no marine accident happens. And, the probabilities $P_j(j = 1, 2, \ldots, 7)$ are the limiting probabilities of occurrence of the states $s_j \in S(j = 1, 2, \ldots, 7)$ of sea-going ship at $t \to \infty$, i.e. the probabilities of

remaining the ship in the unserviceability states resulting from the mentioned collisions $z_i \in Z$ (i = 1, 2, …, 7).

The example realization of the process {W(t): t ≥ 0}, which illustrates occurring the ship's reliability states s∈ S(j = = 0, 1, 2, …, 7) during ship's service, is presented in Fig. 2. In order to calculate values of the probabilities P_j(j = 0, 1, 2, …, 7) it is necessary to estimate p_{ij} and $E(T_j)$.

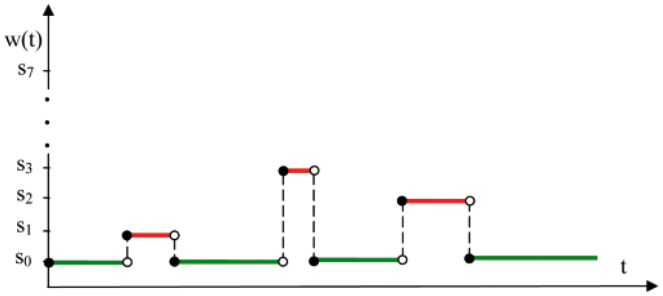

Fig. 2. *The example of the process {W(t): t ≥ 0} for the considered ship:* s_0 *– serviceability state of the ship,* s_1 *– unserviceability state of the ship, as a result of grounding on the approach way to port,* s_2 *– unserviceability state of the ship, as a result of collision with another ship on the approach line to port,* s_3 *– unserviceability state of the ship, as a result of crashing into an entrance head when passing by*

Estimating the probabilities p_{ij} and expected values $E(T_j)$ is possible after obtaining the realization w(t) of the process{W(t): t∈ 0} within an appropriately long investigation time interval, i.e. for t∈ [0, t_b], where the investigation time of the process, $t_b >> 0$. It is then possible to set the numbers n_{ij}(i,j = 0, 1, 2, 3; i ≠ j), of transitions of the process {W(t): t∈ 0} from the state s_i to s_j in an approporiately long time and to determine values of the estimator $\hat{P}_{ij}$ of the unknown probability p_{ij}. Statistic is the most credible estimator of the transition probability p_{ij} [6, 11]:

$$\hat{P}_{ij} = \frac{N_{ij}}{\sum_j N_{ij}}, \quad i \neq j; \;\; i, j = 0,\; 1,\; 2,\; 3 \qquad (10)$$

whose value:

$$\hat{p}_{ij} = \frac{n_{ij}}{\sum_j n_{ij}}$$

is an estimation of the unknown transition probability p_{ij}.

From the mentioned run of w(t) of the process W(t) it is also possible to obtain the realizations $t_j^{(m)}$, m = 1, 2,..., n_{ij}, of the random variables T_j. Application of the point estimation makes it possible to easily estimate $E(T_j)$ by counting arithmetic mean value of the realization $t_j^{(m)}$ [3, 13].

$E(T_j)$ is expected value of the random variable T_j(j = 0, 1, 2, ..., 7) equivalent to lasting time of the state s_j ∈ S(j = = 0, 1, 2, ..., 7) of the process {W(t): t ≥ 0} independently of that to which state the process goes through from the state in question.

The expected values $E(T_j)$ depend on the expected values $E(T_{ij})$ as well as the probabilities p_{ij} , as follows:

$$E(T_j) = E(T_i) = \sum_j p_{ij} E(T_{ij}), \quad i, j = \overline{0,7}; \quad i \neq j \qquad (11)$$

The probability P_0 can be considered a measure of safe operation of ship. And, the probability:

$$\overline{P}_0 = \sum_{j=1}^{7} P_j$$

can be considered a measure which characterizes possibility of collision occurrence during executing critical manoeuvres by ship entering the port and moving over it in difficult conditions.

In order to obtain values (approximated of course) of the probabilities P_j(j = 0, 1, 2, …, 7) it is necessary to estimate p_{ij} and $E(T_j)$, as it was already mentioned. In the case when the probability is greater than (P_a), i.e. that accepted by shipowner, ($\overline{P}_0 > P_a$), the ship operator should angage towing services. Tugs are capable of aiding the ship either in safe entering the port or leaving it.

COMMENTSS AND CONCLUSIONS

The proposal, presented in this paper, of determining the probability which characterizes possible occurrence of marine accident during ship's entering the port or leaving it, deals only with the seven-state set of events resulting in collisions as well as the state of correct execution of critical manouvre. If requested, the proposed model of the process of accidents associated with incorrect execution of critical manoeuvres may be extended by taking into account ship's unserviceability states caused by additional collisions.

To make rational operational decisions connected with the use of tugs for moving the ship into and out of port in ship's operational phase, with accounting for its safety, is possible in the case of knowing, a.o.:

- the probabilities P_j (j = 1, 2, 3, …, 7) of occurrence of accident during execution of critical manoeuvres by the ship entering the port or leaving it,
- the probabilities P_0 of correct execution of critical manoeuvres by the ship, i.e. its safe entering the port or leaving it.

To determine of the mentioned probabilities was applied the theory of semi-Markov processes.

Possible application of semi-Markov process, instead of Markov process, for modelling sequential occurrence of the mentioned situations in which ship's moving can be realized during execution of critical manoeuvres, results from that it should be expected that the random variables T_{ij} and T_i have arbitrary distributions concentrated in the set $R_+ = [0, +\infty)$. Application of Markov process would be justified if only it were be allowed to assume that the random variables T_{ij} and T_i have exponential distributions.

The presented model of the process of marine accidents resulting from collisions during execution of critical manoeuvres, can be of practical importance because it is easy to determine estimators for the transition probabilities p_{ij} and to estimate the expected values $E(T_j)$. It should be simultaneously taken into account that the point estimation of the expected value $E(T_j)$ does not make it possible to determine accuracy of its estimation. To assess such accuracy is possible by using the interval estimation [3, 13] in which is determined the confidence interval [t_{dj}, t_{gj}] of random limits, which contains the expected value $E(T_j)$ with a determined probability (confidence level) β.

BIBLIOGRAPHY

1. Abramowicz-Gerigk T.: *Safety of critical manoeuvres of ships in sea highway transport system*(in Polish). Prace Naukowe (Scientific bulletin). Transport, issue 83. Oficyna Wydawnicza Politechniki Warszawskiej (Publishing House of Warsaw University of Technology), Warszawa 2012.
2. Benjamin J. R., Cornell C. A.: *Calculus of probability, mathematical statistics and decision-making theory for engineers* (in Polish). WNT (Scientific Technical Publishers), Warszawa 1977.
3. Firkowicz S.: *Statistical assessment of quality and reliability of electronic lamps (in Polish)*. WNT (idem), Warszawa 1963.

4. Girtler J., Kuszmider S., Plewiński L.: *Selected problems of operation of sea-going ships in the aspect of safety at sea* (in Polish). Monograph. WSM (Szczecin Maritime Academy), Szczecin 2003.
5. Girtler J., Kitowski Z., Kuriata A.: *Safety of ship at sea. Systematic approach* (in Polish). WKiŁ (Transport and Telecommunication Publishers), Warszawa 1995.
6. Girler J.: *Controlling the operation process of ship diesel engines on the basis of a diagnostic decision-making model* (in Polish). Zeszyty Naukowe AMW(Scientific Bulletins of Polish Naval Academy), No. 100A, Gdynia 1989.
7. Girtler J.: *Suggestion of interpretation of action and the rule of taking decision with regard to safety of sea ships traffic*. Zagadnienia Eksploatacji Maszyn (Operational Problems of Machines), issue 2(122), vol. 35, 2000.
8. Girtler J.: *Diagnostics – a condition for controlling ship diesel engines in service* (in Polish). Study No. 28. WSM (Szczecin Maritime Academy), Szczecin 1997.
9. Girtler J.: *Availability of sea transport means.* Archives of Transport. Polish Academy of Sciences Committee of Transport. Quarterly, vol. 9, iss. 3-4, Warsaw 1997.
10. Girtler J.: *Possibility of valuation of marine diesel engines*. Journal of Polish CIMAC, No. 1,Vol. 4,, Gdańsk 2009.
11. Grabski F.: *Theory of semi-Markov processes of operation of technical objects* (in Polish). Zeszyty Naukowe WSMW (AMW) (Scientific Bulletins of Polish Naval Academy), No. 75A, Gdynia 1982.
12. Jaźwiński J., Borgoń J.: *Operational reliability and safety of flights* (in Polish). WKiŁ (Transport and Telecommunication Publishers), Warszawa 1989.
13. Krzysztofiak M., Urbanek D.: *Statistical methods* (in Polish). PWN (Polish Scientific Publishers), Warszawa 1979.
14. Plewiński L.: *Accidents at sea. Collisions of ships* (in Polish). Publ. WSM (Szczecin Maritime Academy), Szczecin 2000.
15. Wiśniewski B.: *Wind-generated waves* (in Polish). Rozprawy i studia (Dissertations and studies), Vol. (CCCIV) 230, Publ. Uniwersytet Szczeciński (Szczecin University), Szczecin 1998.

CONTACT WITH THE AUTHOR

Jerzy Girtler, Prof.
Department of Ship Power Plants
Faculty of Ocean Engineering and Ship Technology
Gdansk University of Technology
Narutowicza 11/12
80-233 Gdansk, POLAND
e-mail: jgirtl@pg.gda.pl

POLISH MARITIME RESEARCH 1(81) 2014 Vol 21; pp. 14-19
10.2478/pomr-2014-0003

Ship course stabilization by feedback linearization with adaptive object model

Piotr Borkowski, Ph.D.
Maritime University of Szczecin, Poland

ABSTRACT

The algorithm of ship course stabilization herein presented is based on a feedback linearization controller with adaptive object model. The described method, consisting in current approximation of unknown object model functions by neuro-fuzzy approximators, represents a new generation of adaptive control methods. The implementation of this algorithm, which may constitute an executive module of a navigational decision support system, will contribute to a higher degree of automation and navigational safety improvement.

Key words: ship course stabilization; feedback linearization controller; GRBF; safety of navigation

INTRODUCTION

Cost-effectiveness and constant need for safety enhancement in shipping call for raising the requirements concerning the accuracy of steering a ship for various control tasks. This is particularly true for fairways with heavy traffic and restricted area or depth waters, such as straits and channels, but also for the ship to be conducted along a safe trajectory in the open sea. These situations may be considered as steering along a preset trajectory. Although course stabilization generally seems to be a simple problem of automatic ship control, the fact the object is a complex one (model non-linearity, uncertainty resulting from external disturbances, changing ship's dynamics) makes the task more difficult. One can consider it as an uncertain system, i.e. one in which the object dynamics description is unknown, or only partially known. The functional, or structural, uncertainty calls for current object model adaptation, that is why such systems, called functionally adaptive, represent a new area of intelligent control systems [4, 5, 15, 16].

The author presents an algorithm of ship course stabilization, operating on the basis of a feedback linearization controller [6]. The object model structure is assumed to be partly known. Current approximation of unknown object model functions is achieved by means of neuro-fuzzy approximators based on Gaussian radial basis functions (GRBF) [4].

FEEDBACK LINEARIZATION WITH OBJECT MODEL ADAPTATION

This chapter is divided into three parts. The first contains a synthesis of the feedback linearization controller, the second part presents a method of object model adaptation, and in the last part the stability of the adaptive system has been proved.

The controller

Let the dynamics of a continuous object be described by a non-linear equation of state:

$$\dot{\mathbf{x}} = \mathbf{f}(\mathbf{x}, \mathbf{u}) \tag{1}$$

where:

- $\mathbf{f}(\mathbf{x}, \mathbf{u})$ - continuous differentiable vector function, containing zero vectors in its domain,
- $\mathbf{x}$ - n-dimensional state vector,
- $\dot{\mathbf{x}}$ - n-dimensional vector of state derivatives versus time (t),
- $\mathbf{u}$ - p-dimensional vector of control signals.

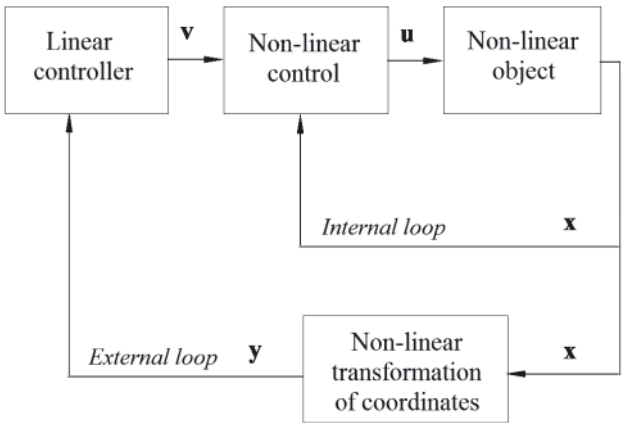

Fig. 1. *Architecture of a controller with linearization feedback (source: own study)*

The fundamental idea of feedback linearization [6] is illustrated in Fig. 1. It consists in building a non-linear control law **u** (assuming the state vector is measurable) as the so called

internal control loop that linearizes a non-linear system after an appropriate transformation of state space coordinates (from **x** to **y**). Then a control **v** can be designed in the external loop in new coordinates, making use of the 'rich store' of linear system control methods.

Our considerations will be limited to the class of non-linear single input and affinity systems, due to the form of control signal:

$$\dot{\mathbf{x}} = \mathbf{f}(\mathbf{x}) + \mathbf{g}(\mathbf{x})u \tag{2}$$

where:

$\mathbf{f}(\mathbf{x})$, $\mathbf{g}(\mathbf{x})$ - smooth vector fields in R^n (infinitely differentiable functions, with a domain and range R^n) and $f(\mathbf{0}) = \mathbf{0}$,
u - control signal (scalar).

The system described by equation (2) can be linearized by feedback, if there exists a nonlinear control law:

$$u = \alpha(\mathbf{x}) + \beta(\mathbf{x})v \tag{3}$$

where:

$\alpha(\mathbf{x})$, $\beta(\mathbf{x})$ - function with a range R and $\beta(\mathbf{x}) \neq 0$,
v - new control input (scalar),

and dipheomorphism (differentiable function, whose inverse function exists and is differentiable) transforming the state vector **x** into **y**:

$$\mathbf{y} = \mathbf{T}(\mathbf{x}) \tag{4}$$

so that for the control (3) the transformed variables satisfy the linear state equation:

$$\dot{\mathbf{y}} = \mathbf{A}\mathbf{y} + \mathbf{b}v \tag{5}$$

where:

A - matrix with $n \times n$ dimensions, whose elements $a_{i,i=1}$ for $1 \leq i \leq n-1$ are equal to one, the others are zeros,
b - n-dimensional vector, whose n-th coordinate is a unity, the others are zeros.

Feedback linearization is called global, if dipheomorphism (4) is determined for any state vector **x**.

We will now derive a condition for the existence of dipheomorphism (4) and a method of its determination, and the determination of control (3). Differentiating both sides of equation (4) against time, we will obtain:

$$\dot{\mathbf{y}} = \frac{\partial \mathbf{T}(\mathbf{x})}{\partial \mathbf{x}} \dot{\mathbf{x}} \tag{6}$$

where:

$\frac{\partial \mathbf{T}(\mathbf{x})}{\partial \mathbf{x}}$ - Jacobian matrix of the transformation $\mathbf{T}(\mathbf{x})$,

which after the application of relation (5) assumes this form:

$$\frac{\partial \mathbf{T}(\mathbf{x})}{\partial \mathbf{x}} \dot{\mathbf{x}} = \mathbf{A}\mathbf{x} + \mathbf{b}v \tag{7}$$

The above equation can be written as the system:

$$\begin{aligned}
&\frac{\partial T_1(\mathbf{x})}{\partial x_1}\dot{x}_1 + K + \frac{\partial T_1(\mathbf{x})}{\partial x_n}\dot{x}_n = T_2(\mathbf{x}) \\
&\frac{\partial T_2(\mathbf{x})}{\partial x_1}\dot{x}_1 + K + \frac{\partial T_2(\mathbf{x})}{\partial x_n}\dot{x}_n = T_3(\mathbf{x}) \\
&\vdots \\
&\frac{\partial T_{n-1}(\mathbf{x})}{\partial x_1}\dot{x}_1 + K + \frac{\partial T_{n-1}(\mathbf{x})}{\partial x_n}\dot{x}_n = T_n(\mathbf{x}) \\
&\frac{\partial T_n(\mathbf{x})}{\partial x_1}\dot{x}_1 + K + \frac{\partial T_n(\mathbf{x})}{\partial x_n}\dot{x}_n = v
\end{aligned} \tag{8}$$

that after the introduction of a Lie derivative [7] takes this form:

$$\begin{aligned}
&L_{\dot{\mathbf{x}}}T_1(\mathbf{x}) = T_2(\mathbf{x}) \\
&L_{\dot{\mathbf{x}}}T_2(\mathbf{x}) = T_3(\mathbf{x}) \\
&\vdots \\
&L_{\dot{\mathbf{x}}}T_{n-1}(\mathbf{x}) = T_n(\mathbf{x}) \\
&L_{\dot{\mathbf{x}}}T_n(\mathbf{x}) = v
\end{aligned} \tag{9}$$

and accounting for relation (2) and the fact that components: T_2, ..., T_n must be independent of u, contrary to the control v, it will be written as:

$$\begin{aligned}
&L_{\mathbf{f}(\mathbf{x})}T_1(\mathbf{x}) = T_2(\mathbf{x}) \\
&L_{\mathbf{f}(\mathbf{x})}T_2(\mathbf{x}) = T_3(\mathbf{x}) \\
&\vdots \\
&L_{\mathbf{f}(\mathbf{x})}T_{n-1}(\mathbf{x}) = T_n(\mathbf{x}) \\
&T_n(\mathbf{x}) + L_{\mathbf{g}(\mathbf{x})}T_n(\mathbf{x})u = v
\end{aligned} \tag{10}$$

At this point one can see that the feedback linearization problem actually requires looking for the component T_1, as later the remaining components T_2, ..., T_n can be determined inductively from the system (10), then the control input (because $L_{\mathbf{g}(\mathbf{x})}T_n(\mathbf{x}) \neq 0$):

$$u = -\frac{L_{\mathbf{f}(\mathbf{x})}T_n(\mathbf{x})}{L_{\mathbf{g}(\mathbf{x})}T_n(\mathbf{x})} + \frac{1}{L_{\mathbf{g}(\mathbf{x})}T_n(\mathbf{x})}v \tag{11}$$

that for:

$$\begin{aligned}
&\alpha(\mathbf{x}) = -\frac{L_{\mathbf{f}(\mathbf{x})}T_n(\mathbf{x})}{L_{\mathbf{g}(\mathbf{x})}T_n(\mathbf{x})} \\
&\beta(\mathbf{x}) = \frac{1}{L_{\mathbf{g}(\mathbf{x})}T_n(\mathbf{x})}
\end{aligned} \tag{12}$$

takes the form (3).

Therefore, how do we determine the component T_1 Using the Lie bracket [7] we get:

$$\begin{aligned}
&L_{\mathrm{ad}_{\mathbf{f}(\mathbf{x})\mathbf{g}(\mathbf{x})}}T_1(\mathbf{x}) = L_{\mathbf{f}(\mathbf{x})}L_{\mathbf{g}(\mathbf{x})}T_1(\mathbf{x}) + \\
&- L_{\mathbf{g}(\mathbf{x})}L_{\mathbf{f}(\mathbf{x})}T_1(\mathbf{x}) = - L_{\mathbf{g}(\mathbf{x})}T_2(\mathbf{x}) = 0
\end{aligned} \tag{13}$$

and performing the above operations inductively, we obtain a system of partial differential equations versus the component T_1:

$$\begin{aligned}
&L_{\mathrm{ad}^0_{\mathbf{f}(\mathbf{x})}\mathbf{g}(\mathbf{x})}T_1(\mathbf{x}) = 0 \\
&L_{\mathrm{ad}^1_{\mathbf{f}(\mathbf{x})}\mathbf{g}(\mathbf{x})}T_1(\mathbf{x}) = 0 \\
&\vdots \\
&L_{\mathrm{ad}^{n-2}_{\mathbf{f}(\mathbf{x})}\mathbf{g}(\mathbf{x})}T_1(\mathbf{x}) = 0
\end{aligned} \tag{14}$$

(whose solution yields T_1) and the relation:

$$L_{\mathrm{ad}^{n-1}_{\mathbf{f}(\mathbf{x})}\mathbf{g}(\mathbf{x})}T_1(\mathbf{x}) \neq 0 \tag{15}$$

thanks to which, by indirect reasoning, we can easily notice that smooth vector fields $\mathrm{ad}^0_{\mathbf{f}(\mathbf{x})}\mathbf{g}(\mathbf{x})$, $\mathrm{ad}^1_{\mathbf{f}(\mathbf{x})}\mathbf{g}(\mathbf{x})$, ..., $\mathrm{ad}^{n-1}_{\mathbf{f}(\mathbf{x})}\mathbf{g}(\mathbf{x})$ must be linearly independent. Therefore, by virtue of Frobenius theorem the system (14) has a solution if and only if the set of vector fields $\{\mathrm{ad}^0_{\mathbf{f}(\mathbf{x})}\mathbf{g}(\mathbf{x}), \mathrm{ad}^1_{\mathbf{f}(\mathbf{x})}\mathbf{g}(\mathbf{x}), ..., \mathrm{ad}^{n-2}_{\mathbf{f}(\mathbf{x})}\mathbf{g}(\mathbf{x})\}$ is involutive, which ultimately gives conditions for the existence of dipheomorphism (4).

The control (3) linearizes the system (2), after the transformation of coordinates (4) and brings it to the form (5), therefore, to obtain asymptotic stability, designing a linear input in the external loop:

$$v = -a_1 y_1 - ... - a_n y_n \tag{16}$$

where:
$a_1, ..., a_n$ - positive settings of the controller,

we should select its coefficient in such a manner that the characteristic polynomial (of the created linear system):

$$\Gamma(s) = s^n + a_n s^{n-1} + ... + a_2 s + a_1 \tag{17}$$

has all roots with negative real part, and for the purpose of the adaptation method we additionally require that at least one pole should have zero imaginary part.

The adaptation

So far the considerations have referred to a situation where the model (2) is in an overt form. In reality this is not the case, so in the formula for the control law in the internal loop (11) there are unknown functions:

$$\begin{aligned} \alpha_f(\mathbf{x}) &= L_{f(x)} T_n(\mathbf{x}) \\ \alpha_g(\mathbf{x}) &= L_{g(x)} T_n(\mathbf{x}) \end{aligned} \tag{18}$$

To identify these functions we will use neuro-fuzzy approximators [4]:

$$\begin{aligned} \hat{\alpha}_f(\mathbf{x}) &= \mathbf{w}_f^T \boldsymbol{\Phi}_f + \alpha_{f0}(\mathbf{x}) \\ \hat{\alpha}_g(\mathbf{x}) &= \mathbf{w}_g^T \boldsymbol{\Phi}_g + \alpha_{g0}(\mathbf{x}) \end{aligned} \tag{19}$$

where:
$\mathbf{w}_f, \mathbf{w}_g$ - k-dimensional vectors of weight parameters,
$\alpha_{f0}(\mathbf{x}), \alpha_{g0}(\mathbf{x})$ - known initial function estimates (18),
$\boldsymbol{\Phi}_f, \boldsymbol{\Phi}_g$ - k-dimensional basis functions,

built on Gaussian radial basis functions (GRBF), whose i-th element has the form ($1 \le i \le k$):

$$\begin{aligned} \Phi_{f_i}(\mathbf{x}) &= \exp\left\{\frac{-\|\mathbf{x} - \boldsymbol{\mu}_{f_i}\|^2}{2\sigma_f^2}\right\} \\ \Phi_{g_i}(\mathbf{x}) &= \exp\left\{\frac{-\|\mathbf{x} - \boldsymbol{\mu}_{g_i}\|^2}{2\sigma_g^2}\right\} \end{aligned} \tag{20}$$

where:
$\mathbf{u}_{f_i}, \mathbf{u}_{g_i}$ - n-dimensional vectors representing centres (symmetry axes) of i-th elements of basis functions,
σ_f^2, σ_g^2 - variances representing the 'width' of basis functions,
$\|\mathbf{x}\|$ - Euclidean norm.

The values of weight parameters should change depending on the dynamics error, which due to the fact that the control:

$$u = -\frac{\hat{\alpha}_f(\mathbf{x})}{\hat{\alpha}_g(\mathbf{x})} + \frac{1}{\hat{\alpha}_g(\mathbf{x})} v \tag{21}$$

generally does not satisfy the last relation of the system (10), should be defined as below (the other equation is created by replacing **v** with a term derived from the control (21)):

$$\begin{aligned} e &= \alpha_f(\mathbf{x}) + \alpha_g(\mathbf{x})u - v = \\ &= \alpha_f(\mathbf{x}) - \hat{\alpha}_f(\mathbf{x}) + [\alpha_g(\mathbf{x}) - \hat{\alpha}_g(\mathbf{x})] \end{aligned} \tag{22}$$

and assuming the vector **y** is measurable, it can be calculated from the following relation, obtained from the last component of the equation (5) and by putting in (16)):

$$\begin{aligned} e &= \dot{y}_n - (-a_1 y_1 - a_2 y_2 - K - a_n y_n) = \\ &= y_1^{(n)} + a_n y_1^{(n-1)} + K + a_2 y_1^{(1)} + a_1 y_1 \end{aligned} \tag{23}$$

If we now apply a Laplace transformation and the notation (17), we get:

$$\begin{aligned} e(s) &= \Gamma(s) y_1(s) = \\ &(s + d)\Gamma_1(s) y_1(s) = (s + d) e_1(s) \end{aligned} \tag{24}$$

where:
d - number opposite to the real root of the polynomial (17),
$\Gamma_1(s)$ - polynomial $s^{n-1} + b_{n-1}s^{n-2} + ... + b_2 s + b_1$, created by dividing (17) by (s + d),
$e_1(s)$ - filtered dynamics error ($e_1(t) = y_1^{(n-1)} + b_{n-1} y_1^{(n-2)} + ... + b_2 y_1^{(1)} + b_1 y_1$).

The error $e_1(t)$ will serve for the determination of the adaptation law of network weight parameters:

$$\dot{\mathbf{w}}_f = \eta_f e_1 \boldsymbol{\Phi}_f \; ; \; \dot{\mathbf{w}}_g = \eta_g e_1 \boldsymbol{\Phi}_g u \tag{25}$$

where:
η_f, η_g - constant coefficients of adaptation.

Stability of the adaptive system

We will now prove the stability of the adaptive system under consideration. Let $\mathbf{w}_f^*, \mathbf{w}_g^*$ be full-network vectors of weight parameters, for which these relations hold:

$$\begin{aligned} \alpha_f(\mathbf{x}) &= \mathbf{w}_f^{*T} \boldsymbol{\Phi}_f + \alpha_{f0}(\mathbf{x}) + \Delta_f \\ \alpha_g(\mathbf{x}) &= \mathbf{w}_g^{*T} \boldsymbol{\Phi}_g + \alpha_{g0}(\mathbf{x}) + \Delta_g \end{aligned} \tag{26}$$

where Δ_f, Δ_g can be regarded as restricted disturbances, and due to their low value they are neglected in practice. Using the relations (22) and (24) and substituting: (19), (26) we get the equation (neglecting: Δ_f, Δ_g):

$$\dot{e}_1 + d e_1 = \mathbf{w}_f^{*T} \boldsymbol{\Phi}_f - \mathbf{w}_f^T \boldsymbol{\Phi}_f + (\mathbf{w}_g^{*T} \boldsymbol{\Phi}_g - \mathbf{w}_g^T \boldsymbol{\Phi}_g) u \tag{27}$$

from which we can determine an error derivative e_1 with respect to time:

$$\dot{e}_1 = -d e_1 - \tilde{\mathbf{w}}_f^T \boldsymbol{\Phi}_f - \tilde{\mathbf{w}}_g^T \boldsymbol{\Phi}_g u \tag{28}$$

where:
$\tilde{\mathbf{w}}_f^T \boldsymbol{\Phi}_f = \mathbf{w}_f^T \boldsymbol{\Phi}_f - \mathbf{w}_f^{*T} \boldsymbol{\Phi}_f$
$\tilde{\mathbf{w}}_g^T \boldsymbol{\Phi}_g = \mathbf{w}_g^T \boldsymbol{\Phi}_g - \mathbf{w}_g^{*T} \boldsymbol{\Phi}_g$

Let the relation below be a Lyapunov function.

$$V(e_1) = \frac{1}{2} e_1^2 + \frac{1}{2\eta_f} \tilde{\mathbf{w}}_f^T \tilde{\mathbf{w}}_f + \frac{1}{2\eta_g} \tilde{\mathbf{w}}_g^T \tilde{\mathbf{w}}_g \tag{29}$$

The time derivative of this function, after substituting the relation (28) has this form:

$$\begin{aligned} \dot{V}(e_1) &= e_1 \dot{e}_1 + \frac{1}{\eta_f} \tilde{\mathbf{w}}_f^T \dot{\mathbf{w}}_f + \frac{1}{\eta_g} \tilde{\mathbf{w}}_g^T \dot{\mathbf{w}}_g = \\ &= -d e_1^2 + \tilde{\mathbf{w}}_f^T \left(\frac{1}{\eta_f} \dot{\mathbf{w}}_f - e_1 \boldsymbol{\Phi}_f \right) + \tilde{\mathbf{w}}_g^T \left(\frac{1}{\eta_g} \dot{\mathbf{w}}_g - e_1 \boldsymbol{\Phi}_g u \right) \end{aligned} \tag{30}$$

and having accounted for the adaptation law of network weight parameters (25) we get for $e_1 \neq 0$:

$$\dot{V}(e_1) < 0 \tag{31}$$

One may conclude from the other Lyapunov's method that the examined adaptive system is asymptotically stable. When we also consider the terms Δ_f, Δ_g to obtain asymptotic stability of the system the sliding mode control has to be used [12]. The method consists in adding a properly selected signal to the control, so that the signal guarantees that the inequality (31) holds. We manage to do so here making an additional assumption: $\alpha_g(\mathbf{x}) > 0$ and knowing the constraints of the relation $\Delta_f + \Delta_g u$, also knowing such number g_{sl}, for which this relation holds:

$$\alpha_g(\mathbf{x}) > g_{sl} > 0 \tag{32}$$

In such case, making similar considerations for the control signal in the form:

$$-\frac{\hat{\alpha}_f(\mathbf{x})}{\hat{\alpha}_g(\mathbf{x})} + \frac{1}{\hat{\alpha}_g(\mathbf{x})} v - \frac{\text{sign}(e_1) \cdot o}{g_{sl}} \tag{33}$$

where:
o - upper constraint of $|\Delta_f + \Delta_g u|$,

we will notice that the inequality (31) will hold, as had to be proven.

SYNTHESIS OF SHIP COURSE STABILIZATION SYSTEM

Let this equation be a model describing the dynamics of ship movement [8]:

$$\dot{r} = -ar - br^3 + c\delta \tag{34}$$

where:
ψ - course deviation,
$r = \dot{\psi}$ - rate of turn,
δ - rudder angle,
a, b, c - constant coefficients.

Then to harmonize the above with (2) the following notations will be made:

$$\mathbf{x} = \begin{bmatrix} \psi \\ r \end{bmatrix}; \quad u = \delta; \quad \mathbf{f}(\mathbf{x}) = \begin{bmatrix} r \\ -ar - br^3 \end{bmatrix}; \quad \mathbf{g}(\mathbf{x}) = \begin{bmatrix} 0 \\ c \end{bmatrix} \tag{35}$$

The control (3) is described by the formula:

$$\delta = \frac{ar + br^3}{c} + \frac{1}{c} v \tag{36}$$

while the dipheomorphism (4) has this form:

$$\mathbf{y} = \mathbf{T}\left(\begin{bmatrix} \psi \\ r \end{bmatrix} \right) = \begin{bmatrix} \psi \\ r \end{bmatrix} \tag{37}$$

therefore, in this case the feedback linearization is global.

Although the state vector will not be transformed, we already get a linear description of the object:

$$\begin{aligned} \dot{\psi} &= r \\ \dot{r} &= v \end{aligned} \tag{38}$$

which for:

$$\mathbf{A} = \begin{bmatrix} 0 & 1 \\ 0 & 0 \end{bmatrix}; \quad \mathbf{b} = \begin{bmatrix} 0 \\ 1 \end{bmatrix}; \quad \mathbf{y} = \begin{bmatrix} \psi \\ r \end{bmatrix} \tag{39}$$

will have the form (5).

Coefficients of linear control in the external loop:

$$v = -a_1\psi - a_2 r \tag{40}$$

should be selected so that the characteristic polynomial of the system (38) executing the control (40):

$$\Gamma(s) = s^2 + a_2 s + a_1 \tag{41}$$

has two real negative roots.

Now, assuming that the functions

$$\alpha_f = ar + br^3; \; \alpha_g = c \tag{42}$$

are not overtly given, and only their initial estimates are available: α_{f0}, α_{g0} we will apply neuro-fuzzy approximators (19) to identify the functions. For the approximators, an i-th ($1 \le i \le k$) element of radial basis functions (20) will have the form:

$$\begin{aligned} \Phi_{f_i} &= \exp\left\{ \frac{-\left| r - \boldsymbol{\mu}_{f_i} \right|^2}{2\sigma_f^2} \right\} \\ \Phi_{g_i} &= \exp\left\{ \frac{-\left| r - \boldsymbol{\mu}_{g_i} \right|^2}{2\sigma_g^2} \right\} \end{aligned} \tag{43}$$

while the adaptation law of weight parameters (25) will be based on the error:

$$e_1 = r + \frac{a_2 - \sqrt{a_2^{\,2} - 4a_1}}{2}\psi \tag{44}$$

An autopilot thus designed guarantees an asymptotic stability of the system on condition that we assume that:

$$\Delta_f \approx 0; \; \Delta_g \approx 0 \tag{45}$$

Otherwise, to achieve an asymptotic system stability, we have to add a signal to the control, as per the relation (33):

$$\frac{-\text{sign}(e_1) \cdot o}{g_{sl}} \tag{46}$$

where:
$g_{sl} = 0.0005$ [1/s^2] - known lower constraint of the function α_g.

COMPUTING EXPERIMENTS

The computing experiments were performed in the Matlab/Simulink environment. Instead of a ship (real object), a de Witt-Oppe model [3] was used, accounting for the dynamics of the steering gear:

$$\begin{aligned} \dot{x}_1 &= u\sin\psi + v\cos\psi \\ \dot{x}_2 &= u\cos\psi - v\sin\psi \\ \dot{\psi} &= r \\ \dot{r} &= -ar - br^3 + c\delta \\ \dot{u} &= -fu - Wr^2 + S \\ v &= -r_1 r - r_3 r^3 \end{aligned} \tag{47}$$

where:
$(x_1, x_2) = (x, y)$ - Cartesian coordinates (ship's position),
u - ship's longitudinal speed,
v - rate of turn,
S - propeller thrust,
a, b, c, f, W, r_1, r_3 - coefficients determined from model tests (varying for different ship types and navigational conditions).

The ship's model coefficients were those of m/s Compass Island [3]. To incorporate disturbances, the simulations

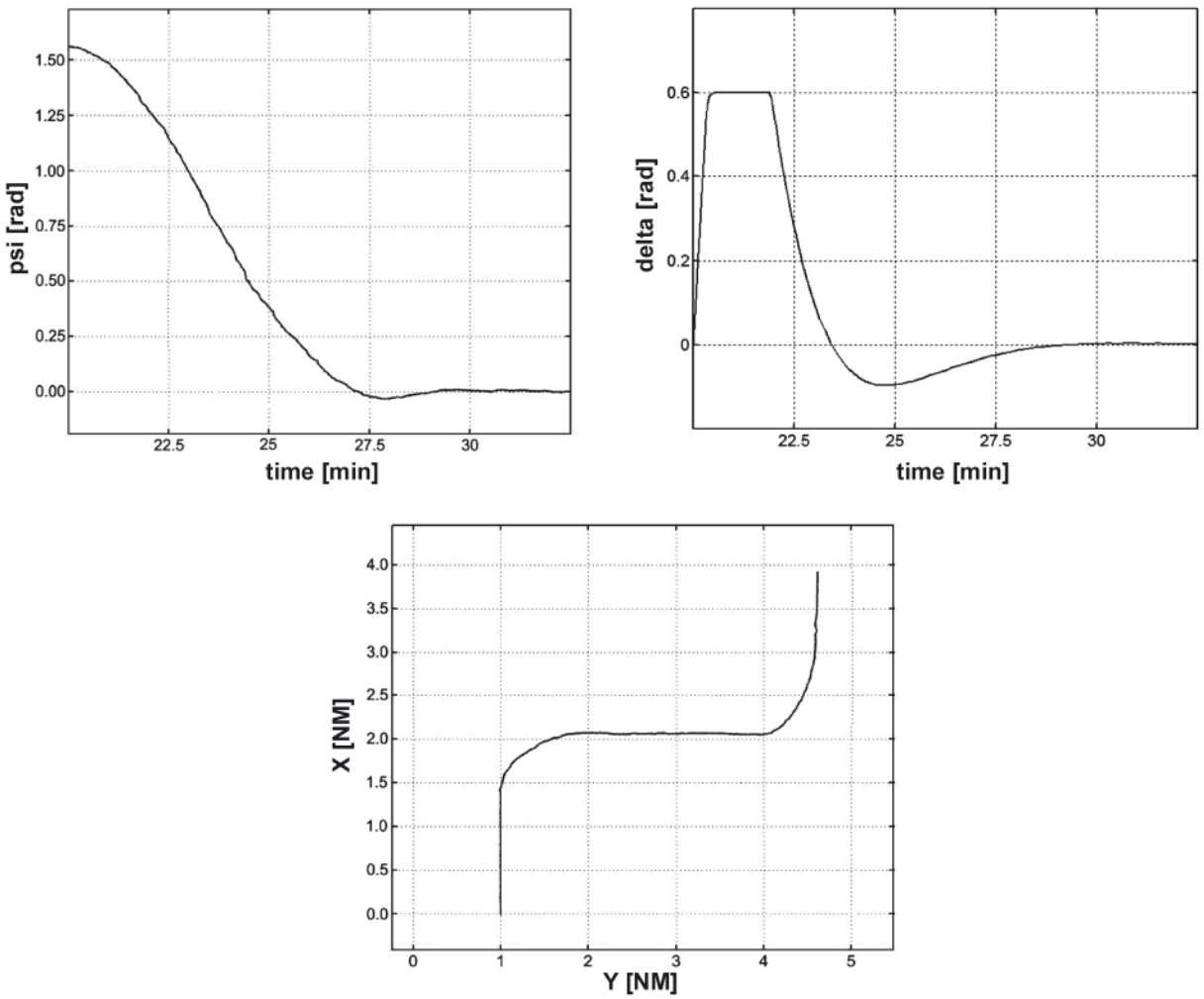

Fig. 2. *Course deviations, rudder angle and ship movement trajectory for an example computing experiment (source: own study)*

included a signal with characteristics of sea waves generated by wind [2]. The coefficients of linear control in the external loop (40) were determined by means of LQR controller synthesis. One-dimensional radial basis functions (43) were assumed, with zero centres and unit variances. The adaptation law of network weight parameters (25) provides for unit coefficients of adaptation.

Results of an example computing experiment are shown in Fig. 2. The plotted trajectory, rudder angle and changes of course deviations illustrate the ship's successive manoeuvres: course alterations 90° to starboard, then 90° to port. The computing experiments confirmed the correct performance of the herein proposed algorithm for ship course stabilization with object model adaptation.

SUMMARY

The article presents an algorithm of ship course stabilization using object model adaptation based on neuro-fuzzy approximators. The presented method belongs to a new generation of adaptive control methods for uncertain systems.

The algorithm is intended for implementation in the executive module of the navigational decision support system NAVDEC [9, 14]. The executive and other modules (e.g. data fusion module [1, 13], manoeuvre planning module [11]) make up a practical implementation of navigational decision support system used in the process of safe ship conduct (invention [10]). The implementation of the presented algorithm will lead to higher degree of automation of navigation and enhancement of navigational safety. Consequently, benefits of this development are as follows:

- social benefits due to lower number of human loss of life or health by crews and passengers of sea-going vessels,
- material benefits due to lower losses of cargo, less ship damage and fewer sunken ships,
- environmental protection and prevention of environmental disasters that might result from collisions of ships carrying hazardous materials.

BIBLIOGRAPHY

1. Borkowski P.: *Data fusion in a navigational decision support system on a sea-going vessel.* Polish Maritime Research vol. 19, no. 4(76), 78, 2012
2. Borkowski P., Zwierzewicz Z.: *Ship course-keeping algorithm based on knowledge base.* Intelligent Automation and Soft Computing vol. 17, no. 2, 149, 2011
3. De Wit C., Oppe J.: *Optimal collision avoidance in unconfined waters.* Journal of the Institute of Navigation, vol. 26, no. 4, 296, 1979
4. Fabri S., Kadirkamanathan V.: *Functional adaptive control.* Springer, Londyn 2001
5. Farrell J., Polycarpou M.: *Adaptive approximation based control.* John Wiley, Hoboken 2006
6. Khalil H.: *Nonlinear systems.* Prentice Hall, Upper Saddle River 2002
7. Marquez H.: *Nonlinear control systems.* John Wiley, New Jork 2003
8. Perez T.: *Ship motion control.* Springer, Londyn 2005
9. Pietrzykowski Z., Borkowski P., Wołejsza P.: *Marine integrated*

navigational decision support system. Telematics in the transport environment, Communications in Computer and Information Science series no. 329, Springer, Berlin, 284, 2012
10. Pietrzykowski Z., Borkowski P. et al.: *A method and system of navigational decision support in the process of safe vessel navigation.*, International patent application under PCT procedure, no. PCT/PL2010/000112, 08-11-2010
11. Pietrzykowski Z., Magaj J., Wołejsza P., Chomski J.: *Fuzzy logic in the navigational decision support process onboard a sea-going vessel*. Lecture Notes in Artificial Intelligence series no. 6113, Springer, Berlin, 185, 2010
12. Slotine J.E., Li W.: *Applied nonlinear control.* Prentice Hall, New Jersey 1991
13. Stateczny A., Kazimierski W.: *Determining manoeuvre detection threshold of GRNN filter in the process of tracking in marine navigational radars.* Proceedings of the International Radar Symposium, Wrocław, 242, 2008
14. www.navdec.com
15. Zwierzewicz Z.: *Nonlinear adaptive tracking-control synthesis for functionally uncertain systems*. International Journal of Adaptive Control and Signal Processing vol. 24, no. 2, 96, 2010
16. Zwierzewicz Z.: *Ship course-keeping via nonlinear adaptive control synthesis.* International Journal of Factory Automation no. 2, 102, 2007

CONTACT WITH AUTHOR

Piotr Borkowski, Ph.D.
Institute of Marine Technologies
Faculty of Navigation
Maritime University of Szczecin
Wały Chrobrego 1-2,
70-500 Szczecin, POLAND
e-mail: p.borkowski@am.szczecin.pl

POLISH MARITIME RESEARCH 1(81) 2014 Vol 21; pp. 20-27
10.2478/pomr-2014-0004

Evolutionary sets of safe ship trajectories with speed reduction manoeuvres within traffic separation schemes

Rafał Szłapczyński, Ph. D.
Gdańsk University of Technology

ABSTRACT

In the previous paper the author presented the evolutionary ship trajectory planning method designed to support Traffic Separation Schemes (TSS). This time the extensions of this method are described which allow to combine evolutionary trajectory planning with speed reduction manoeuvres. On TSS regions with higher than usual density of traffic and smaller distances between ships, the course alterations alone are not always sufficient or effective means of collision avoidance. Therefore they must be supplemented by speed reduction manoeuvres to a larger extent than on open waters. The paper includes a brief description of the optimisation problem, descriptions of the new elements of the method (fitness function, algorithms and the evolutionary cycle) and the examples of how the extended method successfully solves the problems unsolvable without applying speed reduction.

Key words: collision avoidance manoeuvres; track planning; Traffic Separation Schemes; speed reduction

INTRODUCTION

In an earlier paper [10] the author has presented the Evolutionary Sets of Safe Ship Trajectories (ESoSST) method working for Traffic Separation Schemes (TSS) and possible to be applied in Vessel Traffic Service (VTS) centres. This method combined evolutionary approach [9] with goals typical for methods based on games theory [7]. However, unlike other methods utilizing evolutionary algorithms [9, 16], genetic algorithms [2, 6, 13] and related heuristics [8, 12, 14, 15], instead of finding an optimal single ship trajectory only, the author's method searches for an optimal set of safe trajectories of all ships involved in an encounter. In the present paper the extensions of this method are described which allow to combine evolutionary trajectory planning with speed reduction manoeuvres. On TSS regions with higher than usual density of traffic and smaller distances between ships, the course alterations alone are not always sufficient or effective means of collision avoidance. Therefore they are supplemented by speed reduction manoeuvres, when necessary. The paper covers all aspects of incorporating speed reduction manoeuvres into the evolutionary method, including generating the initial population, the evaluation phase and the general scheme of the evolutionary cycle.

OPTIMISATION PROBLEM

The goal of the optimisation process is to find a set of trajectories, which minimizes the average time loss or way loss spent on manoeuvring, while fulfilling the following conditions:

- none of the stationary constraints (including TSS Inshore Traffic Zone [ITZ] and separation zones) are violated,
- none of the ship domains are violated [4],
- minimum and maximum alteration values are configurable and by default are set to 15 and 60 degrees respectively,
- a ship only manoeuvres when she is obliged to and, in case of head-on and crossing encounters, manoeuvres to starboard are favoured over manoeuvres to port,
- COLREGS rules [3, 5] are not violated (especially Rule 10 and Rules 13 to 17),
- speed alterations are not to be applied unless necessary (collision cannot be avoided by a configured maximum course alteration value),
- if speed alteration has to be applied, the number of speed alterations should be minimized (e.g. a ship can reduce her speed to avoid collision and get back to a normal speed once the situation is safe again).

It is assumed that we are given the following data:

- stationary constraints (landmasses and other obstacles and the locations and parameters of each TSS's parts),
- positions, courses and speeds of all ships involved,
- additional ship parameters used for estimating the manoeuvre's dynamics and ship domains

The method directly handles the following COLREGS [5] rules: Rule 13 (Overtaking), Rule 14 (Head-on Situations), Rule 15 (Crossing Situations), Rule 16 (The Give-Way Vessel) and Rule 17(The Stand-On Vessel). Apart from them, the updated version of the method presented here also applies Rule 10 of COLREGS, which governs the behaviour of ships within a TSS [1].

WHEN IS SPEED REDUCTION NECESSARY?

In this section some example scenarios are shown, where it is not possible or not economic to avoid collision by course alteration alone. In general, such situations may be divided into four cases:

- course alterations alone are not economic – large manoeuvres are necessary,
- course alterations alone are misleading – multiple or strange looking manoeuvres are necessary, which might not be understandable for other ships,
- course alterations alone are not sufficient because it is too late – the ships are already too close to each other or their speeds are too large,
- course alterations alone are not possible because there is not enough room to perform them (due to stationary constraints such as safety isobaths or width of traffic lanes).

Examples of situations when course alterations alone are not sufficient are presented below. All scenarios are set in the Gulf of Gdansk TSS (fully shown in Figure 13). For all scenarios the ship domains have been set to values which enable two ships only to transit through a lane parallel to each other.

Scenario 1. positions, courses and speeds are given in Fig. 1. A ship, which is about to cross traffic lanes encounters two ships, which are about to use the incoming lane.

The result (the final set of trajectories) returned by the method, which does not apply speed alterations, is shown in Fig. 2. To avoid collision the crossing ship partially uses the outgoing lane and avoids violating the incoming lane, but its trajectory is considerably longer than would be in case of speed reduction and the manoeuvres of the crossing ship might be misleading for other ships

Scenario 2. Ships positions, courses and speeds are given in Fig. 3. A faster ship encounters two slower ships, one on its starboard, the other on its port board. The result (the final set of trajectories) returned by the method, which does not apply speed alterations, is shown in Fig. 4. The faster ship cannot overtake the slower ships on the incoming lane due to its limited width, so performs the overtaking manoeuvre outside the lane and joins the lane at later stage.

Scenario 3. Ships positions, courses and speeds are given in Fig. 5. This time a faster ship encounters three slower ships which makes it impossible to use the closest outgoing lane. The result (the final set of trajectories) returned by the method, which does not apply speed alterations, is shown in Fig. 6. The faster ship performs a wide course alteration manoeuvre to starboard so as to avoid collision with the slower ships and avoid violating the incoming lane and the separation zone. In case of enlarging the lane encouragement factor - formula (4) to enforce using the outgoing lane, the method returns alternative solution (Fig. 7), a distant outgoing lane is used and the way loss is significant.

TRAJECTORY PLANNING WITH SPEED REDUCTION

The possible approaches to applying the speed reduction in the evolutionary method, which have been considered, are as follows:

1. Allowing ships for speed alterations throughout the encounter situation. This means adding another dimension (speed) to the search space, which originally had two dimensions for each node (its geographical coordinates). Conceptually it is the simplest and most natural approach because speed alteration manoeuvres are planned automatically by evolutionary algorithm. Unfortunately it has the following disadvantages:
   - may lead to numerous speed alterations thus violating COLREGS which allows for speed alteration only when necessary,
   - assumes than any speed within a given range is possible, which might not always be true (sometimes discreet speed values may only be possible depending on the propeller's type),
   - largely increases the computational time because of this additional dimension of the computational space.
2. Allowing for one speed reduction manoeuvre only, chosen from a predefined set, and then getting back to the

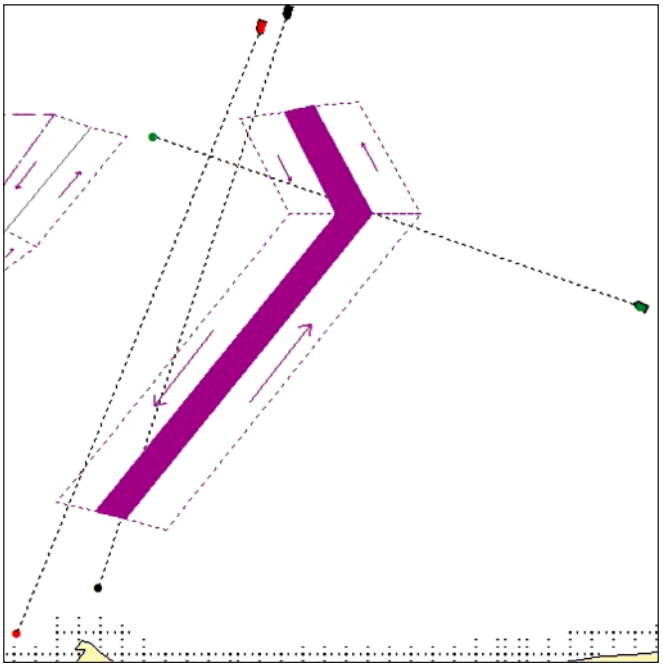

Fig. 1. *Scenario 1: Three ships in an encounter situation, speeds (left to right): 14, 14 and 14 knots*

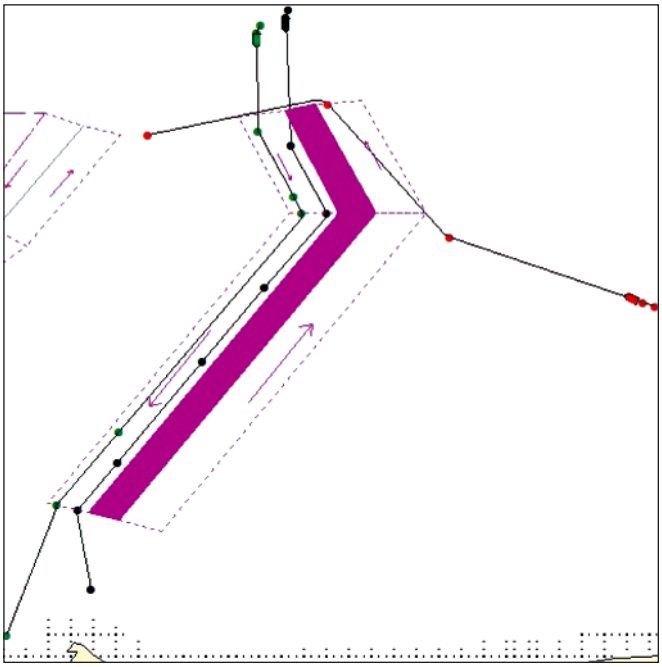

Fig. 2. *A solution returned by the method without speed reduction for Scenario 2*

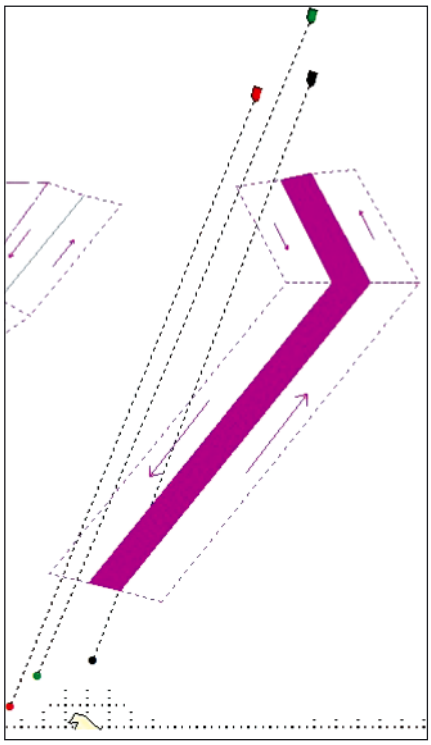

Fig. 3. *Scenario 2: Three ships in an encounter situation, speeds (left to right): 10, 15 and 10 knots*

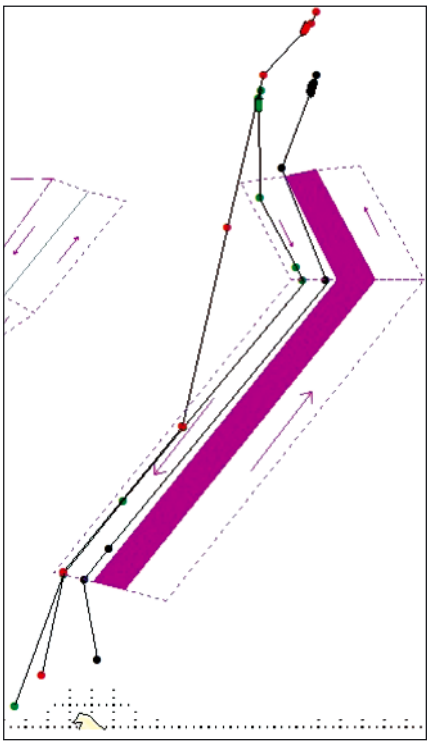

Fig. 4. *A solution returned by the method without speed reduction for Scenario 2*

Fig. 5. *Scenario 3: Four ships in an encounter situation, speeds (left to right): 10, 12, 10 and 10 knots*

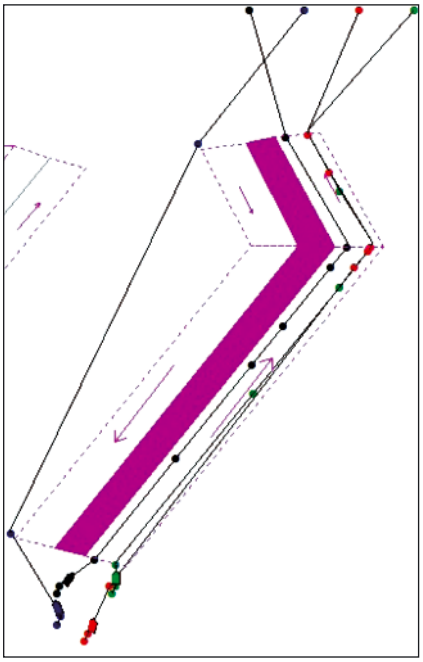

Fig. 6. *A solution returned by the method without speed reduction for Scenario 3*

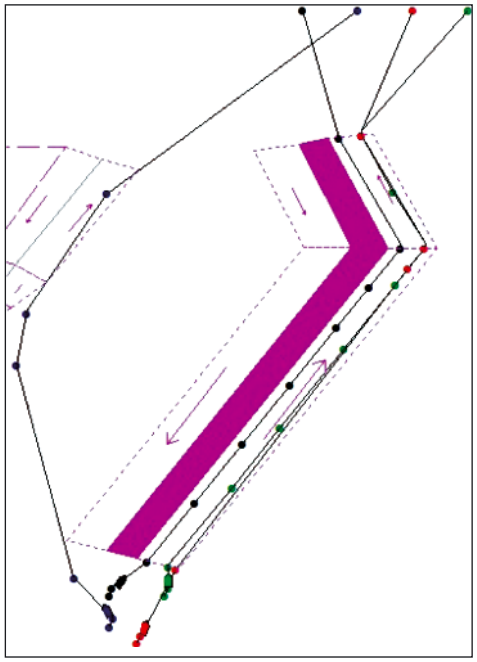

Fig. 7. *An alternative solution returned by the method without speed reduction for Scenario 3*

original speed when possible. This approach is void of the disadvantages typical for the previous one:

- it naturally supports discreet speed values,
- it keeps the constant number of speed alterations equal 2,
- it keeps reasonable computational space and time.

Unfortunately this approach involves applying speed reduction manoeuvres partially outside of the main evolutionary algorithm, which limits the benefits from the evolutionary process.

Taking into account all abovementioned factors, the author has decided to follow the second approach. It is described more thoroughly below.

A new scheme of the ESoSST method

The basic scheme of the ESoSST method without speed reduction is shown in Fig. 8. As can be seen, Specialised operators and mutation is preceding reproduction here, as opposed to the traditional approach. The reason for this is that specialised operators utilize information from evaluation and

therefore they cannot be applied after reproduction (which introduces new individuals into population) but can be applied after succession (which only reduces the number of individuals without affecting any of them).

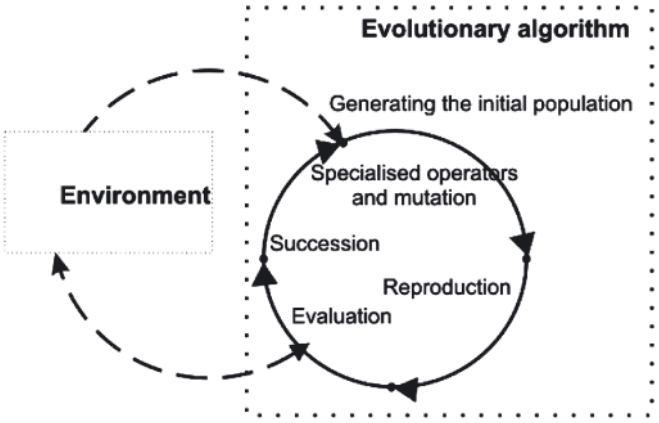

Fig. 8. *The scheme of EA used by ESoSST method without speed reduction*

To apply speed reduction this scheme is extended by additional operations shown in Fig. 9.

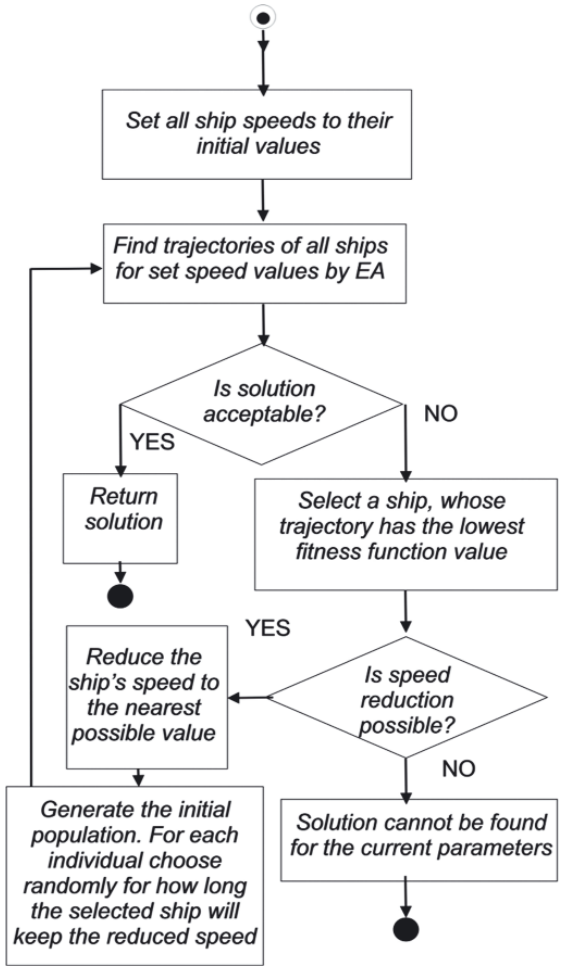

Fig. 9. *The ESoSST method with speed reduction*

This new algorithm works as follows:

1. The EA is run normally as depicted in Fig. 8.
2. If the results are unsatisfactory and indicate that using course alterations alone does not suffice, then EA is run again but with the following changes.
   a. The previously found highest-rated set of ship trajectories is analysed and the speed of the ship which had lowest-rated trajectory (when compared to other ships in the set) will have its speed reduced (changed to the nearest possible speed, e.g. 70% of the original speed).
   b. The reduced speed is to be applied after the pre-configured decision time and it is kept for a randomly chosen number of segments. This is a part of the process of generating the initial population. As a result, each of the initial sets of ship trajectories has the selected ship travelling at the reduced speed for a number of segments and then getting back to the original speed again.
   c. When evaluating the sets of ship trajectories, the new value of the selected ship's speeds is considered, when necessary to determine approach factors for potential collisions with other ships. The new values of the selected ship's speed affects the total passage time, which is also taken into account when computing the fitness function value (1).
3. If the results are still unsatisfactory and still indicate that using course alterations alone might be the reason of the problem, then EA is run once more.
   a. The previously found highest-rated set of ship trajectories is analysed again. If the ship having the lowest-fitted trajectory is the same as before, than the procedure described in points 2a to 2c. is repeated for the further reduced speed (e.g. 50% of the original value).
4. If the results are still unsatisfactory and the ship having the lowest-fitted trajectory cannot have its speed reduced any further then the method returns the best of the previously found sets of trajectories accompanied with a message that acceptable solution could not been found.

Fitness function of the ESoSST method

The formula for the fitness function including speed reduction manoeuvres is as follows.

$$f = \sum_{i=1}^{n} [f_i] \tag{1}$$

where:

$$f_i = e_i s_i a_i c_i t_i \tag{2}$$

s_i (static constraint factor), a_i (collision avoidance factor), c_i (COLREGS-compliance factor) have already been described in [10]. Symbol e_i (trajectory economy factor) is computed in a different way for ships which have to reduce their speed than for those, which do not.

For changing propeller's settings, that is for ships, which reduce their speed:

$$e_i = \left(\frac{l_i - w_i}{l_i} \right) \tag{3}$$

where:

i – the index of the current ship,
l_i – the total length of the i-th ship's trajectory [nautical miles].
w_i – the difference between the length of the i-th ship's trajectory and the length of a predetermined trajectory of the i-th ship (obtained without other ships affecting j-th ship trajectory) [nautical miles].

For fixed propeller's settings, that is for ships which do not reduce their speed time and time loss are used instead of length and way loss respectively. In case of speed reduction, the trajectory economy factor would be much lower when

using total time and time loss. This would lead to unacceptably low trajectory fitness value and total fitness function value. Consequently, the algorithm (Fig. 10) would make the same ship further reduce its speed, even when not necessary. To avoid it, the length-oriented trajectory economy factor (3) is used for ships, which reduce their speed.

Symbol t_i factor from formula (2) is responsible for TSS-compliance and is computed as given by (4).

$$t_i = \left(1 - \sum_{k=1}^{m} [p_k]\right) * [1 + r_i(g-1)] \tag{4}$$

where:

- m – the number of TSS rules violations registered for the current ship,
- k – the index of a registered violation,
- p_k – the penalty for the k-th of the registered TSS rules violations,
- g – lane encouragement factor applied to encourage using traffic lanes, set to 1.5 by default,
- r_i – trajectory's lane percentage factor (a percentage of the trajectory's length that transits through a traffic lane).

Ship priority groups

An additional extension to the ESoSST scheme is introducing ship priority groups. They are used for convenience of the system's user as well as for optimizing the method's performance. The number of ships within a TSS or within a region supervised by a VTS centre can be quite large and finding an optimal set of all trajectories within a single algorithm run would be time consuming. Instead, depending on the ships' parameters and the areas of a TSS, which they transit, ships can be divided into priority groups to save on computational time (two or three smaller groups of ships will be processed faster than one large group). In the ESoSST method a two-digit priority numbering is used, where the first digit denotes the class of service for a given ship and the second digit – the priority number within this class. Ships with dangerous loads or limited manoeuvring capability would be privileged by being assigned a lower first digit and their trajectories would be planned first. Other ships trajectories would then be planned in such a way so as not to collide with each other and with the trajectories planned previously. The second digit might be assigned manually or automatically (based on the area of a TSS or traffic lane, which the ship is supposed to transit through). An example is presented in Fig. 10.

In Fig. 13 three ships are shown. Two of them will traverse the west (left) part of the TSS and one will traverse the east (right) part of the TSS. It is assumed that the first of the ships traversing the west part of the TSS is carrying a dangerous load and therefore is assigned a higher priority (lower first digit). As a result the ships are given priority numbers: 11, 21 and 22 and their routes would be planned in the ascending order of these numbers.

When ship priority groups are applied, the operations presented previously on the algorithm from Fig. 10 are performed in turns for each of the priority groups. The trajectories of ships from each priority groups are checked for potential collisions with each other as well as with the trajectories already found for previous priority groups.

EVOLUTIONARY OPERATORS AND TECHNIQUES

In this section details on elements of the evolutionary method from Fig. 11 are described. The evaluation (fitness function) has already been presented, so the remaining elements are: generating the initial population, specialised operators and mutation, reproduction and selection.

An individual's structure and generating the initial population

Each individual consists of a set of trajectories, each of them representing one of the ships involved in an encounter situation. Each trajectory is a sequence of nodes containing geographical coordinates X and Y.

Apart from straight segments and randomly generated individuals used in previous versions of the ESoSSt method, in the TSS-oriented version the initial population also includes

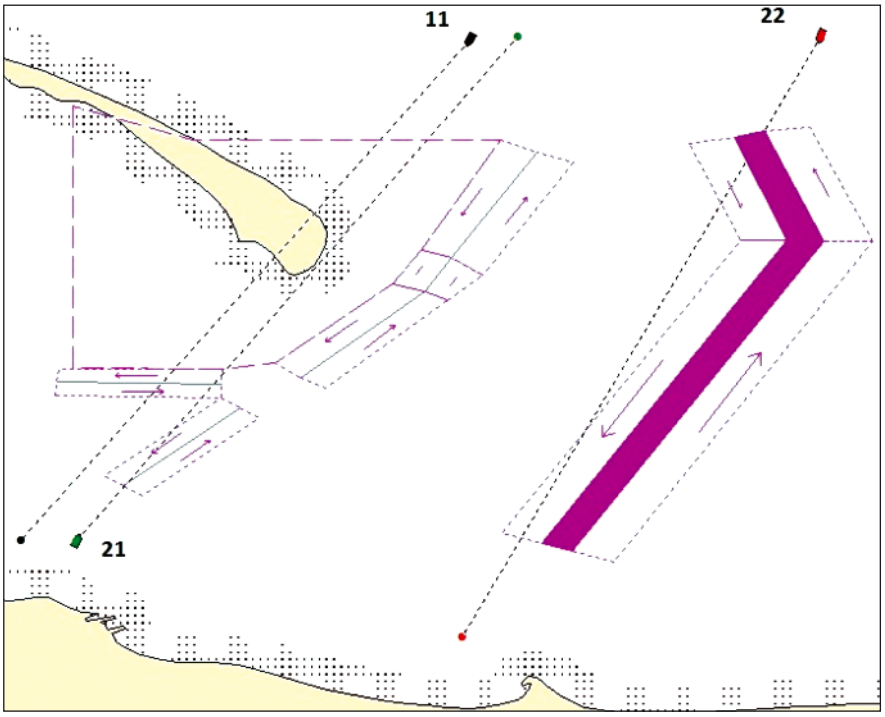

Fig. 10. *Three ships and the priority numbers assigned to them by the method*

individuals consisting of predefined, TSS-compliant tracks, generated automatically for each ship. The random sets of trajectories, which constitute the majority of the initial population, are necessary for wide exploration, while the predefined tracks result in a faster convergence to a solution.

The size of the population is configurable (100 by default). It doubles during specialised operators and mutation phase and then doubles again during reproduction. It is reduced to its original size during succession.

Specialised operators and mutation

Four types of mutation operators (node insertion, nodes joining, node shift and node deletion) have been used. More important than them however are the specialised operators designed to handle particular problems and selected depending on the particular situation (time remaining to collision etc.). They include five types of ship collision-avoidance operators (segment insertion, segment shift, first node shift, second node shift and node insertion) all of which are parameterised and semi-deterministic as opposed to random mutation operators. Analogically to ship collision avoidance operators, five kinds of operators avoiding collisions with static obstacles have been used. Apart from that, three types of additional operators (reduction of unnecessary nodes, smoothing and adjusting) have been applied. The TSS-oriented version of the method includes ten new operators handling TSS-violations. Altogether, twenty seven different operators have been used, the majority of them being problem-dedicated. Problem-dedicated operators were applied always if collision or rule violation was registered. Only in case of a lack of need for applying a specialised operator, mutation operators were used. The probability of mutation decreased with the increase of fitness function value of a particular trajectory of an individual, so as to improve low-fitted trajectories without spoiling the high fitted ones.

Reproduction

In the reproduction phase pairs of individuals (parents) are crossed to generate new individuals (offspring). Four types of crossover operators have been designed and implemented:

a) An offspring inherits whole trajectories from both parents and the higher-valued of the two possible trajectories is chosen.
b) An offspring inherits whole trajectories from both parents and the choice of a particular trajectory (from the first or the second parent) is done randomly.
c) Each of the trajectories of the offspring is a crossover of the appropriate trajectories of the parents.
d) Each node of a trajectory is an arithmetical crossover of the nodes in the parents' trajectories.

Of these four types the first one has been eliminated eventually because it involved doubling the evaluation phase and its benefits were not enough to justify the this additional computational cost.

Selection

Prior to implementing the TSS-oriented version of the method various methods of pre-selection (selection for crossover purpose) and post-selection (selection for succession) purpose have been tested including proportional (roulette wheel) and modified proportional (modified roulette wheel). Eventually uniform pre-selection and threshold post-selection were chosen as their results were competitive and they worked were faster than proportional and modified proportional.

Number of generations and the computational time

The process was stopped if a satisfying (configurable) value of a normalized fitness function was reached (0.99 by default) and there were no collisions or rule violations registered. Otherwise, the stop criterion of a maximum number of generations or maximum time was used. In case of a collision threat, an Officer Of the Watch (OOW) should make a decision and initiate a manoeuvre within 6 minutes. Therefore a 1-minute time for returning the results was chosen: it should satisfy the needs of navigators and VTS operators alike. In practice, it allowed for 100-200 generations (depending on the number of ships) and the process would nearly always converge by then and the total fitness function would be above 0.97 (way loss below 3%). This was due to the specialised operators and predefined tracks which greatly increased the convergence rate, though occasionally at the cost of a slightly larger way loss (up to 5%). All experiments were carried out on a standard PC machine (processor Intel Core i7-2600k, 3.40 GHz, 8 GB RAM).

SOLVING THE ENCOUNTER SITUATIONS BY THE ESOSST METHOD WITH SPEED REDUCTION MANOEUVRES

In this section the examples of situations previously shown as unsolvable by the method without speed reduction, are now dealt with by the extended version of the ESoSST method.

Scenario 1. The result (the final set of trajectories) returned by the method with speed reduction is shown in Fig. 11. The crossing ship reduces its speed and passes safely astern of the two ships, which transit the incoming lane.

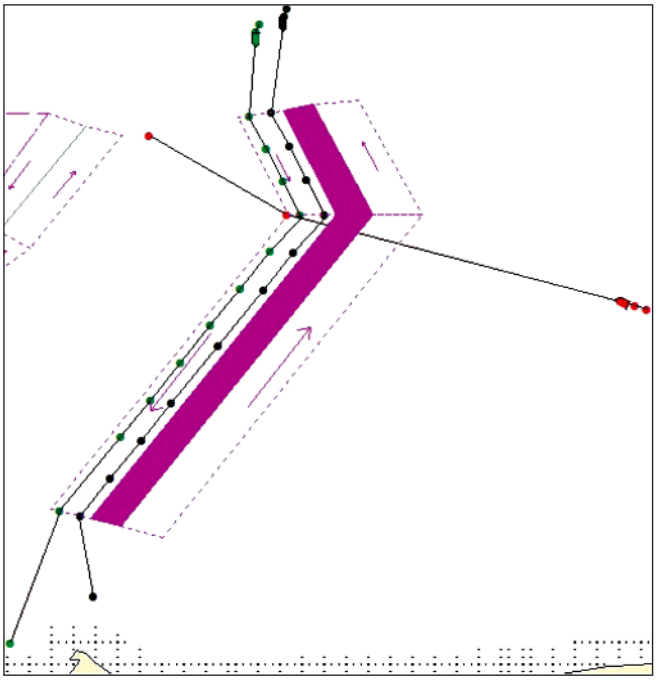

Fig. 11. *A solution returned by the method with speed reduction for Scenario 1*

Scenario 2. The result (the final set of trajectories) returned by the method with speed reduction is shown in Fig. 12. The faster ship reduces its speed which enables it to use the outgoing lane as recommended by COLREGS.

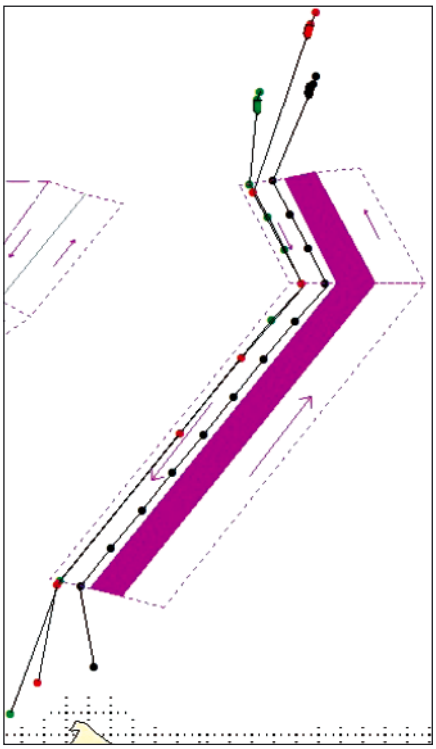

Fig. 12. A solution returned by the method with speed reduction for Scenario 2

Scenario 3. The result (the final set of trajectories) returned by the method with speed reduction is shown in Fig. 13. Similarly to Scenario 2, the faster ship reduces its speed which enables it to use the outgoing lane as recommended by COLREGS.

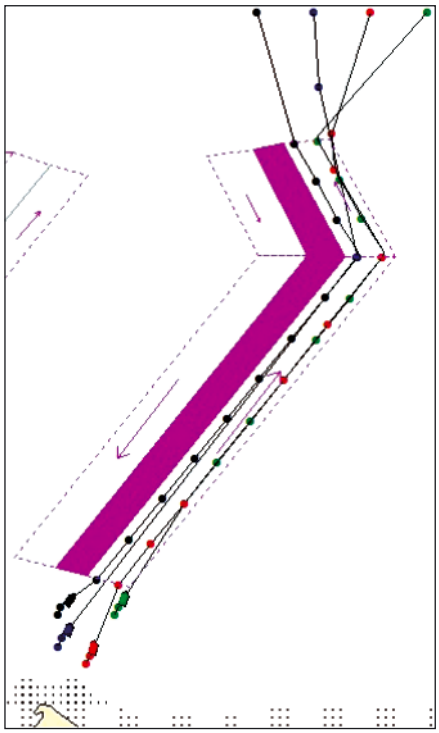

Fig. 13. A solution returned by the method with speed reduction for Scenario 3

In general in all of the test scenarios speed reduction enabled larger number of ships to use traffic lanes in a way recommended by COLREGS, either transiting the lanes or crossing them while avoiding collisions. The way loss spent on collision avoidance maneuvers was insignificant (always below 3%) and therefore all results can be considered satisfactory. It was additionally tested that further evolution (larger number of generations) would only bring insignificant rise in fitness value (below 0.5%) or no rise at all.

SUMMARY AND CONCLUSIONS

In the paper an extended version of the author's ESoSST method has been presented. The method works for Traffic Separation Scheme and applies speed reduction manoeuvres when necessary. The experiments that have been carried out confirmed the correctness of the presented approach to speed reduction problem:

- speed reduction manoeuvres are only applied when necessary,
- applying speed reduction effectively solves encounter situation in situations when course alterations alone are not sufficient or would result in significant way loss,
- the presented extension to the method does not affect any of the advantages of the previous version.

The further research on the method will be focused on:

- scalability of this approach (for larger number of ships and larger maps),
- optimising this approach by testing various evolutionary techniques,
- ensuring the reliability of the method, especially partial solutions in situations when the optimisation problem cannot be fully solved due to very strict safety constraints.

BIBLIOGRAPHY

1. Anwar N., Khalique A.: *Passage Planning Principles*. Witherby Seamanship International, Livingston, United Kingdom, 2006.
2. Cheng X. and Liu Z.: T*rajectory Optimization for Ship Navigation Safety Using Genetic Annealing Algorithm*. Proceedings of ICNC 2007 Third International Conference on Natural Computation, 4., 385 – 392, 2007.
3. Cockcroft A.N. and Lameijer J.N.F.: *A Guide to Collision Avoidance Rules*. Butterworth-Heinemann, 2011.
4. Coldwell T.G.: *Marine Traffic Behaviour in Restricted Waters*. The Journal of Navigation. 36, 431-444, 1983.
5. COLREGS. *Convention on the International Regulations for Preventing Collisions at Sea*. International Maritime Organization, London, 1972 (with amendments adopted from December 2009).
6. Ito M., Feifei Z., Yoshida N.: *Collision avoidance control of ship with genetic algorithm*. Proceedings of the 1999 IEEE International Conference on Control Applications, vol. 2, 1791-1796, 1999.
7. Lisowski J.: *The Dynamic Game Models of Safe Navigation*, International Journal on Marine Navigation and Safety of Sea Transportation, 1, no. 1., 11-18, 2007.
8. Statheros T., Howells G. and McDonald-Maier K.: *Autonomous Ship Collision Avoidance Navigation Concepts*, Technologies and Techniques, The Journal of Navigation, 61, 129-142, 2008.
9. Smierzchalski R., Michalewicz Z.: *Modelling of a Ship Trajectory in Collision Situations at Sea by Evolutionary Algorithm*, IEEE Transactions on Evolutionary Computation. No. 3 Vol. 4, 227-241, 2000.
10. Szlapczynski R.: *Evolutionary Sets of Safe Ship Trajectories within Traffic Separation Schemes*. The Journal of Navigation. vol. 66, iss. 1 65-81, 2012.
11. Tam C.K. and Bucknall R.: *Path-Planning Algorithm for Ships in Close-Range Encounters*. Journal of Marine Science Technology. 15, 395-407, 2010.

12. Tsou M. C. and Hsueh C. K.: *The Study of Ship Collision Avoidance Route Planning by Ant Colony Algorithm*. Journal of Marine Science and Technology. 18(5), 746-756, 2010a.
13. Tsou M. C., Kao S.L. and Su C.M.: *Decision Support from Genetic Algorithms for Ship Collision Avoidance Route Planning and Alerts*. The Journal of Navigation, 63, 167-182, 2010b.
14. Xue Y., Lee B.S. and Han D.: *Automatic Collision Avoidance of Ships. Proceedings of the Institution of Mechanical Engineers*, Part M: Journal of Engineering for the Maritime Environment, 33-46, 2009.
15. Yang L. L., Cao S. H. and Li B.Z.: *A Summary of Studies on the Automation of Ship Collision Avoidance Intelligence*. Journal of Jimei University (Natural Science), 2006.
16. Zeng X.: *Evolution of the Safe Path for Ship Navigation*. Applied Artificial Intelligence. 17., 87-104, 2003.

CONTACT WITH AUTHOR

Rafał Szłapczyński, Ph. D.
Faculty of Ocean Engineering
and Ship Technology,
Gdańsk University of Technology
Narutowicza 11/12
80-233 Gdańsk, POLAND
e-mail: rafal@pg.gda.pl

POLISH MARITIME RESEARCH 1(81) 2014 Vol 21; pp. 28-34
10.2478/pomr-2014-0005

Expert judgement-based tuning of the system reliability neural network

Brandowski A., Prof.,
Hoang Nguyen, Ph. D.,
Wojciech Frąckowiak, M. Sc.,
Gdynia Maritime University, Poland

ABSTRACT

The neural network tuning procedure applied to reliability analyses of anthrop technical systems, based on judgements of experts - experienced operating practicians. Numerical and linguistic elicitation of the judgements, analyses of the network input and output data correlation and of the AHP method processing deviation are presented. Example of data elicitation and correlation analysis of a reliability arrangement of the seagoing ship propulsion system are included to the article.

Key words: neural network; reliability; elicitation; parameter; correlation

INTRODUCTION

Neural networks (NNs) can be useful wherever there are difficulties with the formulation and/or solution of an analytical model but where the network tuning data are available. The data may be objective or subjective, i.e. derived from human memory. Such fields include, among other domains, reliability and safety of anthrop technical systems, in particular complex systems where formal models may be burdened with considerable uncertainty.

Tuning a neural network consists in determining the values of network input/output (I/O) parameters. When objective data are not available, the tuning may be based on expert judgement. There are fields of technology where experts can be found only among experienced operators. This is the case discussed in this paper.

The neural network I/O values must be correlated - the non-correlated values are obviously useless for tuning. Obtaining correlated subjective data is an essential difficulty in the considered case. There are several ways of effecting the level of correlation. First of all it is proper selection of experts and methods of judgement elicitation, and applying effective methods of processing the obtained data.

EXPERTS AND ELICITATION PROCEDURE

The expert is assumed to be a person well acquainted with the subject he is expected to formulate his judgement on. The knowledge is connected with the experience acquired by years-long practice. The expert should also be capable of formulating his judgement. This is connected with the level of his education and the language used in the elicitation process, particularly as regards the parameters the expert is expected to estimate. This may be the language of numerical or linguistic values. Numerical values are better but are more difficult to articulate - also errors in judgements are more likely. The analyst designing the reliability investigation method must in each case select properly the category of available experts, the number of experts and the elicitation language to be used. The number and qualifications of the available experts may be a limitation.

In the case of reliability, tuning pertains to characteristics expressed by probabilistic values, e.g. reliability function, unreliability function, failure rate, intensity function, or to physical values - operands in those expressions - e.g. failure frequency, time to failure or time between failures.

Preferred candidates for experts are persons having experience in observing the operation process of the elicitation objects for sufficiently long time and having proper theoretical knowledge. The reliability analyst must determine the elicitation language and choose the available expert category. For instance, in the reliability investigation of nuclear power stations, operators of those objects may be considered high-class specialists with knowledge of the calculus of probability, and on seagoing ships - members of the crew with various education levels, generally not familiar with the probability.

Man is not good as a probability estimator. His judgements show biases, weak calibration, incoherence, and overconfidence tendency. Dependences may occur between expert judgements. These flaws cannot be fully removed in the elicitation phase [4, 9].

Table 1 contains data on presentation forms of probabilistic judgements. The type of probability distribution is connected with the character of the respective event. For instance, the up time or maintenance time distributions are continuous and the human error probability is generally estimated by discrete distributions. Distributions of dangerous event circumstances, appearing in the event trees, are generally estimated by discrete two-point distributions. The distribution dimension may be essential in the case of estimation of probability distributions of different categories of losses and also in distributions of state parameters of the risk analysis object environment, e.g. meteorological conditions.

Tab. 1. *Taxonomy of the forms of probabilistic judgements used in reliability*

Distribution type	Discrete or continuous. If discrete then two-point or multipoint. If continuous then in known functional form or empirical.
Models of probability distributions	Empirical. Formal - e.g. exponential, normal or Markov processes.
Distribution dimension	Single-dimensional or multi-dimensional.
Frequency of events	Frequent ($p > 0.01$) or rare ($p < 0.01$).
Calibration	With or without calibration by objective data.

Differentiation of frequent and rare events is essential. The latter may be out of the experience of experts, who have not observed them. The estimation of the probability of occurrence of rare events is based on intuition.

As regards the information in the last row of Table 1, significant is the fact of having or not having objective information which could be used for the calibration of expert judgements. Without such information the estimation results may bear considerable uncertainty.

Reference [4] describes conditions to be fulfilled in the expert judgement elicitation phase. The main conditions pertain to the selection of experts, instructions, questionnaires and the way they should be filled-in, and also to the independence of judgements and the interview duration. Experts are chosen according to the subject of investigation. They are informed about the purpose and procedure of the investigation, data processing method and other possible questions. They are asked to formulate their judgements in a straightforward and honest way. Experts present their judgements by filling in the prepared questionnaires; give numbers or linguistic values by marking the appropriate fields. They cannot answer questions on subjects they have no knowledge about. The questionnaires should be as simple as possible.

The expert judgements must be formulated independently, which means that the experts must not contact with each other during the elicitation process. They are supposed to formulate their judgements entirely on their own, relying on their personal experience [1, 4, 9].

TUNING THE NEURAL NETWORKS OF RELIABILITY

The anthrop technical object of interest will be treated as a reliability system. It may be a no-repairable or repairable system with negligible or non-negligible renewal time. The catastrophic failure state will be modeled as the absorbing state.

Let's assume that the task to be done by the neural network is to determine system reliability model parameters. If we choose a specific reliability model then the basic problem is to determine its parameters. In general, the uncertainty of a model is connected mainly with the uncertainty of its parameters. By identifying parameters of the model we obtain sufficient material to be able to control its reliability, and the neural network model becomes simpler than that of the system as a whole.

The first step in programming an investigation is to define its objective and assumptions concerning the investigation subject (definitions of the system and its operational states, formal reliability model, characteristics of the environment). With these assumptions the system fault tree (FT) can be constructed. The fault tree allows determining the sets of elements effecting the system reliability, and also indirect relations if it appears helpful in the elicitation process.

We shall continue the consideration with, for instance, the exponential reliability system and the Markov chain. The task of the neural network will be to determine parameters of those systems.

Exponential distribution

$$R(t) = \exp(-\lambda t) \tag{1}$$

where:
$\lambda = 1/MTTF$ - the failure rate,
MTTF - the mean time to failures, which can be estimated by an expert without difficulties,
t - is the time.

Markov chain

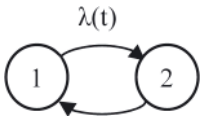

The graph presents the simplest case of a chain with two states: 1 – the state of operational use with $\lambda(t)$ failure rate, and 2 – the maintenance state with $\mu(t)$ repair rate of the reliability system. It is a nonhomogeneous process with finite renewal time. When the transition rates are not time-dependent then the process becomes homogeneous and the distributions of the state 1 and 2 duration times are exponential. The availability formula for an asymptotic homogenous version of the system takes the form:

$$a(t) = P_1(t) = \frac{\mu}{\lambda+\mu} + \frac{\lambda}{\lambda+\mu}\exp[-(\lambda+\mu)t] \tag{2}$$

Parameters of model (2) are the rates of failure λ and repair μ. In general, they are time-dependent, but may be approximated by constant or constant in time intervals. Statistical verification of such simplification is recommended [6, 11]. From the renewal equations:

$$\lim_{t\to\infty}\frac{H(t)}{t} = \frac{1}{T_0} \tag{3}$$

where:
$H(t) = E[\nu(t)]$ - he expected value of $\nu(t)$,
$\nu(t)$ - the number of failures in time interval t,
T_0 = MTBF.

From formula (3) - after sufficiently long time:

$$MTBF = \frac{t}{\overline{\nu(t)}} \tag{4}$$

where:

$\overline{\nu(t)}$ - the mean number of failures in time interval t, which can be easily determined from the expert judgements.

In the case of identical exponential distributions of times between failures

$$\lambda = 1/MTBF \tag{5}$$

It is generally assumed that the maintenance times have also exponential distributions with time-independent transition rates μ. This assumption pertains to direct maintenance work time without organizational preparation time and waiting time for beginning the work. In practice, that preparation period may be chaotic, which makes probabilistic estimation of the parameter μ difficult or even impossible. The following approach to the estimation of parameter μ is proposed:

1) adopting the model with negligible renewal time when that time is short compared with the usage time;
2) adopting constant renewal times for individual devices;
3) determining μ from the formula:

$$\mu = \frac{1}{\overline{\Theta}} \tag{6}$$

where:

$\overline{\Theta}$ - the mean renewal time, to be estimated by the experts.

In general, the reliability model parameters are functions of operands - physical values - like the time to failure, time between failures, duration times of specific reliability or operational states, and/or the number of failures in a time interval (event frequencies). These values are easier to be determined by an expert than the probabilistic model parameters. They are suggested to be used in elicitation.

The above presented considerations deal with the neural network output parameters, i.e. the top event (TE) in the tree FT, which is the system failure. Now we shall deal with the determination of the input parameters, i.e. basic events (BEs) in relation to TE. These are the system element failures. It is possible to obtain linguistic values of shares of the basic events in the top event frequencies. The linguistic variables have associated sets of values (very rare, rare, occasional, frequent, and very frequent). The linguistic values determined in the elicitation process allow to apply the pairwise comparison method in order to determine the preferences linking individual pairs and then, using the AHP method, the corresponding numerical values [10, 12]. The correlation level between the neural network output and input parameters should then be verified.

In the case of a large reliability system, the elicitation process of the shares of system elements in the failure frequencies may be subdivided into "layers", for instance in the case of two FT system layers - higher and lower - first determine the shares of higher layer elements in the system failure frequencies and then the shares of lower layer elements in the failure frequencies of

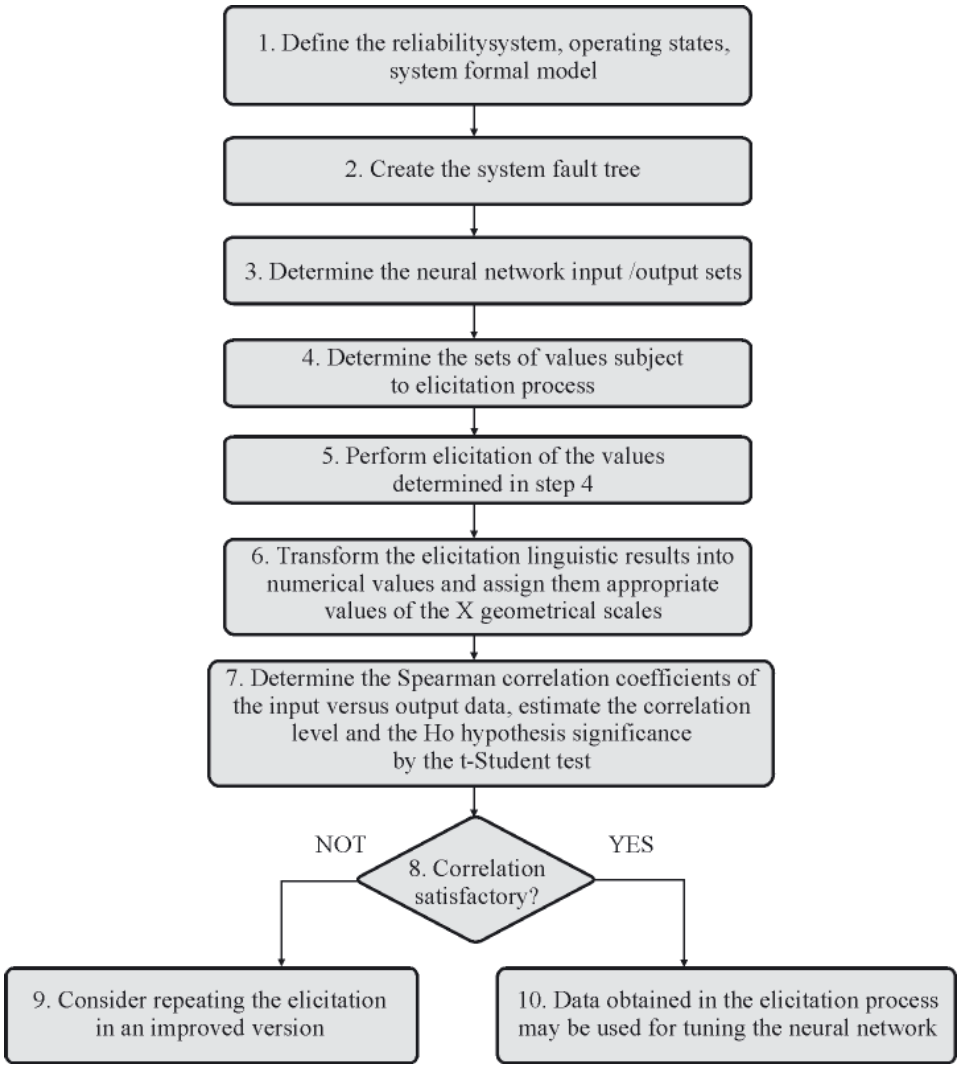

Fig. 1. *Network of the algorithm of data elicitation and processing for tuning the neural network*

the higher layer objects. The principles of completeness and disjointness should be maintained. This procedure will increase the correctness of expert estimates.

Let φ be an parameter of a NN and $\mathbf{p} = (p_1, p_2, ..., p_n)^T$ - vector of parameter sequences of BS event shares in the system fault tree, being the network inputs determined by the AHP method. Then the input vector will take the form [10, 12]:

$$\boldsymbol{\varphi} = \varphi\mathbf{p} = (\varphi_1, \varphi_2, ..., \varphi_n)^T \tag{7}$$

The preferred method of determining the sequence vector is the logarithmic least squares method [10].

Fig. 1 presents the flow diagram of the elicitation and data processing algorithm for obtaining correlated sets suitable for NN tuning.

PROCESSING OF EXPERT DATA BY THE AHP METHOD

Linguistic estimates of the shares of reliability system elements in the system failure frequency consist in expert choice of the share value from the set of five values. The estimates are given numbers from 1 to 5. Differences of experts' judgements indicate the scale of preferences in the pairwise comparison of the linguistic estimates. Depending on these differences, the preferences are assigned weights r(s) in accordance with a scale function. Then the linguistic judgment matrix **R** is determined and transformed into the priority vector **p**:

$$\mathbf{R} = \begin{bmatrix} r_{11} & \cdots & r_{1n} \\ \vdots & \ddots & \vdots \\ r_{n1} & \cdots & r_{nn} \end{bmatrix} \tag{8}$$

where:

R - the linguistic judgement matrix

r_{ij} - the preference of i-th to j-th share (i,j = 1, 2,…, n), with properties: $r_{ij} > 0$, $\forall_{i,j} r_{i,j} = 1/r_{j,i}$.

Matrix **R** is consistent if its elements fulfill the condition: $r_{i,j}r_{j,k} = r_{ik}$ $\forall$i,j,k = 1, 2, ..., n.

The priority vector $\mathbf{p} = (p_1, ..., p_n)^T$ is determined by approximation of matrix **R** with matrix **P,** where:

$$\mathbf{P} = \begin{bmatrix} p_1/p_1 & \cdots & p_1/p_n \\ \vdots & \ddots & \vdots \\ p_n/p_1 & \cdots & p_n/p_n \end{bmatrix} \tag{9}$$

The measure of consistency of the Xu processing is the difference between matrices **P** and **R** [14]:

$$d(R,P) = \sqrt{\frac{2}{n(n-1)} \sum_{i=1}^{n} \sum_{j=1}^{n} (r_{ij} - p_{ij})^2} \tag{10}$$

The Xu scale [14] is a geometrical scale with parameter c = 2, in the form:

$$r(s) = (\sqrt{c})^{I(s)} \tag{11}$$

where:

I(s) - the index of the preference symbol s,

c - the parameter.

It was proved [14] that with this particular value of c the difference between the linguistic judgment matrix and the matrix derived from the priority vector is at a minimum. Table 2 shows the Xu scale data with parameter c = 2.

Tab. 2. *AHP geometrical scale data (c = 2)*

Differences of expert judgments	AHP geometrical scale with parameter c = 2			
	s_i	I(s)	r(s)	Description of preference
0	s_o	0	1	equally import ant
1	s_2	2	2	moderately more important
2	s_4	4	4	strongly more important
3	s_6	6	8	evidently more important
4	s_8	8	16	extremely more important
-1	s_{-2}	-2	0.5	moderately less important
-2	s_{-4}	-4	0.25	strongly less important
-3	s_{-6}	-6	0.125	evidently less important
-4	s_{-8}	-8	0.0625	extremely less important

DATA CORRELATION PROBLEM

The data elicited from the experts may have a numerical or linguistic form. The latter are adjectives valuating the intensity of the measured variable of an object's feature, process or phenomenon. These adjectives may be assigned natural numbers, ascending with the increasing intensity, i.e. perform ranking of the measured value. The estimates of the linguistic values are done by means of ordered scales. The scales have order relations.

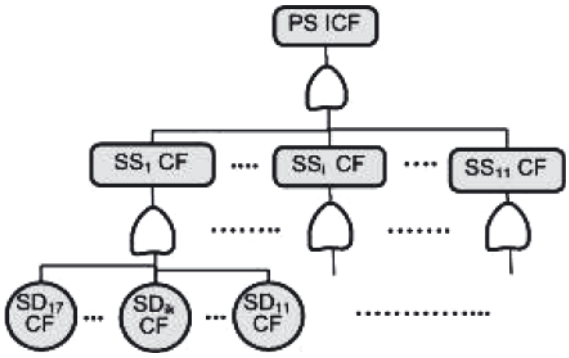

Fig. 2. *Fault tree of a ship propulsion system ICF*
***Legend**: **PS** – propulsion system; **ICF** – immediate catastrophic failure; **CF** – catastrophic failure.*
***SS**$_i$ – subsystem, **i = 1** – fuel oil subsystem, **2** – sea water cooling subs.; **3** – low temperature fresh water cooling subs.; **4** – high temperature fresh water cooling subs.; **5** – starting air subs.; **6** – lubrication oil subs.; **7** – cylinder lubrication oil subs.; **8** – electrical subs.; **9** – main engine subs.; **10** – remote control subs.; **11** – propeller + shaft line subs.*
***SD**$_{ik}$ – set of devices; **ik = 11** – fuel oil service tanks; **12** – f. o. supply pumps; **13** – f. o. circulating pumps; **14** – f. o. heaters; **15** – filters; **16** – viscosity control arrangement; **17** – piping heating up steam arrangement*

As indicated above, in the case of physical objects observed in the operation process the numerical values pertain to independent variables in expressions defining the reliability model parameters. They are estimated in interval scales. Such scales have a constant unit of measurement, the order relation and an optionally chosen zero point.

The correlation analysis of the values measured on the above presented scales is carried out using non-parametric methods.

They compensate the effects of the standing-out measurements and the non-normality of the elicited values [13].

To the correlation analysis of the data obtained from the elicitation process the R. Spearman's method is applied. The output and input data are ranked by assigning them ascending natural numbers starting from 1. The numbers are ranks. The ranking process may be performed also with the decreasing sequence. The Spearman's rank correlation coefficient is determined from the following formula [13]:

$$r_s = 1 - \frac{6\sum_{i=1}^{n} d_i^2}{n(n^2-1)} \tag{12}$$

where:

d_i - the difference between the ranks of corresponding characteristic values. The correlation coefficient ranges within $-1 \le r_s \le 1$.

The correlation coefficient determined by formula (11) is applicable only to a random sample, and the correlation of the general population should also be checked. For that the zero hypothesis H_o: $\rho = 0$, where ρ is the correlation coefficient of the general population, is verified against the alternative hypothesis H_1: $\rho \neq 0$. The *t-Student* test is used for verification. It is assumed that the population has the Student distribution with n -1 degrees of freedom. The test has the form:

$$t = \frac{r_s}{\sqrt{1-r_s^2}}\sqrt{n-1} \tag{13}$$

where:

n - the size of the sample.

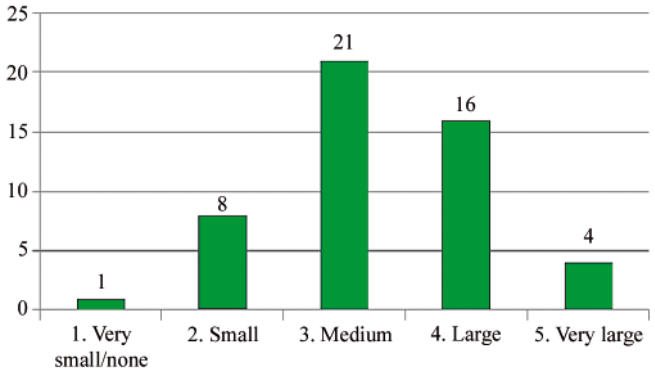

Fig. 3. *Distribution of propulsion system ICF type failure numbers*

The test value t is compared with the critical value t_p determined from the Student tables for an assumed significance level p and n - 2 degrees of freedom. If $t > t_p$ then hypothesis H_0 is rejected and hypothesis H_1 is accepted (the correlation exists also in the general population) [13].

EXAMPLE

Object of analysis, elicitation

The example illustrates the reliability analysis of a container carrier propulsion system (PS) with slow-speed piston internal combustion engine and screw propeller, operating in the North Atlantic (*). The reliability was analysed for immediate catastrophic failures (ICF) of the PS; it is substantial in the case of the risk analysis of PS. Fig. 2 presents the FT of the PS. It was assumed that ICFs can occur only during the active usage state of the system, i.e. during the ship sea voyage. Detailed data of this example can be found in [1, 2, 3].

A questionnaire was presented with definitions of the investigated object, "immediately catastrophic failure of PS" and "sea traffic", as well as tables to be filled in by the experts and suggestions how to do it. The questionnaire was filled in by 50 experts - ship engineers with multi-year experience. Questions were asked about the annual frequency of propulsion system ICF type events, the share of subsystem (SS) failures in the PS system failure frequency and the share of module (set of devices - SD) ICF type failures in the SS failure frequencies. Appendix 1 shows fragments of the questionnaire.

The data elicitated by the experts have been multiplied in the neural network tuning process to 2 - 3 hundreds base on uniform distribution.

Analysis of the correlation of elicitation results

As regards the propulsion system as a whole, the experts gave their subjective estimates of the ICF type failures per year in numbers, and linguistically by marking one of fields in the order scale containing numbers and descriptions of that failure frequency (see Appendix 1). For instance, Fig. 3 presents a histogram of the system PS failure frequency per year. The histogram shows a distribution close to the normal distribution, which may be considered correct in the case of observation of dangerous events with more or less steady frequency of occurrence.

The elicitation of the ICF type failures of SS subsystems and their SD modules consisted in marking appropriate fields in the questionnaire order scales (see Appendix 1). They indicated the share of a given SS or SD in the ICF type failure frequency of a direct higher level object, i.e. of the propulsion system in the case of SSs and of a specific SS in the case of SD modules. The shares were pairwise compared and respective differences of numbers were treated as numerical estimates of experts' preferences. The preferences were assigned values in accordance with the geometrical scale function.

Appendix 2 presents selected verification results of correlation between the PS – SS_i, (i = 1, 2, …, 11), SS_{1k} – SD_{ik}, (11, 12, …, 17) and PS – SD_{ik}, (11, 12, …, 17) data. The correlation coefficients ranged within 0.9716 – 0.9909, so the data sets appeared well correlated (*nearly total correlation* according to [13]). The zero correlation in the general population H_0 hypothesis was rejected at the 0.01 level. The consistency measure Xu (8) was zero.

CONCLUSION

The above text presents the method to tune the neural network. The network is only directed to determine subjective parameters of the complex reliability system model. The numerical elicitation of the system's failure frequency is performed, with further linguistic elicitation of the shares of failures in system's elements in that value. The first value serves for determining the network's output parameter and the second one serves for determining the set of network's input parameters. The linguistic values are subjected to pairwise comparison and assigned numerical values by means of the AHP method. The correlation between the output and input parameters is investigated. When it is positive we can find that the tuning parameters are corrected for general population.

The content presented above allows concluding that the used neural network tuning procedure gives correct results. It appears appropriate when makes use of experts who are experienced operators of the reliability analysis objects. It may be useful for network tuning in reliability analyses and for the technical system risk management.

BIBLIOGRAPHY

1. Brandowski A.: *Estimation of the Probability of Propulsion Loss by a Seagoing Ship Based on Expert Opinions*. Polish Maritime Research. 59. 73-77, 2009.
2. Brandowski A., Mielewczyk A., Nguyen H., Frackowiak W.: *Certain propulsion risk prediction model of a seagoing ship.* Proceedings of ESREL 2010 Conference. Rhodes: CRS PRESS / BALKEMA, 42-48, 2010.
3. Brandowski A., Mielewczyk A., Nguyen H., Frackowiak W.: *A fuzzy - neuron model of the ship propulsion risk prediction.* Szczecin - Świnoujście: Journal of KONBiN, 2010.
4. Cooke R. M.: *Experts in Uncertainty*. New York, Oxford: Oxford University Press, 1991.
5. Elliot M. A.: *Selecting numerical scales for pairwise comparisons.* Reliability Engineering and System Safety 95, 750-763, 2010.
6. Gniedienko B. W., Bielajew J. K., Sołowiew A. D.: *Mathematical methods in the reliability theory* (in Polish). Warszawa: Wydawnictwa Naukowo-Techniczne, 1968.
7. IMO – Resolution A. 849(20).: *Code for the investigation of marine casualties and incidents.* London: IMO, 1997.
8. Jaźwiński J., Smalko Z.: *The use of expert method for estimation of the beta distribution parameters for evaluation of non-delectability and safety of technical means of transport* (in Polish). Radom: Wyd. Instytutu Technologii Eksploatacji, 2001.
9. *Judgment under uncertainty: Heuristics and biases* (edited by: Kahneman G., Slovic P., Tversky A.). Cambridge University Press, 2001.
10. Kwiesielewicz M.: *Analytical hierarchical decision process. Non-fuzzy and fuzzy pairwise comparison* (in Polish). Warsaw: System Research Institute PAN, 2002.
11. Modarres M., Kaminskiy M., Krivtsov: *Reliability Engineering and Risk Analysis.* New York, Basel: Marcel Dekker Inc, 1999.
12. Saaty T.L.: *The analytic hierarchy process*. New York: McGraw Hill, 1980.
13. Stanisz A.: *Intelligible course of statistics*. Vol. 1 (in Polish). Cracow: StatSoft, 2006.
14. Yucheng Dong, Yinfeng Xu, Hongyi Li, Min Dai.: *A comparative study of the numerical scales and the prioritization methods in AHP.* European Journal of Operational Research 186, 226-242, 2008.

CONTACT WITH THE AUTHORS

Brandowski A., Prof.,
Hoang Nguyen, Ph. D.,
Wojciech Frąckowiak, M. Sc.,
Faculty of Marine Engineering
Gdynia Maritime University,
Morska 81-87
81-225 Gdynia, POLAND
e-mail: a.brandowski@gmail.com
mobile: +48 668 548 525

Appendix 1. Fragments of PS and SS questionnaire

13. Propulsion system (as a whole) – main task of the system is ship propulsion and additional task is electric energy generation (not included in the investigation).

The following ranges of the propulsion system critical failure frequencies are distinguished:

A – very rare – the failure occurrence seems unlikely but is possible;
B – rare – probability of failure is low but failure may be expected;
C – occasional – failures happen several times in the ship life;
D – frequent – failures occur frequently;
E – very frequent – failures recur regularly.

Please give in the table below:

- your own estimate of average frequency per year of the propulsion system catastrophic failures, which caused immediate stoppage or impossibility of starting the system at sea;
- mark (X), at your discretion, the appropriate frequency range.

Frequency per year of the propulsion system critical failures:				.....[year^{-1}]
Propulsion system failure frequency range:				
1 – very rare	2 – rare	3 – occasional	4 – frequent	5 – very frequent

14. Subsystems of the propulsion system (main engine, installations, assemblies) – Please mark (X) appropriate table fields, in accordance with your professional experience

Subsystem	Share of failures of the installation / engine / assembly in the total number of propulsion system critical failures causing its immediate stoppage				
	5. very large	4. large	3. medium	2. small	1. very small / none
1. Propeller + shaft line SS					
2. Remote control SS					
3. Main engine SS					
4. Electric SS					
5. Cylinder lubrication SS					
6. Lubrication SS					
7. Starting air SS					
8. High temperature fresh water cooling SS					
9. Low temperature fresh water cooling SS					
10. Sea water cooling SS					
11. Fuel oil SS					

Appendix 2. Results of expert data correlation analysis after processing by the AHP method (geometrical scale, c = 2)

Spearman correlations between PS and SS_i, (i = 1, 2, …, 11) estimates, after processing by the AHP method

SS_i*	SS_1	SS_2	SS_3	SS_4	SS_5	SS_6	SS_7	SS_8	SS_9	SS_{10}	SS_{11}
Spearman ranking	0.9905	0.9835	0.9830	0.9845	0.9874	0.9855	0.9827	0.9921	0.9930	0.9879	0.9825
t test	50.303237	38.047424	37.437767	39.233811	43.732864	40.671667	37.169861	55.318965	58.65185	44.60928	36.907435
t crit. (p = 0.01)	2.682204										
0 hypothesis	rejected	rejected	rejected	rejected	rejected	rejected	rejected	rejected	rejected	rejected	rejected

Spearman correlations between SS_1 and SD_{1k}, (k = 1, 2, …, 7) estimates, after AHP

SD_{1k}*	SD_{11}	SD_{12}	SD_{13}	SD_{14}	SD_{15}	SD_{16}	SD_{17}
Spearman ranking	0.9716	0.9857	0.9864	0.9761	0.9829	0.9877	0.9787
t test	28.752914	41.002746	42.02624	31.463987	37.316519	44.142822	33.393157
t crit. (p = 0.01)	2.682204						
0 hypothesis	rejected	rejected	rejected	rejected	rejected	rejected	rejected

Spearman's correlation between estimates of PS and SD_{1k}, (k = 1, 2, …, 7) belonging to SS_1, after processing by the AHP method

SD_{1k}*	SD_{11}	SD_{12}	SD_{13}	SD_{14}	SD_{15}	SD_{16}	SD_{17}
Spearman ranking	0.9827	0.9908	0.9905	0.9873	0.9909	0.9931	0.9879
t test	37.126849	51.387827	50.391728	43.579343	51.456312	59.202177	44.671438
t crit. (p = 0.01)	2.682204						
0 hypothesis	rejected	rejected	rejected	rejected	rejected	rejected	rejected

* Descriptions of the SS_i and SD_{1k} modules as in Fig. 2

POLISH MARITIME RESEARCH 1(81) 2014 Vol 21; pp. 35-41
10.2478/pomr-2014-0006

Regression Analysis of Principal Dimensions and Speed of Aircraft Carriers

J.Y. Bi, Ph. D.,
Ludong University, China
Z. Zong, Ph. D.,
Dalian University of Technology, China

ABSTRACT

In this paper empirical formulas relating the speed to principal dimensions of aircraft carriers have been obtained through regression analysis of the data of 105 aircraft carriers. To reduce uncertainty as much as possible, aircraft carriers are classified into several different categories. In each category, regression analysis is separately performed such that a variety of regression (empirical) formulas have thus been obtained for possible use at the initial design stage of a carrier. The goodness of fit of these formulas is finally analyzed through variance analysis.

Key words: aircraft carriers; speed; principal dimensions; regression; variance

1. INTRODUCTION

At the initial design stage of a ship, only speed is provided in the design specifications. Its principal dimensions are usually predicted based on the prescribed ship speed. Or inversely, its speed is predicted based on its principal dimensions. More often than not, the principal dimensions are evaluated either through empirical formulas or through parent ships. This paper is focused on the study of empirical formulas. The method of parent ships will be ignored throughout the paper.

A variety of empirical formulas have been obtained through regression of ship data of various types [2]. For example, there have been empirical formulas for bulk carriers, container ships, oil tankers and passenger liners to estimate their principal dimensions based on given ship speed or vice versa. There is, however, a lack of regression formulas relating the speed to principal dimensions of an aircraft carrier. It is thus needed to find the regression formulas for evaluating the relations between principal dimensions and the speed for aircraft carriers.

To obtain empirical formulas for evaluating speed of an aircraft carrier, 125 sets of data of aircraft carriers [3] are collected. Among them, only 105 have been used in our regression analysis [6] because the information provided in the rest 20 sets of data is not complete. In this paper, regression analysis of available data is presented based on aircraft carriers and regression formulas are obtained for predicting the principal dimensions based on speed performance of an aircraft carrier or vice versa. Different regression formulas are determined through application of various regression forms. The confidence of each regression formula is analyzed through variance [4, 7]. So the most suitable regression formulas for various types of aircraft carriers are given and different regression formulas can be chosen to use for diverse purposes.

2. REGRESSION ANALYSIS

The scatters of available data of aircraft carriers are large. To reduce uncertainty aircraft carriers data are divided into different categories. In each category regression analysis is separately performed.

2.1. Classification by Froude number

Based on Froude number (Fr) surface vessels of displacement type fall into three categories: low-speed vessel, medium-speed vessel and high-speed vessel. Fr [1] is defined by:

$$Fr = v_s / \sqrt{gL} \tag{1}$$

where:
L – ship length [m],
v_s – speed [m/s],
g – acceleration of gravity [m/s^2].

Low-speed ships are those which Froude numbers are smaller than 0.18, that is, Fr < 0.18; Medium-speed ships are those which Froude numbers are between 0.18 and 0.30, that is, 0.18 < Fr < 0.30; High-speed ships are those which Froude numbers are larger than 0.30, that is, Fr > 0.30. Analyzing the speed data of aircraft carriers shows that the Froude numbers of aircraft carriers are almost all larger than 0.18. Therefore the regression analysis will be focused on medium-speed and high-speed aircraft carriers.

2.1.1. Medium-speed aircraft carriers

a) Ayre formula regression

Ayre formula relates Froude number to the ratio of ship length to the cubic root of its displacement. The Ayre formula for civil vessels and merchant ships which lengths are between 120 m and 140 m is known to be [5]:

$$L/\Delta^{1/3} = 3.344 + 10.225Fr \tag{2}$$

where:
Δ – the displacement [t].

Based on the available data regression analysis is performed for medium-speed aircraft carriers in the form of Ayre formula. The finally obtained regression formula for medium-speed aircraft carriers is:

$$L/\Delta^{1/3} = 12.636Fr + 4.235 \tag{3}$$

In Fig. 1 the data pairs ($L/\Delta^{1/3}$, Fr) based on 49 carriers are plotted. The curve corresponding to the above formula is also given in the figure. The variance estimated from the data is 0.566, thus showing an unsatisfactory agreement. To improve the accuracy and reduce the variance, quadratic form is employed in the following section for the regression.

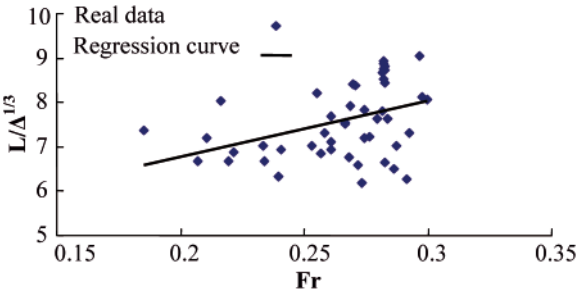

Fig. 1. *Ayre regression analysis of medium-speed aircraft carriers*

b) Quadratic regression

In the Ayre formula the quantity $L/\Delta^{1/3}$ is assumed a linear function of Froude number, which does not describe the data very well as shown in Fig. 1. A regression formula of quadratic form is therefore used to replace Ayre formula in the hope to reduce the variance. Following the same procedures as above, the regression formula of quadratic form is obtained for medium-speed aircraft carriers as follows:

$$L/\Delta^{1/3} = 202.37Fr^2 - 88.407Fr + 16.663 \tag{4}$$

The data and the regression curve are all plotted in Fig. 2. The variance in this case is 0.541.

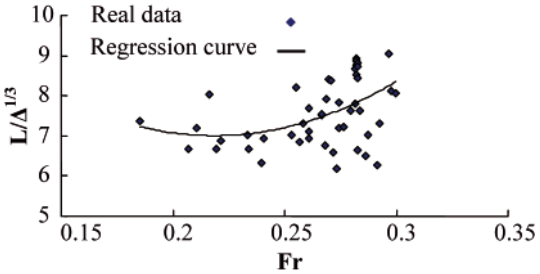

Fig. 2. *Polynomial regression analysis of medium-speed aircraft carriers*

Comparing the variance of Ayre formula with quadratic formula, we conclude that the latter does not improve much over the former (one being 0.566 and the other 0.541). The reason is that the scatters of the data as shown in Figs. 1 and 2 are large. This problem will be discussed further in the following section.

c) Three-dimensional regression

The above analyses indicate that the regression results are not satisfactory even quadratic form regression is employed. To reduce variance further one more variable is introduced, that is, ship beam into the regression formula. Although the beam is often used to represent stability, the variance is indeed reduced somewhat through introduction of the beam into the regression formula. Because three variables are involved the regression formula is thus a three-dimensional one. The three non-dimensional variables are $L/\Delta^{1/3}$, $B/\Delta^{1/3}$ and Fr.

Regression analysis in three-dimensional form has been performed based on 49 sets of data. The obtained three-dimensional regression formula is given in the form of:

$$L/\Delta^{1/3} = 242.93Fr^2 - 9.015(B/\Delta^{1/3})^2 - 70.332Fr(B/\Delta^{1/3}) +$$
$$- 46.746Fr + 38.508(B/\Delta^{1/3}) - 7.898 \tag{5}$$

where:
B – beam [m].

The data and the regression surface corresponding to the three-dimensional regression formula are plotted in Fig. 3. The variance estimated from the data is 0.483, having been improved slightly over the quadratic regression formula.

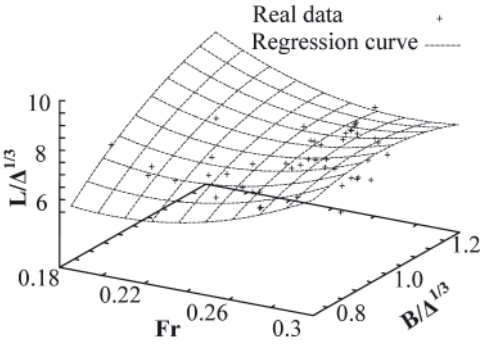

Fig. 3. *Three-dimensional regression analysis of medium-speed aircraft carriers*

2.1.2. High-speed aircraft carriers

a) Ayre formula regression

Again, Ayre formula for high-speed aircraft carriers is first used to represent the linear relationship between displacement length $L/\Delta^{1/3}$ and Froude number (Fr). Regression based on the data of 54 carriers yields the Ayre formula in the form of:

$$L/\Delta^{1/3} = 1.148Fr + 7.913 \tag{6}$$

The regression curve corresponding to the above formula and the 54 pairs of data are all plotted in Fig. 4. The variance

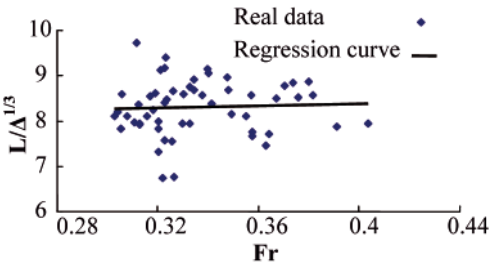

Fig. 4. *Ayre regression analysis of high-speed aircraft carriers*

estimated from the data is 0.355. Comparing with the Ayre formula for medium-speed carriers, we conclude that the Ayre formula for high-speed carriers is better in terms of variance.

b) Quadratic regression

In order to reduce the variance the quadratic form is used to replace the linear form, that is, quadratic regression formula is obtained to replace the Ayre formula which does not represent the data very well as shown in Fig. 4. The obtained regression formula for high-speed aircraft carriers is:

$$L/\Delta^{1/3} = -101.58Fr^2 + 71.466Fr - 4.186 \quad (7)$$

The variance in this case is 0.350 by analyzing the data and the regression curve plotted in Fig. 5, showing negligible improvement over the Ayre formula.

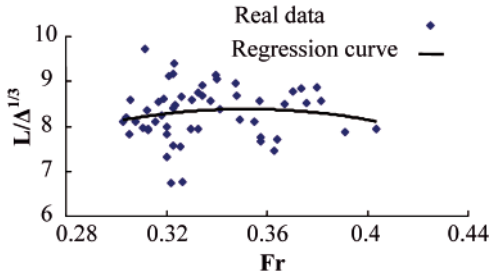

Fig. 5. Polynomial regression analysis of high-speed aircraft carriers

c) Three-dimensional regression

A regression formula of three-dimensional form for high-speed aircraft carriers has been obtained based on the available data of 54 carriers as follows:

$$L/\Delta^{1/3} = -98.788Fr^2 + 15.538(B/\Delta^{1/3})^2 - 17.314Fr(B/\Delta^{1/3}) + $$
$$+ 86.640Fr - 23.222(B/\Delta^{1/3}) + 3.864 \quad (8)$$

The variance in this case is 0.330. The regression surface is shown in Fig. 6.

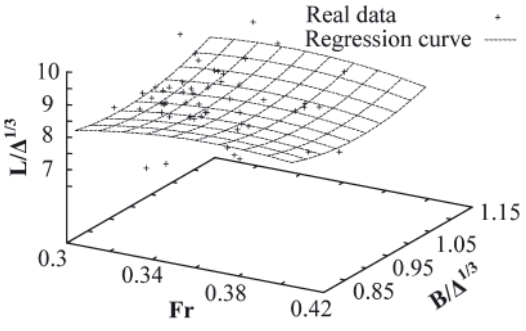

Fig. 6. Three-dimensional regression analysis of high-speed aircraft carriers

2.2. Classification by Displacement

Alternatively, aircraft carriers may also fall into three categories: light aircraft carriers, medium aircraft carriers and large aircraft carriers based on displacement. Large aircraft carriers are those which displacements are over 60000 tons, medium aircraft carriers are those which displacements are between 30000 to 60000 tons and light aircraft carriers are those which displacements are less than 30000 tons.

2.2.1. Light aircraft carriers

a) Ayre formula regression

Regression analysis for light aircraft carriers in the form of Ayre formula has been performed based on 83 sets of data. The obtained regression formula for light aircraft carriers is:

$$L/\Delta^{1/3} = 10.301Fr + 4.856 \quad (9)$$

The 83 sets of data and the regression curve are plotted in Fig. 7, and the estimated variance is 0.541. The variance shows an unsatisfactory agreement. Again, quadratic form is employed in the following section for the regression.

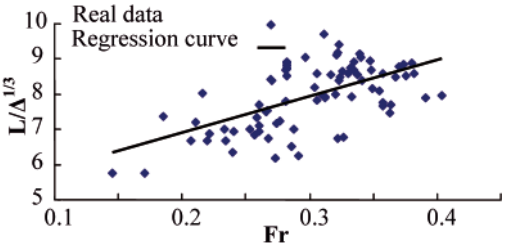

Fig. 7. Ayre regression analysis of light aircraft carriers

b) Quadratic regression

A regression formula of quadratic form for light aircraft carriers is employed in the hope to improve the accuracy. The obtained quadratic regression formula for light aircraft carriers is:

$$L/\Delta^{1/3} = -54.373Fr^2 + 41.579Fr + 0.513 \quad (10)$$

The variance is estimated to be 0.501. Again the conclusion is drawn that the quadratic regression does not improve much over the Ayre formula (see Fig. 8).

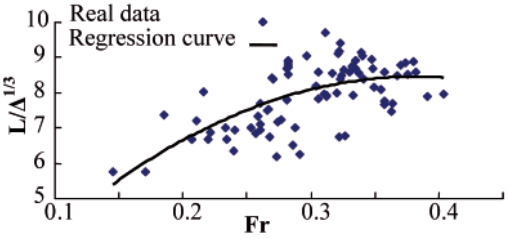

Fig. 8. Polynomial regression analysis of light aircraft carriers

c) Three-dimensional regression

Regression analysis in the form of three-dimensional formula for light aircraft carriers has been performed. The final regression formula in the three-dimensional form is:

$$L/\Delta^{1/3} = -36.888Fr^2 - 6.661(B/\Delta^{1/3})^2 + 4.124Fr(B/\Delta^{1/3}) + $$
$$+ 26.755Fr + 13.540(B/\Delta^{1/3}) - 4.645 \quad (11)$$

The variance estimated from the data is 0.473. The data and the regression surface are shown in Fig. 9.

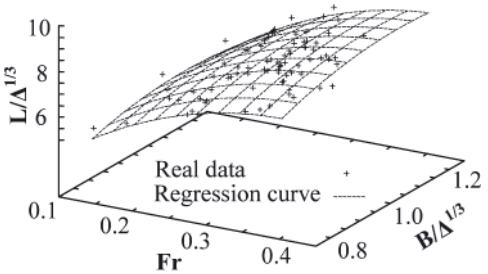

Fig. 9. Three-dimensional regression analysis of light aircraft carriers

2.2.2. Medium aircraft carriers

a) Ayre formula regression

Available data for medium aircraft carriers are not plenty. Only 15 sets of data are used for regression analysis. The obtained regression result in the form of Ayre formula for this case is:

$$L/\Delta^{1/3} = 0.662\mathrm{Fr} + 7.659 \tag{12}$$

The variance estimated from the data is 0.249. The regression curve is nearly flat in this case as shown in Fig. 10.

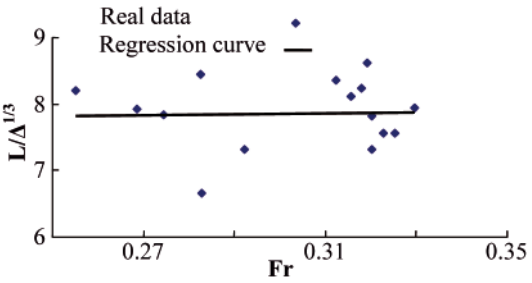

Fig. 10. Ayre regression analysis of medium aircraft carriers

b) Quadratic regression

The regression formula in the form of quadratic form is again used for medium aircraft carriers. The obtained formula is:

$$L/\Delta^{1/3} = 256.08\mathrm{Fr}^2 - 150.42\mathrm{Fr} + 29.789 \tag{13}$$

The variance estimated from the data is 0.239. It is just a little better than Ayre formula (see Fig. 11).

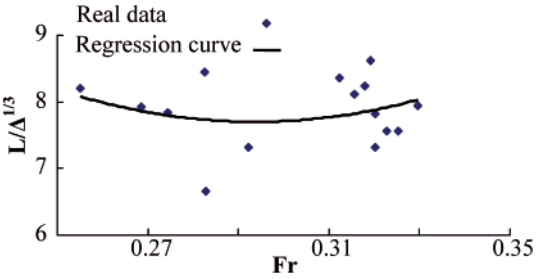

Fig. 11. Polynomial regression analysis of medium aircraft carriers

c) Three-dimensional regression

Based on the above data, regression analysis of three-dimensional form is performed for medium aircraft carriers. The following regression formula is obtained:

$$L/\Delta^{1/3} = 209.623\mathrm{Fr}^2 - 164.361(B/\Delta^{1/3})^2 + \\ - 209.951\mathrm{Fr}(B/\Delta^{1/3}) + 81.066\mathrm{Fr} + \\ + 383.134(B/\Delta^{1/3}) - 191.213 \tag{14}$$

The variance estimated from the data is 0.204. The regression surface and the data are plotted in Fig. 12.

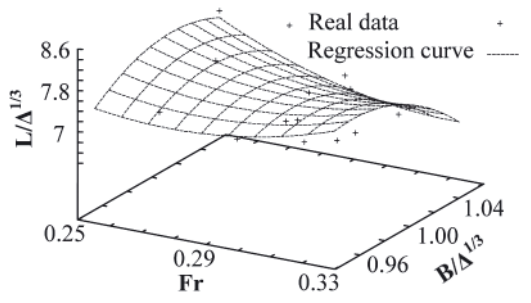

Fig. 12. Three-dimensional regression analysis of medium aircraft carriers

2.2.3. Large aircraft carriers

a) Ayre formula regression

Data for large carriers are even less, only 7 sets of data available. Based on the 7 sets of data, the following regression curve is obtained in the form of Ayre formula:

$$L/\Delta^{1/3} = 36.416\mathrm{Fr} - 2.881 \tag{15}$$

The data and regression curve are plotted in Fig. 13. The variance estimated from the data for this case is 5.995×10^{-2}.

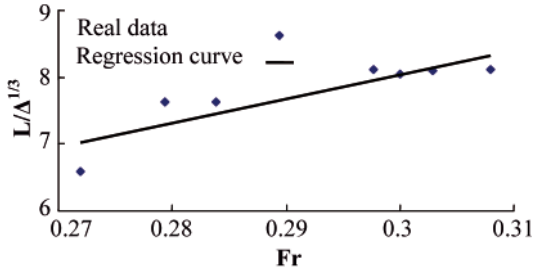

Fig. 13. Ayre regression analysis of large aircraft carriers

b) Quadratic regression

Again quadratic regression analysis is performed for large aircraft carriers. The obtained quadratic regression formula is:

$$L/\Delta^{1/3} = -1934.4\mathrm{Fr}^2 + 1158.1\mathrm{Fr} - 165.17 \tag{16}$$

The variance for this case is 1.508×10^{-2} (see Fig. 14). Because the sample size is small, both the Ayre formula [(Eq. (12)] and the regression formula of quadratic form [Eq. (13)] are in excellent agreement with the data.

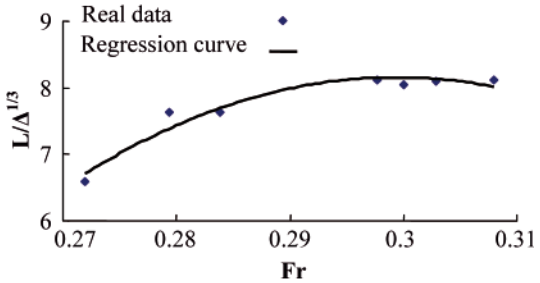

Fig. 14. Polynomial regression analysis of large aircraft carriers

c) Three-dimensional regression

Regression analysis in the form of three-dimensional formula has been performed based on the 7 sets of data. The obtained three-dimensional regression formula is given in the form of:

$$L/\Delta^{1/3} = 1848.83\mathrm{Fr}^2 + 10.308(B/\Delta^{1/3})^2 - 1207.71\mathrm{Fr}(B/\Delta^{1/3}) \\ + 95.248\mathrm{Fr} + 338.47(B/\Delta^{1/3}) - 173.441 \tag{17}$$

The data based on 7 carriers and regression surface are plotted in Fig. 15. The variance in this case is 4.561×10^{-3}.

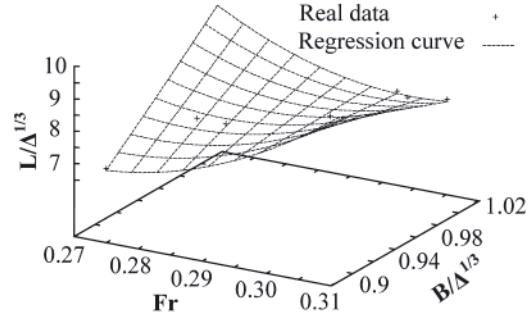

Fig. 15. Three-dimensional regression analysis of large aircraft carriers

2.3. Classification by Power

The third approach used to classify aircraft carriers is based on the power plant. Based on power plant aircraft carriers are classified into conventional-powered aircraft carriers and nuclear-powered aircraft carriers. There are 12 carriers of nuclear-powered class in the world. They are Enterprise, Nimitz class, Improved Nimitz class and Charles de Gaulle. The rest are all conventional-powered.

2.3.1. Conventional-powered aircraft carriers

a) Ayre formula regression

The regression formula in the form of Ayre formula for conventional-powered aircraft carriers is:

$$L/\Delta^{1/3} = 10.094\mathrm{Fr} + 4.894 \tag{18}$$

The variance estimated from the data based on 102 carriers is 0.497. The data and regression curve are shown in Fig. 16. In this case, the variance is large due to the large scatters in the data.

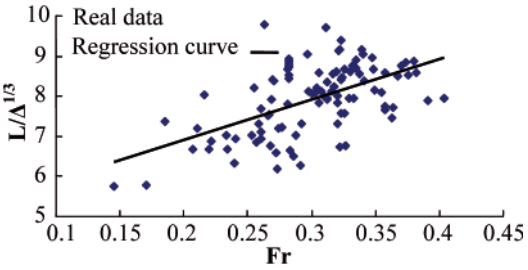

Fig. 16. Ayre regression analysis of conventional-powered aircraft carriers

b) Quadratic regression

The quadratic form regression formula for conventional-powered carriers based on 102 sets of data is:

$$L/\Delta^{1/3} = -47.549\mathrm{Fr}^2 + 37.453\mathrm{Fr} + 1.075 \tag{19}$$

The variance is 0.471. Both the data and the regression curve are shown in Fig. 17. No much improvement has been observed by replacing Ayre regression formula with the quadratic regression formula.

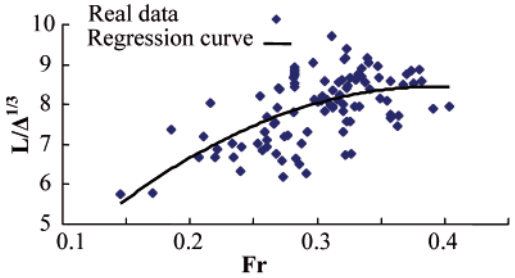

Fig. 17. Polynomial regression analysis of conventional-powered aircraft carriers

c) Three-dimensional regression

Again the following regression formula in three-dimensional form is obtained as follow:

$$L/\Delta^{1/3} = -24.546\mathrm{Fr}^2 - 4.816(B/\Delta^{1/3})^2 - 3.430\mathrm{Fr}(B/\Delta^{1/3}) + \\ + 26.435\mathrm{Fr} + 12.236(B/\Delta^{1/3}) - 4.026 \tag{20}$$

The variance estimated from the data based on 102 carriers is 0.448. The correlation between the data and regression surface is clearly shown in Fig. 18.

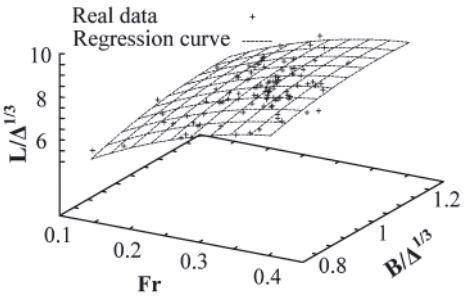

Fig. 18. Three-dimensional regression analysis of conventional-powered aircraft carriers

2.3.2. Nuclear-powered aircraft carriers

a) Ayre formula regression

There are 12 nuclear-powered aircraft carriers ever built. They are however pertaining to only four different types, that is, Enterprise (only one), Nimitz class (3), Improved Nimitz class (7) and Charles de Gaulle (only one). Therefore, there have only been four sets of data available for nuclear-powered carriers. The regression formula relating the displacement length to Froude number is:

$$L/\Delta^{1/3} = 28.769\mathrm{Fr} - 0.277 \tag{21}$$

The variance estimated from the data is 3.049×10^{-2} (see Fig. 19).

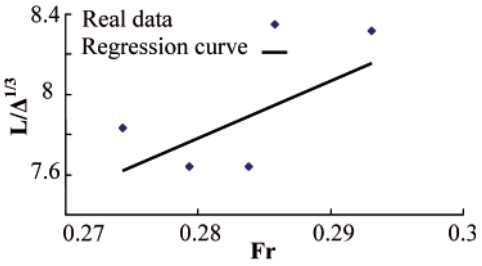

Fig. 19. Ayre regression analysis of nuclear-powered aircraft carriers

b) Quadratic regression

A regression formula in the quadratic form has also been tried with excellent results obtained due to the small sample size. The final regression formula is:

$$L/\Delta^{1/3} = 4904.8\mathrm{Fr}^2 - 2757.6\mathrm{Fr} + 395.21 \tag{22}$$

The variance in this case is 9.943×10^{-5}. In Fig. 20, the data and the regression formula are in perfect agreement as expected because there are only four sets of data.

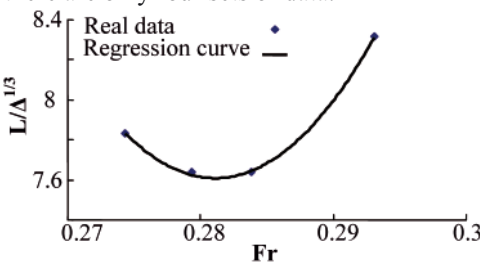

Fig. 20. Polynomial regression analysis of nuclear-powered aircraft carriers

c) Three-dimensional regression

The regression formula in three-dimensional form has also been performed with excellent results. The obtained three-dimensional regression formula is:

$$L/\Delta^{1/3} = 789.71Fr^2 - 411.993(B/\Delta^{1/3})^2 - 637.36Fr(B/\Delta^{1/3}) +$$
$$+ 154.037Fr + 992.573(B/\Delta^{1/3}) - 498.617 \qquad (23)$$

The variance in this case is 4.896×10^{-10}. It is a perfect surface as shown in Fig. 21.

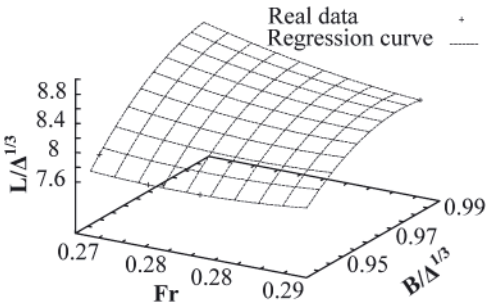

Fig. 21. *Three-dimensional regression analysis of nuclear-powered aircraft carriers*

3. DISCUSSION

Regression theory states that the smaller the variance is the better the regression is. For comparison all the previous results are placed in Tab. 1. From the Table, conclusion may be drawn that in general the variances of regression formulas of quadratic form are smaller than those of the Ayre formula, thus the latter being better than the former. Moreover, the variances of three-dimensional regression formulas are smaller than the other two forms of regression formulas. Therefore, three-dimensional regression formulas are the best among the three regression methods. Although ship beam B is generally not present in such regression formulas for civil vessels, three-dimensional regression formulas for carriers are recommended because they do improve the regression accuracy apparently.

Of particular interest are large carriers and nuclear-powered carriers. Their regression is excellent. This may be attributed to the fact that large carriers are smaller in number and thus the sample scatters are small, too. Another reason is that these large carriers are built following almost the same plans. Take nuclear-powered carriers for instance. Twelve nuclear-powered carriers are in fact built based on four different categories.

4. EXAMPLE

In this section, several examples are given to demonstrate the use of the regression formulas obtained in this paper. Based on given displacement, length and beam of a given aircraft carrier, its speed is predicted as shown in Table 2. In the Table, the real-ship speed is also given for comparison.

In general, 3-D regression formulas are better than the other. From Table 2, however, there are occasional cases where speed predictions from quadratic form or Ayre form are better than 3-D form, but the differences are not significant. Therefore, three-dimensional regression formulas are recommended for use at the initial design stage of a carrier.

5. CONCLUSION

Empirical formulas relating speed with other principal dimensions of a ship play an important role at the initial stage of design. In this paper such empirical formulas for carriers are

Tab. 1. *Variance analysis for each category of carriers*

Classification	Type of aircraft carriers	Principal dimensions regression		
		Ayre regression	Quadratic regression	Three-dimensional regression
Speed	Medium-speed	0.566	0.541	0.483
Displacement	High-speed	0.355	0.350	0.330
	Light	0.541	0.501	0.473
	Medium	0.249	0.239	0.204
Power	Large	5.995×10^{-2}	1.508×10^{-2}	4.561×10^{-3}
	Conventional-power	0.497	0.471	0.448
	Nuclear-power	3.049×10^{-2}	9.943×10^{-5}	4.896×10^{-10}

Tab. 2. *The comparison of estimated speed and real speed*

Name	Displacement [t]	Length [m]	Beam [m]	Real speed [m/s]	Formula to use	speed predicted		
						3-D formula [kn]	quadratic formula [kn]	Ayre formula [kn]
Theodore Roosevelt	82500.0	332.5	40.9	31.0	nuclear powered	31.0	30.9	30.5
Theodore Roosevelt	82500.0	332.5	40.9	31.0	large	30.5	31.4	32.1
John F. Kennedy	61850.0	320.6	39.4	33.0	conventional powered	33.0	33.7	34.7
John F. Kennedy	61850.0	320.6	39.4	33.0	Large	33.5	33.2	32.9
Lexington	39450.0	270.5	32.1	33.0	conventional powered	29.4	29.1	30.3
Lexington	39450.0	270.5	32.1	33.0	medium	31.9	32.5	43.3

studied and obtained through regression analysis of 105 sets of data. These data are classified into different categories based on speed, displacement and power plant. In each category three forms of regression formulas are obtained for speed prediction or for prediction of principal dimensions. The variances of these formulas are also given for correct choice of the formula used in the design.

Acknowledgements

The authors are grateful to the financial support from Chinese NSF (51221961), Programme 973 (2010CB832704, 2013CB036101), High-tech Ship programme and Chinese NSF (51279030).

BIBLIOGRAPHY

1. Carrica P.M., Wilson R.V. and Stern F.: *Unsteady RANS simulation of the ship forward speed diffraction problem*, Computers & Fluids, 35, 6, 545-570, 2006.
2. Gu M.T.: *The principles of ship design*, Shanghai Jiao Tong University Press, Shanghai, 2001.
3. Ireland B.: *The Illustrated Guide to Aircraft Carriers of the World*, Hermes House, London, 2005.
4. Paroka D., Ohkura Y. and Umeda N.: *Analytical Prediction of Capsizing Probability of a Ship in Beam Wind and Waves*, Journal of Ship Research, 50, 2, 187-195(9) , 2006.
5. Schneekluth H. and Bertram V.: *Ship Design for Efficiency and Economy*, Butterworth & Heinemann, Oxford, 1998.
6. Sen A. and Srivastava M.: *Regression Analysis: Theory, Methods, and Applications*, Springer, New York, 1997.
7. Zong Z.: *Information-Theoretic Methods for Estimating Complicated Probability Distributions*, Elsevie Science, Amsterdam, 2006.

CONTACT WITH THE AUTHORS

J.Y. Bi, Ph. D.,
School of Transportation,
Ludong University,
Yantai 264025, China
e-mail: bijunying@gmail.com

Z. Zong, Ph. D.,
School of Naval Architecture Engineering,
Dalian University of Technology,
Dalian 116024, China

POLISH MARITIME RESEARCH 1(81) 2014 Vol 21; pp. 42-53
10.2478/pomr-2014-0007

Investigations of harbour brick structures by using operational modal analysis

Mariusz Żółtowski, Ph. D.,
University of Technology and Life Science in Bydgoszcz, Poland

ABSTRACT

Historic harbour brick objects are subject to large dynamic loads clearly reflected by generated vibration processes. The vibrations may affect state of serviceability of structures by lowering comfort of persons working there as well as possible reaching the level hazardous to safety of the structures. The effect of vibrations to structure is mainly manifested by additional stresses in a given cross-section, which are summed up with those resulting from static loads. Moreover often occur consequences associated with environmental conditions and fatigue of materials which accelerate destruction of the objects. Therefore the dynamic loads may cause damaging effects in buildings of various structural types or even lead to their catastrofic destruction. Judging the necessity of improving the quality assessment methods of building structures for purposes of estimation of their state as well as safety factors for brick structures (see PN-B-03002 standard, p.3.1.3 and 4.6), the author of this work undertook an attempt to investigate destruction process of selected building structures by using the method of operational modal analysis.

Key words: modal analysis; natural vibration frequency; stabilization diagram; structural vibrations

INTRODUCTION

Modern building structures, production of silent-running machines and devices are associated with a high precision level of their manufacturing and appropriate selection of materials that greatly influence their quality, reliability and durability [5, 17, 21].

In investigating real systems (structures, buildings, machines, devices) the main problem is to determine quantity of energy stored, dissipated and transmitted by particular elements of the systems. Knowledge of the quantities serves to assessing material effort, fatigue, diagnostic investigations as well as predicting noise levels, and also to facilitate designing system's elements (e.g. vibration isolation) [3, 10, 15, 21].

Development of measurement methods, especially those for measuring energy quantities, has substantially extended possibility of research on sound radiation by structures as well as made it possible to calculate sound power radiated to a remote field on the basis of close-field measurements. Methods for quantitative and qualitative research on vibroacoustic energy propagation within space of complex boundary areas, have been developed. It has been connected with quantitative assessment of vibroacoustic energy stored in structural elements as well as assessment of energy radiated by the elements and also that transmitted in different ways [2, 7, 14, 20].

Contemporary structural dynamics in building engineering makes use of various research tools from the state identification area such as: boundary element method, finite element method and modal analysis methods, which enable – by modelling and investigating state changes – to better understand behaviour of complex structures, perform their optimization during design process and assess their current, often hazardous, states [4, 6, 12, 20].

Acknowledging necessity of improving research methods dealing with quality of brick building structures for purposes of assessing their state, as well as safety factors for brick structures (see PN-B-03002 standard, p.3.1.3 and 4.6), in this work the author has undertaken an attempt to elaborate research methods for quality assessment of destruction of selected building structures by means of the operational modal analysis method [20, 21].

For this reason an important place is taken by non-destructive tests of brick wall elements in laboratory conditions, presently often used, as well as in-situ tests - by using sclerometric methods (indentation measurement method, rebound measurement method), impulse methods (ultrasonic and hammer ones), radiologic methods (radiographic, radiometric ones), electromagnetic methods (magnetic and dielectric ones) as well as special methods (e.g. electric ones) [1, 3, 5, 15, 20].

It is necessary to improve methods for research on dynamic characteristics of structures especially those exposed on large dynamic loads. New materials and technology methods have been introduced to building engineering as well as novel structural solutions make it possible to increase productivity and quality of products, however they are accompanied with large,

often dangerous dynamic loads. To the problems more and more attention has been presently devoted [11, 15, 16, 17, 20].

In building engineeering, vibrations - a process which accompanies any motion - may be considered in the categories of noxiuos, favourable or information containing vibrations. Vibrations are primary process and their (secondary) effect is acoustic signal in the form of longitudinal sound wave. Vibration and noise processes form the basis for a scientific research area - vibroacoustics. Modern building structures are accompanied by vibroacoustic phenomena which endanger people, environment, and their products. Trends of contemporary engineering and technology connected with rising dynamic loads, rotational speeds, minimization of weights and gabarites, make growing level of vibrations and noise inevitable. The tendencies together with mass application of technical means provide hazards to people, natural and technical environment [2, 7, 10, 13].

In most cases met in practice, analyses of dynamic properties are performed on the basis of analysis of structural model behaviour. Quality of the analysis depends on credibility of the model, which is measured by means of conformation of the object's behaviour and the model, both subject to disturbances of the same kind. Structural model may be built in the process of analytical transformations used for description of system's dynamics or on the basis of results of experiments performed on a real object [3, 8, 9, 20].

Analysis of dynamic properties of structure is carried out mainly by examining behaviour of dynamic model of a given structure, which is realized by using analytical description of quantities which characterize system's dynamics, or experimental methods directly applied to real objects [13, 21].

Novel tools in this research area deal with possible application of modal analysis methods as well as a modern ways of achieving and processing vibration process for assessing quality of brick wall structures and elements which is the subject of considerations in this work. In practical applications they make it possible to better understand behaviour of complex structures, optimize them during design process and assess hazardous states. In the latter area is contained the clue of the investigated problems, i.e. searching for assessment measures for degradation state of brick wall structures and elements, new and aged ones, and often those of unknown destruction state and safety factor values.

Modal analysis is widely used for investigating degradation state and fault location, modification of dynamics of tested structures, description and updating analytical model, as well as monitoring structural vibrations in aircraft and civil engineering. In the subject-matter literature the following notions can be found: modal analysis, experimental modal analysis and operational modal analysis [4, 8, 9, 13, 20]. In the majority of practical applications of modal analysis a multi-channel experiment and complex calculations connected with the processing of measured signals and estimation of model's parameters, are required. The so seen application possibilities allows to distiguish the following kinds of modal analysis [13, 21]:

- theoretical - which requires to solve eigenvalue problem for a given structural model of investigated object,
- experimental - which requires to control identification experiment during which object's motion (e.g. vibration) is excited and measurements of excitation and response are performed in many measuring points,
- operational - which is based on experiment carried out in real conditions, during which only system's response is measured and object's motion results from real operational excitations.

From the beginning of 1990 close attention was more and more paid to possible application of the so called operational modal analysis (OMA) to testing the existing building structures. In this case object's vibrations (of platforms, buildings, towers and bridges) are excited by environment and only system's responses to generated vibrations, differentiated according to a degradation state, are measured.

In this paper are presented research results of differentiated state of building structure, obtained by applying the operational modal analysis. For this aim was used the LMS SCADAS Recorder, the device which combines features of analyzer and classical recorder, as well as LMS Test.Lab software serving for performing the tests and vizualizing their results [19].

VIBRATIONS IN DESCRIPTION OF STRUCTURES

Vibroacoustics is a domain of science which deals with any vibration, acoustic and pulsation processes occurring in nature, building engineering, technology, machines, devices, communication and transport means, i.e. in the environment. Among the tasks of vibroacoustics the following may be rated [16, 18]:

- the identification of vibroacoustic energy sources which consists in location particular sources within structure of object, machine or environment, determination of their characteristics and mutual relationship, determination of vibroacoustic power as well as character of vibration and sound generation;
- the elaboration of vibroacoustic energy propagation paths in real structures and environment (buildings, machines, objects etc), theory of energy transmission and transformation, passive and active control means for phenomena, methods for analyzing and testing phenomena at the border area between wave and discrete approach;
- the elaboration of control methods for vibroacoustic energy (emission, propagation) in building structures, machines and environment, and also elaboration of methods for steering the phenomena, that is associated with active methods which are presently under development worldwide;
- the use of vibroacoustic signals for purposes of technical state diagnostics as they constitute a good carrier of information on state of object's destruction as well as technological process under way (vibroacoustic diagnostics);
- the vibroacoustic synthesis of objects, performed to obtain optimum vibroacoustic activity (structural, kinematic, dynamic one), which covers synthesis of parameters used in active methods for vibration and noise mitigation, and structural, kinematic and dynamic synthesis of objects and machines;
- the active applications of vibroacoustic energy to realizing various technological processes, beginning from ultrasonic welding and cleaning, transport of materials and machine elements along technological lines, consolidation of moulding sands, shaking out and cleaning castings, ending at consolidation of soils and concretes.

Vibroacoustic process may be presented as:

- generation of time-varying forces acting onto a structure and its environment;
- propagation and transformation of energy in different environment structures;
- sound radiation through material elements of environment.

In analysis of vibroacoustic processes the following is taken into account:
- time – space distribution of run of energy coming from a (primary), source;
- response of a system (structure, liquid) as well as energy transmission through propagating media;
- mutual relationship between sources.

The notion of measurement means a process of acquisition and transformation of information about a measured quantity to get – by comparing it with measurement unit – a quantitative result in a form most comfortable to be acquired by human sense organs, its transmission in space or time (recording), mathematical processing or application to steering. To carry out such measurements is necessary for [2, 20]:
- the determining of time runs of vibrations and their parameters to determine kinds of the vibrations, their characteristic quantities and to perform detail analysis;
- the finding of vibration sources and places of their occurrence;
- the determining of characteristic features of systems (e.g. determining loads during vibrations and their dependence on object's parameters, its shape, dimensions, material properties etc);
- the minimizing of vibrations harmful for reliable operation of devices and their human operators;
- the determining of harmfulness level of occurring vibrations and the implementing of preventive measures.

In practice, vibration signal is more often used than noise one, due to its easiness of transferring and exactness of measuring [5, 16].

System's vibrations resulting from upsetting state of equilibrium of an object which then moves under action of elastic, gravity or friction forces, are called free vibrations. In one-degree-of-freedom (d.o.f) systems the upsetting of state of equilibrium is characterized by the initial conditions: the initial position x_0 and initial velocity v_o. If the system is of one d.o.f. (single mass m) and linear characteristics of elasticity (k) and damping (c) – Fig. 1, and the harmonic excitation force F(t) acts onto it, then its motion equation is expressed by the following formula:

$$m\ddot{x} + c\dot{x} + kx = F(t)$$

which represents the equation of harmonic vibrations or harmonic oscillator vibrations.

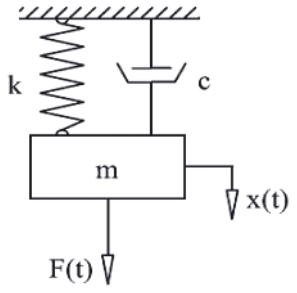

Fig. 1. *One-d.o.f. system to perform translation motion*

As results from it, natural vibration of one-d.o.f system is entirely determined by natural frequency of vibration. Amplitude of the vibration depends on initial conditions but natural frequencies and vibration period do not depend on them. The solution of the equation (i.e. translation) takes the following form:

$$x = A\sin(\omega_0 t + \varphi)$$

By differentiating this equation the vibration velocity is obtained:

$$\dot{x} = A\omega_0\cos(\omega_0 t + \varphi)$$

which is also a periodical function of time, of the same period as that of translation. And, by differentiating the velocity equation the value of vibration acceleration is obtained:

$$\ddot{x} = -A\omega_0^2 \sin(\omega_0 t + \varphi) = -\omega_0^2 x$$

It is a periodical function of time, of the same period as that of translation and velocity. Acceleration is proportional to translation and directed against it, i.e. it always is pointing position of equilibrium.

The parameters: a, v, x – are those of vibration process,which convinces that the vibrations properly describe state of structure.

In the low frequency range, building structures can be modelled by means of discrete systems of a few d.o.f.s – and rather often – one – d.o.f system. The discrete system – in contrast to continuous one – is characterized by point distribution of mass, stiffness and damping and dimensions of the elements do not play any role. Number of d.o.f.s determines number of independent coordinates which should be introduced to get unambiguous description of system's motion (number of d.o.f.s is equal to number of mass elements in the system in question). In practice, the system presented in Fig. 1 can model:
- the building machine of mass **m**, seated on shock absorbers (**k, c**) and fastened to a big mass fundation;
- the work machine of mass **m**, seated on shock absorbers (**k, c**) and moving along an even road;
- the high building structure (high chimney, mast) under wind action.

Many systems can be preliminarily modelled by using one - d.o.f. system, to search for its properties by means of mathematical description and analysis of solutions of equations which describe it. It is possible to investigate system's properties by using the vibration parameters ($\ddot{x}$, $\dot{x}$, x) which – being results of solutions of mathematical description of the model – interchangeably describe the same properties but from the viepoint of the system's vibration measuring process. In industrial practice it is common to measure vibrations instead to perform complex theoretical considerations.

The use of vibrations for testing quality of building structures results from the following reasons:
- vibration processes reflect physical phenomena occurring in structures (displacements, stresses, fractures), on which degree of their destruction (serviceability) and correct operation depends, that results from character of spreading the vibration process;
- easiness of performing measurments of vibration processes in normal operational conditions of an object without necessity of exclusion it from service and performing special preparation, hence it makes it possible to assess its state of destruction without disassembling the structure;
- vibration processes are characterized by a high speed of information transmission per time unit, defined by Shanon formula:

$$C = F\lg_2(1+\frac{N_S}{N_Z})$$

dependening on spectrum band of the process F and the rate of the useful signal power N_S and the disturbing noise power N_Z;

- vibration processes are characterized by a complex structure of time, amplitude and frequency, which, if only correctly processed, makes it possible to assess state of entire structure as well as its particular elements.

During service of structure, due to occurrence of many external factors (excitations from the side of environment and other structures) and internal factors (ageing, wear, interaction of elements) in the structure take place disturbances of its equilibrium state, which propagate within elastic body, i.e. material of which the structure is made. The disturbances are of dynamic character and maintain equilibrium conditions between inertia, elasticity, damping and excitation state. Consequently, it results in energy dissipation of waves, their deflection, reflection and mutual superimposing. Existence of sources and propagation of disturbances cause vibration of structural elements and surrounding environment to occur.

When separating - during dynamic state analysis - the input processes X, object's structure A and output processes S, one should remember about their random character - Fig. 2.

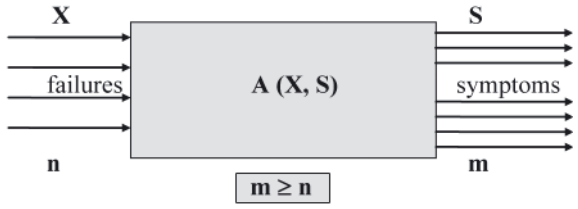

Fig. 2. *Schematic model of an object and its description*

Internal input taken as a set of excitation quantities which determine object's structure (shape, manufacturing quality, clearances etc) and a way of interaction of its elements is formed in random conditions during manufacturing, that reveals object's random properties in service.

External input which determine conditions of interaction between structure elements and other elements of a system (changes of loads, speed, environment impact) is also practically of a random character.

Many possible occurrences of randomness and disturbances result in additional assumptions dealing with inputs and occurring transformations of states of destruction of structures. They concern with assumptions on linearity, stationarity and ergodity of models of objects and processes [6, 12, 19, 20].

As a result of existence of the input and realization of transformation of states which represent processses occurring in structure, many measurable characteristic symptoms contained in output processes emitted from structure, are obtained. The processes form the basis for elaboration of a signal generation model which determines a way of forming, functioning and changing states of object's destruction [21].

Features of model of transition of vibration signals for building structure in random disturbance conditions

The assumptions

1. State of structure is unambigously determined by the characteristic signal $\varphi_i(t, \theta)$ generated seperately at every excitation. The signal undergoes changes within the dynamic (short) time t and evolution within the (long) time θ.
2. The characteristic signal is composed of the determined process φ_o and random one n and its intensity and dynamics characterize state of destruction of structure. Hence, during i-th excitation the following signal is generated:

$$\varphi_i(t, \theta) = \varphi_0(t, \theta) + n_i(t, \theta)$$

3. The transformed characteristic signal which represents internal actions – material destruction – is achieved in the form of y(t, θ) and, in the simplest case, it constitutes response of a tested material of the characteristics h(t, θ) to the excitation x(t, θ). Taking into account the spatial wideness (dimensions) r of structure one can write as follows:

$$y(\theta, r) = \sum_{i=1}^{\infty} \varphi_i(t, \theta, r) * h(t, \theta, r) * \delta(t - iT)$$

4. The output processes from structure reciprocately influence (selectively) destruction processes and consequently state of structure (element) due to positive destructive feedback, that deforms the initial signal $\varphi_i(t, \theta)$.
5. For a given value of service time, θ_i = const, all building objects are considered to be linear, stationary systems whose features are unambiguously described by the impulse response h(t, θ, r) or its tramsforms: Laplace operator, H(p, θ, r), or Fourier spectrum, H(jω, θ, r).

The above described set of assumptions which leads to a model of generation of signals can be presented in the form of the schematic diagram shown in Fig. 3.

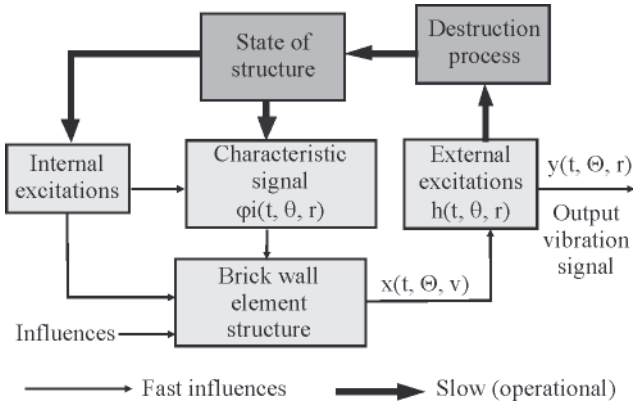

Fig. 3. *Model of signal transmission through tested brick wall element*

The output vibration signal at any reception point can be approximately expressed by the following formula [2, 16]

$$y_k(\theta, r) = \sum_{i=1}^{k} a(k) h_i(t, \theta, r) * [u_i(t, \theta, r) + n_i(t, \theta, r)]$$

where:
- the impulse transition function **h(*)** which covers material destruction properties;
- **a(k)** - term which provides different summation weights connected with the reception place r.

The above presented way of interpretation of the output signal (θ, r) is – in the general case of excitations of periodical service objects - correct, but not always so simple as that shown in Fig. 4 where is illustrated occurrence of excitations due to random actions of wind onto high buildings, chimneys, towers, and record of relevant response in the form of complex vibration signal.

The output signal received in an arbitrary point of structure is the weighted sum of responses to all elementary events φi(t, θ, r) which occur always in the same sequence in particular points of the dynamic system of the pulse transition function h(t, θ, r).

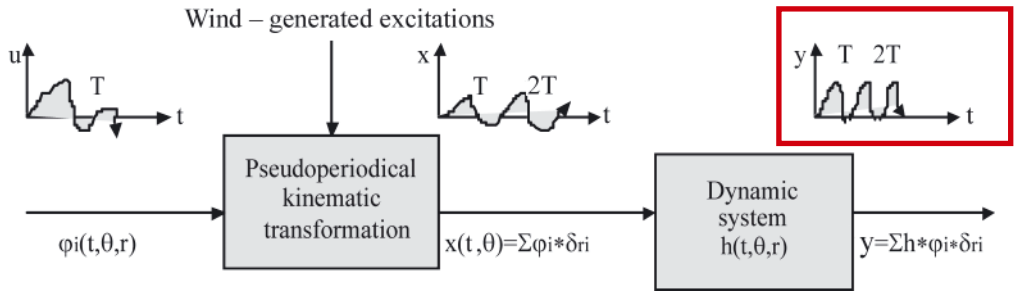

Fig. 4. *Transformation of the characteristic signal φi(*) into the output signal y(*), considered to be a model of signal generation in objects under environmental excitation [7, 21]*

The influences sum up together and subject to additional transformation along different reference axes, and a change of signal reception point r is associated also with change of transmittance.

Model of vibration signal transmitting through tested structures or brick wall elements is described practically by FRF function which is determined by means of experimental modal analysis in the form of ratio of vibration excitation force and vibration acceleration amplitude at output. The transmittance H(f) defined as the response-to-excitation ratio is inversion of the FRF function.

The indicated properties of the elaborated model of signal transition through tested materials were further used for assessing changes of degree of degradation of structures or brick wall elements during testing transition of vibration signals through various structures of brick wall elements and segments.

Modal analysis is widely applied to removing damages resulting from vibrations, modifying structure dynamics, updating analytical model or state control, and also used for monitoring vibrations in aircraft industry and civil engineering [7, 9, 13, 19].

Theoretical modal analysis is defined as a matrix eigenvalue problem dependent on matrices of mass, stiffness and damping. It requires the eigenvalue problem for an assumed structural model of investigated structure to be solved [13, 21]. The determined sets of natural frequencies, damping coefficients for the natural frequencies and forms of natural vibrations make it possible to simulate behaviour of structure under arbitrary excitations, choice of steering means, structural modifications and other issues.

Analysis of natural fequencies and vectors is obtained on the basis of motion equations (after neglecting terms which contain damping matrix and external load vector). Then the motion equation of natural vibrations obtains the following form:

$$B\ddot{q} + Kq = 0$$

For one d.o.f. system its solution is as follows:

$$q(t) = \vec{q}\sin(\varpi t + \varphi)$$

where:

$\vec{q}$ - vector of amplitudes of natural vibrations.

On substitution of the above given equation and 2nd derivative to the motion equation the following is obtained:

$$(-\varpi^2 B + K)\vec{q}\sin(\varpi t + \varphi) = 0$$

The equation is to be satisfied for arbitrary instant t, then the set of algebraic equations is yielded as follows:

$$(K - \varpi^2 B)\vec{q} = 0$$

$$(k_{11} - \omega^2 m_{11})q_1 + (k_{12} - \omega^2 m_{12})q_2 + \\ + \cdots + (k_{1n} - \omega^2 m_{1n})q_n = 0$$

$$(k_{21} - \omega^2 m_{21})q_1 + (k_{22} - \omega^2 m_{22})q_2 + \\ + \cdots + (k_{2n} - \omega^2 m_{2n})q_n = 0$$

$$\ldots\ldots\ \ldots\ldots\ \ldots\ldots\ \ldots\ldots\ \ldots\ldots$$

$$(k_{41} - \omega^2 m_{41})q_1 + (k_{42} - \omega^2 m_{42})q_2 + \\ + \cdots + (k_{nn} - \omega^2 m_{nn})q_n = 0$$

This way was produced the set of linear homogeneous algebraic equations, which has non-zero solution only when the condition:

$$\det(K - \varpi^2 B) = 0$$

is fulfilled.

On transformations the n-order polynomial is obtained. Among its roots multifold ones may be present, and the vector built from the set of frequencies ϖ^2 ordered according to increasing value sequence is called the frequency vector, and the first frequency is called the fundamental one [21].

$$\varpi = [\varpi_1, \varpi_2 \ldots, \varpi_n]$$

The theoretical modal analysis is mainly used in design process, i.e.when it is not possible to perform tests on objects.

The traditional experimental modal analysis (EAM) makes use of input (excitation) to output (response) relation and it is measured in order to assess modal parameters consisted of modal frequencies and damping. However the traditional EAM has some limitations such as:

- in the traditional EAM, artificial excitation is used to measure vibration frequencies,
- the traditional EAM is usually performed in laboratory conditions.

However in many cases a real state of degradation may greatly differ from those observed in laboratory environment. In experimental modal analysis the identification experiment consists in exciting object's vibrations at simultaneous measuring excitation force and system's response usually in the form of vibration acceleration amplitude.

Beginning from 1990 more and more attention has been paid to application of the operational (service) modal analysis (OMA) to the testing of existing building structures. In this case the environment serves as a vibration exciter

for platforms, buildings, towers, bridges etc. Only system's responses to vibrations generated by the environment are measured, Fig. 5.

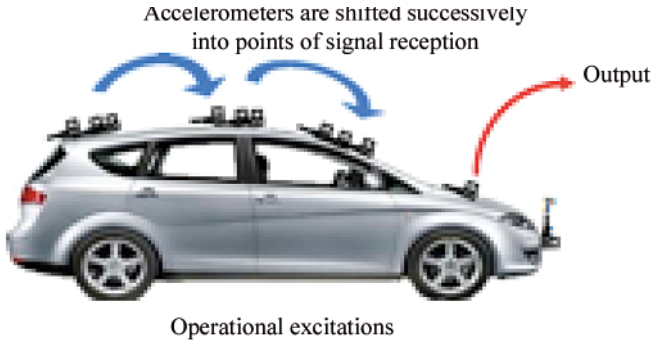

Fig. 5. *Essence of the operational modal analysis*

The OMA is very attractive for industrial testing due to its many merits such as:
- it is cheap and allows to fast carry out measurements;
- lack of the problem with artificial excitation of vibrations;
- assessing dynamic features of entire existing system is possible;
- operation of the simple measuring instruments is easy;
- testing results which are more representative than those from laboratory, can be obtained;
- because of a broad band of random excitation testing results are more representative.

As a result of modal analysis, is obtained a modal model of structure, which can be used for solving many engineering problems, e.g. synthesis of building systems, analysis of structure behaviour under action of various excitations, modification of dynamic properties, minimization of acoustic energy radiation, fatigue analysis.

The modal model of tested building structure (or its elements) is considered as an ordered set of natural frequencies, damping coefficients as well as vibration forms for particular loading excitations [6, 13, 20].

By making use of the statement that state of destruction of object (tested material) can be alternatively described, instead to model changes in the categories (**m, k, c**), by the vibration description in the categories (**a, v, x**)] - as is the case in the tests in question, one could assess state of degradation of structures or brick wall elements by means of natural vibration frequencies directly resulting from modal analysis.

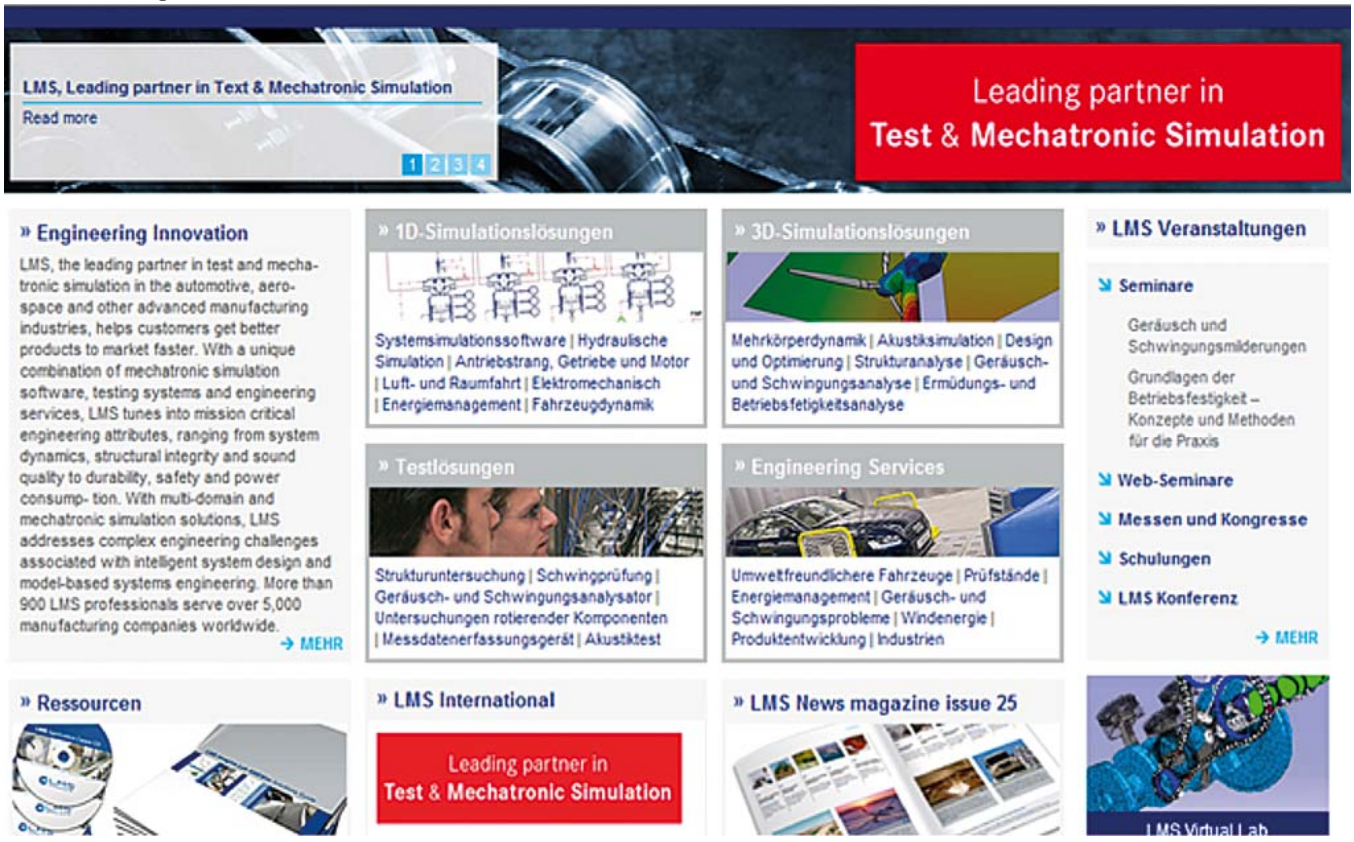

Fig. 6. *The web site and LMS instrument*

Determining individual modal models for partial excitations in a tested element and further summing up them for the entire object's structure, one obtains an evolutionary model which unambiguously describes changes in state estimators in varying load conditions. This way is revealed fractal nature of energy transformation processes, which makes possible ways of approximating description of real world, more perfect.

MEASUREMENT SOFTWARE

The recorded vibration signals (excitations and responses) are subject to rather complicated processing for purposes of

determination of measures of destruction state of brick wall elements and structures [13, 21].

For measuring time runs of system's excitation and response as well as determining modal model parameters during the testing the LMS TEST.XPRESS instrument, the most modern measuring device, was used (Fig. 6). The device and relevant software makes it possible to easily perform modal analysis of brick elements as well as another building structures.

The software in question is equipped with a user-friendly interface. After starting the software one should open a new project and call it according to its task. Beginning from this moment all the performed measurements will be recorded in this active project - Fig. 7.

The first step is to define a system in the aspect of calibration of measurement channel. For purposes of the tests performed during the present stage the action was started from the defining of a number of active measurement channels. Their number is limited only by a number of inputs on the measurement card, which is different for different models of measurement segments.

The dialogue window open during measurements is presented in Fig. 8.

The LMS software makes it possible to produce a stabilization diagram for a given single measurement (option: „Selected function") as well as to produce a stabilization diagram from all measurements together (option: „SUM"). The example

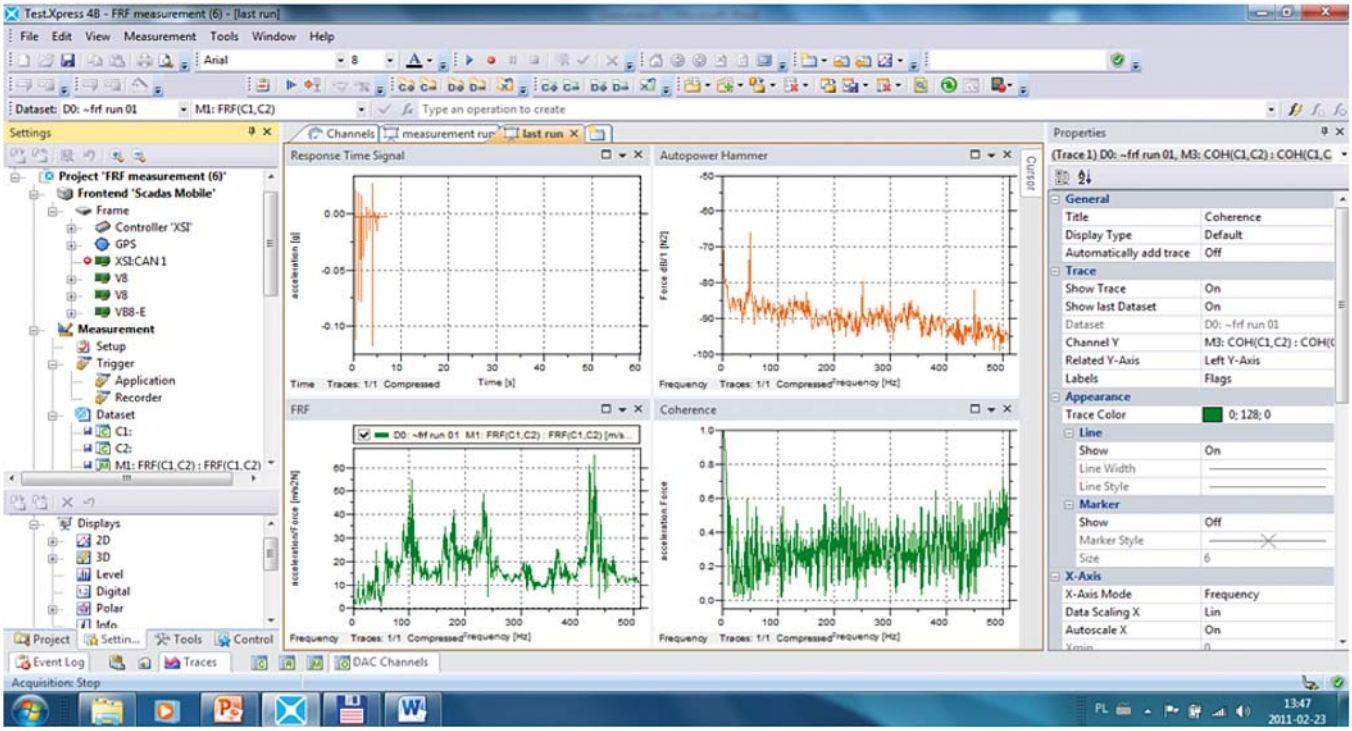

Fig. 7. Interface of LMS software

Fig. 8. The main dialogue window during measurements

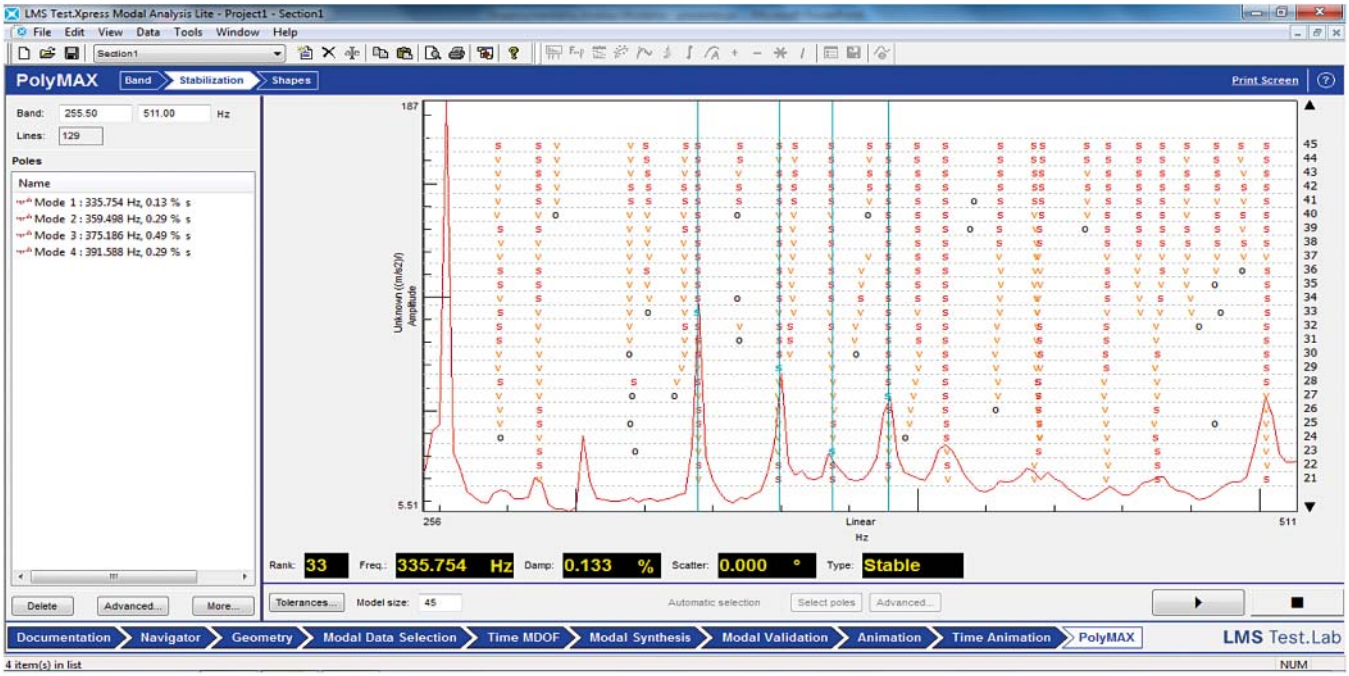

Fig. 9. *„Stabilization" window displaying a stabilization diagram*

stabilization diagram is shown in Fig. 9. where poles are marked as follows: S – stable, V – modal vector, D – damping. The option „Mode" available in the software is capable of visualizing deformations of geometrical model.

In Fig. 10 is shown testing instrumentation (modal hammer, LMS SCADAS Recorder) and examples of materials selected for testing, and a view of tested building structure.

Fig. 10. View of materials,a fragment of structure used for testing, and testing instrumentation

The tests were performed for two existing building structures. The first of them was a brick wall of 18 cm in thickness and 200 cm in height. The wall structure was tested both in place of a damage which produced drop of strength and endangered safety of the structure, and – for comparison – the same wall structure but in place of its correct (serviceable) state. (Fig. 11).

Fig. 11. *View of both serviceable and damaged brick wall structure*

In the first case gauges were placed on a surface without any symptoms of faults and then measurements were performed for the structure modelled as that serviceable. Next, the gauges were fixed between the existing fracture on the wall and for this arrangement of gauges the measurements were done.

Another existing building structure under testing was a reinforced concrete wall of a didactic building, deriberately structurally weakened by two cuts (scratches) made to change its stiffness. For purposes of testing by using operational modal analysis, 8 measuring channels were defined. In compliance with the theoretical assumptions of the modal analysis the first response gauge was defined to be reference one, and the next seven - the structural response gauges. Owing to that it was possible to determine the cross-correlation function for signal transition through tested structure, which is the basis for signal processing. Preparation of the object to the tests consisted of arranging and fastening the gauges for measurements, Fig. 12, their connection with the measuring device and calibration of the entire system.

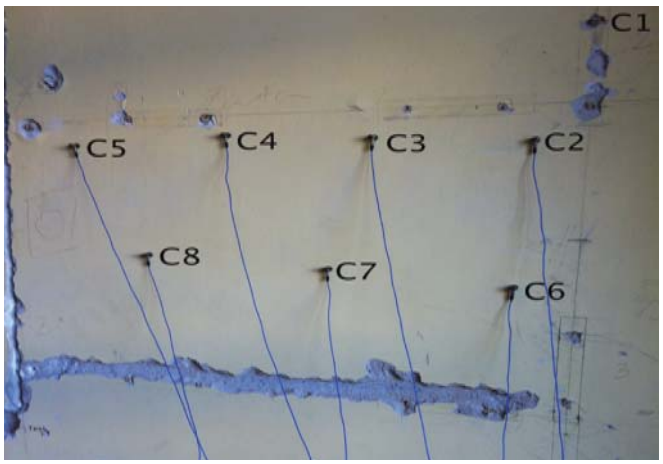

Fig. 12. *View of the tested wall structure and arrangement of the gauges*

RESULTS OF THE TESTS

Results of the tests are presented in the following sequence: first, for the wall shown in Fig. 13, where the cross-corelation functions were measured between the reference point (C1 gauge) whose place was selected according to the theory of operational modal analysis, and seven gauges assumed in the model and placed on the structure in question. On the basis of the generated cross-power spectrum function it was possible, in the further stage of signal processing, to generate stabilization diagrams and next fundamental vibration frequencies.

To visualize possible changes of structure degradation the measurements were performed in a few variants. It was at first the measurements made for serviceable and unserviceable structure without any external interference, and then the comparative tests carried out for serviceable and unserviceable structure at simultaneous excitation of vibrations by rhythmic knocking onto structure with the use of the modal hammer. Each test lasted 30 seconds.

Below, are presented selected results of the tests in the form of visualization of stabilization diagrams and deformations occurring in different dynamic states of the structure.

Near, is presented Tab. 1 which contains the set of the natural vibration frequencies generated for measuring different states of degradation of the existing brick structure.

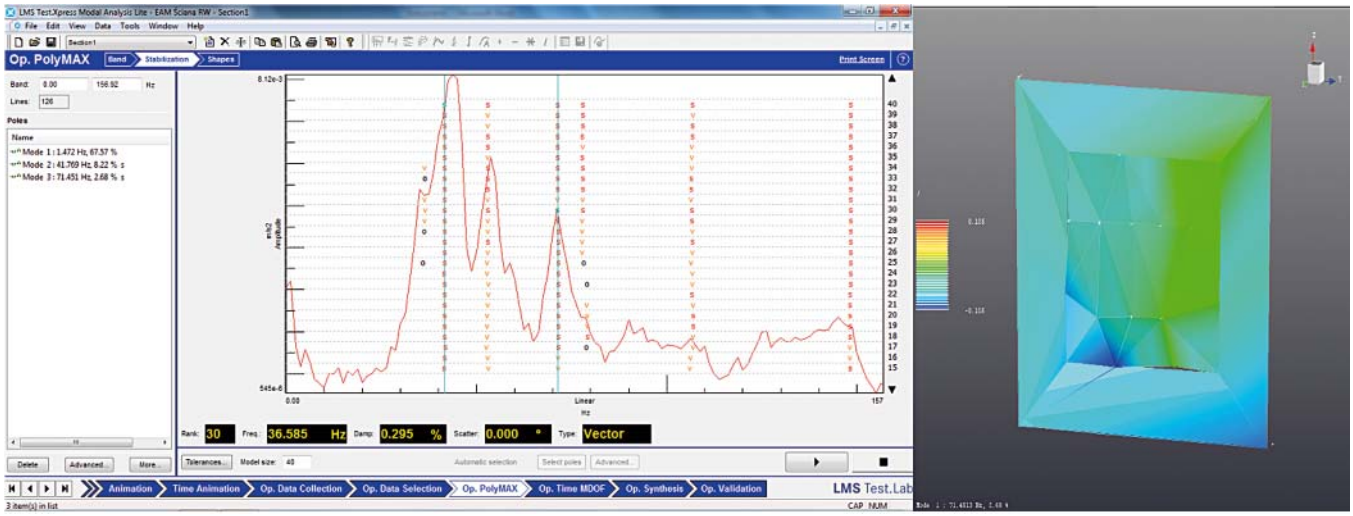

Fig. 13. *Test results for the wall without damages, under excitations*

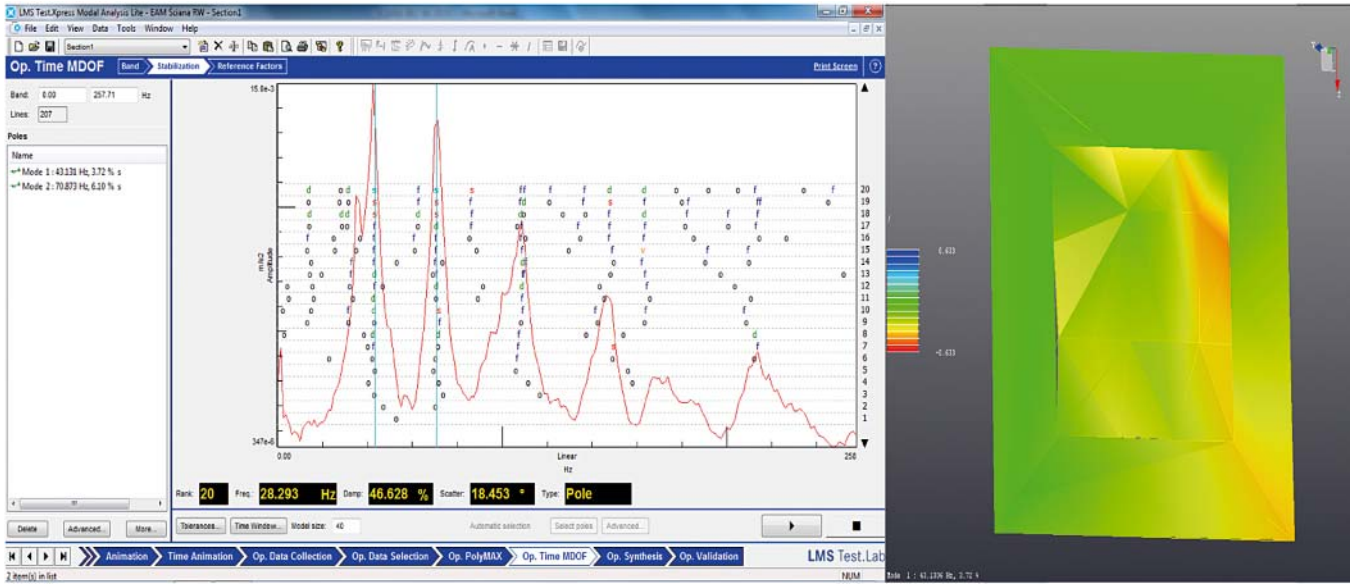

Fig. 14. *Test results for the wall with one scratch, under excitations*

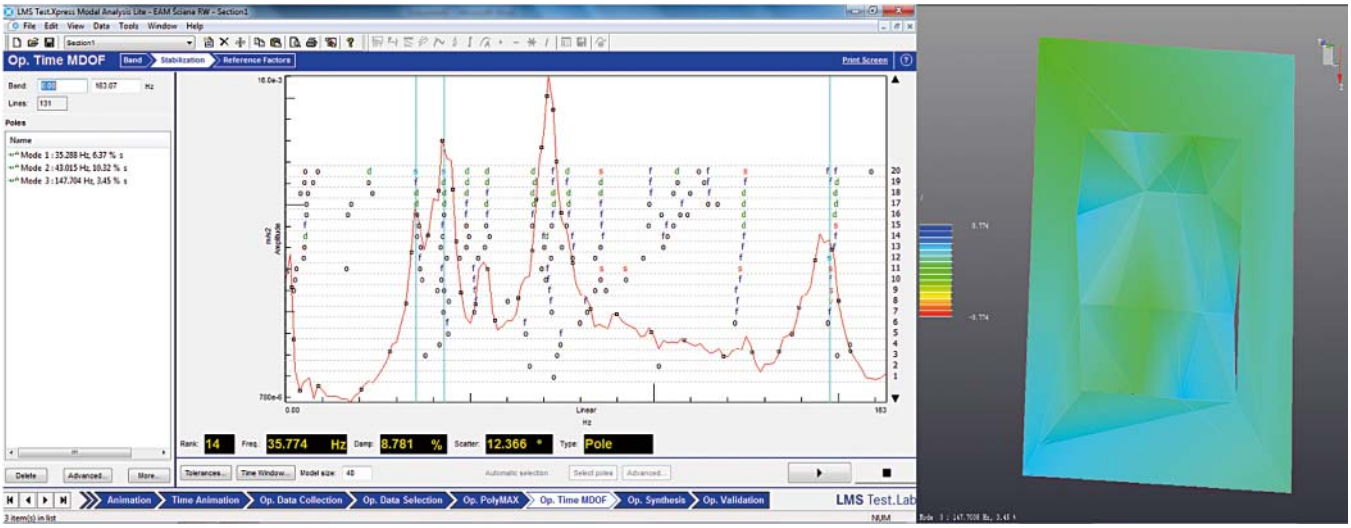

Fig. 15. Test results for the wall with two scratches, under excitations

Tab. 1. Set of natural vibration frequencies for different states of degradation of the brick structure

EXCITATIONS	Serviceable wall	Wall with one scratch	Wall with two scratches
without excitation	71.388Hz	39.999Hz	29.831Hz
without excitation	81.699Hz	40.806Hz	39.207Hz
with excitation	43.526Hz	41.271Hz	70.844Hz
with excitation	81.699Hz	147.588Hz	110.296Hz

Quantitative results of testing the brick wall without damages as well as that with damages (see Fig. 13) performed with the use of the method of operational modal analysis are presented in successive figures. The complete set of natural vibration frequencies characteristic for the tested states of degradation of the wall, obtained with the use the experimental and operational modal analysis, is presented in Tab. 2.

Below, is presented Tab. 2 which contains the set of natural vibration frequencies generated during testing the existing brick wall.

Tab. 2. The complete set of natural vibration frequencies for the tested brick wall

EXCITATIONS	Serviceable element	Damaged element
with excitation (EAM)	865.612Hz	1025.813Hz 1060.857Hz 1112.476Hz 1121.607Hz
without excitation (OAM)	0.777Hz	2.289Hz 4.446Hz 15.417Hz
with excitation (OAM)	0.805HZ	0.772Hz 14.043Hz

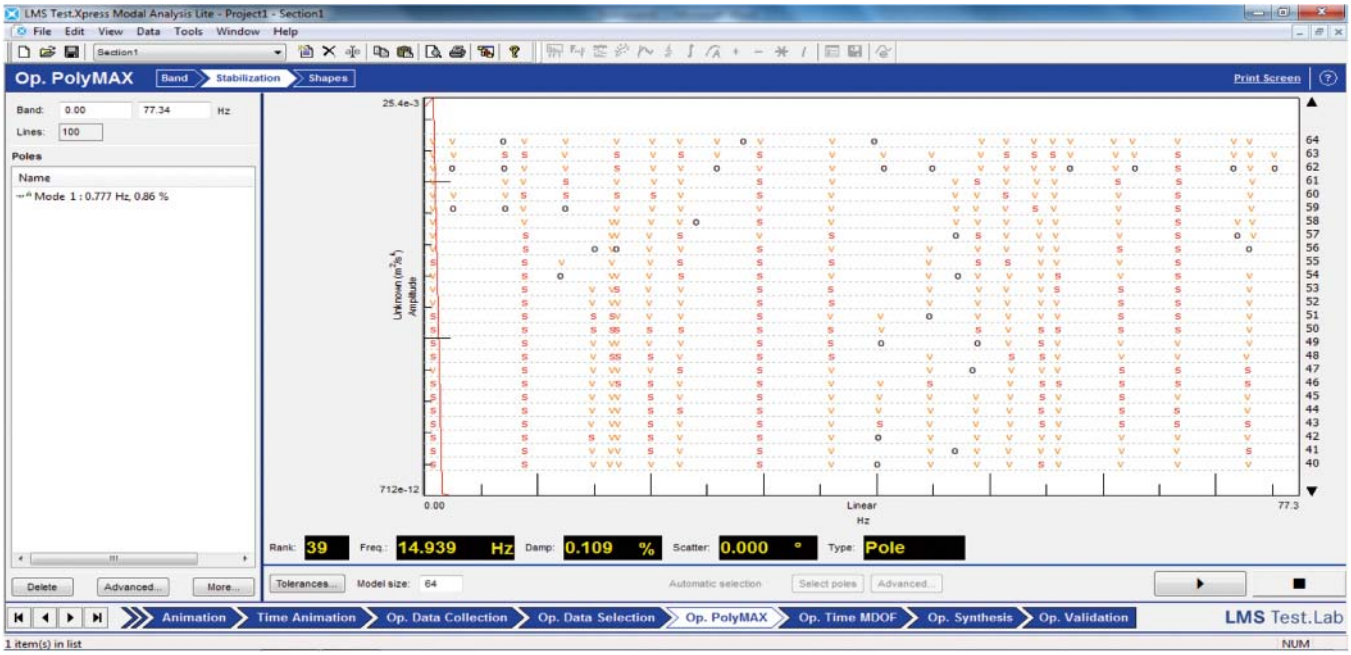

Fig. 16. Stabilization diagram for the serviceable brick wall (OAM)

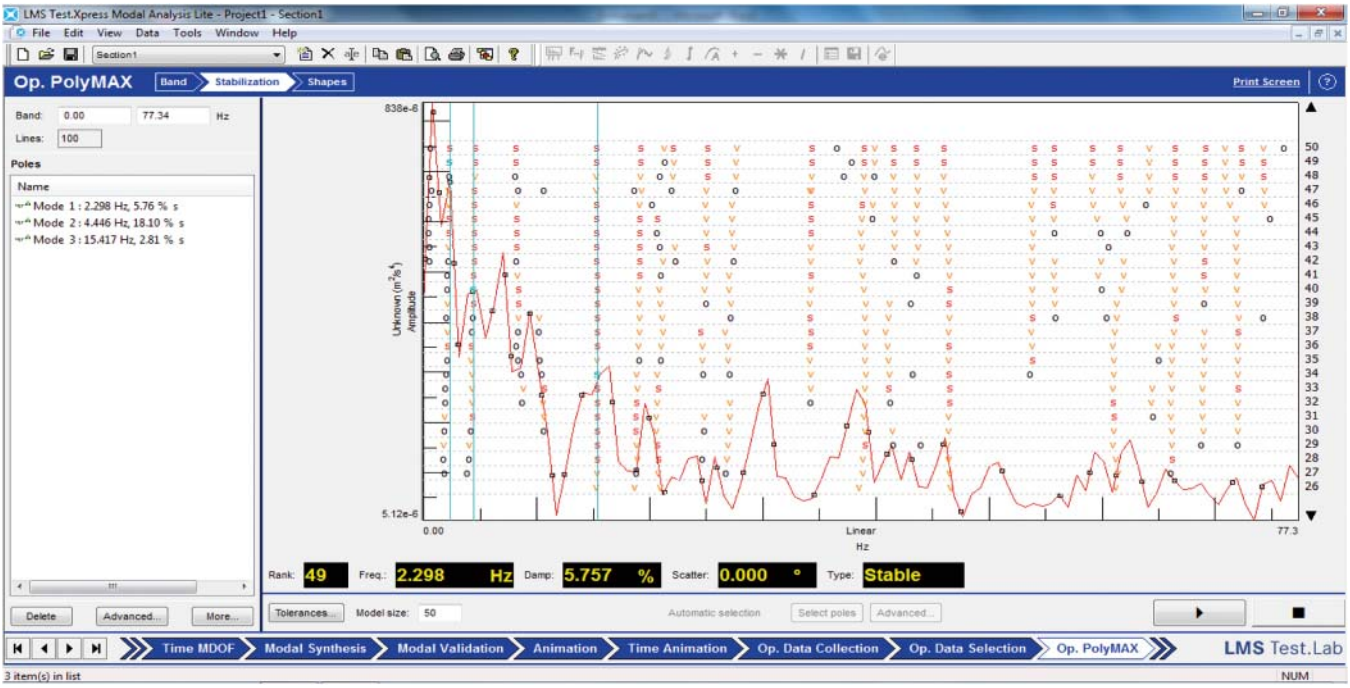

Fig. 17. *Stabilization diagram for the damaged brick wall (OAM)*

CONCLUSIONS

The searching for of non-destructive testing methods for buildings and harbour structures indicates that to apply modal analysis to assess their degradation is possible, that has been shown in this paper. Out of different available kinds of form of modal analysis the operational modal analysis was used to the reported investigations on structure destruction.

The presented results of the testing indicate that it is possible to distinguish degradation features of brick materials, that show influence on possible assessment of hazards and their strength aspects. The in-situ and operational tests confirmed that the LMS instruments are useful for performing operational modal analysis of real building structures.

From the presented test results it can be preliminarily concluded that for the serviceable brick wall structures the generated natural vibration frequencies were contained within the range of 70 ÷ 80Hz. For the damaged structures the generated natural vibration frequencies were of much lower values, i.e. in the range of 30 ÷ 40Hz. The implemented graphic presentation of deformations resulting from action of natural vibrations of a given frequency is useful for qualitative assessment of degradation state.

The practically verified sensitivity of assessment of modal analysis to degree of brick structure degradation, reveals – in a practically satisfactory degree – differences between serviceable structure and damaged one. Therefore it becomes possible to determine hazards to a building (harbour) structure on the basis of examining values of frequencies of natural vibrations and their forms by using the operational modal analysis.

BIBLIOGRAPHY

1. Batel M.: *Operational modal analysis – another way of doing modal testing.* Sound and Vibration, August 2002.
2. Bishop R., Johnson D.: *The mechanics of vibration.* Cambridge University, Press, 1980.
3. Brandt S.: *Data analysis* (in Polish). Wydawnictwo Naukowe PWN (Scientific Publishing House), Warszawa 1999.
4. Brown D., Allemang R.: *Multiple Input Experimental Modal Analysis*. Fall Technical Meeting, Society of Experimental Stress Analysis, Salt Lake City, UT, November 1983.
5. Brunarski L.: *Non-destructive methods for concrete testing* (in Polish). Arkady, Warszawa 1996.
6. Formenti D., Richardson M.: *Parameter estimation from frequency response measurements using rational fraction polynomials (twenty years of progress).* Proceedings of International Modal Analysis Conference XX, Los Angeles, CA, February 4-7, 2002.
7. Ibrahim S., Mikulcik E.A.: *Method for the direct identification of vibration parameters from the free response.* Shock and Vibration Bulletin, Vol. 47, Part 4, 1977.
8. Peeters B., Ventura C.: *Comparative study of modal analysis techniques for bridge dynamic characteristics.* Submitted to Mechanical Systems and Signal Processing, 2001.
9. Pickrel C.R.: *Airplane ground vibration testing – nominal modal model correlation*. Sound and Vibration, November 2002.
10. Richardson M.: *Is it a mode shape or an operating deflection shape?* Sound and Vibration, February 1997.
11. Richardson M.: *Structural dynamics measurements.* Structural Dynamics @ 2000: *Current status and future directions*, Research Studies Press, Ltd. Baldock, Hertfordshire, England, December 2000
12. Shih C., Tsuei Y., Allemang, R., Brown D.: *Complex mode indication function and its applications to spatial domain parameter estimation.* Proceedings of International Modal Analysis Conference VII, January 1989.
13. Uhl T.: *Computer-aided identification of mechanical structure models* (in Polish). WNT (Scientific Technical Publishers), Warszawa 1997.
14. Williams R., Crowley J., Vold H.: *The multivariate mode indicator function in modal analysis*. Proceedings of International Modal Analysis Conference III, January 1985.
15. Vold H., Schwarz B., Richardson M.: *Display operating deflection shapes from non-stationary data.* Sound and Vibration, June 2000.
16. Vold H., Kundrat J., Rocklin G.A.: *Multi-input modal estimation algorithm for mini-computers.* S.A.E. paper No. 820194, 1982.
17. Żółtowski M.: *Identification of vibration hazards to building objects* (in Polish). Budownictwo Ogólne (General Building), ZN ATR, Bydgoszcz 2005
18. Żółtowski M.: *Measurements of acoustic properties of materials* (in Polish). Diagnostyka, PTDT, Polska Akademia Nauk (Polish Academy of Sciences), vol.33, 2005

19. Żółtowski M.: *Selection of information on identification of the state of machine*. UWM, Acta Academia 310, Olsztyn 2007.
20. Żółtowski M.: *Computer-aided management of system's operation in production enterprise. Integrated management* (in Polish). Oficyna Wydawnicza Polskiego Towarzystwa Zarządzania Produkcją (Publishing House of Polish Society on Production Management), vol. 2, Opole 2011.
21. Żółtowski M.: *Modal analysis in the testing of building materials* (in Polish). ITE-PIB, Radom 2011.

CONTACT WITH THE AUTHOR

Mariusz Żółtowski, Ph.D.,
University of Technology and Life Science
in Bydgoszcz,
Ks. Kordeckiego 20,
85-225 Bydgoszcz, POLAND
mazolto@utp.edu.pl

POLISH MARITIME RESEARCH 1(81) 2014 Vol 21; pp. 54-61
10.2478/pomr-2014-0008

Monitoring of underdeck corrosion by using acoustic emission method

Krzysztof Emilianowicz, M. Sc.,
Gdańsk University of Technology, Poland

ABSTRACT

This paper presents first short characteristics of underdeck corrosion process as well as a problem of its monitoring. Next is described an acoustic emission (AE) method elaborated by Department of Ship Technology, Quality Systems and Material Engineering, Gdańsk University of Technology in cooperation with partners of CORFAT project realized within 7th EU Frame Program. Further are presented short characteristics of the emission process, used measuring instrumentation of Vallen Systeme GmbH, as well as TESTER, corrosion testing device, and a corrosion solution used in the tests. Finally, results of the tests performed on selected marine units, are presented.

*1*GUT - Gdańsk University of Technology*
*2*TÜV- Austria*
*3*TESTER - a device used for simulation of corrosion processes without destruction of tested material surface.*
*4*Corrosive solution - a solution which catalizes corrosion processes in the tester*
*5*SMW S.A.- Naval Shipyard Co.*

Key words: underdeck corrosion; acoustic emission (AE); corrosion tester; marine units

INTRODUCTION

Underdeck corrosion - It is impossible to unambiguously define this notion as - depending on a place of its ocurring - it may be of a typical electrochemical, chemical or fatigue character. Usually it may be:
- pitting corrosion,
- fatigue corrosion,
- oxygen corrosion,
- microbiological corrosion.

The most obvious places of appearing corrosion wastage are tanks of any kind, e.g.:
- ballast tanks,
- fresh water tanks,
- tanks for crude oil and oil products,
- sewage tanks.

Also, it may happen in such places as e.g.:
- connections of decks,
- connections of underdeck stiffeners,
- connections of stiffeners with deck plating,
- drains from heat exchange devices.

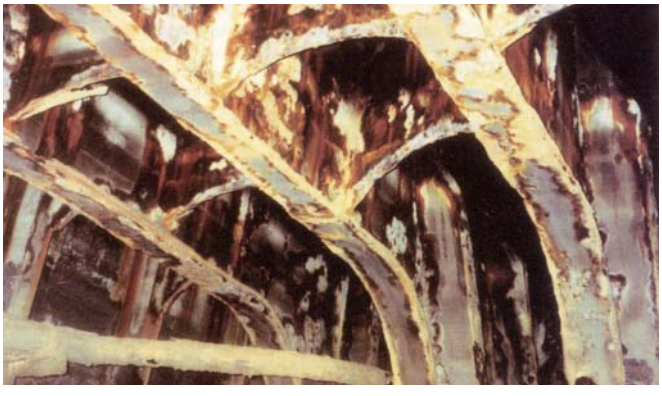

Fig. 1. *An example of ship underdeck corrosion [5]*

As results from the above given description this is a serious problem as the places exposed to such destruction are as a rule hardly accessible or non-accessible at all during ship (unit) service. The question hence arises: how to monitor the process ?

This work has been aimed at presentation of a method which is enough promising and providing suffciently good results to make monitoring the process possible.

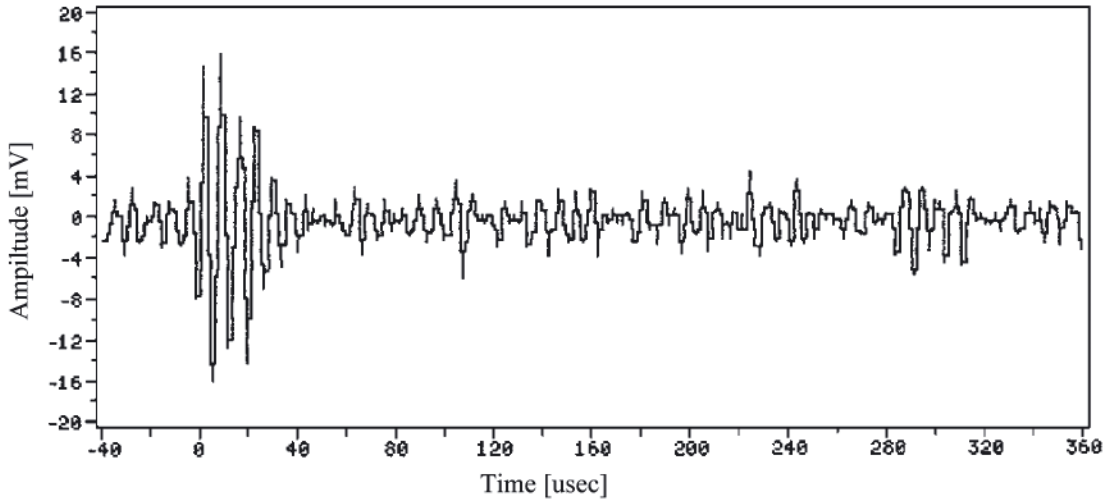

Fig. 2. Run of short wave [4]

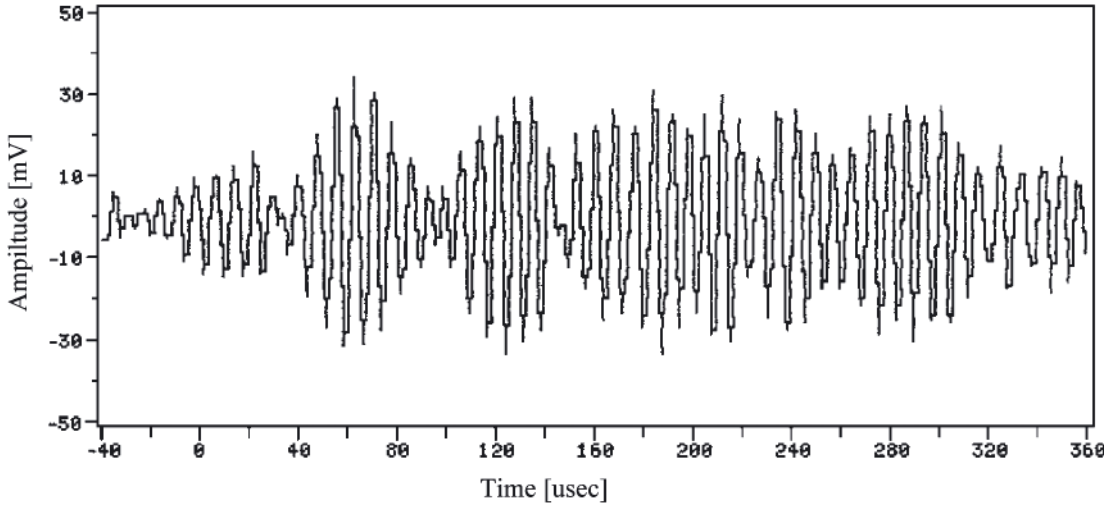

Fig. 3. Run of reflected wave [4]

Historical outline

The acoustic emission phenomenon was first implemented by Parry to test pitting corrosion inside a pipe. He observed that acoustic emission can be generated by different cracks resulting from oxygen depositions on surface of corrosion defects if only a stable hydrostatic pressure flow is exerted to the tested segment of pipe [9, 14]. In 1976 two scientists, Reting and Felsen, proved that the relationship between acoustic emission and amount of oxygen released from aluminium rods immersed in salt water, is linear. They also suggested that it is possible to test other physical chemical properties by means of acoustic emission [9, 14]. In 1976 Mansfeld and Stocker showed accurate relation between activity of acoustic events occurring in Al-alloys immersed in 3% NaCl solution, and amount of pitting corrosion. While running the tests many acoustic signal fluctuations were observed during anodic polarisation [9, 14].

Acoustic emission (AE) method

Acoustic emission is formed by sound signals which accompany changes of material structure during violent release of internal energy stored in it. During transferring wave through material, in the case of its coming across a defect, dispersion and reflection of the wave occurs. The phenomenon is called acoustic event. During such event, occurs acoustic wave emission which results from released internal energy. The so formed wave (Fig. 2) is recorded by an acoustic sensor. Events which become sources of wave emission can be of a low-energy or high-energy character [14,4].

Criteria for determining acoustic emission

In measuring and investigating acoustic emission, counting number of pulses or events or acoustic emission rate (number of events per time unit) is usually used as a measure of the phenomenon. For AE analysis to measure amplitude and duration of pulses lasting from a few micro-seconds to decimal parts of seconds, is necessary [4].

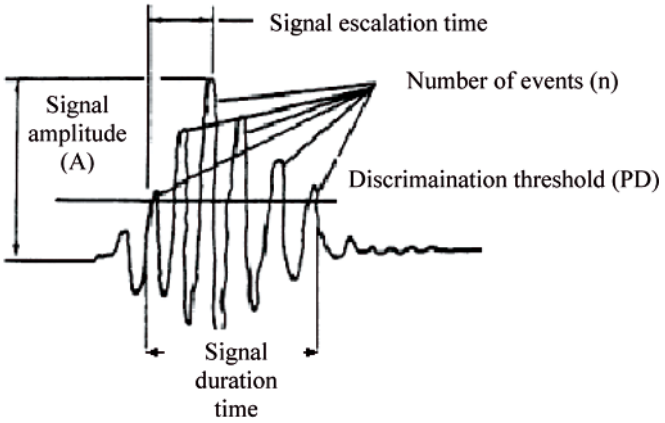

Fig. 4. A single acoustic emission signal [4, 14]

Advantages of AE method [4, 14]

Advantages of AE method are the following:
- possible continuous performing investigations,
- possible monitoring defect initiation place and time,
- possible testing large structures,
- owing to a large number of acoustic sensors, to precisely locate signal source, thus to determine place of defect occurrence, is possible.

The AE method is one of the non-destructive testing methods (NDT) and found wide application in the following areas of corrosion monitoring and - first of all - to assessing consequences of corrosion processes:
- analyzing and detecting corrosion cracks,
- testing corrosion in steel rods of reinforced concrete structures,
- detecting cracks of any kind and leakages from piping and tanks,
- testing degradation of laminates and linings [14].

Acoustic wave sensors [14]

Sensor is a device for transforming chemical, biolgical or physical stimulus coming from external environment, into electric signal which is a function of the output signal [14].

Acoustic sensors are divided, depending on a way of execution of measurements, into the following kinds:
- capacity ones,
- piezoelectric ones,
- electro-dynamic ones,
- nterferometric ones.

During the tests described in Ch. 3 piezoelectric acoustic sensors of 20 ÷ 80 kHz frequency range were used for monitoring corrosion and corrosion - fatigue processes.

METHOD OF VERIFYING THE ASSSUMED AIM

The method elaborated by the Department of Ship Technology, Quality Systems and Material Engineering in the frames of CORFAT project realized within 7th EU Frame Program, takes into account interaction of the three elements:
- the Vallen AMSY-5 measuring system together with sensors,
- the corrosion tester,
- the corrosive solution.

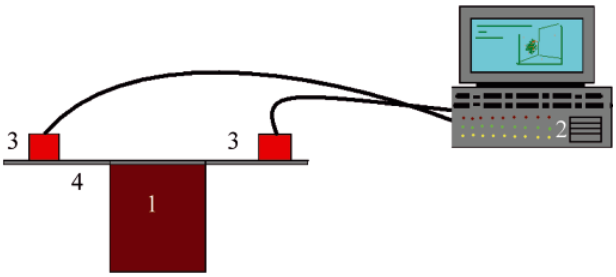

Fig. 5. *Schematic diagram of the system used for underdeck corrosion measurements:* ***1)*** *corrosion tester;* ***2)*** *Valen AMSY-5 measuring system;* ***3)*** *measurement sensors;* ***4)*** *ship's deck*

AMSY-5 measuring system

For recording AE signals and their analysis a specialty software of Vallen Systeme GmbH was used, namely:
- Visual AE,
- Visual TR,
- Visual Class.

Fig. 6. *AMSY-5 system of Vallen Systeme GmbH for AE testing [2]*

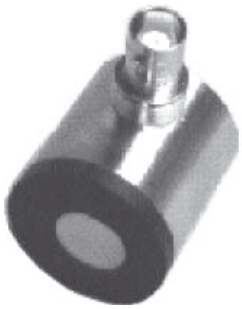

Fig. 7. *VS 150-RIC measurement sensor of Vallen Systeme GmbH [2]*

Corrosion tester

In the tests corrosion testers were used as AE sources since they make it possible to simulate corrosion without any destructive influence on the tested material of ship structure.

Which are criteria for selecting such tester?

Tester is to be built in such a way as to simulate most credibly conditions existing in a given place under testing, hence, the following items are to be appropriately selected:

a) size of the tester;
b) material for the tester, which should be the same or close to that to be tested;

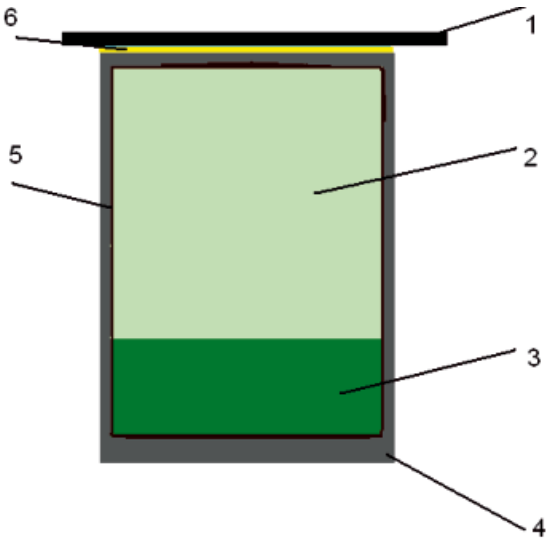

Fig. 8. *Schematic diagram of corrosion tester:* ***1)*** *ship's deck;* ***2)*** *corrosive gas;* ***3)*** *corrosive solution;* ***4)*** *tester's reaction cylinder;* ***5)*** *initiated corrosion;* ***6)*** *acoustic contact*

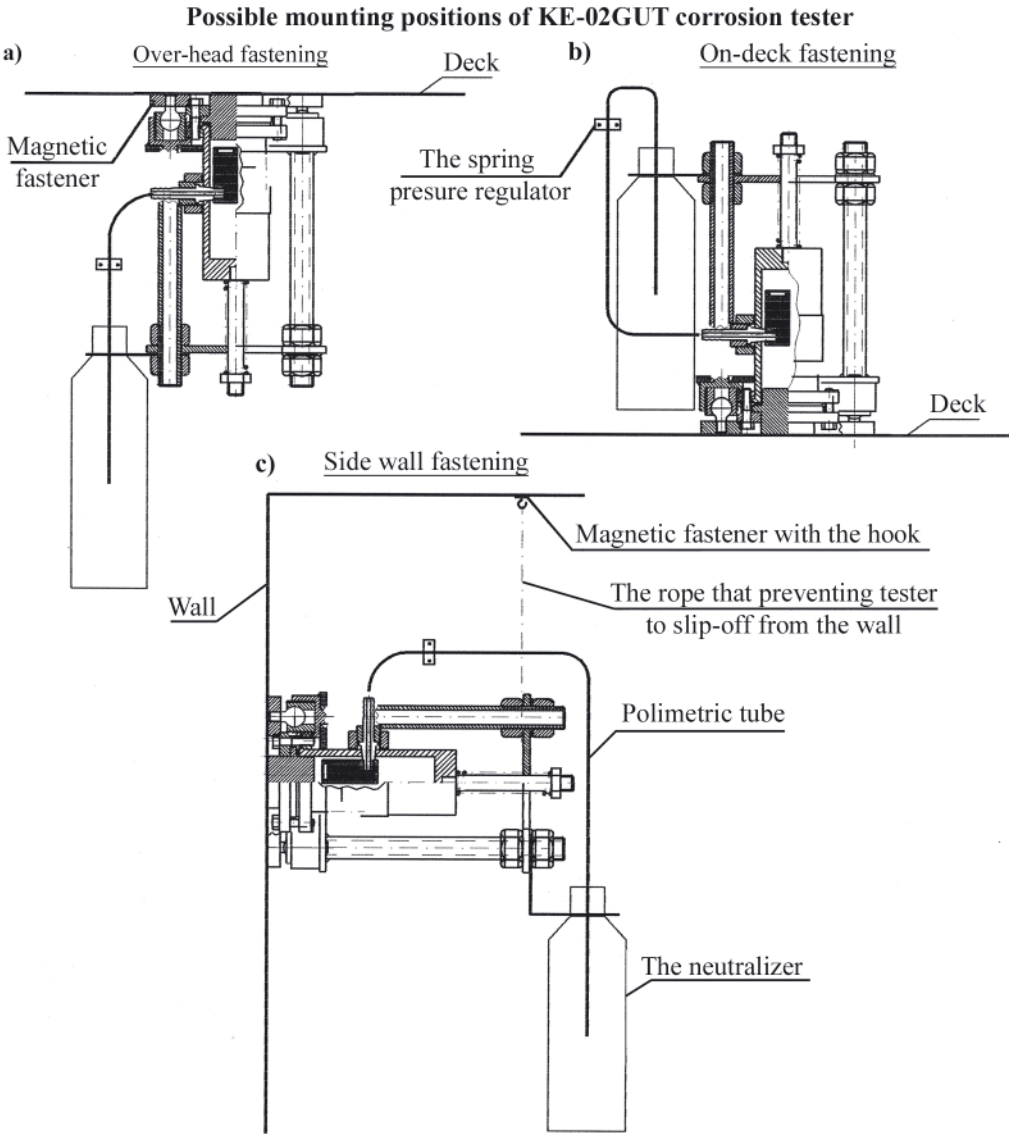

Fig. 9. *Schematic diagram presenting possible positions of KE-02(GUT) corrosion tester against ship's deck:* ***a)*** *over-head fastening,* ***b)*** *on-deck fastening,* ***c)*** *side wall fastening*

Fig. 10. *Naval Shipyard Co floating dock of 135 m in length, and 35 m in breadth*

c) surface area of contact of the tester with the tested surface, which should be sufficiently large as to correctly transfer acoustic signal, that is equivalent to tester's detectability;
d) corrosive solution.

The tester is fastened to a tested surface by means of magnetic fasteners but a way of fastening or image of corrosion cylinder depends on a type of tester.

RESULTS OF THE TESTS

The presented measurements were aimed at the following:
- detection of signals generated by active corrosion sources, by using the existing AE signal classificator,
- collection of data base on background noise coming from: operation of main and auxiliary electric generating sets, main engines, performed welding work etc, which will make it possible to elaborate a better version of AE classificator and improve this way detection quality of signal coming from active corrosion sources as well as corrosion fatigue defects.

Place of the tests performed on Naval Shipyard Co floating dock

The tank No. 11 7,95 m long and 4,7 m broad was the object in which the tests in question were performed. The test was performed for both two measurement conditions:
- dry tank,
- tank filled with sea water up to l' of its height.

The applied measuring instrumentation consited of:
- EA AMSY-5 Vallen system,
- VS75 and VS-150 RIC sensors as well as novel ISAS3 Vallen ones,

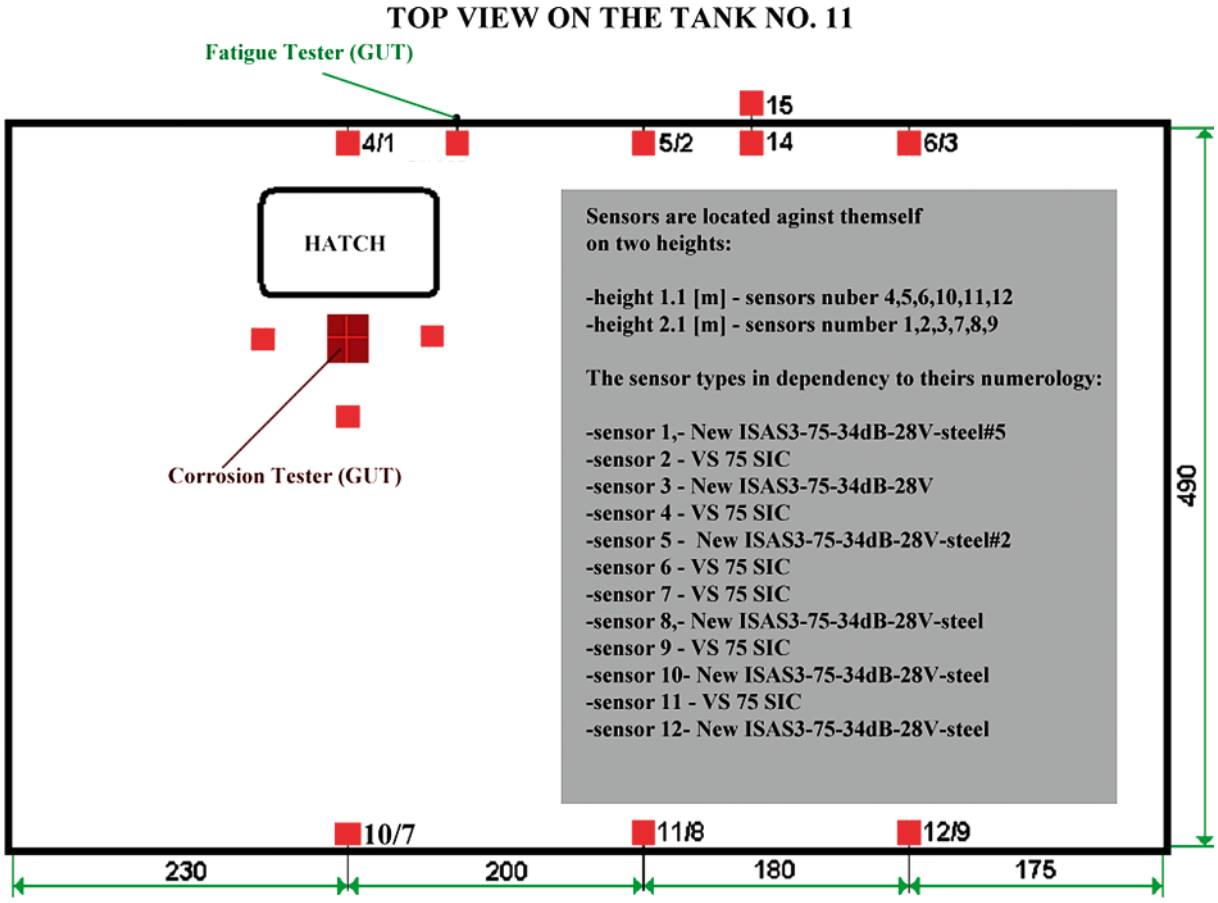

Fig. 11. *Schematic diagram of arrangement of sensors and corrosion testers inside the tank No. 11 of the Naval Shipyard Co floating dock*

- for calibration HSU 0.5 mm sensor and internal AMSY-5 system was used,
- the GUT and TÜV-Austria corrosion testers were implemented to serve as sources of AE corrosion signals,
- for fastening the sensors magnetic fasteners were used.

The corrosive solution of TÜV-Austria (4.13L H_20, 0.18L 68 % HNO_3, 0.18L 98 % H_2SO_4 0.14 kg NaCl) was applied.

Prior to measurements, paint coating was locally removed from plate surface and then the sensors and testers were fixed in this place. The entity was connected together by means of an acoustic silicone interface. Thickness of the plate was equal to about 10 mm.

The corrosion tester was placed overhead on tanktop internal surface, about 100 mm from a manhole; additional AE sensors (measuring signal coming directly from the GUT tester) were located on external surface, about 300 mm from corrosion source, directly over the tester.

Results of the tests performed on the Naval Shipyard Co floating dock

Because of some technical problems as well as dificult weather conditions (air temperature close to 0°C resulting in a drop of rate of corrosion processes, strong wind disturbing measurements) all the tests with the use of the GUT tester, TUV corrosion testers and GUT fatigue tester, did not bring expected results. But it was managed to record and collect measurement data on background noise generated by welding and repair work carried out on the Naval Shipyard Co dock, that will be helpful for building a background noise data base for signal classificator in a further project.

Fig. 12. *View of the deck in the vicinity of the tank No. 11 of the Naval Shipyard Co floating dock*

Fig. 13. *View of the Polish Navy tanker „Bałtyk"*

Place of the tests performed on the Polish Navy tanker „Bałtyk”

The next place of the tests was the tank V12 of cofferdam on the Polish Navy tanker „Bałtyk”. On the contrary to the earlier tests it was not allowed to locally remove paint coating, that was however taken into account during measurements. Also, no data on paint coating thickness were available because it was impossible to get access to painting documentation of the ship. Thickness of the plate was equal to about 6 mm.

The tests were performed for two variants of measurement conditions:

a) during standstill of the ship (at a low activity of onboard equipment),

b) durin voyage of the ship (at regular operation of onboard equipment).

Instrumentation used for the tests:

- Vallen AMSY-5 system fitted with ASIP2 filters
- Novel ISAS 3 sensors
- VS-75 and VS-150 RIC sensors
- GUT tester used as a corrosion source

Both the sensors and testers were fastened on the tank walls by means of the magnetic fasteners. GUT - Gdansk corrosive solution (2L H_20, 0.3L 68 % HNO_3, 0.25L 98 % H_2SO_4 0.07 kg NaCl) was applied.

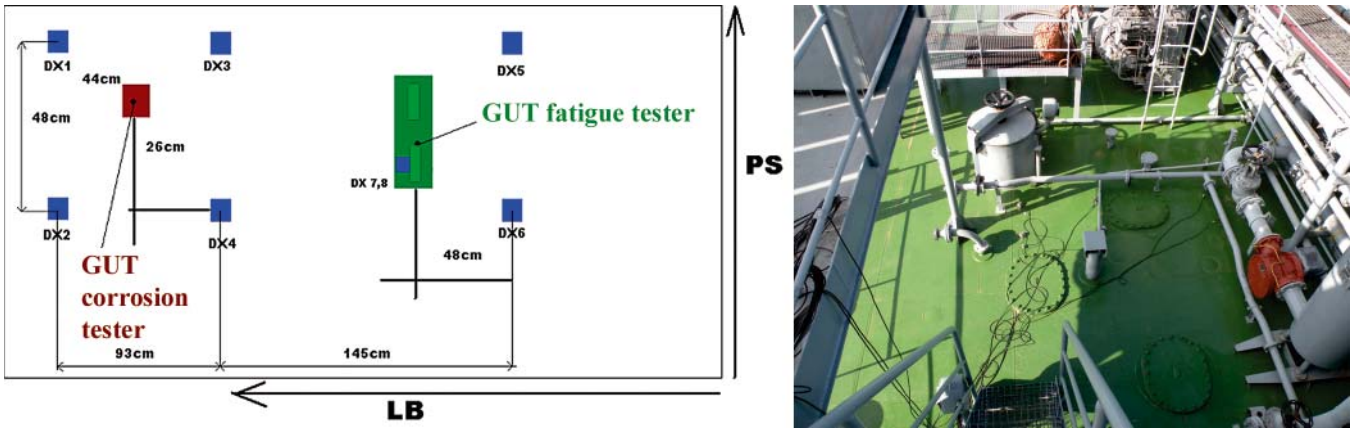

Fig. 14. Location of the test site (the tank No. V12 of cofferdam) and arrangement plan of the sensors on the deck of the Polish Navy tanker „Baltyk”

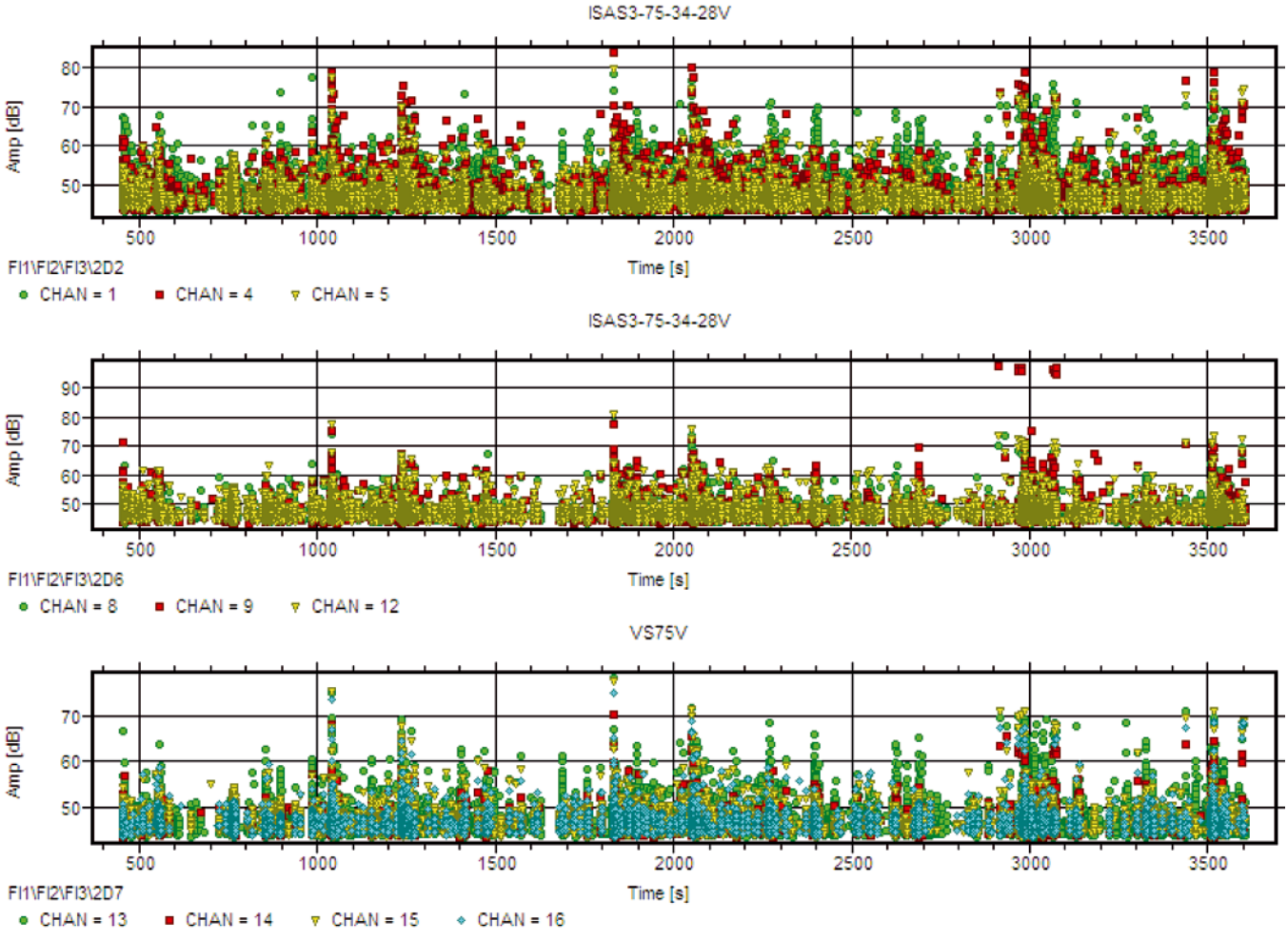

Fig. 15. Standstill test; records of external noise - AE signal amplitude for all measurement signals. Th = 43 dB

Results of the tests performed on the Polish Navy tanker „Bałtyk"

The tests were performed for two measurement conditions:

a) During ship's laying at anchor, at minimum number of ship's systems under operation, when the signal coming from the corrosion tester was so strong that it was possible to locate it. Results for the first testing conditions are presented in Fig. 15 and 16.
b) During sea voyage with the ship's systems under operation (main engines etc), when the signal coming from the corrosion tester, however weaker, was possible to be located due to application of a set of filters, e.g. frequency ones. Results for the second testing conditions are presented in Fig. 17 and 18.

Simultaneously, were performed the tests with the use of GUT fatigue tester, whose presentation was ommitted in this paper as they were beyond the scope of this author's work and whose realization did not influence detection quality of AE signal coming from the GUT corrosion tester.

SUMMARY

The described AE method shows many adventages in relation to other non-destructive testing methods, namely:

- speed of measurements,
- effectiveness of corrosion signal detection,
- repeatability,
- detection possible even at one -side access.

From the above described measurements results that AE signals coming from the corrosion tester can be detected both in the tanks with paint-coating and without it.

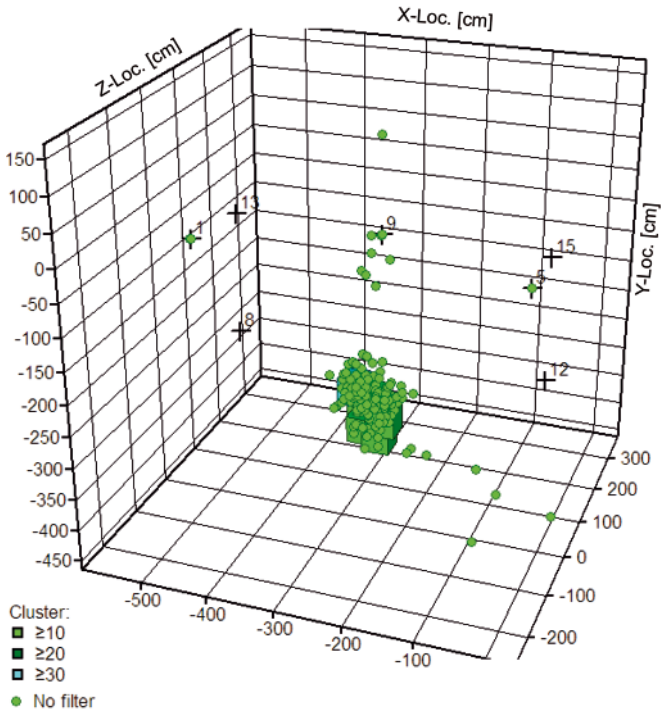

Fig. 16. Standstill test; 3-D location of corrosion source (the tester) close to DX4sensor.Th = 43 dB

However, results of the tests may be influenced by various factors such as: atmospheric conditions, ambient temperature and energy and intensity of external noise (e.g. operation of engines). They can make locating and identifying AE signals coming from active corrosion sources, difficult. In many cases it is possible, despite the unfavourable factors, to separate signals

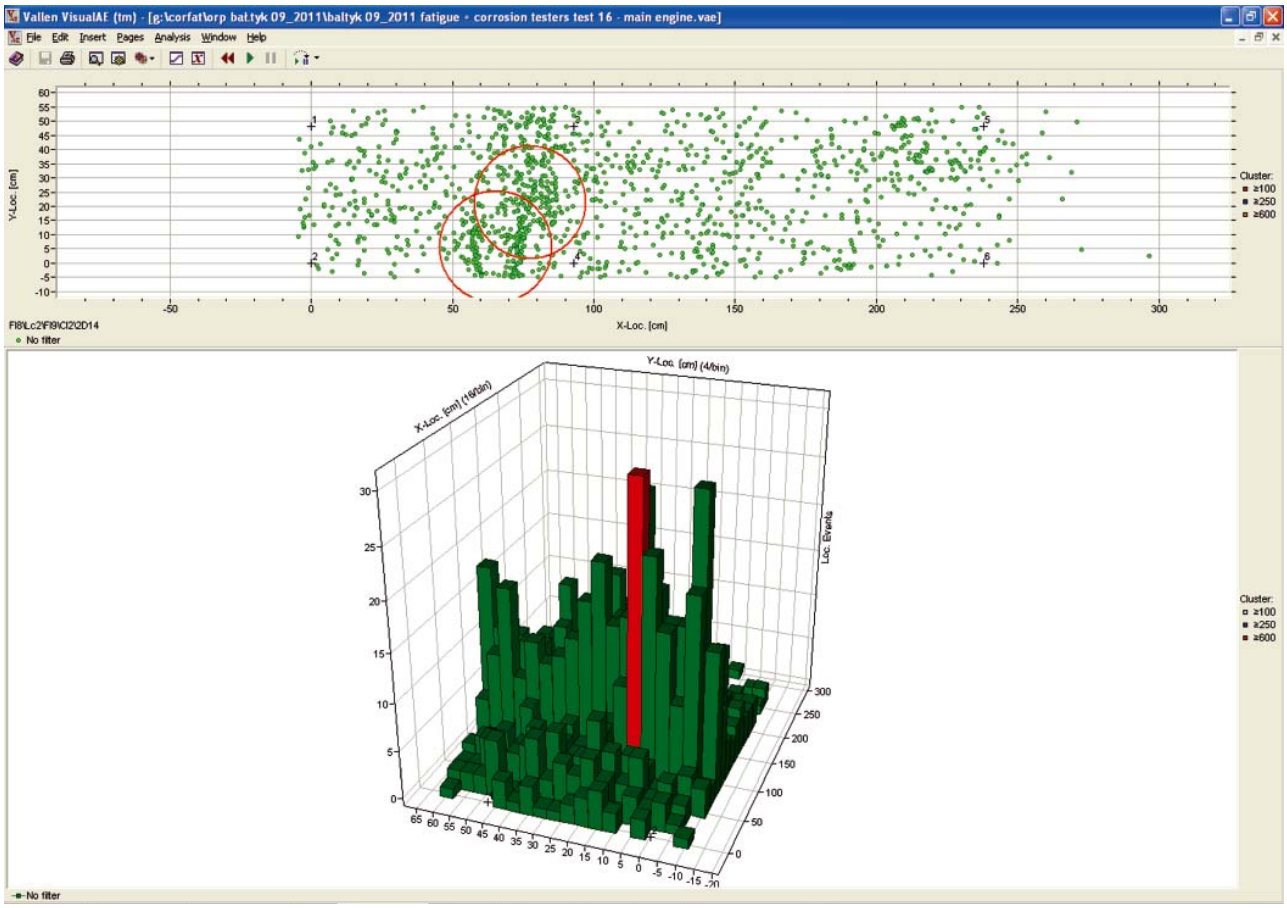

Fig. 17. Location of the corrosion tester and partial location of the tester during operation of engines

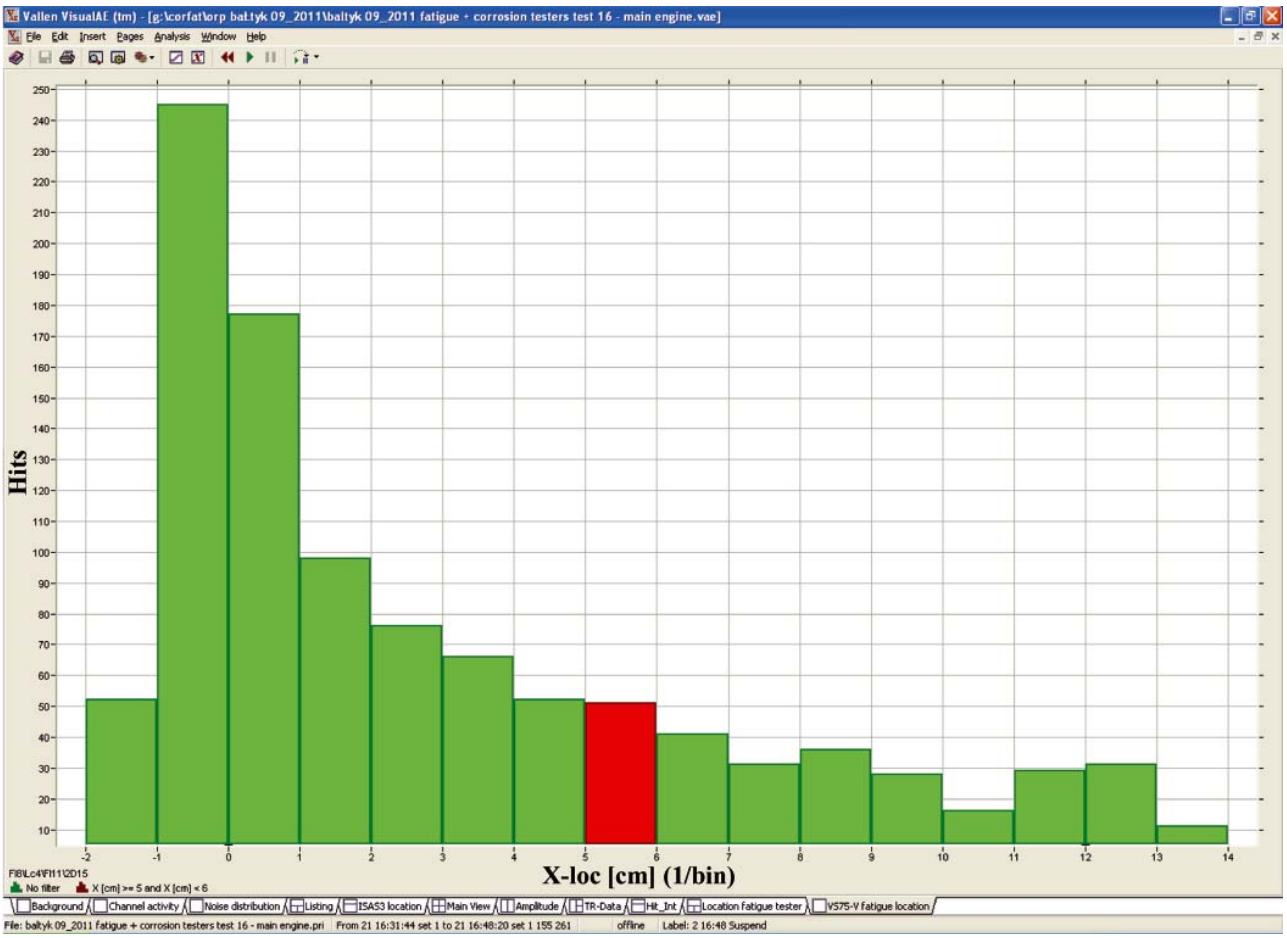

Fig. 18. *Diagram of output from ISAS3 sensor - signal coming from the corrosion tester during operation of engines*

out of the background; however in some cases their detection is completely impossible, that produces difficulties in applying the method in question.

Note

The tests were performed in the frame of CORFAT project (Contract No. SCP7-GA-2008-218637 - *Cost effective corrosion and fatigue monitoring for transport products*) realized within 7th EU Frame Program.

BIBLIOGRAPHY

1. TÜV Austria: *Corrosion testing of ships*. Project of V FPEU "CORRSHIP". Contract EVG1-CT-2002-00067, 2003÷2006.
2. Vallen Systeme GmbH*: AMSY-5 Specification.* The Acoustic Emission Company. Icking Germany.
3. PN-EN 1330-9: 2002 Polish standard: *Non-destructive tests - Terminology - Part 9: Terms applicable to acoustic emission tests* (in Polish), 2002.
4. Malecki I., Ranachowski J. (Editors): *Acoustic emission. Sources. Methods. Applications* (in Polish). PAN IPPT, Warszawa 1994.
5. TÜV Austria: *Cost effective corrosion and fatigue monitoring for transport products*. Project of 7th FPEU "CORFAT". Contract SCP7-GA-2008-218637. TÜV Austria 2008.
6. Tscheliesnig P.: *Corrosion testing of ship building materials with acoustic emission*. In Proceedings of EWGAE 2004 Conference.
7. Assouli B., et al.: *Detection and identification of concrete cracking during corrosion of reinforced concrete by acoustic emission coupled to the electrochemical techniques* NDT&E International 38, pp. 682-689, 2005.
8. Bellenger F., *et al.: Use of acoustic emission for the early detection of aluminum alloys exfoliation corrosion* NDT&E International 35, pp. 385-392, 2002.
9. Fregonse M., *et al.: Initiation and propagation steps in pitting corrosionof austenitic stainless steels: monitoring by acoustic emission* Corrosion Science 43, pp. 627-641, 2001.
10. Fregonse M., *et al.:* Monitoring pitting corrosion of AISI 316L austenitic stainless steels by aocuistic emission technique: Choice of representative acousitc parameters Journal of Materials Science 36, pp. 557-563, 2001.
11. Kim Y. P., *et al.: Ability of acoustic emission technique for detecting and monitoring of cravice corrosion on 304L austenitic stainless steels* NDT&E International 36, pp. 553-562, 2003.
12. Mazille H., *et al.: An acoustic emission technique for monitoring pitting corrosion of austenitic stainless steels* Corrosion Science, Vol. 37, No 9, pp. 1365-1375, 1995.
13. Assouli B., *et al.: Characterization and control of selective corrosion of* α,β*'-brass by acoustic emission* NDT&E International 36, pp. 117-126, 2003.
14. Emilianowicz K.: *Electrochemical and acoustic tetsts of 5754 alloy in presence of corrosion inhibitor* (in Polish). M.Sc thesis, Chemistry Dept., Gdansk University of Technology, Gdańsk 2008.

CONTACT WITH AUTHOR

Krzysztof Emilianowicz, M. Sc.
Faculty of Ocean Engineering
and Ship Technology,
Gdańsk University of Technology
Narutowicza 11/12
80-233 Gdańsk, POLAND

POLISH MARITIME RESEARCH 1(81) 2014 Vol 21; pp. 62-69
10.2478/pomr-2014-0009

Influence of pitting corrosion on fatigue and corrosion fatigue of ship structures
Part I
Pitting corrosion of ship structures

Marek Jakubowski, Assoc. Prof.
Gdansk University of Technology

ABSTRACT

The present paper is a literature survey focused on a specific kind of corrosion, i.e. pitting corrosion and its influence on fatigue of ship and offshore steels. Mechanisms of a short- and long-term pitting corrosion in marine environment have been described including pit nucleation and growth phases. Some models of pit growth versus time of exposure have been presented. Some factors which influence the pit growth rate have been discussed briefly.

Key words: pitting corrosion; ship structures; offshore structures

INTRODUCTION

There are two groups of actions which can lead to damages of real structures:

- chemical or electrochemical, if undesirable, are identified with corrosion (**C**)
- mechanical, usually identified with stresses or strains (**S**).

Damages resulting from interaction of both stresses and corrosion are usually considered as an aspect of one of them: influence of stress on corrosive damage, or influence of corrosion on mechanical damage. In this author's opinion interaction of corrosive and mechanical factors is the most general case. Almost all corroding structures are stressed. Almost all stressed structures are operated in an environment not neutral for mechanical damage process. In fact any damage (**D**) can be considered as: $D = (C + S)_D$.

Pure mechanical or pure corrosive damage can be considered to be specific and unusual cases. In the case of vacuum or inert gas environment **C** = 0 can be assumed and damage is purely mechanical in nature, while for very low stress levels **S** = 0 can be assumed and damage is purely corrosive.

The above given statement is especially true for ship structures which are the main object of the present research. Corrosive environment of the structures in question is also the main source of service loads.

There are many kinds of corrosion but for ship hull structures which work in sea environment, electrochemical corrosion is important. Both general (almost uniform) and local (pitting) corrosion is observed in low and medium strength steels and their welded joints in sea environment. The uniform corrosion is not ideally uniform, i.e. the thickness reduction is not uniform over the whole corroding surface, and pits are not classic in shape – their depths are often much smaller than diameters (low aspect ratios).

Metal surface always exhibits some differences in potential of different areas. Corrosion results in corrosion cells. Anodes and cathodes in such cells are in short circuits with negligible ohmic resistance. At the areas of lower potentials, i.e. **anodes**, metal ions come off the metal surface to the corrosive electrolyte (seawater) and they leave free electrons on the metal surface. This process is called anodic dissolution. The electrons flow to the adjoining cathodic areas where they are taken off the metal surface by so called depolarizers D (atoms, molecules or ions) that are reduced.

Faraday's law and polarization curves evaluated in short-duration laboratory tests were used for calculation of corrosion rates and life of corroding structures. Such approach is correct for a relatively short life of structure. It is well known, however, that corrosion products are deposited over the metal surface, e.g. red-brown rust is produced in low-carbon low-alloy steels.

Presence of rust layer of increasing thickness on the surface of structure changes the kinetics of corrosive reactions leading to a decrease of the corrosion rate with the rusting progress thus also with time. Many authors have considered limitation of the main depolarizer, i.e. oxygen supplied to cathodic areas by diffusion through the rust. A simplified formula is usually proposed for the corrosion loss y in function of the exposure time t [29]:

$$y = At^B \tag{1}$$

where A and B are empirical constants. Although B should be equal to 0.5 for Fickian diffusion and homogeneous rust layer, calibration to field data shows values between 0.3 and 0.8 [29].

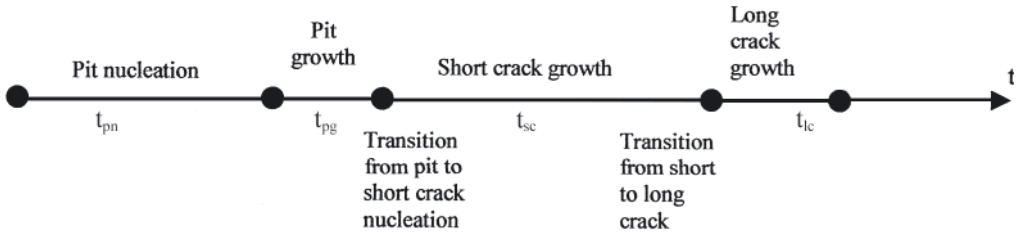

Fig. 1. *Seven stages of pitting corrosion fatigue life [4]*

Predictions of very long-term corrosion wastages based on the above given equation (1) lead to significant deviations from field data and do not explain a large scatter band of the data.

Melchers [29] stated that the corrosion process is more complex than that approximated by simple empirical models and a single formula of type (1a). In his numerous publications (not referred to here) he elaborated a new multi-phase model.

In common opinion, pits, if they are present on the material surface, are almost always the potential sites of the fatigue cracks initiation. Pits formation period is a part of total fatigue and corrosion fatigue life of structures exposed to marine environment during manufacturing or service stage. Every model of pitting corrosion fatigue process which could be applied to in-service life prediction, contains pit growth, pit-to - crack transition and fatigue crack growth. Most complete seems to be the assumption, originally proposed by T. K. Goswani and D. W. Hoeppner and accepted by Shi and Mahadevan [3, 4] that the pitting corrosion fatigue process proceeds in seven stages shown in Fig. 1.

Total pitting corrosion fatigue life of a structure where damaging crack is initiated at pit, can be calculated as the sum of the duration times of the following four phases:

$$t_f = t_{pn} + t_{pg} + t_{sc} + t_{lc} \tag{2}$$

where:

t_{pn} - the time for pit nucleation,
t_{pg} - the time for pit growth,
t_{sc} - the time for short crack growth,
t_{lc} - the time for long crack growth.

The present paper describes the phenomena and modelling of first two stages of the process, i.e. pit nucleation (initiation) and pit growth (propagation).

1. MECHANISM OF PITTING CORROSION

1.1. Pit nucleation (initiation)

In marine environment pitting occurs when the anodic area are fixed at the structure surface.

Butler [5] tested pure iron and its alloys. On pure iron the grain boundary region rather than the grain boundary itself is preferred site of initial attack of pitting corrosion. It suggests that even high-purity iron may have some metallurgical or chemical heterogeneity. Some pits can be initiated near inclusions. The greater tendency for pitting to originate at such sites may be associated with stresses in the crystal lattice surrounding the inclusions. In this author's opinion, however, it could be caused by electrochemical potentials of inclusion and iron.

In technical metals and alloys, corrosion pits almost always initiate at some chemical or physical heterogeneity on the metal surface, such as inclusions, second phase particles, flaws, mechanical damage, or dislocation [6]. In steels, however, pitting corrosion is almost always initiated at sulphide inclusion - this is commonly accepted opinion since the beginning of 20th century [7]. As a rule, sulphides contain about 90% MnS, remaining sulphides in mild and low alloy steels are mainly FeS.

Sulphides have usually cathodic potential, while the surrounding matrix is anodic [42]. There are different theories, but it is generally agreed that the sulphide inclusions or the immediate area surrounding the inclusions (contaminated by sulphur) are anodic with respect to the steel matrix, and that the hydrogen sulphide H_2S and HS^- ions enhance the local corrosion [7, 8, and 9]. The hydrogen sulphide and HS^- catalyse the anodic dissolution of iron and poison the cathodic reaction of hydrogen depolarisation [7, 8, 9]. The dissolved Fe^{2+} and Fe^{3+} ions are hydrolysed. These reactions cause local acidification of the electrolyte and enhance (catalyze) further dissolution of the steel and dissolution of sulphide inclusion producing H_2S and HS^- and originating micro pits. Both MnS and FeS inclusions exhibit sufficient solubility even in neutral water. Local attacks first occur in only a few places at the interface between the inclusion and matrix. Next macro pits are generated as a result of formation, growth and coalescence of micro pits at the mentioned interface [9]. Less soluble FeS are much more detrimental due to: (i) higher solubility in the steel matrix, and (ii) higher electric conductivity.

A micro-pit of only a few microns is formed very quickly after immersion and this time is a true initiation time [8]. The moment when the initiation stage transforms to propagation is not distinct. Sometimes corrosive attack starts from existing voids between the sulphide and the matrix [7, 9]. In standard non-alloy steels having small content of active sulphides, most of pits reach the depth of $100 \div 200$ μm and then stop to propagate [7, 8]. Such pits are called micro-pits. They can continue their growth only under a layer of dirt or corrosion products. In classical approach, the early development of mini-pitting is entirely attributed to dissolution of sulphide inclusions. If proportion of active sulphides in the steel is high enough, the dissolution of active iron around the sulphide inclusion may expose a new underlying active sulphide, the attack around the latter exposes still another active sulphide, and so on. In this way a macroscopic pit is generated [7].

All engineering alloys are covered with passive films of some oxides [10] which - in some cases - can facilitate local corrosion initiation in local sites of the film breakdown by an active anion (usually Cl^-). Further growth of micro-pit is driven by difference of potentials between cathodic film and anodic alloy. This is often the case for high-alloy Cr or Cr-Ni stainless steels. In non-alloy structural steels the oxide film exhibits very weak passive properties and does not effectively protect the steels against general uniform corrosion which takes place all over the steel surface, not only at the film local breakdown sites.

Role of paint coating for the pitting nucleation can be interpreted analogously to the role of passive films. Until the classification rules were amended in 1992, the coating of hold frames was not required and the frames were not coated [11]. Then, only general corrosion of the frames was observed. Now, when the hold frames have protective coatings such as tar epoxy paints, pitting corrosion is observed [11]. It means

that the coating which protects steel structures against general corrosion, facilitates the pitting corrosion process. The pits are presumably created at some inherent defects of coating or in-service - produced damages like scratches etc.

1.2. Pit growth (propagation)

When a pit has reached a certain depth, it has passed the initiation (or nucleation) stage and the propagation (or growth) stage begins. The propagation stage usually is much longer than the initiation period. However, if this pit nucleation period is neglected in the predictions of the total life of the structure, the final results are slightly more conservative [12].

An oxygen concentration cell is now formed with a small anode within the pit and a large cathode on surrounding steel surface. The metal ions produced by anodic dissolution are hydrolyzed, that leads to acidification of electrolyte in pits. Novokshchenov [13] has reviewed many literature data showing more or less marked potential and pH drop within pits compared to the external conditions. Butler *et al.* [5] reported relatively shallow pits (of the depth below 50 μm) in pure iron and the potential fallen by about 100mV at the pit centre, while pH dropped from a value about 8 well away from the pit to a value of about 2 at its centre. The acidity was not confined to the pit but extended over a region of about 15 - pit diameter. Thus the processes realized within the pit create favourable conditions for the pit growth, and the growth is autocatalytic.

The pit growth mechanism with the main electrochemical reactions is shown in Fig. 2. The scheme first proposed by Wranglen (Fig. 2a) [7] has been adapted and simplified by Novokshchenov [13] for steel in concrete, and the Novokshchenov's scheme has been again adapted for steel in marine environment with some modifications and simplifications introduced by Biezma and Rio-Cologne (Fig. 2b) [14]. The Wranglen's scheme gives the most complete picture of the pit propagation.

From the bottom and side walls of the pit, iron is dissolved anodically as Fe^{2+} ions which migrate and diffuse outwards, whereas anions, e.g. chloride ions, migrate into the pit. On their way outwards Fe^{2+} ions are partly hydrolyzed with the acidification of the inside-pit electrolyte. In low-alloy steels,by further reactions, they create precipitations of black magnetite and red-brown rust, often forming a crust (blister, dome) above the pit. Hydrogen ions discharged at the sides of the pit, partly form adsorbed atoms H_{ads} and next they are absorbed, and partly form H_2 gas that causes occasional bursting of the blister.

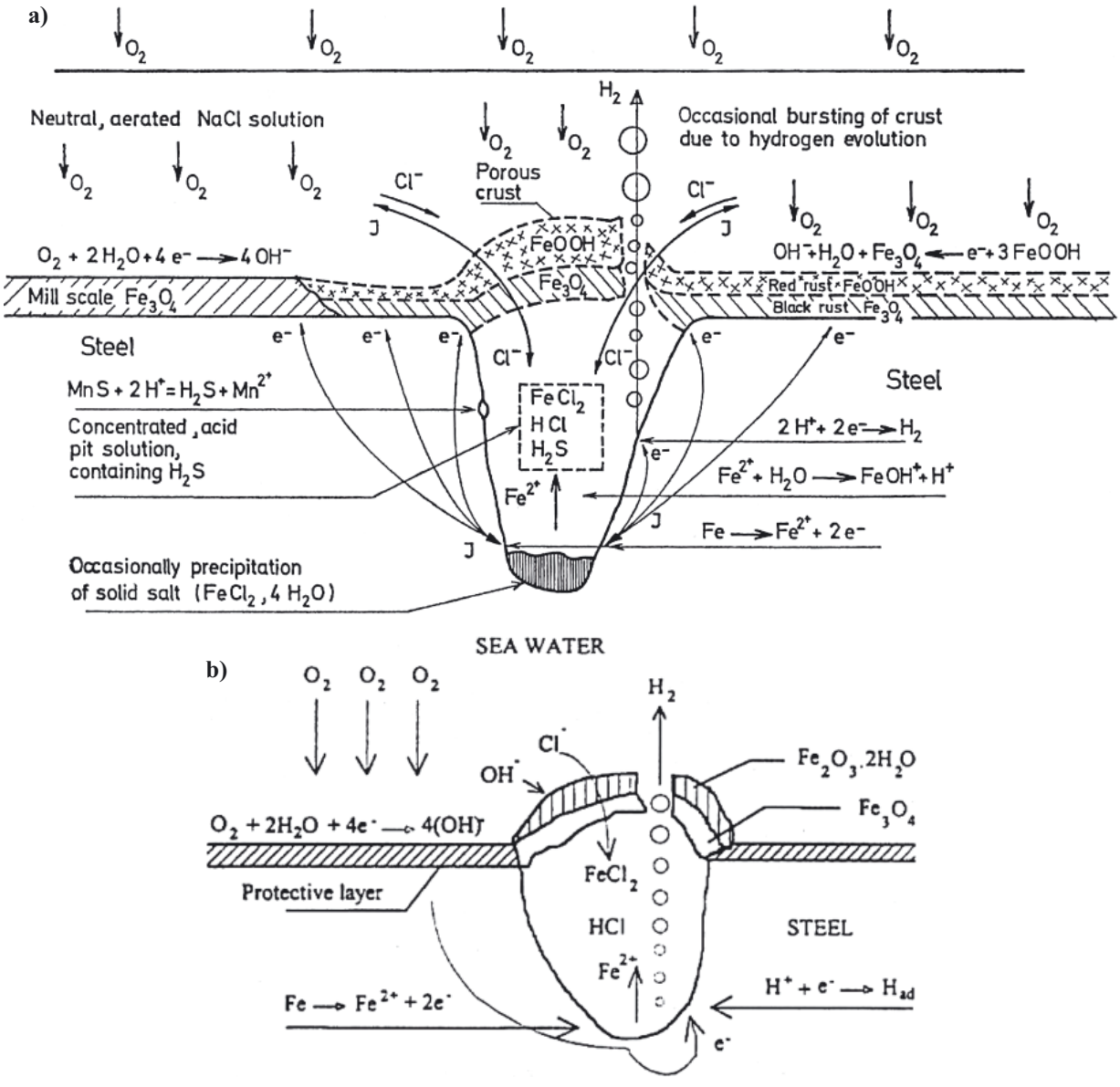

Fig. 2. *Growth of steel corrosion pits to be in near - neutral chloride solutions* ***(a)*** *[7];* ***(b)*** *[14]*

The autocatalytic conditions created by a pit are the following [7]:

1) within the pit:
   - preventing passivation:
   a) small supply of oxygen;
   b) generation of an acidic pit solution by hydrolysis reaction;
   c) dissolution of sulphides, resulting in H_2S;
   d) enrichment of anions (Cl^-, SO^{2-}) attracted by cathions in the pit;
   e) high electric conductivity of high-concentrated pit solution;
2) in the pit mouth:
   - formation of the crust, counter-acting mixing of the pit and bulk solutions, thus maintaining the oxygen concentration cell;
3) around the pit:
   - reducing general corrosion:
   a) partial cathodic protection by the corrosion current;
   b) passivation due to cathodically formed alkali, particularly in hard water.

The above described mechanism suggests that pits should grow still deeper and deeper. The author's own observations and literature information show that real macro pits on surfaces of steel ship structures are rather very broad and not very deep, e.g. 50 mm broad, 2 ÷ 3 mm deep, all over their surfaces, i.e. with approximately flat, but irregular bottom. It can be deduced that at least some of pits begin to grow into diameter direction and, in consequence, coalescence with adjacent pits occurs. Also, investigations of pure iron showed that some pits grow by coalescence. The reason why their growth in depth direction slows down is not clear for this author, but its possible explanation is - as shown in Fig. 2a – that occasionally solid salts can be deposited over the bottom of the pit.

Propagation of pit depth conventionally is described by power-law model [8] analogous to that for general corrosion rate:

$$a_p = A \cdot (t - t_i)^B \tag{1b}$$

In practice the time for the pit nucleation (t_i) is negligible compared to the pit propagation time hence the pit growth is usually described by:

$$a_p = A \cdot (t)^B \tag{1c}$$

Exemplary constants are as follows:

- A = 0.092 and B = 0.511 for a carbon steel immersed in salt water [15], and
- A = 0.0028 and B = 0.3877 for a typical mild steel used for ship structures sprinkled with sea water twice a day over 20 days period [16].

Exponent $B = 0.3 \div 0.5$ has been evaluated for aluminium alloys and solid stainless steels (i.e. the materials covered with a stable oxide films) in salt water [17]. Eq. (1c) is relevant for micro-pits rather than for macro-pits, and for exposure periods usually much shorter than 1 year and usually measured only in hours or days [8]. Wang *et al* [18] tried to apply the model (1c) to describe eight-year test results of macro pits (up to 2.4 mm deep) in different steels. They obtained relatively satisfactory values of coefficient of determination $R^2 = 0.915 \div 0.98$, but in this case for shorter exposure periods (1 year) and $a_p < 0.4 \div 0.6$ mm the pit depth was markedly overestimated while for a longer exposure the pit depth was a little underestimated (up to about 10%).

2. INFLUENCE OF BIOLOGICAL ACTIVITY OF MARINE ENVIRONMENT

2.1. Introduction

Kobzaruk et al [19] exposed some specimens of mild steel in natural sea water (of 1.8% salinity) *in situ* and in the very same natural sea water in laboratory tanks. Marked differences were found in results. Many deep and sharp corrosion pits were observed in specimens tested *in situ*, while sporadic, shallow and non-sharp pits were revealed in specimens tested in laboratory. The difference was attributed to the biological activity of water *in situ* with marine growth on the specimen surfaces and lack of such activity of the same water stored in laboratory. Therefore the metal surfaces submerged in sea were non-uniform from electrochemical point of view and some bacteria could influence the pits growth too. Authors did not consider that, but the conditions around and within the pits were rather aerobic since the exposition time was 5500 hours, while Melchers [20] considered that aerobic conditions are likely to exist up to about 1÷1.5 years of *in situ* exposition. Thus aerobic bacteria played presumably the main role in the case of investigations [19].

Sulphate-reducing bacteria (SRB) play a very important role in pitting corrosion in anaerobic conditions that presumably dominate within pits and in their neighbourhood after longer periods of the steel surface exposition to seawater *in situ*, e.g. longer than 1.5÷2 years of exposition. At the bottom of cargo tanks on tankers and of fuel tanks such conditions can occur even earlier.

There is always an at least thin layer of water under fuel and oil in tanks. Marine SRB proliferate in the anaerobic conditions often existing in seawater underlying fuels [21]. Sulphur and sulphur compounds are produced by the metabolic reduction of sulphate by anaerobic bacteria. Different kinds of bacteria have been found in water on the bottom of the tanks. The association of the different species of micro - organisms causes, through a symbiotic action, favourable conditions for the growth of anaerobic bacteria. Steel in seawater contaminated by SRB is characterized by a change of pitting and corrosion potential to more active (more negative) potentials. The breakdown of passivity is accomplished easily in deaerated solutions where low levels of sulphide or metabolic products are needed. Therefore at the bottom plates of cargo holds of many tankers some extremely deep hemispherical pits of order of 10 mm or more in depth can be sometimes found.

2.2. Melchers model

Real pit depths in ship structures, especially after a long-term exposition to marine environment, do not agree with predictions by the conventional power-law equations (1c). In Melchers' opinion [9] the reason is that after long period of exposure, conditions on the corroding surface change from an essentially aerobic to an essentially anaerobic environment, thereby creating conditions that allow a much greater rate of corrosion through the metabolism of SRB. Melchers [9] elaborated a multi-phase model of pit depth growth including this observation. The model is shown in Fig. 3.

In the phases 0, 1, 2 the corrosion rate is controlled mainly by oxygen supply rate to the bottom of the pit, and the pit depth growth can be described approximately by the relation (1c), at least for the phases 0 and 1. At the end of the phase 2, corrosion rate is sufficiently declined mainly due to build-up of corrosion products reducing the rate of oxygen transport to the corroding surface (mainly the pit bottom), and - to a lesser

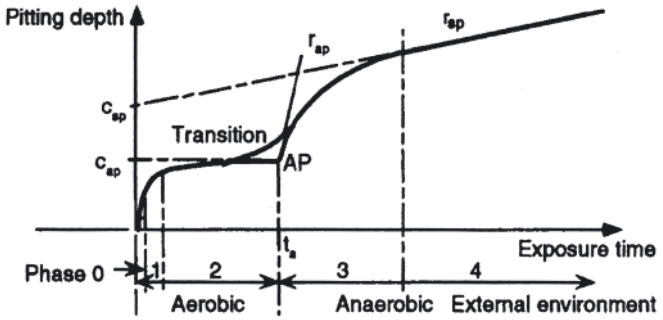

Fig. 3. Melchers' pitting corrosion model including the SRB activity [9]

extent - the effect of fouling. The life (t_a) of the phases 1 ÷ 3 strongly depends on the seawater temperature (T) and is given by [8]:

$$t_a = 9.91 \exp(-0.088\ T) \tag{3}$$

For cold North Sea water this is 4-years period while for warm waters of temperature 20°C or more this is less than 1 year. This is also idealized beginning of the anaerobic phase 3. Total maximum pit depth at this moment (c_{ap} - see Fig. 3) is given by an equation of the analogous form [8]:

$$c_{ap} = 9.91 \exp(-0.052\ T) \tag{4}$$

Thus, at the moment of commencement of the anaerobic phase 3, for warm water the pit depths are still in the range of micro-pits (200 μm) while for cold water they are evidently of macro-pits (800 μm). The pit depth in these equations means its absolute value, i.e. the depth "as measured" (relative value) plus the equivalent, one - sided, general corrosion loss.

Although some SRB activity is likely to occur soon after immersion, it tends to be suppressed in the early stage of the corrosion process. Renewal of the SRB activity is observed at the end of the phase 2, when the corrosion products layer is thick and regular and creates appropriate anaerobic conditions for the entire metal surface. Therefore similar trends are observed for pitting corrosion (Fig. 3) and general corrosion described in [9]. It means that there is an interaction between pitting and general corrosion loss [9].

To sustain the corrosion process in the phase 3 and 4 in particular, nutrient must be transported through the corrosion products. It is likely that the rate of this supply will control the rate of corrosion in the mentioned phases. The SRB-induced corrosion produces new products which reduce the rate of supply of nutrients, leading to reduction of corrosion rate in the phase 3 and eventually to near-steady corrosion process in the last phase 4.

The above statements concerned pitting which proceeds in external anaerobic conditions in the late phases of a structure work. Conditions within pits, however, are locally favourable for SRB activity even in aerobic external environment because of lower pH, lower oxygen concentration, some H_2S, $FeCl_3$ and HCl content [9]. Near the edges of the pit the aerobic bacteria which can exist in the external environment, will become dormant or die because of local oxygen deficiency. This provides a source of nutrient additional to nutrient from the external environment. The nutrients transported to the pit interior, provide conductive conditions for the rapid growth and metabolism of SRB. Thus even (i) under generally external aerobic conditions (ii) without the presence of further sulphide inclusions around the pitted area, further pit growth could occur due to local generation of H_2S.

Melchers proposed the following explanations for widening of pits and coalescence of them during the phase 3:

- availability and rate of supply of nutrients to SRB,
- their rate of metabolism as governed by energy supply rate and temperature and concomitant rate of production of hydrogen sulphide H_2S,
- the interaction with other bacteria and with marine growth,
- the morphology of the pits,
- usual presence of partially protective deposits at the bottom of the pits (Fig. 2a).

Melchers [8] has evaluated some exponential equations which enable to calculate the pitting rate at the commencement of the phase 3 (r_{ap}) and the constants (c_{sp} and r_{sp} – meanings of the constants are explained in Fig. 3). He concludes that the rate of pit growth eventually steadies, in the last anaerobic phase, to a rate about the same as that for general corrosion. Thus, the size of pit measured from the actual material surface will practically not increase during this phase.

2.3. Wang et al. model [18]

Wang *et al.* [18] did not consider complex multiphase physical-chemical-biological mechanism of pitting corrosion but they proposed a simple engineering model. They adopted a Weibull function to describe the growth of macro-pits in function of exposure time:

$$a_p = d(t) = d_m \{1 - \exp[-[\alpha \cdot (t - T_i)]^m]\} \tag{5}$$

the corresponding pit growth rate is given by:

$$a_p' = d'(t) = \tag{6}$$

$$= d_m \cdot m\ \alpha^m\ (t - T_i)^{m-1} \exp[-[\alpha \cdot (t - T_i)]^m]$$

where: d_m means the long-term depth of pits; m is the shape parameter; α is the scale parameter. For $m > 1$ the pit growth rates exhibit an increasing phase, next the maximum and a decreasing phase (Fig. 4a), while for $m \leq 1$ the pitting corrosion rates drop monotonically.

The new model is only applicable to the growth phase of macro-pits. Exemplary conformance of the model with the data on the maximum depths of pits, published by Melchers, is shown in Fig. 4b. The data points for micro-pits cannot be well described by this simple model because of the high non-linear phenomena in the considered phase of pitting. The authors [18] ascertained that for assessment of time-dependent reliability of ship structures it is essential to inspect the weakening of structural load - carrying capacity in the long term. Therefore, the influence of micro-pits may be neglected in the meaning of engineering practice. This statement seems to be controversial in the light of many investigations (discussed below) which showed marked influence of micro-pits on fatigue and corrosion fatigue life of specimens made of different materials.

Wang *et al* [18] evaluated influence of environmental variables and the steel composition on the parameters d_m, m and α. Contrary to Melchers [8] who considered all steels (even medium-carbon ones) as one population independently on the chemical composition, Wang and co-workers stated a marked influence of carbon, sulphur and manganese content in steel on the model parameters d_m, m and α.

2.4 Conical pits

Most of published papers are focused on pits of a hemispherical (or a spherical sector) shape (Fig. 5a) [22]. Investigations of actual corroded hold frames of bulk carriers which carry exclusively coal or iron ore, revealed that corrosion pits are often of a conical shape (Fig. 5b) [23]. The pits are

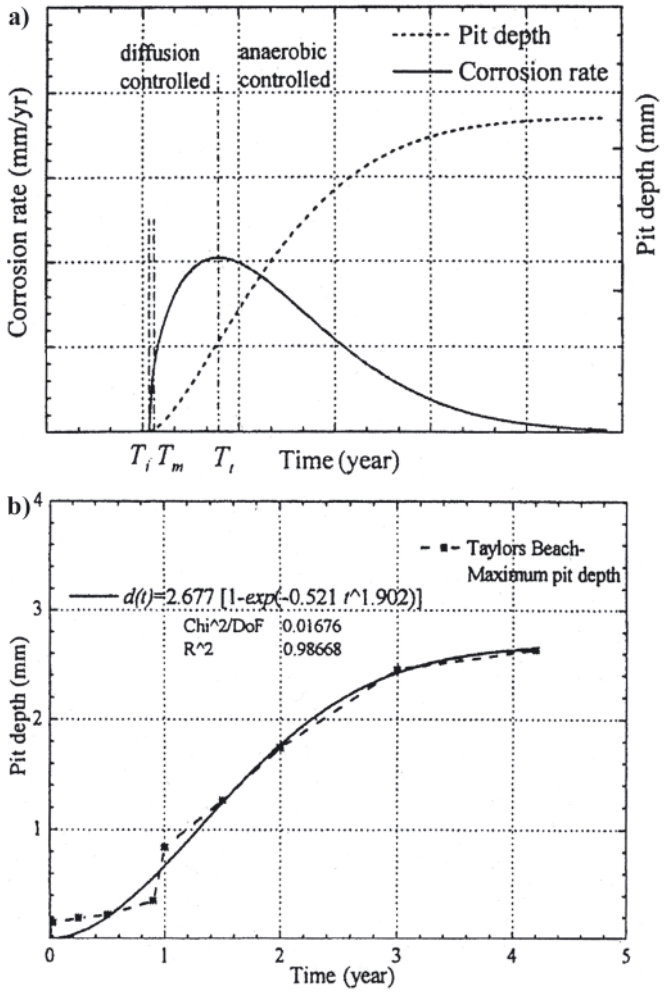

*Fig. 4. Wang et al model [18]: (**a**) schematic plot of basic relations; (**b**) the model fitting to all maximum pit depth data from a research at Taylor's Beach, Australia*

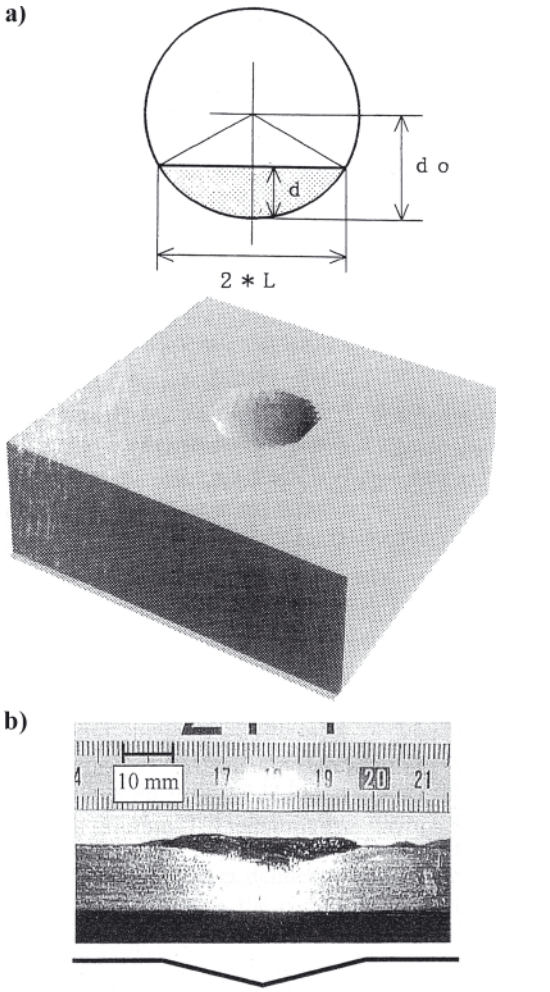

*Fig. 5. Pits: (**a**) view of a spherical one (typical for e.g. tankers) [22]; and (**b**) cross-sectional view of a conical one (typical for hold frames in bulk carriers) [23]*

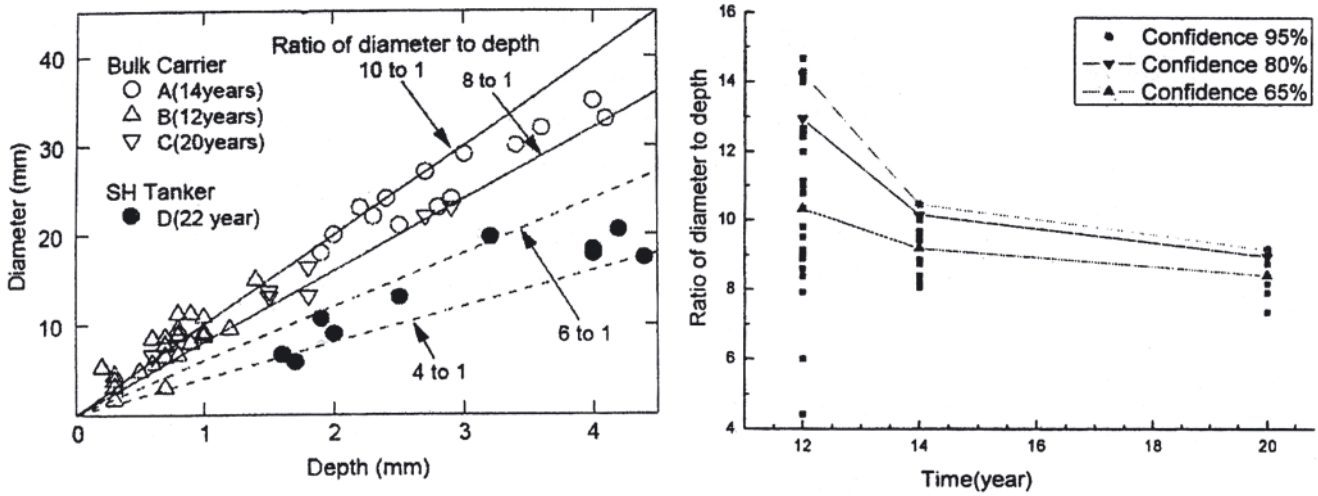

Fig. 6. Pit's shape and its evolution on different ships (diameter-to-depth ratio is an inverse of the aspect ratio) [24]

considered not generated at sulphides and spherical ones. It is considered that mechanical damage to the coatings occurs at very small points due to scratches by cargoes, then the corrosion process starts locally at these points, that leads to the formation of corrosion pits. As the number of the pits increases, the pits can coalesce and overlap. They are initiated exactly on surface of steel, therefore they exhibit lower aspect ratios (depth-to-diameter ratio equal to 0.1 ÷ 0.125) than spherical pits (0.167 ÷ 0.25) originated inside material within "caverns" placed at dissolute sulphide inclusions (Fig. 6a). In earlier stages of exposure the aspect ratio is often lower than 0.1 (Fig. 6b). This is evident that in 20-year old bulk carriers pits (as measured) are smaller than in 14-year old ones. This is presumably a result of general corrosion progress and overlapping of individual pits.

2.5. Grooving corrosion

Grooving corrosion is a form of pitting corrosion with joined pits. This form of corrosion is usually observed along

welds, and heat affected zones (HAZ) are attacked most intensively. Cross section of fillet welded joints with grooving corrosion, general corrosion and a transitional form of corrosion are compared in Fig. 7a, 7c and 7b, respectively. The main reason presumably is electrochemical potential of the heat affected zone which is less noble than parent material and weld metal. A relative potential difference of about 100 mV between HAZ and the central part of the weld has been reported [25]. An additional reason can be dust and dirt accumulated at the region of the toe of weld. Yuasa and Watanabe [25] have fairly stated that, in practice, the cause of this corrosion is generally defective painting. Grooving corrosion can be prevented by satisfactory painting. However, during repair work, the quality of the painting work is generally poor, that leads to the problem in question.

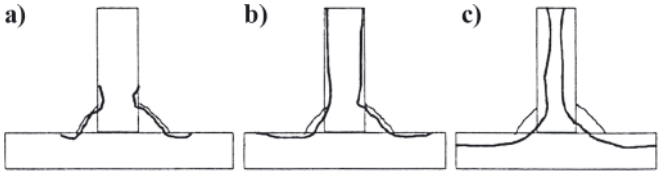

*Fig. 7. Cross sectional view of corroded fillet welded joints of frames of bulk carriers: (**a**) 12 -year old, and (**b**) 14-year old; and a 22- year old tanker bottom plate: (**c**) [26]*

3. RELATION BETWEEN MICROSTRUCTURE AND PITTING SUSCEPTIBILITY

In steels with martensite-ferrite structure pits are predominantly initiated in the ferrite bands [27]. In steels with martensite-pearlite structure pits are preferentially initiated on martensite [27]. In a pearlitic-ferritic steel commonly applied to ship and offshore structures, tested in salt water, pits were initiated earlier and grew faster in pearlite then in ferrite [28]. As pits start growing in one phase they will give cathodic protection to growing pits in the other phase and therefore deactivate the growing process [5]. Miller and Akid [29] reported that some micro-structural barriers (such as grain boundary) can influence the pit growth rate – the rate drops when the pit approaches the barrier.

A new bainite-ferrite steel for application in shipbuilding industry has been developed in Japan [30]. The new steel with bainite-ferrite microstructure exhibited longer corrosion fatigue crack initiation life as compared to conventional ferrite-pearlite steels. This extended crack initiation life in the ferrite-bainite steel has been attributed [30] to small number of corrosion pits which are potential sites of initiation of corrosion fatigue cracks. The small number of the pits might be caused by high homogeneity of ferrite-bainite steel to general corrosion which is slower than for ferrite-pearlite steel. General corrosion of ferrite-bainite steel is uniform and evidently slower than for ferrite-pearlite steels because of fine and homogenous microstructure. The ferrite-pearlite microstructure is not so homogeneous, therefore in this case general corrosion is non-uniform.

4. STATISTICAL DISTRIBUTION OF CORROSION PIT DEPTHS

Modelling of pitting-induced corrosion fatigue process requires to know statistical distribution of the pit depths since the distribution of corrosion pits have a substantial effect on the distribution of fatigue life [31]

Melchers [20] analysed the uncertainty (or scatter) in the data concerning pit depth at any given point of time. For pit growth under aerobic conditions (i.e. in the phases 1 and 2 of the model shown in Fig. 3), pit depth distribution, at least for deeper pits, approximately satisfies the normal distribution. For anaerobic conditions (the phases 3 and 4), both supply rate of nutrient and proportion of surface covered by pits, with no knowledge of the probability density of each, may be represented by a unimodal distribution as the normal distribution. Thus the individual pit depth will be distributed in compliance with Cauchy distribution. Then the extreme pit depths are asymptotically distributed in compliance with Fretchet distribution. However, if the density of pitting is relatively well described with little uncertainty, the underlying pit depth distribution is approximately normal and hence the asymptotic extreme value model is of a Gumbel type.

Not only distribution of pit depths seems to be important, but also a rigorous probabilistic analysis to quantify the probability of the crack initiation at pits of different sizes, would be useful [32].

CONCLUSIONS

1. Pitting corrosion in steels is almost always initiated at sulphide inclusions (90% MnS, remaining mainly FeS), which are cathodic, but their surfaces and the surface of surrounding steel are contaminated with sulphur, therefore they are more anodic than matrix far from inclusion.
2. Grooving corrosion takes place in HAZ close to toe of weld due to electrochemical potential difference between separate zones of welded joints.
3. Protective coatings like paints successfully prevent general corrosion during a relatively long period but they enhance tendency for local corrosion like pitting corrosion and grooving corrosion to be initiated in sites of inherent defects of coating (blisters or pores) or in-service - generated defects (pop -offs, scratches, etc).
4. In ferrite-pearlite steels, pearlite is more liable to suffer corrosion pitting. Therefore the greater carbon content the greater pearlite content, and the higher pitting corrosion susceptibility of steel could be probably expected. Melchers [8] is of opposite opinion. Corrosion of a new ferrite-bainite steel for shipbuilding industry is almost uniform with much smaller number of pits compared to conventional ferrite-pearlite steels because of much fine and much homogeneous microstructure of the ferrite-bainite steels compared to conventional steels.
5. Oxygen access to the initiated pit is restricted by its shape and a rust blister covering the pit, therefore an oxygen concentration cell which facilitates the pit growth, exists. Many authors reported evident drop of electrochemical potential within the pit, where iron is dissolved anodically as Fe^{2+} ions which diffuse outwards, whereas chloride anions migrate into the pit. On their way outwards, anions Fe^{2+} are partly hydrolysed with the acidification of electrolyte within the pit. This acidification and a higher concentration of Cl^- within the pit accelerates the pit growth rate too.
6. Biological activity of sea water can play an important role in pitting corrosion in case of both short-term exposure (measured in days and months) and long-term exposure (measured in years). Anaerobic conditions built up even after short-term exposure at the bottom of fuel and oil tanks but after a long-term exposure of structures working in seawater, are propitious for sulphate-reducing bacteria (SRB), that markedly enhance the pit growth rates.

Acknowledgements

This work has been performed in the scope of the project RISPECT ("Risk-Based Expert System for Through-Life Ship Structural Inspection and Maintenance and New-Built Ship Structural Design") which has been financed by the UE under the contract SCP7-GA-2008-218499.

BIBLIOGRAPHY

1. Domański A., Birn J.: *Corrosion of ships and their prevention* (in Polish). Wydawnictwo Morskie, Gdańsk, 1970,
2. Melchers R.E.: *Development of new applied models for steel corrosion in marine applications including shipping*. SAOS, 2008, Vol.3, No.2, pp.135-144.
3. Shi P., Mahadevan S.: *Probabilistic corrosion fatigue life prediction.* 8th ASCE Specialty Conference: Probabilistic Mechanics and Structural Reliability. 2000
4. Zhang R., Mahadevan S.: *Reliability based reassessment of corrosion fatigue life*. Structural Safety, 2001, Vol.23, pp.77-91.
5. Butler G., Stretton P., Beynon J.G.: *Initiation and growth of pits on high purity iron and its alloys with chromium and copper in neutral chloride solution*. British Corrosion Journal, 1972, Vol.7. July, pp. 168-173.
6. Wang Q.Y., Kawagoishi N., Chen Q.: *Effect of pitting corrosion on very high cycle fatigue behaviour.* Scripta Materialia 2003, Vol.49, pp.711-716.
7. Wranglen G.: *Pitting and sulphide inclusions in steel.* Corrosion Science, 1974, Vol.14, pp.319-349.
8. Melchers R.E.: *Pitting corrosion of mild steel in marine immersion environment – Part 1: Maximum pit depth.* Corrosion, 2004, Vol.60, No. 9, pp.824-836.
9. Melchers R.E.: *Pitting corrosion under marine anaerobic conditions – Part 1: Experimental observations.* 2006, Vol.62, No. 11, pp.981-988.
10. Akid R., Dmytrakh I.M., Gonzales-Sanchez J.: *Fatigue damage accumulation: the role of corrosion on the early stages of crack development.* Corrosion Engineering, Science and Technology, 2006, Vol.41, No.4, pp.328-335.
11. Nakai T., Matsushita H., Yamamoto N., Arai H.: *Effect of pitting corrosion on local strength of hull structural members.* Class NK Technical Bulletin, 2005, pp.29-49.
12. Ishihara S., Saka S., Nan Z.Y., Goshima T., Sunada S.: *Prediction of corrosion fatigue lives of aluminium alloy on the basis of corrosion pit growth law*. Fatigue & Fracture of Engineering Materials & Structures, 2006, Vol.29, pp.472-480.
13. Novokshchenov V.: *Brittle fracture of prestressed bridge steel exposed to chloride-bearing environment by corrosion-generated hydrogen.* Corrosion, 1994, Vol.50, No.6, pp.477-484.
14. Biezma M.V., Rio-Cologne B.: *Influence of various marine conditions on corrosion behaviour of AISI C1118 steel.* Inżynieria Materiałowa (Material Engineering), 2001, Vol. 22, No.4, pp.227-230.
15. Linder J., Blom R.: *Development of a method for corrosion fatigue life prediction of structurally loaded bearing steel.* Corrosion, 2001, Vol. 57, No.5, pp.404-412.
16. Kumakura Y., Takanashi M., Fuji A., Kitagawa M., Ojima M., Kobayashi Y.: *Fatigue strength of coated steel plate in seawater.* Proc. Ninth Int. Offshore and Polar Engineering Conference, Brest, France, May 30 – June 4, 1999, Vol.4, pp. 108-113.
17. Kawai S., Kasai K.: *Considerations of allowable stress of corrosion fatigue (focused on the influence of pitting).* Fatigue & Fracture of Engineering Materials & Structures, 1985, Vol.8, pp.115-127.
18. Wang Y., Wang Y., Huang X. Cui W.: *A simplified maximum pit depth model of mild and low alloy steels in marine immersion environment.* Journal of Ship Mechanics, 2008, Vol.6, No.1, pp.401-417.
19. Kobzaruk K.A.V., Marichev V.A.: *Corrosion and corrosion fatigue resistance of steels in real marine environment and in laboratory* (in Russian). Physical Chemical Mechanics of Materials,1981, Vol.16, No 2, pp.15-21.
20. Melchers R.E.: *Pitting corrosion under marine anaerobic conditions – Part 2: Statistical representation of maximum pit depth,* 2006, Vol.62, No 12, pp.1074-1081.
21. Salvarezza R.C., Videla H.A.: *Passivity breakdown of mild steel in seawater in the presence of sulphate reducing bacteria.* Corrosion, 1980, Vol.36, No.10, pp.550-554.
22. Matoba M., Yamamoto N., Watanabe T., Umino M.: *Effect of corrosion and its protection on hull strength (1st report)* (in Japanese). J. Society of the Naval Architects of Japan, 1994, Vol.175, pp.271-280.
23. Nakai T., Matsushita H., Yamamoto N.: *Effect of pitting corrosion on the ultimate strength of steel plates subjected to in-plane compression and bending.* J. Marine Science and Technology, 2006, pp.52-64.
24. Wang Y, Wu X., Zhang Y., Huang X., Cui W.: *Pitting corrosion model of mild and low-alloy steel in marine environment – Part 2: The shape of corrosion pit* (in Chinese). Journal of Ship Mechanics, 2007, Vol.11, No.5.
25. Yuasa M, Watanabe T.: *Fatigue strength of corroded weld joints.* Class NK Technical Bulletin, 1996, Vol.14, pp.51-61.
26. Matsushita H., Nakai T., Yamamoto N.: *A study on static strength of corroded fillet welded joints for ship structures* (in Japanese). J. Society of the Naval Architects of Japan, 2004, Vol. 195, pp.291-297.
27. Cui N., Qiao L.J., Luo J.L., Chiovelli S.: *Pitting of carbon steel with banded microstructures in chloride solutions.* British Corrosion Journal, 2000, Vol.35.
28. Boukerrou A., Cottis R.A.: *Crack initiation in the corrosion fatigue of structural steels in salt solutions.* Corrosion Science, 1993, Vol.35, pp.577-585.
29. Miller K.J., Akid R.: *The application of microstructural Fracture Mechanics to various metal surface states.* Proc. Royal Society A ?, 1996, Vol. 452, pp. 1411-1432.
30. Konda N., Suzuki S., Tada N., Kho Y., Kazushige A., Watanabe E., Yamamoto M and Yaima H.: *Effect of microstructure on fatigue properties of steel in seawater – development of steels for high resistance to fatigue in ships, Part 2.* J. Soc. Naval Architects of Japan, 2001, Vol.191, pp.229-237.
31. Dolley E.J., Lee B., Wei R.P.: *The effect of pitting corrosion on fatigue life.* Fatigue & Fracture of Engineering Materials & Structures, 2000, Vol.23, pp.555-560.
32. Sankaran K.K., Perez R., Jata K.V.: *Effect of pitting corrosion on the fatigue behaviour of aluminium alloy 7075-T6: Modelling and experimental studies.* Materials Science and Engineering, 2001, Vol. A 297, pp223-229.

CONTACT WITH THE AUTHOR
Marek Jakubowski, Assoc. Prof.
Faculty of Ocean Engineering
and Ship Technology
Gdansk University of Technology
Narutowicza 11/12
80-233 Gdansk, POLAND
e-mail: marjak@pg.gda.pl

POLISH MARITIME RESEARCH 1(81) 2014 Vol 21; pp. 70-76
10.2478/pomr-2014-0010

A method to improve repeatability and reproducibility of the results of examination of the rate of heat released by shipbuilding materials

Krzysztof Sychta, Ph. D.,
Sychta Laboratory General Partnership, Poland

ABSTRACT

A specialised integrated research rig has been designed and built to validate the method of heat release dynamic error correction based on the FTP Code, part 5, and to control the rig operation and calibration. The basic rig component is a programmed gas burner with an option to select the function and parameters of burner's operation. The use of the programmed burner increased the level of consistency (reproducibility and correlation) of the results of heat release rate measurements.

Key words: intensity of the secretion of the warmth; dynamic measurements; dynamic error

INTRODUCTION

The energy potential collected in materials can, but does not have to, be released during the fire. The final effect will depend on:
- resistance of materials to the action of external ignition sources,
- combustion efficiency of particular materials, defined by the mass which was subject to gasification,
- rate of heat release during thermal decomposition and combustion of the material,

a result of which successive portions of the burning material, or adjacent materials, can, but do not have to, be subject to ignition.

The heat release rate is also decisive for the rate of fire temperature changes, and the emission of smoke and toxic decomposition products during thermal decomposition and combustion of materials. Therefore from the point of view of prevention of fire spreading in an arbitrary technical object the object of interest, among other factors, is:
- **resistance** of the material or product to the action of external ignition sources,
- **analysis of possible ignition** caused by this material or product to the next successive elements of its surface and adjacent materials.

Propagation of flames over the material surface can be described by parameters determining this propagation, which are:
- critical heat flux,
- heat needed to maintain flaming combustion,
- heat release rate,
- heat emitted during thermal decomposition and combustion,
- possibility to create droplet fall.

The above quantities characterise thermal conditions which are necessary to start and maintain flaming combustion. The two first parameters are responsible for the resistance of the material (product) to the action of external ignition sources, while the remaining three – for material's potential to ignite fire in adjacent materials.

The critical heat flux and the heat needed to maintain flaming combustion are the measures of minimal thermal power of the ignition source which is necessary to start the self-maintaining process of material combustion.

Important material parameters which are decisive for fire danger in technical objects are the heat release rate and thermal potential of the material used. In the shipbuilding industry the heat release rate is determined during the examination of the surface flammability level of materials, done using the method described in FTP Code, part 5, IMO [1]. The surface of the sample of the examined material is placed vertically (Fig. 1) and heated by the heat flux of standardised distribution generated by the gas-fired radiant heating panel.

Fig. 1. *Research rig examining surface flammability level of materials according to FTP Code, part 5*

The flame spreads along the sample in the decreasing heat flux direction before it autonomously extincts. The material

sample is examined at the presence of the flame of a pilot burner. The heat release rate – $\dot{q}(t)$ and the amount of heat Q_t released by the sample are calculated from the formulas:

$$q_p = \beta(T) \cdot (T_m - T_o) \tag{1}$$

$$Q_t = \int_0^{t_k} \beta(T) \cdot (T(t) - T_o) \cdot dt \tag{2}$$

where:

$\beta(T)$ - thermal equivalent of the research rig chimney duct, determined experimentally during rig calibration, [kW/K],
$T(t)$ - maximal temperature of gases in the chimney duct, [K],
T_o - initial temperature of gases in the chimney duct, [K],
t - time, [s].

FACTORS AFFECTING THE RESULT OF THE MEASUREMENT OF THE INTENSITY OF THE HEAT

The rate of heat release during thermal decomposition and combustion of the examined materials is measured using the method described in the FTP Code, part 5, in the open system (Fig. 1) without any forced gas flow through the chimney.

For the assumed initial conditions (without the burning sample or reference gas) the total thermal balance has the form:

$$\dot{Q}_{gpr} + \dot{Q}_{gp} = \dot{Q}^o_{gk} + \dot{Q}^o_{strat} \tag{3}$$

$$\dot{Q}^o_{gk} = \dot{V}^o_{gk} \cdot c_p \cdot (T_o - T_{ot}) = \dot{V}^o_{gk} \cdot c_p \cdot \Delta T_o \tag{4}$$

$$\dot{Q}^o_{strat} = \sum_{i=1}^{4} \sum_{j=1}^{3} \dot{Q}^o_{ijo} \tag{5}$$

where:

$\dot{Q}^o_{gk}$ - heat flux carried out with the gases flowing through the chimney duct at given initial conditions, [kW],
$\dot{Q}_{gpr}$ - thermal power of the radiant heating panel, [kW],
$\dot{Q}_{gp}$ - thermal power of the gas pilot burner, [kW],
$\dot{Q}^o_{strat}$ - total heat flux carried out to the environment at initial conditions, [kW],
$\dot{Q}_{ijo}$ - heat flux of j-th type (1 – radiation, 2 – convection, 3 – conduction) flowing from the source and to the environment, [kW],
$\dot{V}^o_{gk}$ - volumetric flow rate of gases in the chimney duct at initial conditions, [$m^3 \cdot s^{-1}$],
c_p - specific heat of gases, [$kJ \cdot m^{-3} \cdot K^{-1}$],
T_o - initial temperature of gases in the chimney duct, [K],
T_{ot} - ambient temperature, [K].

The total thermal balance for the rig with the burning sample or reference gas has the form:

$$\dot{Q}_{gpr} + \dot{Q}_{gp} + \dot{Q}_p = \dot{Q}_{gk} + \dot{Q}_{strat} \tag{6}$$

$$\dot{Q}_{gk} = \dot{V}_{gk} \cdot c_p \cdot (T_g - T_{ot}) = \dot{V}_{gk} \cdot c_p \cdot \Delta T_g \tag{7}$$

$$\dot{Q}_{strat} = \sum_{i=1}^{4} \sum_{j=1}^{3} \dot{Q}_{ijo} \tag{8}$$

where:

$\dot{Q}_p$ - rate of heat release during thermal decomposition and combustion of the sample of the examined material or reference gas, [kW],
$\dot{Q}_{gk}$ - heat flux carried out with gases flowing through the chimney duct, [kW],
$\dot{Q}_{strat}$ - total heat flux carried out to the environment, [kW],
$\dot{Q}_{ijo}$ - heat flux of j-th type (1 – radiation, 2 – convection, 3 – conduction) flowing from the source and to the environment, [kW],
$\dot{V}_{gk}$ - volumetric flow rate of gases in the chimney duct, [$m^3 \cdot s^{-1}$],
c_p - specific heat of gases, [$kJ \cdot m^{-3} \cdot K^{-1}$],
T_g - temperature of gases in the chimney duct, [K],
T_{ot} - ambient temperature, [K].

After transformation of the research rig thermal balance equation system we get the formula for the heat release rate during thermal decomposition and combustion of the sample of the examined material or reference gas [2]:

$$\begin{aligned} \dot{Q}_p &= (\dot{Q}_{gk} - \dot{Q}^o_{gk}) + (\dot{Q}_{strat} - \dot{Q}^o_{strat}) = \\ &= \dot{V}_{gk} \cdot c_p \cdot \Delta T_g - \dot{V}^o_{gk} \cdot c_p \cdot \Delta T_o + (\dot{Q}_{strat} - \dot{Q}^o_{strat}) \end{aligned} \tag{9}$$

$$\begin{aligned} \dot{Q}_p &= \beta_1 \cdot (\Delta T_g - \Delta T_o) + \beta_2 \cdot (\Delta T_g - \Delta T_o) = \\ &= (\beta_1 + \beta_2) \cdot (\Delta T_g - \Delta T_o) \end{aligned} \tag{10}$$

$$\dot{Q}_p = \beta(\Delta T_g) \cdot (\Delta T_g - \Delta T_o) \tag{11}$$

where:

$\beta_1 \cdot (\Delta T_g - \Delta T_o) = \dot{V}_{gk} \cdot c_p \cdot \Delta T_g - \dot{V}^o_{gk} \cdot c_p \cdot \Delta T_o$
$\beta_2 \cdot (\Delta T_g - \Delta T_o) = \dot{Q}_{strat} - \dot{Q}^o_{strat}$
$\beta(\Delta T_g) = \beta_1 + \beta_2$

It results from the above analysis that the **rig is a converter measuring the heat release rate** during thermal decomposition and combustion of samples of examined materials. High repeatability of the measured results can be obtained when repeatable conditions are preserved for:

- heat transfer between rig components and the environment,
- thermal decomposition and combustion of the examined material.

That means absolute necessity to preserve conditions, defined by a relevant standard for the given method, for thermal decomposition and combustion of samples of the examined materials. This requirement also refers to the environment and geometrical structure of the rig, which affect considerably the heat transfer between its individual components and that taking place in the zone of thermal decomposition and combustion of samples of examined materials.

The converter used for measuring heat release rate during thermal decomposition and combustion of samples of the examined materials with the aid of the calorimetric method given in the FTP Code, part 5, is the entire research rig which converts the measured quantity (heat release rate) to voltage. The heat release rate measured on the rig is a function of voltage signal at measuring system output:

$$\dot{Q}_p(t) = \beta(U) \cdot [U(t) - U_o] \tag{12}$$

where:

$\beta(U)$ - thermal equivalent of the rig, calculated experimentally during its calibration, [$kW \cdot mV^{-1}$],
U - voltage at output of the difference system measuring the temperature of gases in the chimney duct, [mV],
U_o - initial voltage at output of the difference system measuring the temperature of gases in the chimney duct, [mV].

The thermal equivalent of the rig is the thermal power which is to be continuously delivered to the chimney duct to keep

the elementary signal increment of the system measuring the temperature of the gases flowing through it steady:

$$\beta = \frac{\dot{q}}{U_m - U_o} \tag{13}$$

where:
β - thermal equivalent of the rig, [kW·mV^{-1}],
$\dot{q}$ - thermal power, [kW],
U_m - maximal signal of the temperature measurement system, [mV],
U_o - initial signal of temperature measurement system, [mV].

The thermal equivalent of the rig is determined experimentally during rig calibration by combusting a gas with known combustion heat in conditions identical to those in which material samples are examined. **The process of calibration of the heat release rate system is to be compatible with the real process of the heat release rate measurement during material examination.** When this condition was not met in the past, it led to different results of examination of the same materials done in different laboratories.

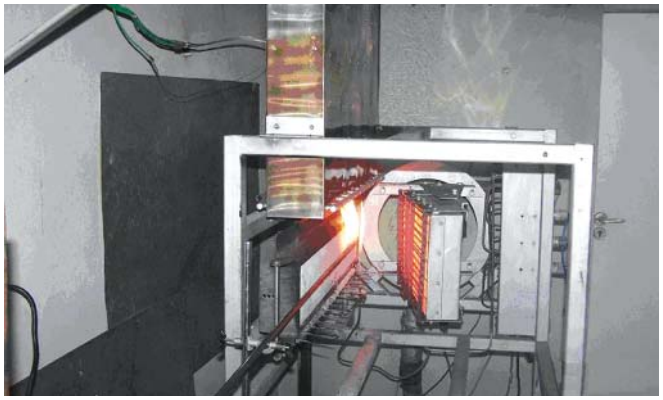

Fig. 2. *Rig measuring surface combustibility level of materials, according to FTP Code, part 5, with a calibration burner for thermal equivalent calculation*

A scheme of the measuring system to determine the thermal equivalent of the rig is given in Fig. 3.

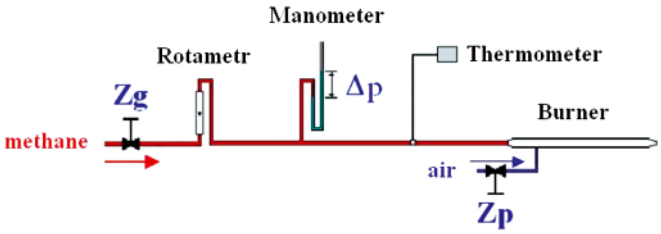

Fig. 3. *Scheme of feeding of the linear burner used for rig calibration*

The amount of the released heat and the rate of its release measured by the system are to be compared with the power of the burner and the amount of the heat delivered to the rig:

$$\dot{q} = \frac{T_o}{T_g} \cdot \frac{p_b + \Delta p}{p_o} \cdot \dot{V} \cdot c_{sp}$$
$$Q_c = \frac{T_o}{T_g} \cdot \frac{p_b + \Delta p}{p_o} \cdot V \cdot c_{sp} \tag{14}$$

where:
T_o - gas temperature at normal conditions, [K],
T_g - temperature of the combusted gas, [K],
p_b - barometric pressure, [Pa],
Δp - overpressure of the combusted gas, [Pa],
p_o - gas pressure at normal conditions, [Pa],
$\dot{V}$ - average volumetric gas flow rate, [m^3·s^{-1}],
V - volume of the combusted gas, [m^3],
c_{sp} - combustion heat of the gas, [kJ·m^{-3}].

The thermal equivalent of the rig is calculated from the formula:

$$\beta = \frac{T_o}{T_g} \cdot \frac{p_b + \Delta p}{p_o} \cdot \frac{\overline{\dot{V}} \cdot c_{sp}}{U_m - U_o} \tag{15}$$

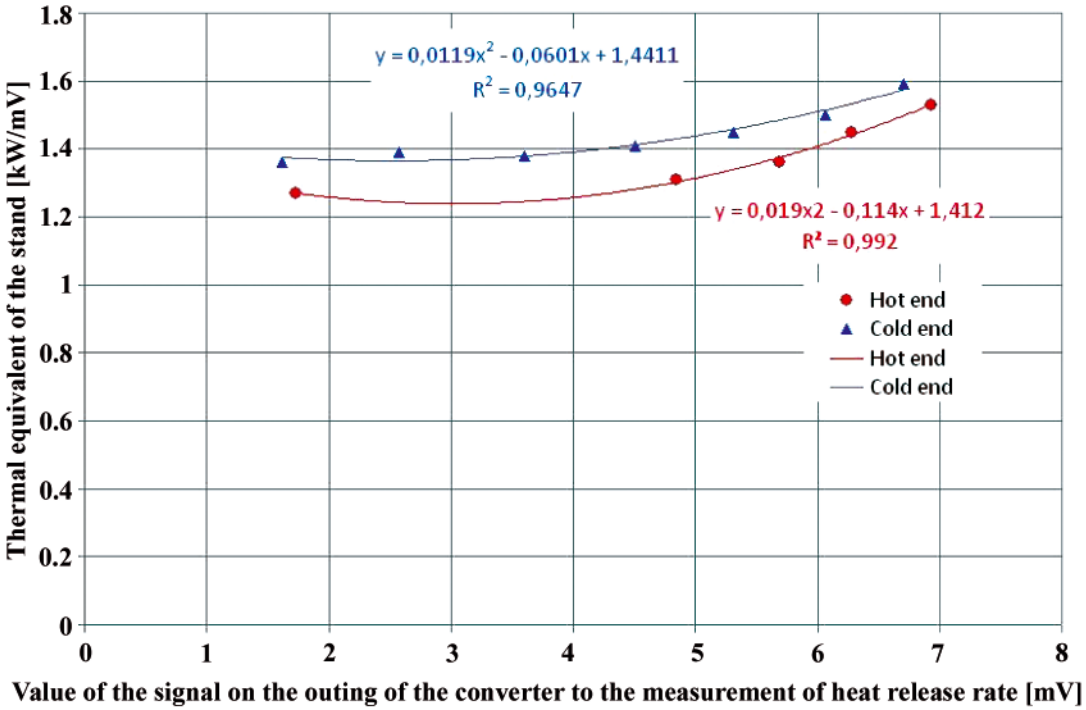

Fig. 4. *Results of measurements of thermal equivalent β of the KTZO rig used for examining surface combustibility of shipbuilding materials with the aid of the method of Resolution A.653(16)*

where:
T_o - gas temperature at normal conditions, [K],
T_g - temperature of the combusted gas, [K],
p_b - barometric pressure, [Pa],
Δp - overpressure of the combusted gas, [Pa],
p_o - gas pressure at normal conditions, [Pa],
$\overline{\dot{V}}$ - average volumetric gas flow rate, [$m^3 \cdot s^{-1}$],
c_{sp} - combustion heat of the gas, [$kJ \cdot m^{-3}$],
U_m - maximal signal of the temperature measurement system, [mV],
U_o - initial signal of the temperature measurement system, [mV].

Due to heat losses, the thermal equivalent of the rig is not constant and depends on the combustion gas temperature, $\beta(U) = f(U)$, while the relevant standard assumes its constant value.

The combined uncertainty of the heat release rate measurement rig is given by the equation system [2]:

$$\frac{u_c(\dot{Q}_p)}{\dot{Q}_p} = \sqrt{\left[\frac{u(\beta)}{\beta}\right]^2 + \left[\frac{u(U)}{U}\right]^2 + \left[\frac{u(U_o)}{U_o}\right]^2} \quad (16)$$

$$\frac{u_c(\beta)}{\beta} = \sqrt{\left[\frac{u(T_g)}{T_g}\right]^2 + \left[\frac{u(p_g)}{p_g}\right]^2 + \left[\frac{u(\dot{V}_g)}{\dot{V}_g}\right]^2 + \left[\frac{u(c_{sp})}{c_{sp}}\right]^2 + \left[\frac{u(U_m)}{U_m}\right]^2 + \left[\frac{u(U_o)}{U_o}\right]^2} \quad (17)$$

where:
$u(\beta)$ - standard uncertainty of measurement of thermal equivalent of the rig, [$kW \cdot mV^{-1}$],
$u(U)$ - standard uncertainty of voltage measurement at outlet of the difference system which measures gas temperature in the chimney duct, [mV],
$u(U_o)$ - standard uncertainty of initial voltage measurement at outlet of the difference system which measures gas temperature in the chimney duct, [mV].
$u(T_g)$ - standard uncertainty of temperature measurement of the gas delivered to the burner, [K],
$u(p_b)$ - standard uncertainty of pressure measurement of the combusted gas, [Pa],
$u(\overline{\dot{V}})$ - standard uncertainty of volumetric gas flow rate measurement, [$m^3 \cdot s^{-1}$],
$u(c_{sp})$ - standard uncertainty of combustion heat measurement for methane, [$kJ \cdot m^{-3}$],
$u(U_m)$ - standard uncertainty of measurement of maximal voltage at outlet of the difference system which measures gas temperature in the chimney duct, [mV],
$u(U_o)$ - standard uncertainty of initial voltage measurement at outlet of the difference system which measures gas temperature in the chimney duct, [mV].

Rig parameters and voltage U at difference system outlet, being the basis for estimating the gas temperature in the chimney duct, were measured using an integrated control and measurement system with a 20-bit A/D converter (Fig. 5). Standard uncertainty for the average value U measured by the voltage system is 0.001 mV. That means that the basic component of uncertainty when measuring heat release rate using the method of the FTP Code, part5, is uncertainty of the measurement of thermal equivalent $\beta(U)$ of the rig.

The extended combined uncertainty of the rig for heat release rate measurements making use of the FTP Code, part 5, method is obtained from the formula:

$$U = k \cdot u_c(y) \quad (18)$$

Since standard partial uncertainties were estimated from small numbers of measurements, the t-Student distribution was used for determining the extension coefficient. For the confidence level equal to 0.95 the assumed extension coefficient was 3.18. The extended uncertainty of the rig owned by the Faculty of Technical Ship Service is 0.2 kW.

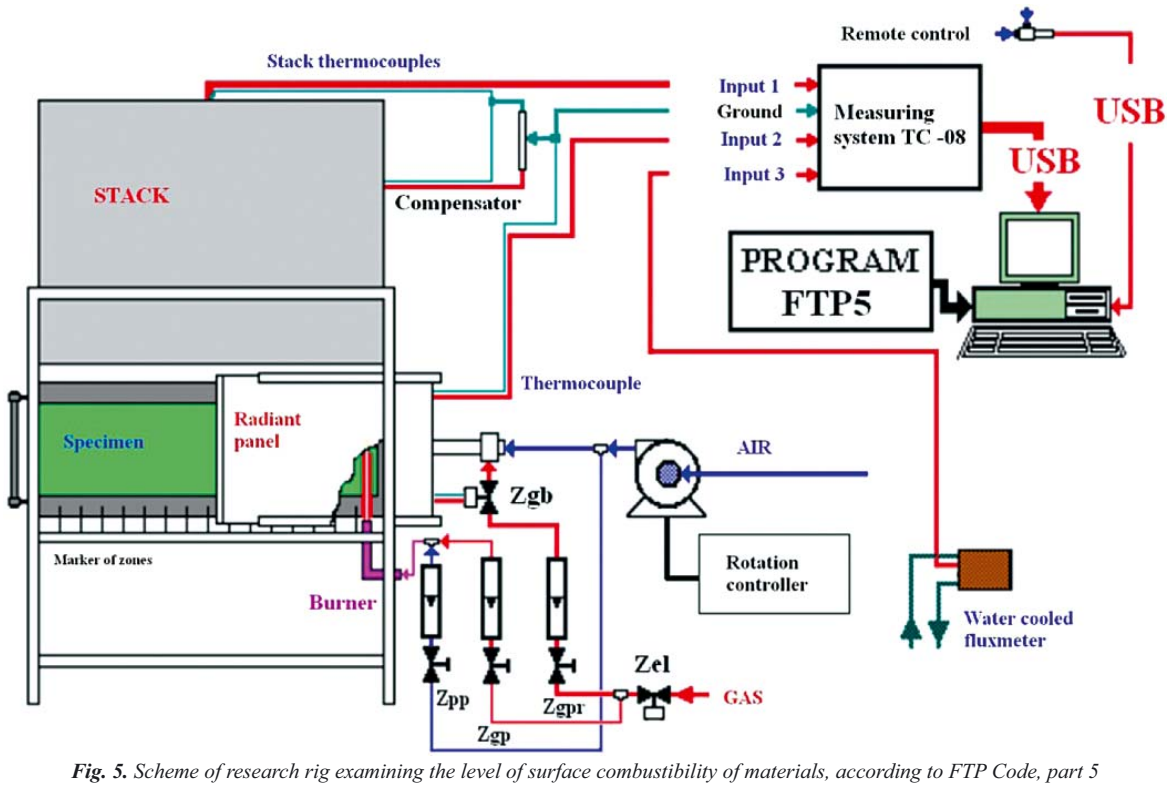

Fig. 5. Scheme of research rig examining the level of surface combustibility of materials, according to FTP Code, part 5

DYNAMIC ERROR CORRECTION METHOD

Since the material combustion is a dynamic process, the heat release rate measurement should also be considered a dynamic measurement. The identification of the research rig as the converter for heat release rate measurement consisted in defining the structure and functional relations which describe dynamic characteristics of the measuring system. This made it possible to conclude that [2, 3] the research rig measuring the heat release rate with the aid of the method of the FTP Code, part 5, (Res. A.653(16)) is the second order converter characterised by: time constant T_1, time constant T_2, attenuation coefficient ζ, and free-vibration pulsation coefficient ω_o.

Correction of the dynamic error of the rig working in accordance with the FTP Code, part 5, was done using the response of the rig to a linearly increasing excitation. The response of the second order converter to the linearly increasing excitation $x(t) = a \cdot t$ has the form [2]:

$$y(t)=a\cdot\left[t-\frac{2\cdot\zeta}{\omega_o}+\frac{\frac{1}{T_2^2}\cdot\exp\left(-\frac{t}{T_1}\right)-\frac{1}{T_1^2}\cdot\exp\left(-\frac{t}{T_2}\right)}{\omega_o^2\cdot\left(\frac{1}{T_2}-\frac{1}{T_1}\right)}\right] \quad (19)$$

For sufficiently large values of t the equation becomes:

$$\lim_{t\to\infty} y(t)=a\cdot\left(t-\frac{2\cdot\zeta}{\omega_o}\right) \quad (20)$$

Consequently it can be assumed that in the time interval: $t_i - \Delta t < t_i < t_i + \Delta t$ (where Δt it the time of measurement) the measured heat release rate is a linear function with the change rate a_i constant in this interval. The corrected value of the heat release rate is calculated from the formula:

$$\dot{q}_k(t_i)=\dot{q}(t_i)+a_i\cdot\frac{2\cdot\zeta}{\omega_o}= \quad (21)$$

$$=\dot{q}(t_i)+\frac{\dot{q}(t_{i+1})-\dot{q}(t_{i-1})}{t_{i+1}-t_{i-1}}\cdot\frac{2\cdot\zeta}{\omega_o}$$

VALIDATION OF A DYNAMIC ERROR CORRECTION METHOD

The validation of the method correcting the dynamic error of the heat release rate measurement making use of the method described in the FTP Code, part 5, was done using a specialised integrated research rig designed and built for this purpose. The basic component of the rig is a programmed gas burner with the option to select the function and parameters of burner's operation.

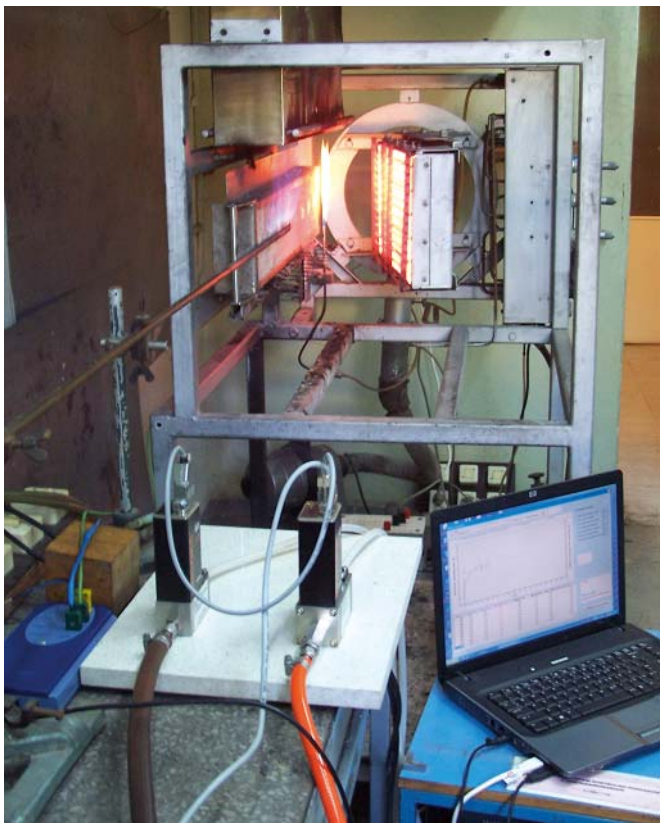

Fig. 7. Rig for examining heat release rate with the aid of the FTP Code, part 5, method

Taking into account dynamic characteristics of the rig has made it possible to improve the level of consistency (reproducibility and correlation) of the results of heat release rate measurements (Fig. 8, Fig. 9, Fig. 10), without introducing any changes to research rig structure and measuring procedures.

Taking into account dynamic characteristics of the rig has made it possible to improve the level of consistency (reproducibility and correlation) of the results of heat release rate measurements done using different methods, without introducing changes to research rig structures and measuring procedures (Fig. 11).

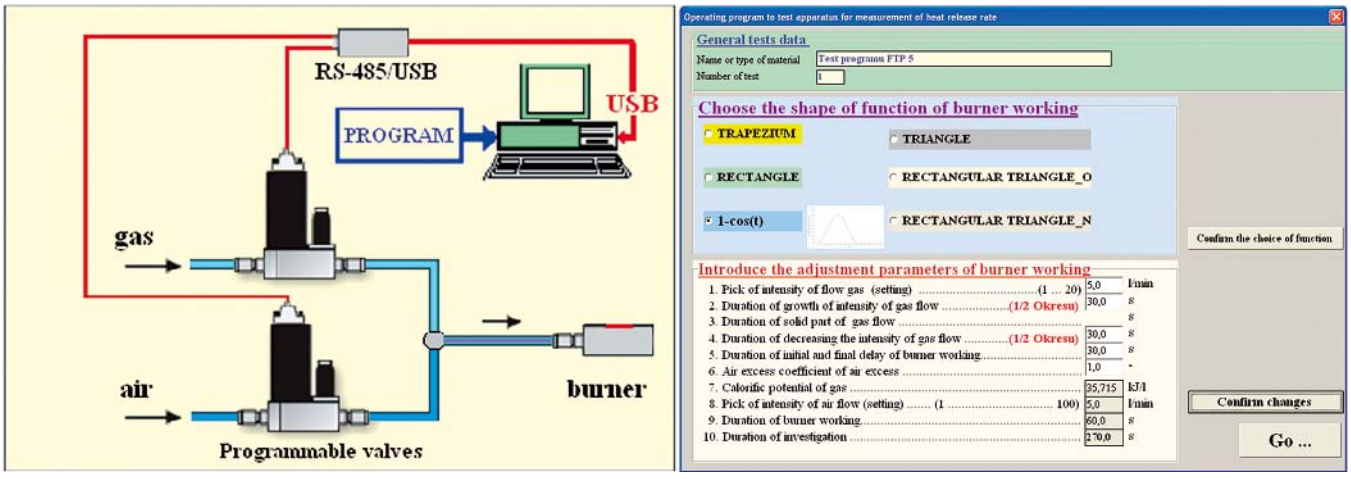

Fig. 6. Scheme of programmed gas burner

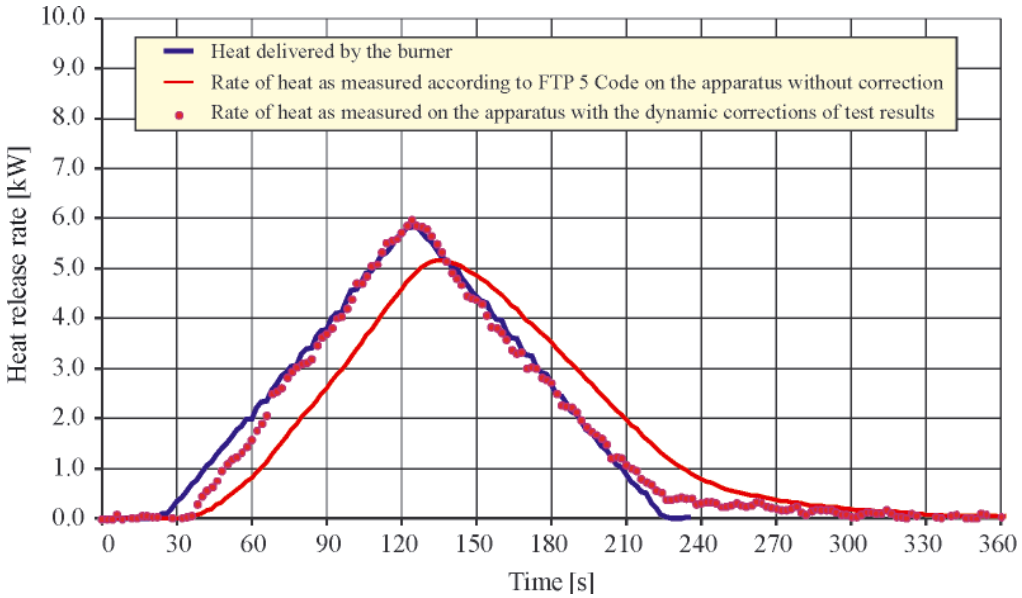

Fig. 8. *Comparing results of the heat release rate of the programmed gas burner with that measured on the rig with the aid of the FTP Code, part 5, method – with and without dynamic error correction*

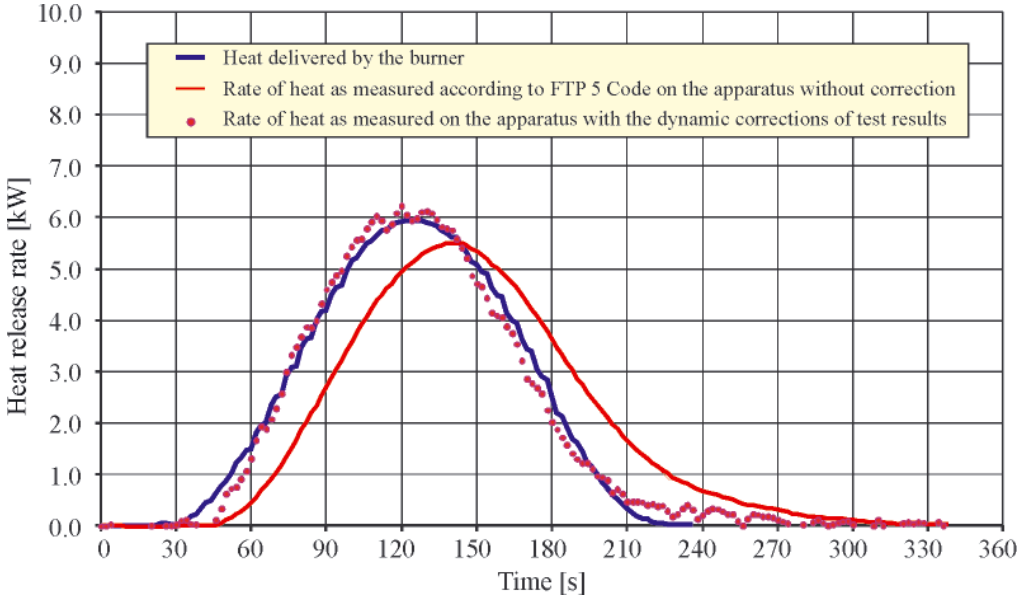

Fig. 9. *Comparing results of the heat release rate of the programmed gas burner with that measured on the rig with the aid of the FTP Code, part 5, method – with and without dynamic error correction*

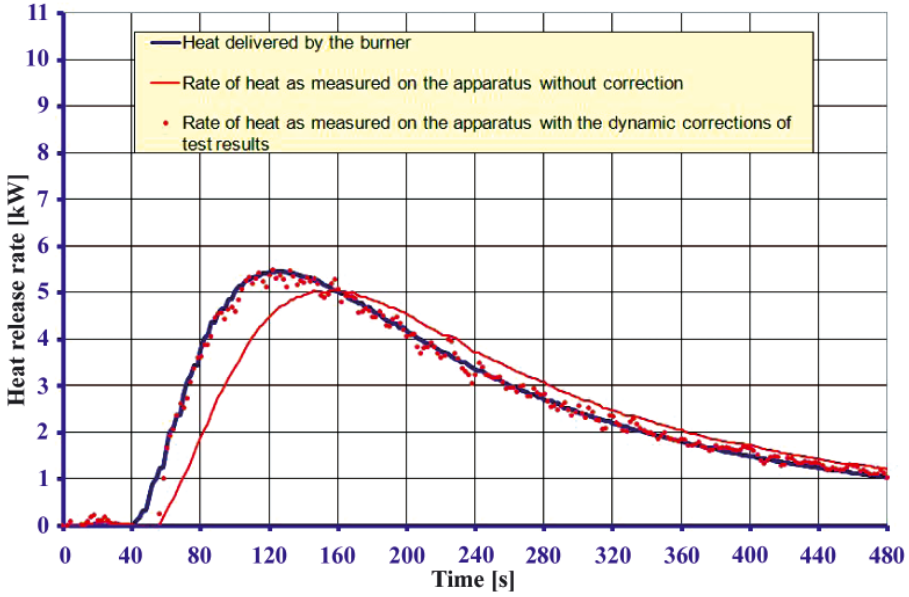

Fig. 10. *Comparing results of the heat release rate of the programmed gas burner with that measured on the rig with the aid of the FTP Code, part 5, method – with and without dynamic error correction*

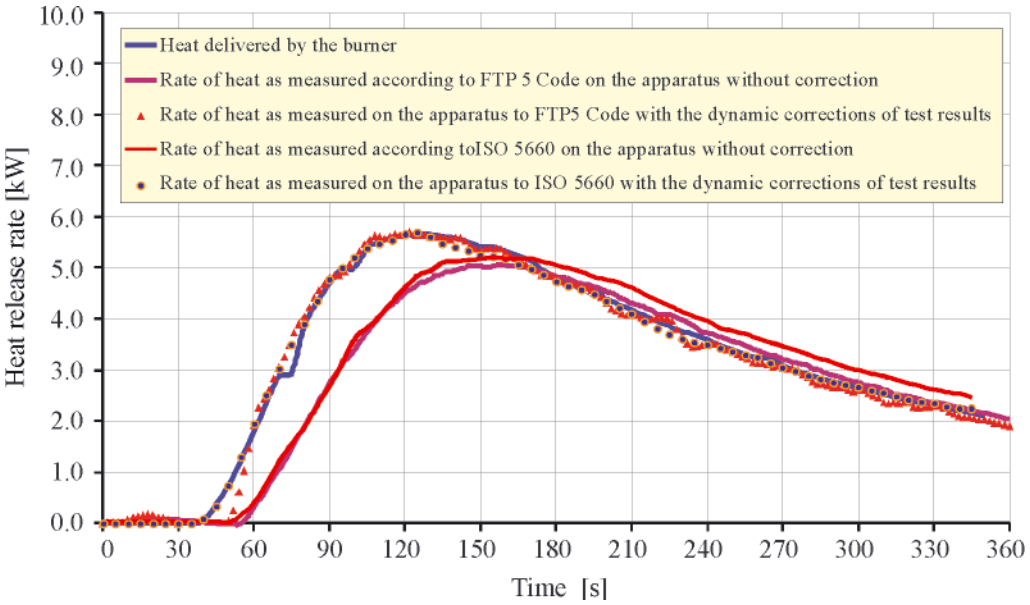

Fig. 11. *Comparing results of the heat release rate of the programmed gas burner with the values measured on the rig using the FTP Code, part 5, method and on the ISO 5660 rig [4] – with and without dynamic error correction*

SUMMARY

A basic factor which is decisive for poor correlation between results of heat release rate measurements done using different methods is treating the measurement in a conventional way as a static measurement. Since material combustion is a time-dependent process, the heat release rate measurement should also be considered a dynamic process.

In order to validate and control the rig operation and the method used to correct the dynamic error of heat release rate measurement making use of the FTP Code, part 5, method, a specialised integrated research rig was designed and built. The basic component of this rig is a programmed gas burner with an option to select a function and parameters of burner's operation.

Taking into account dynamic parameters of the rig has made it possible to increase the level of consistency (reproducibility and correlation) of the results of heat release rate measurements obtained using different methods, without introducing any changes to research rigs and/or measuring procedures.

BIBLIOGRAPHY

1. International Code for Fire Test Procedures. Annex 1. Part 5. Surface Flammability Test. International Maritime Organization, London 1998
2. K. Sychta: *Analiza porównawcza badań intensywności wydzielania ciepła przez materiały okrętowe oraz metoda poprawy dokładności pomiaru. (Comparison and analysis of tests of the rate of heat release results of shipbuilding materials and the method of improvement of reproducibility of results).* Doctors Thesis, Faculty of Maritime Technology, Szczecin Technical University, Szczecin 2006
3. K. Sychta: *The analysis of research results concerning heat release rates of ship materials with regard to dynamic parameters of the research station*. Polish Maritime Research, Vol. 15 (2008) pp. 56-59
4. ISO 5660-1: 2002, Reaction-to-fire tests . Heat release, smoke production and mass loss rate. Part 1: Heat release rate (cone calorimeter method)

CONTACT WITH THE AUTHOR

Krzysztof Sychta, Ph. D.,
Sychta Laboratory General Partnership,
Ofiar Stutthofu 50,
72-010 Police, POLAND
e-mail: biuro@sychta.eu
phone: +48 91 3170161

POLISH MARITIME RESEARCH 1(81) 2014 Vol 21; pp. 77-88
10.2478/pomr-2014-0011

On board LNG reliquefaction technology: a comparative study

J. Romero Gómez, Ph. D.,
M. Romero Gómez, Ph. D.,
R. Ferreiro Garcia, Prof.,
A. De Miguel Catoira, Ph. D.,
University of A Coruna, Spain

ABSTRACT

Reliquefaction technologies are being currently applied on board liquefied natural gas (LNG) carriers on the basis of economic criteria and energy efficiency. A variety of reliquefaction techniques have been developed so far during the last decade. Nevertheless, technology enhancement continues being a research area of interest. In this article the different technologies applied to the reliquefaction of the boil-off gas (BOG) on LNG carriers have been described, analysed and discussed, contributing to highlight the process and operation characteristics as well as selection plant criteria. Finally, a comparison of the different reliquefaction plants, considering their capacities and efficiencies as well as other technical data of interest has been carried out.

Key words: reliquefaction; boil-off gas; vessel; Brayton Cycle; efficiency

1. INTRODUCTION

Among merchant ships, the LNG carriers are of the highest speed, their average service speed varies usually in the range of 19 ÷ 21 knots [1]. Since the introduction of LNG transport ships, steam turbines have almost exclusively been the method of propulsion. This is namely due to the simplicity of using the gas from the evaporation of the cargo in steam boilers to produce steam for the turbines, while controlling the pressure in the cargo tanks. The overall efficiency of this method is estimated to be of around 30% [2].

In recent years, due to the increasing cost of LNG, the shipbuilding industry has called for alternative propulsion systems to the steam turbine, opting for more efficient propulsion systems.

Thanks to recent technological developments, electric propulsion with dual 4-stroke engines has become the most demanded option for LNG carriers between 140,000 and 210,000 m^3. The use of 2-stroke engines in combination with the BOG reliquefaction is the most used on larger vessels. Electric propulsion with 4-stroke dual-powered engines and the propulsion of 2-stroke engines combined with reliquefaction provide efficiencies above 40% (43% and 48% respectively) [2], while reducing emissions to the atmosphere of NOx, SOx and CO_2. Fig. 1 shows the possible propulsion options for LNG carriers depending on the method of processing the BOG.

The implementation of reliquefaction techniques on board has acquired a very important role in recent years, in an effort to reduce operating costs and increasing energy efficiency in large LNG carriers. Despite this, there has been no literature with a detailed technical report in the academic field wherein a comparative description of reliquefaction plants currently on the market is carried out. Although some studies [3, 4] have described the process, the scope of studies is limited to only some characteristics or, in particular, the analysis of the operating cycle. The efforts undertaken in the development and implementation of this new technology installed on board Qatargas 2 in the Q-Flex and Q-Max ships are reviewed in [5]. By means of performing a thermodynamic study, in [6] the conditions, parameters and energy consumption required in the process of reliquefaction on board under the Brayton cycle were analysed and evaluated, including the influence of the choice and variation of diverse factors on the operating conditions and power. A design of the reliquefaction process based on the Brayton cycle is carried out in [7], followed by dynamic simulations for all operation modes. [8] analyses the availability and security of propulsion systems with reliquefaction for LNG vessels along with other studied alternatives to propulsion.

The optimization of redundancy and the maintenance strategy of reliquefaction systems are studied in [9] to provide reliability and reduce costs in case of system failure.

A comparison of the various technologies implemented on-board has become necessary as a result of the increasing number of manufacturers who seek to apply these new techniques on ships in order to reduce operating costs and increase efficiency. In the following sections of this paper a general reliquefaction technology on board is carried out as are the processes of reliquefaction technology already in place, a comparative study of available technologies and the study's con clusions.

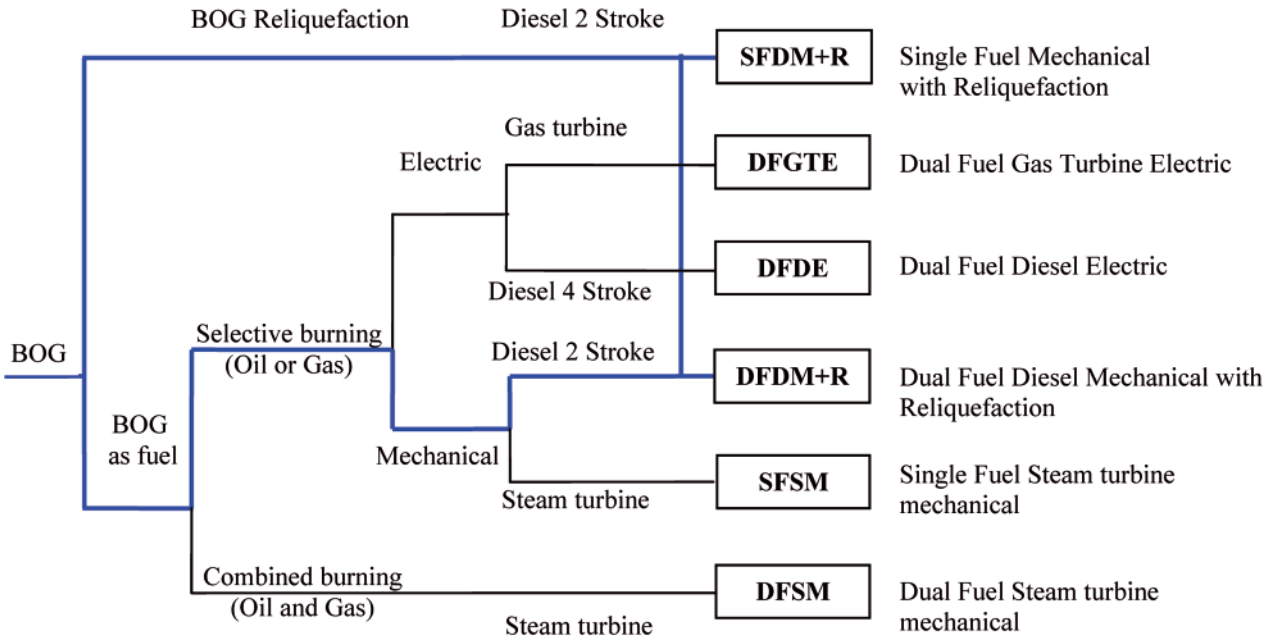

Fig. 1. *Different propulsion systems for LNG carriers*

2. RELIQUEFACTION TECHNOLOGY ON BOARD

The reliquefaction of BOG on board has different processing requirements to traditional LNG plants on shore. While the thermodynamic efficiency of liquefaction plants on-shore is the most contentious criteria, other different factors are more important in re-liquefied projects on board. Therefore, when selecting the reliquefaction technology, several key points should be analysed that outweigh the efficiency of the process and determine the election:

- The limited space on board requires the plant to be compact and lightweight.
- The conditions at sea shouldn´t effect the operation of the plant. It must be stable with swaying and pitch.
- Must provide high security and inherent reliability in the process.
- Quick startup with high availability and operability.
- Small amount of equipment, easy installation and low cost.
- Easy maintenance.

It is because of the above points that the leading manufacturers of this technology incline towards the Brayton cooling cycle (with N_2 as the working fluid), instead of other more efficient technologies installed in onshore LNG trains such as:

- Traditional waterfall cycle or mixed refrigerants.
- Simple mixed refrigerant cycle.
- Pre-cooling propane cycle and mixed refrigerant.

These technologies operating onshore reach extremely low rates of liquefaction consumption, around 0.3 kWh/kg [10].

2.1. Basic principles of operation of the Brayton cooling cycle

The Brayton cooling cycle is the inverse of the closed Brayton power cycle. A basic representation of the reverse Brayton cycle used for on board reliquefaction is shown in Fig. 2.

The working fluid is N_2 as a number of conditions need to be met that make it ideal for the process. The boiling point of

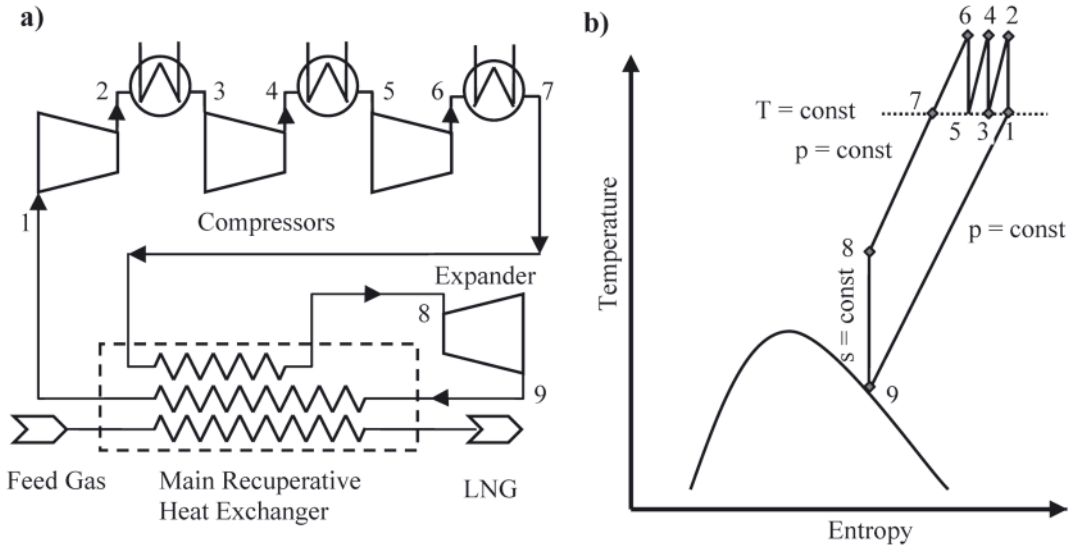

Fig. 2. *Schematic diagram of the reverse Brayton Cycle.* ***a)*** *the plant structure,* ***b)*** *the T-S diagram*

the N_2 is below methane, it is inert, not a fuel, it´s safe and it´s acquirement is possible on board.

The working cycle is described as follows: N_2 is compressed in stages with intercooling, process 1-7 as shown in Fig. 2. The intercoolers, with sea water or a medium fluid necessary to reduce the compression work.

After the final cooling in the compression, the nitrogen is sub-cooled countercurrent (stage 7-8) with the same N_2 in an exchanger. At this temperature it undergoes an isentropic expansion in an expander (stage 8-9), thereby obtaining the cold current to liquefy the BOG and sub-cool the nitrogen before expansion, while recovering a percentage (about 20%) of power expended in the compression of nitrogen.

3. RELIQUEFACTION PLANT STRUCTURES IMPLEMENTED ON BOARD

Current technology of BOG reliquefaction offers seven different processes for LNG carriers. These are listed in Tab. 1 alongwith the company, year of implementation, work cycle and licensor. It is noted that Hamworthy Gas System (HGS) is the manufacturer with most technological influence and that the Brayton refrigeration cycle predominates over other alternatives used.

Tab. 1. *Current technology for reliquefaction of BOG on LNG carriers*

Plant model	Manufacturer	Work Cycle	Year
LNG Jamal	Osaka Gas	Inverse Brayton	2000
TGE	Tractebel	Inverse Brayton	2004
Mark I	HGS	Inverse Brayton	2006
EcoRel	Cryostar	Inverse Brayton	2008
Mark III	HGS	Inverse Brayton	2008
Mark III Laby-GI	HGS	Inverse Brayton	2009
TGE Laby-GI	Tractebel	Waterfall	2009

3.1. LNG Jamal

The first reliquefaction plant on board a LNG carrier was installed in the Jamal with a cargo capacity approaching 135.000 m^3 [11]. It was intended to pave the way toward the use of new propulsion systems and better the efficiency in the transport of LNG. Due to lack of experience with the implementation of reliquefaction technology on board, a steam turbine plant with a propulsion system was installed instead of the other possible more efficient systems.

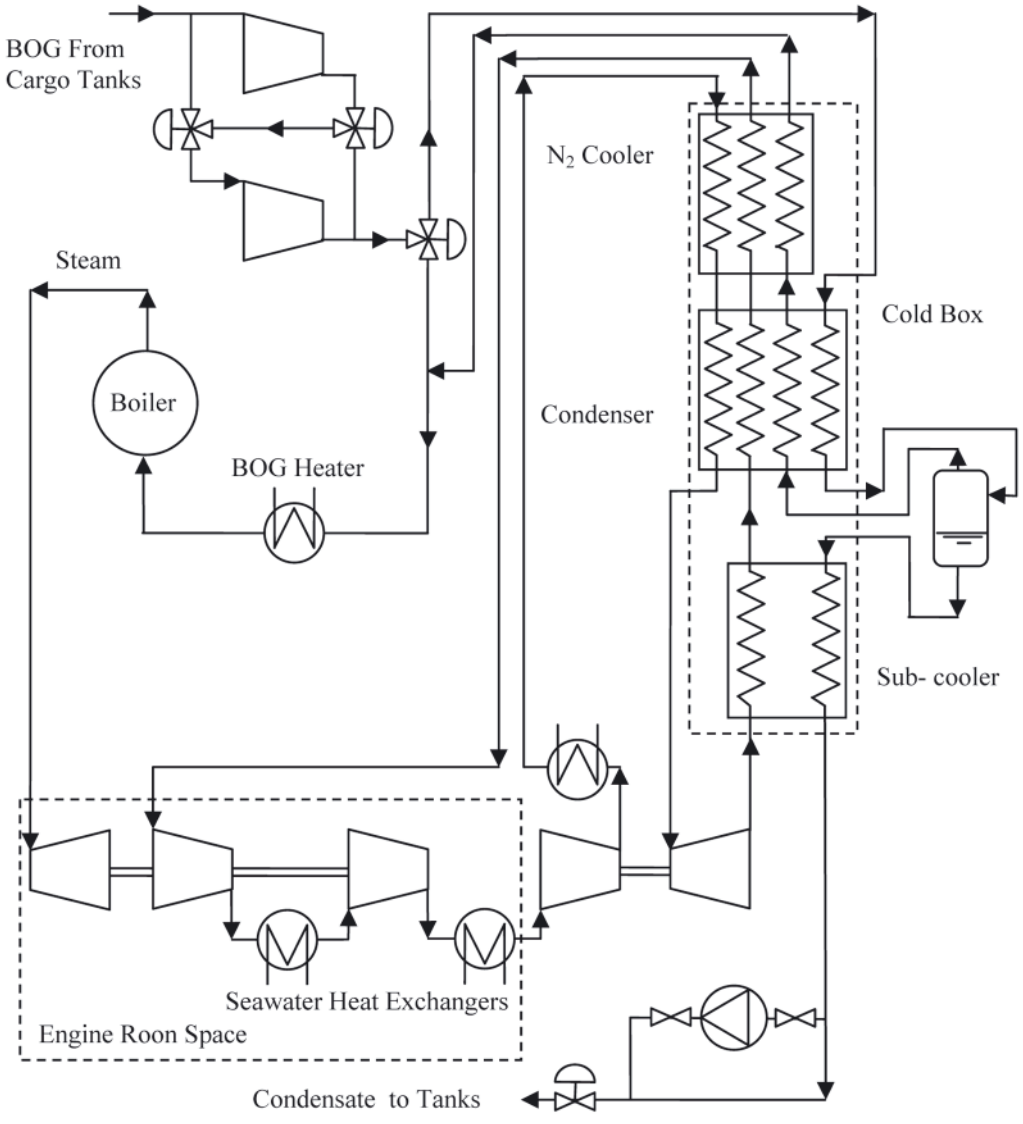

Fig. 3. *BOG reliquefaction process flow diagram of the Jamal*

The plant is based on the reverse Brayton cycle using nitrogen as the working fluid. It was designed for a nominal reliquefaction capacity of 3 Tons/h based on a BOG rate (BOR) of 0.14 %/day. The power required to process a nominal capacity is 3 MW.

Under normal conditions all the BOG is processed through the plant and a heavy fuel is used for propulsion, burned in boilers to produce steam for the turbines. In case of failure of the reliquefaction plant BOG is sent to the boiler to generate steam for the turbines, the ship is operated as a conventional tanker.

The cooling power is obtained from the nitrogen circulating in a closed reverse Brayton cycle. A schematic of the plant is depicted Fig. 3. The N_2 is compressed to 35 bar by three-stage centrifugal compressors with intercooling by means of sea water. Once compressed it is introduced into a cold box, which houses most of the cryogenic equipment. This consists of three sections: the nitrogen cooler, a condenser and a subcooler. Here the nitrogen is cooled before entering an expander, where it makes the expansion from 35 bar to 6.5 bar. Thus obtaining the cold current that leads to the cold box upstream to subcool the LNG and the N_2 before undergoing expansion.

The energy for the first two stages of compression of N_2 is obtained from a turbine powered by steam from the main boiler, while the third stage of compression is the energy recovered in the expander. The problem with this is the pressure loss that occurs in the nitrogen cycle, to travel great distances to the engine room to be driven by the turbine.

BOG system is composed by 2 centrifugal compressors, which can be batch or parallel as required. When demand is high BOG compressors operate in both tandem and when it is low or the BOG is burned in boilers as in a traditional LNG, are arranged in parallel and the other remain in stand-by.

To condition the BOG for reliquefaction, it is compressed to 4.5 bar with the two compressors in series. As the BOG passes through the cold box and the heat exchange performed on the N_2, it condenses and heads toward the separator gas/liquid. Here the non-condensable gases of the condensed BOG are separated. Condensable gases are directed against the current in the condenser and the nitrogen heat exchanger, to act as a coolant, conditioning it to turn for combustion in the steam boiler. The BOG condensate is then sent to the sub-cooler and back to the tanks by pressure difference. In certain processes, where the pressure of the condensed BOG is not sufficient to overcome the column of LNG of the tanks, there is a pump that raises the pressure.

Except in the case of BOG compressors, which are used as much in plant mode as in conventional mode, the system implemented on the Jamal has used no additional redundancy methods for the reliquefaction plant. Instead, the steam boiler has the same redundancy as that of any conventional carriers.

3.2. Tractebel Gas Engineering TGE

As a result of heightened awareness that TGE liquefaction technologies has, this process is also based on reverse Brayton cycle with nitrogen. Fig. 4 shows the diagram of this process. The plant has been designed for a carrier of 228 000 m^3, with a BOR of 0.14 %/day, which means 6.25 t/h.

The BOG from the tanks is compressed by a centrifugal compressor at a pressure ranging from about 3 to 6 bar, and liquefied in the main heat exchanger by the cold current of N_2. It is previously expanded to the pressure tank through a valve. For the start-up process, in cases where liquefaction of the BOG isn´t achieved, the plant has a larger diameter valve to facilitate the exit. An exchanger is located at the entrance of the reliquefaction plant to condition the BOG by means of injecting LNG. In this way the inlet temperature is controlled in extreme cases and eases startups. This exchanger also acts as a pre-cleaner to prevent liquid from entering the compressor.

The cooled nitrogen is compressed in a three-stage turbo compressor exchangers shell and tube to room temperature with seawater. It is then introduced into the heat exchanger until reaching temperatures of between -80°C and -110°C.

The cooled nitrogen is sent via the expander, whose transmission shaft is connected to the third stage of compression named a Compander. Hence the nitrogen temperature reaches -170°C /-180°C with expansion.

Due to the different boiling points of LNG components (ranging from -196°C to +36°C), vaporization is not homogeneous: components with the lowest boiling point (N_2 and CH_4) tend to evaporate in a more important amount than heavy components [ethane (C2) and propane (C3), and traces of i-butane (i-C4), n-butane (n-C4), i-pentane (i-C5) and n-pentane (n-C5)] [12]. This phenomenon is known as the aging of LNG and its main consequence is the change of the composition and its properties during the trip. In this plant, the incondensable BOG gases are injected into the cargo tanks for its reabsorption by a piping system. This prevents the enrichment of the load and maintains a relatively constant composition.

BOG and N_2 equipment are separated by a bulkhead, ensuring safety while allowing the use of lower cost devices on the N_2.

The control system is through a conventional PLC integrated into the architecture of the plant cargo system. The boot sequence is programmed to reach operating temperature in 2 hours from room temperature. The plant is designed to work 9-12 hours a day on a loaded voyage. During the period of operation the tanks are cooled and then remain stopped until the pressure increases again and the control system proceeds to initiate the boot sequence. Once the plant is cooled, the sequences of stop/start are reduced to one hour.

The installed power for compression of N_2 is of 4.700 kW and 2x330 kW for the compression of the BOG. The power recovered in the expander is of the order of 1200 kW. The water flow required for the intermediate cooling of N_2 increases to approximately 700 m^3/h. The total energy consumption is about 0.75 kWh/kg [13].

The redundancy of the compression equipment includes margins of tolerance of 5% and 25% for the cryogenic heat exchanger. A redundant system, that is, two compressors of equal capacity, is available for the compression of BOG. In the case of reliquefaction system failure, the plant has a combustion unit (CGU, Combustion Gas Unit) to maintain steady pressure in the tanks.

3.3. Mark I

This plant was developed by Hamworthy Gas System (HGS), based on the reverse Brayton cycle. Qatargas and ExxonMobil chose it as the reliquefaction system for the first Q-Flex ships of 210.000 m^3, combined with a slow propulsion system. It´s design is based on a BOR of approximately 0.14 %/day of the cargo volume and has a maximum capacity of 6 t/h reliquefaction plant, with an approximate electric power consumption of 5.8 MW. A flowchart of the reliquefaction system is shown in Fig. 5.

The BOG at the entrance of the plant is pre-cooled in a heat exchanger by flashing a small stream of BOG condensate from the separator. Since the BOG is being heated when transferred from the LNG tanks to the plant suction, a pre-cooling allows for the temperature compensation before entering the

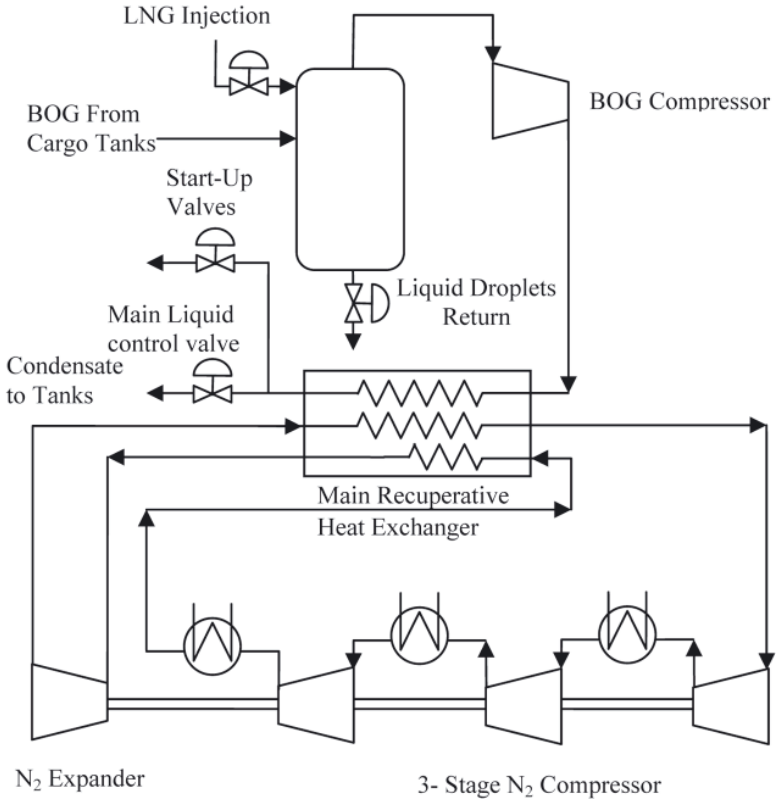

Fig. 4. *Flow Diagram of the reliquefaction of TGE process*

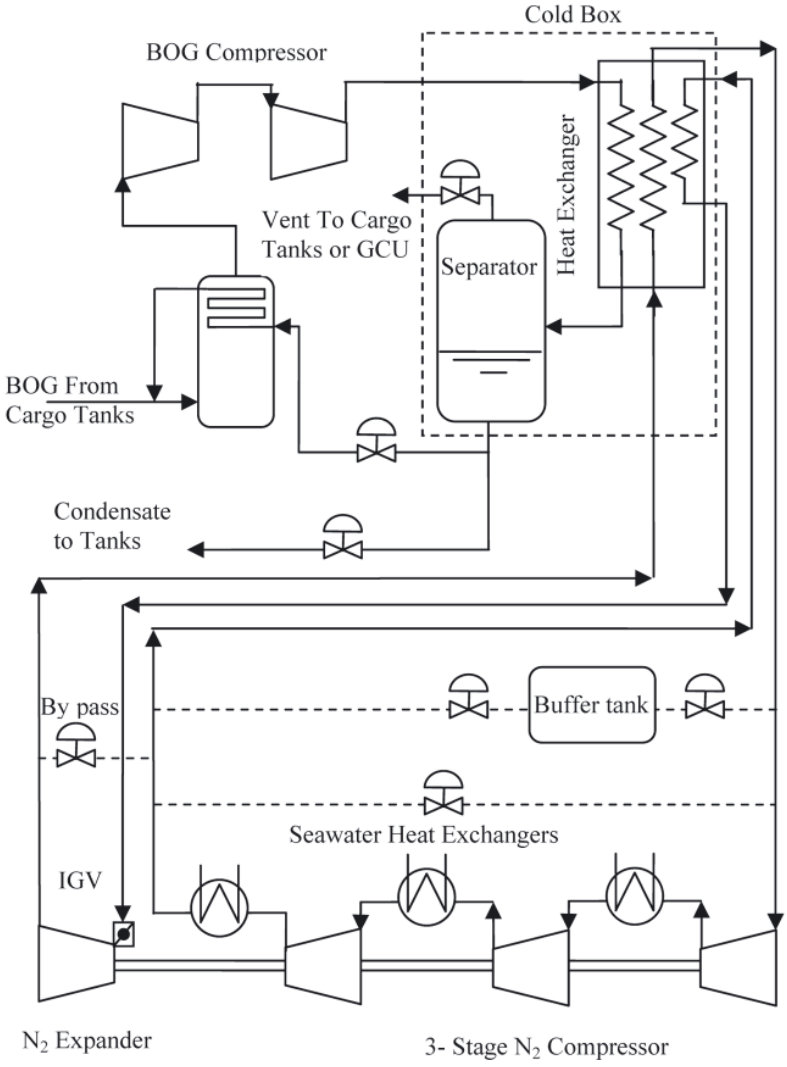

Fig. 5. *Flow diagram of HGS Mark I reliquefaction process*

reliquefaction plant, thus maintaining a stable temperature at the entrance of the process. The pre-cooling heat exchanger is designed to remove any possible heavy components formed by condensation and in effect protect the compressors.

Precooled BOG is compressed to approximately 4.5 bar in two stages with centrifugal compressors with a capacity regulation by DGVs (diffuser guide vanes). This allows the variation of the flow of BOG through the compressors in order to adapt to BOR changes in the tanks and therefore control the pressure.

Once the BOG is compressed it is condensed counter current with the cold N_2 in the cryogenic heat exchanger. The BOG condensate is collected in a separator to remove non-condensable gases, and from here as a result of the pressure difference with the cargo tanks, is returned. The cryogenic heat exchanger and the separator form a single insulated cold box to minimize the heat input.

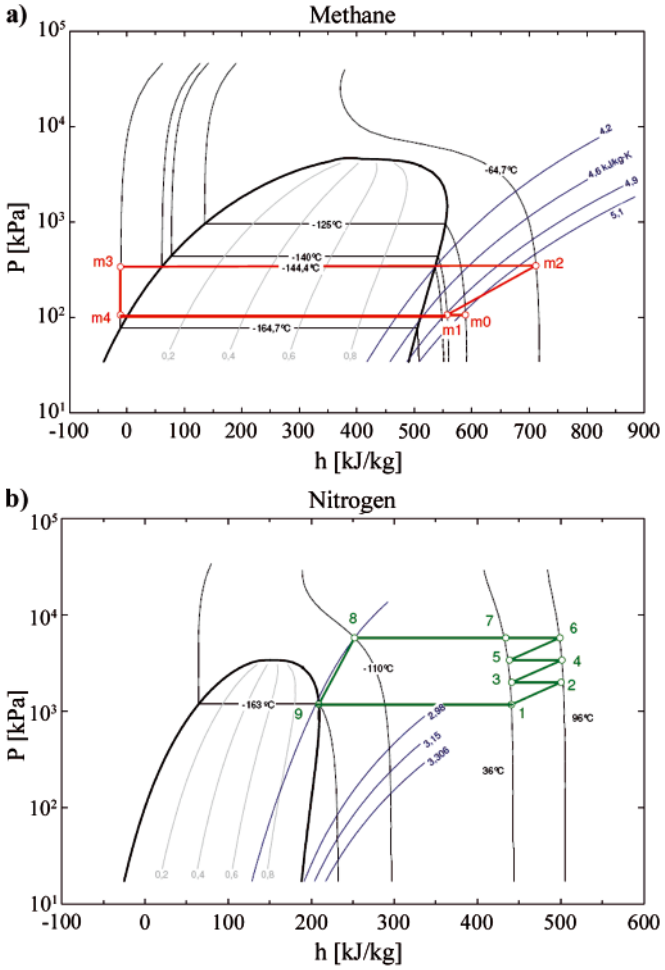

Fig. 6. a) *Mollier diagram of different stages of BOG in the reliquefaction process;* ***b)*** *Mollier diagram of the Brayton refrigeration cycle*

Fig. 6(a) shows the different stages of cooling process by the BOG. The process (m0-m1) is the pre-cooling of the BOG on entry to the plant, before the double compression (m1-m2). This pre-cooling is due to the evaporation (m4-m1) of the flashed fraction of BOG condensate (m3-m4).

In the reverse Brayton cycle, in terms of design, N_2 is compressed to 58 bar in three-compression stage with intercooling and cooled down to -110°C in the cryogenic heat exchanger. In the expansion, the pressure drops to 14.5 bar and the temperature to -163°C.

The plant´s control software is designed to handle all the changes in the BOG. The control can be summarized in two ways: start-up and normal operation. In start-up mode a pre-cooling of the heat exchanger is carried out at a rate of -2 °C/min to a temperature close to -163°C, operating only the N_2 cycle. Once the pre-cooling is complete it passes to normal operating mode with the BOG compressor running to process the BOG. During normal operation, the expander outlet temperature is controlled to keep it as low as possible, but above the saturation limit. At the same time, the amount of circulating N_2 is continuously controlled to meet the thermal demands of the BOG to condense.

To control the final expansion temperature of the plant it is equipped with three capacity control actuators: Buffer tank valves, Inlet guide vane (IGV) and bypass valve, arranged as shown in Fig. 5.

In medium and high work mode, the control of the reliquefaction capacity is achieved by varying the N_2 mass flow circulating in the circuit, through the buffer tank connected between the suction and discharge with its corresponding valves.

If the cooling capacity is too low, the outlet temperature of the expander is increased and so opens the control valve of the nitrogen container located at stage 1 of the compressor suction and nitrogen is added to the Brayton cycle until the setpoint temperature at the outlet of the expander is achieved. If, however, the cooling capacity is too high, the expander outlet temperature decreases, thus opening the nitrogen container´s control valve located after the last compression cooling and nitrogen is removed from the cycle until the setpoint temperature is reached at the exit of the expander.

The nitrogen container, located on deck, is designed to engender a sufficient volume to store the N2 at room temperature and an intermediate pressure between suction and discharge. This pressure varies depending on the work situation of the plant. If the plant operates near the nominal point, the pressure in the container will be closer to the suction pressure of Stage 1, while if working part-load the pressure value is close to the discharge.

At low load operation, to control the final temperature of expansion, cross-sectional area is reduced via the inlet guide vane mediate (IGV) of the expander. This ensures the expansion outside the zone of saturation. If this control loop is not enough the by-pass valve control loop opens it, introducing hot gas at the end of the expansion process.

For the control of flash gases produced in the separator, the plant installs an automatic gas purger which returns the gas to the tanks or send it to the CGU.

The process uses full redundancy for all rotating parts as specified by the regulations on international gas carrierss. The CGU is able to handle 150% of normal BOR, to ensure the treatment of BOG in case of total failure of the BOG reliquefaction system.

3.4. Ecorel

The Ecorel plant was developed by the Cryostar company for Q-Max ships of 266.000 m³, on the Qatargas-2 project. The operating principle is similar to the Mark I, HGS plant. A flowchart of the Ecorel plant is shown in Fig. 7. The plant has a reliquefaction capacity of 7 t/h of the BOG, with a power consumption of about 6 MW.

BOG is compressed in two-stages with centrifugal compressors equipped with capacity control by DGVs up to 4.8 bar. The compression between stages is cooled by a fraction of N_2 from the BOG condenser, which reduces the required compression work. Before passing to the condenser

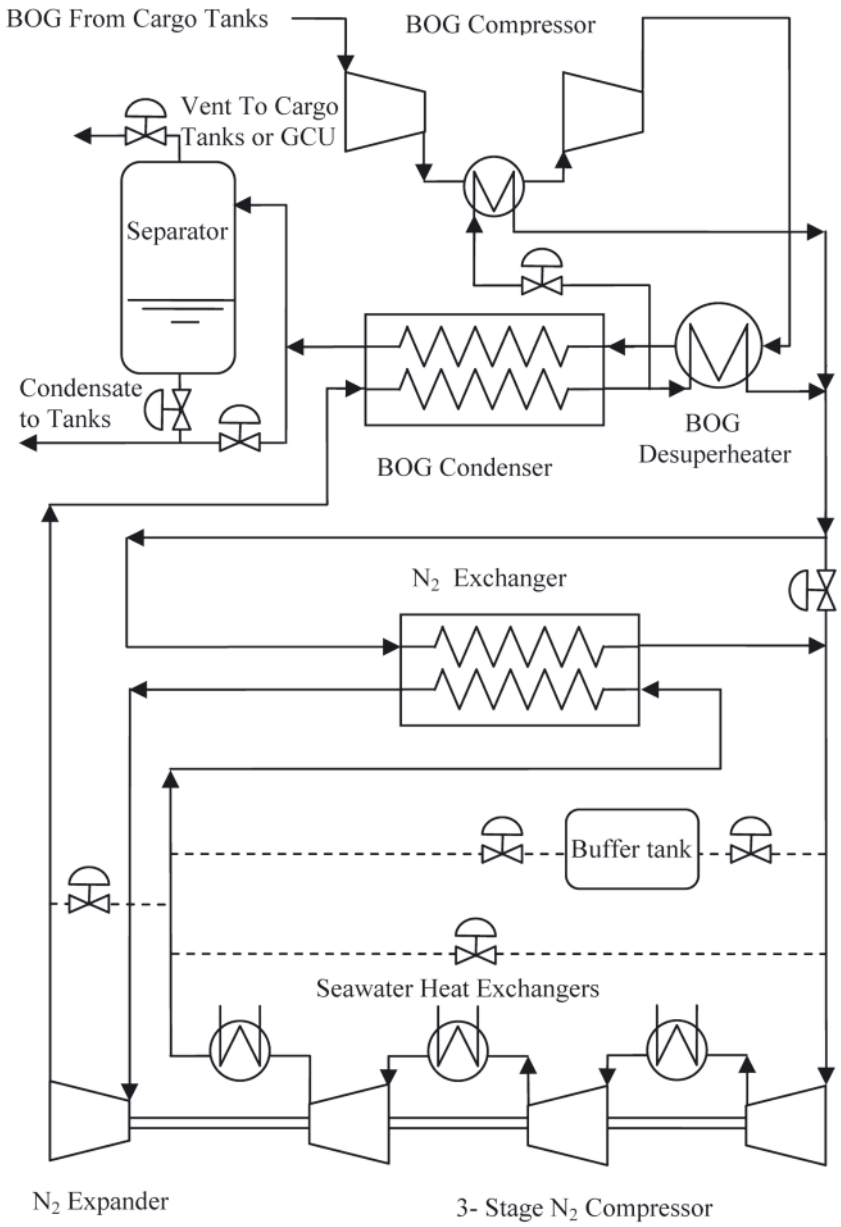

Fig. 7. *Flow diagram of the Cryostar Ecorel reliquefaction plant*

the compressed BOG is cooled in a heat exchanger constructed of stainless steel. This exchanger gives strength to the plant, since the stainless steel heat exchanger can better absorb fluctuations in temperature of the process while protecting the BOG condenser, made of aluminum plates. The two heat exchangers are individually isolated and not in a cold box, as in the Mark I, HGS plant.

In terms of design, the N_2 is compressed to 47 bar in three compression stages with intercooling and cooled down to -105°C before it expands to 9.5 bar and -168°C.

The BOG condensate is slightly sub-cooled, so it can be returned to the tanks back directly, without passing through the separator. For cargoes with higher content of N_2 in the BOG, the system switches to partial reliquefaction. In this mode for a BOG compressor and phase mixture coming from the condenser is redirected to a separator. Depending on the pressure of the cargo tanks, the vapor separator is returned back to the tank or CGU.

The variation of cooling capacity of the plant is controlled in a manner similar to the HGS system. However, Ecorel´s plant´s system has additional by-passes in all the N_2 cycle operation that gives a better operational capacity.

3.5. Mark III

HGS designed Mark III as an improvement on the previous Mark I, with the intention of reducing power consumption and completely with the Ecorel Cryostar plant. Fig. 8 shows the process flow diagram.

In Mark III BOG compression is performed at temperatures close to room temperature, using 3 centrifugal compressors with intercooling with seawater. Compression at room temperature is a result of heat transfer given by the BOG in a heat exchanger at the entrance of the plant, with a stream of N_2 from the cooler of the third compression stage. The advantages of compression at room temperature are as follows:

- Installation of conventional compressors
- The use of regular oil
- Removal of heat of BOG compression with seawater
- Reduces the losses of exergy in the ColdBox.
- Allows to condense BOG at high pressure

The N_2, as in Marck I, is compressed into 3 stages with centrifugal compressors. After third stage cooling, the current is divided into two different streams. One stream is

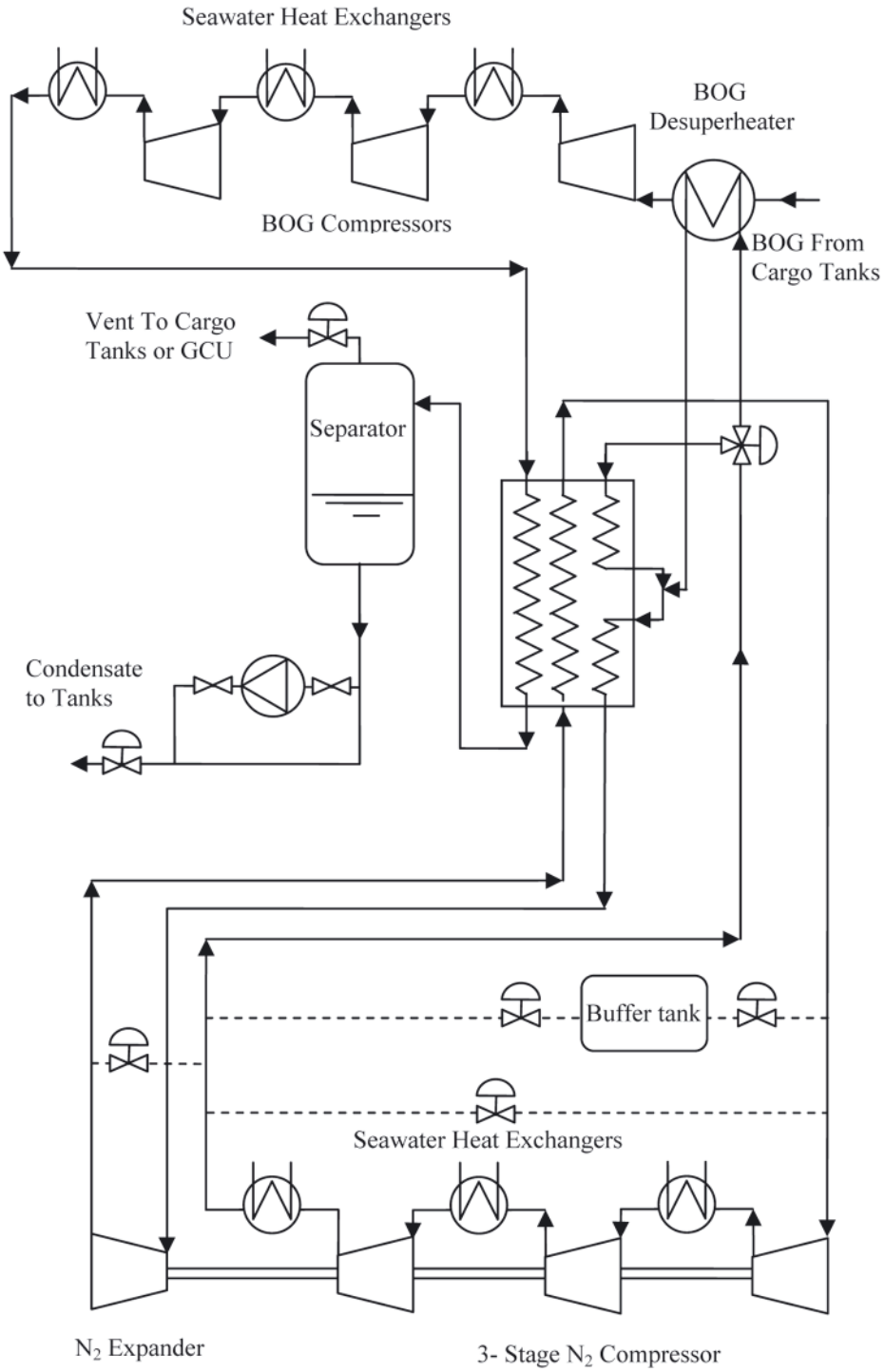

Fig. 8. *Flow Diagramof the Cryostar Ecorel reliquefaction process*

used to preheat the BOG and the other is driven to the hot part of the cold box. After N_2 exchanged heat with the BOG coming into the plant, the two streams are mixed again and reintroduced into the cold box. With this implementation and according to manufacturer's specifications [14], for a Q-Max ship considering the BOG 100% methane, a requirement of approximately 5.5 MW is needed for reliquefaction of 7 t/ h.

3.6. Laby-GI Mark III

This plant is designed to be implanted in combination with a propulsion system with a 2-stroke dual combustion engines.

The reliquefaction plant is the same as Mark III, with the exception of the compressors and the integration of the fuel system compressed to feed the dual motors. The principle scheme is shown in Fig. 9. The BOG compression system is replaced by a vertical reciprocating compressor manufactured by Burckhardt called Laby®-GI. This compressor is if 5 stages type, of which the first two are part of the reliquefaction plant. The BOG is compressed in the first and second stages up to 5-6 bar and the pressure of the other following 3 is risen to 300 bar. Such high pressure is necessary to ensure injection into the combustion chamber of the dual engines.

BOG compression at room temperature is achieved, as in Mark III, as a result of heat transfer experienced by the BOG in a heat exchanger at the entrance of the plant with

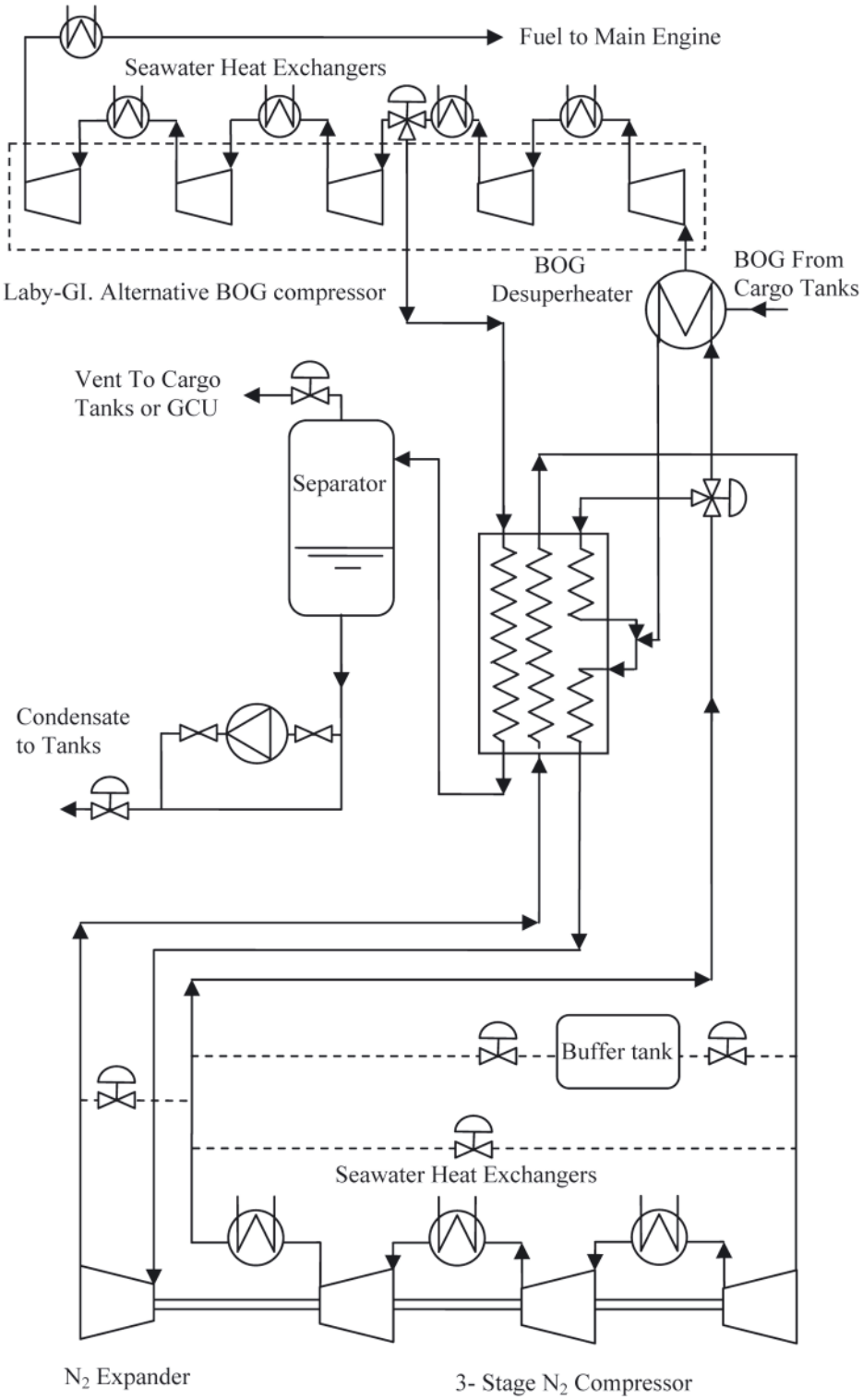

Fig. 9. *Flow Diagram of the Laby-GI Mark III HGS reliquefaction process*

a stream of N_2 from the cooler of the third stage compression. This configuration ensures that the compression heat can be dissipated through the cooling water in intercoolers.

When the main engine works in gas mode, the BOG is compressed to 300 bar by the compressor and is not processed by the reliquefaction plant. If excess of BOG is produced, after the second stage of compression, the BOG is diverted for condensation in the reliquefaction plant. When the engine operates in HFO the entire BOG is processed by the plant.

When in ballast, the propulsion system can go in HFO mode and with the plant running for the liquefaction of BOG in order to keep the cargo tanks cool or use the BOG to fuel the engine.

3.7. Laby-GI TGE

This plant has a special feature meaning it does not use the Brayton cycle, but a cascade process with ethylene and propylene of higher thermodynamic efficiency. Fig. 10 schematically shows the process. Tractebel Gas Engineering and Burckhardt developed the reliquefaction plant with the intention of combining the propulsion system with dual engines

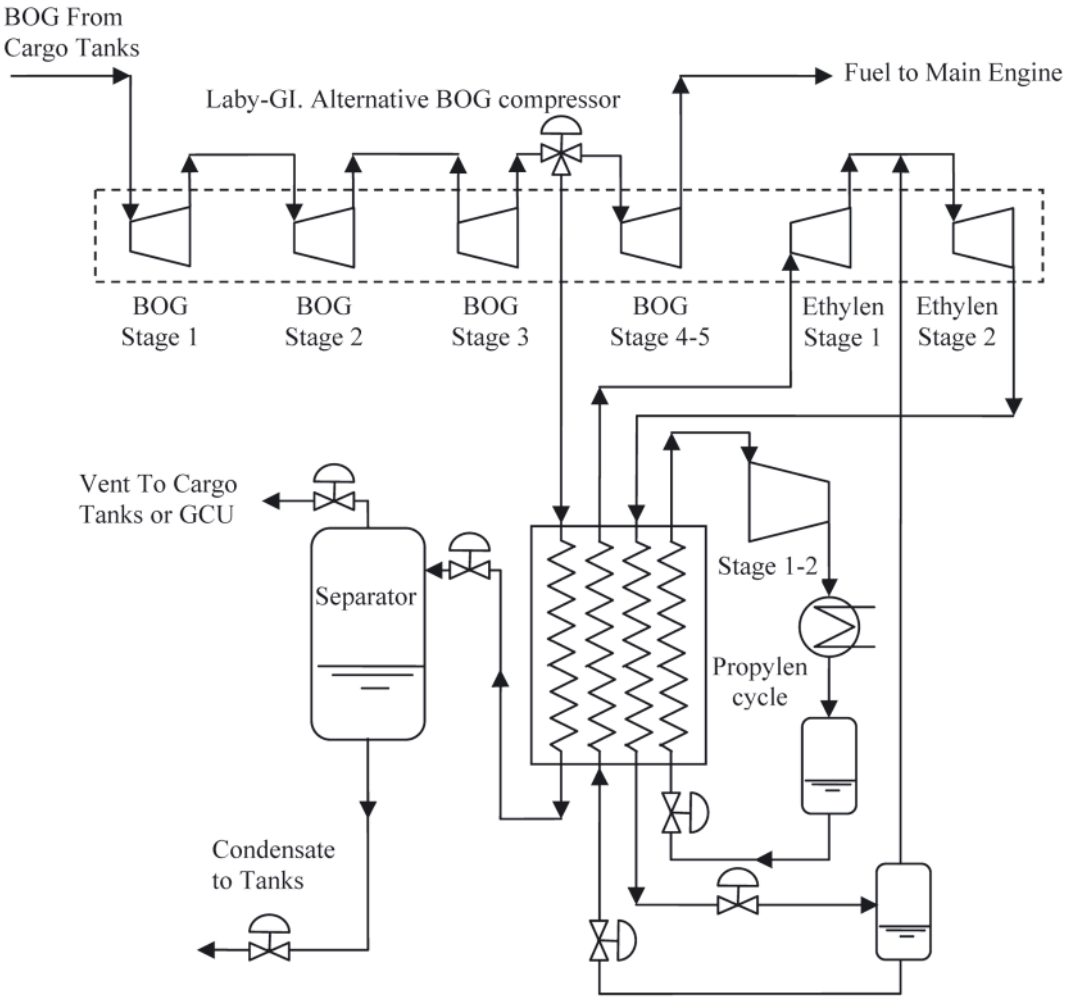

Fig. 10. *Outline of the cascade process for the TGE´s liquefaction of BOG*

for LNG carriers with a capacity of between 170.000 m^3 and 210.000 m^3.

The BOG compression process both for the reliquefaction as for burning in the dual motors, and compression of ethylene that corresponds to the cascade cycle, is carried out with the Burckhardt´s Laby-GI compressor. Fig. 11 shows the distribution of the compression stages and structure.

In reliquefaction mode, the BOG from the tanks is compressed in three stages up to 45 bar and condensed to -100°C by a cycle of ethylene of double compression with intercooling. The ethylene is condensed at -30°C and 19 bar with propylene in the same exchanger as where condensation of the BOG takes place. Propylene compression is performed in a separate screw compressor and condensed at 17 bar and 40°C with seawater.

The BOG condensate is flashed in a gas/liquid separator and returned to the tanks.

The variable for the operation of the Laby-GI compressor is the feed pressure of the dual engines. It is capable of varying the feed pressure between 150÷300 bar, depending on the engine load. When the engine load does not consume all of the BOG demand, the reliquefaction plant is put into operation.

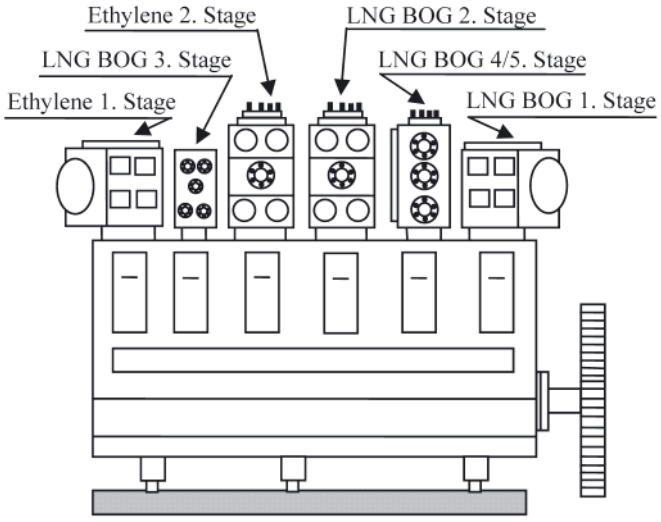

Fig. 11. *Representation of Burckhardt´s Laby-GI compressor and the distribution of the BOG compression stages and cascade modes*

4. COMPARISON OF PROCESSES

In the descriptive analysis of different manufacturers´ reliquefaction processes, data of the various capabilities and power consumption was provided, as well as other technical and business data. The information is based primarily on technical information provided by plant manufacturers and equipment suppliers. Tab. 2 summarizes this information intended to assess the tendencies in the implementation of reliquefaction processes.

Despite it's high energy consumption, the choice of the Brayton cycle for reliquefaction is characterized by its compactness and robustness, its simplicity and it´s small number of additional equipment. The objective of lowering the

Tab. 2. Some relevant data regarding capacities, plant power, as well as some useful technical data of the reliquefaction plant architectures provided by the manufacturers

	Reliquefaction Plant						
	Jamal	**TGE**	**Mark I**	**EcoRel**	**Mark III**	**Mark III Laby-GI**	**TGE Laby-GI**
SUPPLIER	OsakaGas	Tractebel	HGS	Cryostar	HGS	HGS	Tractebel
YEAR	2000	2004	2006	2008	2008	2009	2009
CICLO Refrigerant Work press. (bar) Expansion temp	Brayton N_2 35-6.5 --	Brayton N_2 -- -170°C	Brayton N_2 58-14.5 -163°C	Brayton N_2 47-9.5 -168°C	Brayton N_2 58-14.5 -163°C	Brayton N_2 58-14.5 -163°C	Cascade C_2H_4/C_3H_6 1-19/1.7-17 -105/-35°C
BOG CYCLE Compressor type N° Compressors Compress. press Suction temp Observations	Centrifuge 2 4.5 bar -140°C	Centrifuge 1 3-6 bar -	Centrifuge 2 4.5 bar -145°C	Centrifuge 2 4.8 bar -120°C Interm.Refrig. with N_2	Centrifuge 3 - Room tem Interm. Refrig sea water	Alternative 2 stages 5-6 bar Room tem Interm. Refrig sea water	Alternative 3 stages 45 bar - Interm. Refrig sea water
CAPACITY Liquefaction	3 t/h 0.83 kg/s	6.25 t/h 1.74 kg/s	6 t/h 1.67 kg/s	7 t/h 1.94 kg/s	7 t/h 1.94 kg/s	--	--
POWER kW *Installed kWh/kg $_{BOG}$	3000 1	5030* 0.75	5.800 0.96	6.000 0.86	5.500 0.78	-- --	-- --
SHIP Capacity (m^3) Propulsion	135.000 Steam turbine	228.000 low speed 2-stroke diesel	Q-flex 210.000 low speed 2-stroke diesel	Q-Max 266.000 low speed 2-stroke diesel	Q-Max 266.000 low speed 2-stroke diesel	-- low speed 2-stroke dual fuel	210.000 low speed 2-stroke dual fuel

power requirements associated with an increased reliquefaction ability in recent years, contributes to an ever-greater complexity of the process and a larger number of necessary equipment. This causes the assessment of the cascade reliquefaction technology developed by TGE, where the process is more efficient due to the phase change. A noteworthy disadvantage is that it requires more safety instrumentation than Brayton cycles due to the inherent use of refrigerant fuels as working fluids. Furthermore, the use of different levels of temperature leads to a more complex and costly installation in both its implementation and maintenance.

CONCLUSIONS

Conducting a descriptive comparison of different technologies has become necessary following the increasing number of manufacturers who seek to apply these new techniques on ships. The knowledge of these is of great importance in order to provide selection criteria and make the correct decisions with the responsibility of selecting the most efficient technology. Based on the conducted review, it can be concluded that the technological contributions of the last 4 years are headed towards the combination of reliquefaction propulsion with dual engine systems, with the aim of maximizing flexibility in the exploitation strategy of LNG ships operating at high efficiency and comply with legislation regarding fuel emissions. Furthermore, the cascade based reliquefaction technology has become a serious alternative to the Brayton cycle due to its greater efficiency and lower maintenance costs despite of some drawbacks such as the use of fossil fuel based refrigerants and higher implementation and maintenance costs.

BIBLIOGRAPHY

1. Bortnowska M.: *Development of new technologies for shipping natural gas by sea*. Polish Maritime Research. No 3(61) Vol 16, pp 70-78, 2009
2. Küver M, Clucas C, Fuhrmann N.: *Evaluation of propulsion options for LNG carriers*. In: The 20th international conference and exhibition for the LNG, LPG and natural gas industries (GASTECH 2002).
3. Romero Gómez, J., Ferreiro García, R., Carbia J.: *Análisis de la relicuación del boil off en buques de GNL Alternativa al proceso basado en el ciclo Brayton de refrigeración*. Ingeniería Quimica No.462, pp 164-176, 2008.
4. Romero Gómez, J., Ferreiro García, R., Bouzón Otero, R., De Miguel Catoira, A.: *Relicuación del boil-off en buques LNG: principios tecnológicos*. Ingenieria Quimica, Vol 504, pp. 44-50, 2012.
5. Thomas N. Anderson, Mark E. Ehrhardt,Robert E. Foglesong, Tom Bolton, David Jonesc and Andy Richardson: *Shipboard Reliquefaction for Large LNG Carriers*. In: Proceedings of the 1st Annual Gas Processing Symposium. (2009) http://www.nt.ntnu.no/users/skoge/prost/proceedings/gas-processing-doha-2009/fscommand/po03.pdf; (Accessed 24/11/2012)
6. Romero, J., Orosa, J.A., Oliveira, A.C.: *Research on the Brayton cycle design conditions for reliquefaction cooling of LNG boil off*. Journal of Marine Science and Technology, pp 1-10, 2012.
7. Younggy Shin, Yoon Pyo Lee: *Design of a boil-off natural gas reliquefaction control system for LNG carriers*. Applied Energy Vol. 86, pp. 37–44, 2009.
8. Daejun Chang, Taejin Rhee, Kiil Nam, Kwangpil Chang, Donghun Lee, Samheon Jeong: *A study on availability and safety of new propulsion systems for LNG carriers*. Reliability Engineering and System Safety, Vol. 93, pp. 1877– 1885, 2008.
9. Chang Kwang Pil, Marvin Rausand, Jřrn Vatn: *Reliability assessment of reliquefaction systems on LNG carriers*.

Reliability Engineering and System Safety Vol. 93, pp. 1345–1353, 2008.
10. Barclay, M.A., Yang, CC.: *Offshore LNG: The Prefect Starting Point for 2-Phase Expander*. Offshore Technology Conference, May 2006.
11. Yoneyama H, Irie T, Hatanaka N.: *The first BOG reliquefaction system on board ship in the world "LNG Jamal"*. In: The 22nd world gas conference, Tokyo, Japan. 2003
12. Mario Miana, Rafael del Hoyo, Vega Rodrigálvarez, José Ramón Valdés, Raúl Llorens: *Calculation models for prediction of Liquefied Natural Gas (LNG) ageing during ship transportation*. Applied Energy Vol. 87, pp. 1687–1700, 2010.
13. Gerdsmeyer, K-D, Harry Isalski, W.(2004) *On-board reliquefaction for lng ships*. http://www.ivt.ntnu.no/ept/fag/tep4215/innhold/LNG%20Conferences/2005/SDS_TIF/050202.pdf; (Accessed 24/11/2012).
14. Hamworthy Ltd., LNG Shipping Operations 27th Sept. 2006. *Hamworthy Reliquefactión & Regasification systems on LNG carriers*. http://www.thedigitalship.com/powerpoints/SMM06/lng/Reidar%20Strande,%20Hamworthy.pdf; (Accessed 24/11/2012).

CONTACT WITH THE AUTHORS

J. Romero Gómez*), Ph. D.,
M. Romero Gómez, Ph. D.,
Department of Energy and Marine Propulsion, ETSNM,
University of A Coruna, ETSNM,
Paseo de Ronda 51,
A Coruna 15011, SPAIN.

R. Ferreiro Garcia, Prof.,
Department of Industrial Engineering, ETSNM,

A. De Miguel Catoira, Ph. D.,
Department of Energy and Marine Propulsion, ETSNM,

*) Corresponding author:
e-mail: j.romero.gomez@udc.es,
phone: +34 981 167000 4233,
fax: +34 981 167100

POLISH MARITIME RESEARCH 1(81) 2014 Vol 21; pp. 89-95
10.2478/pomr-2014-0012

Investigating the impact of intranet resistance and intranet withdrawal in Malaysian maritime industry

Norzaidi Mohd Daud, Assoc. Prof.,
Intan Salwani Mohamed, Ph. D.,
Universiti Teknologi MARA, Malaysia

Saad Alghanim, Ph. D.,
Rashid Alhamali, Ph. D.,
King Saud University, Saudi Arabia

ABSTRACT

This article investigates the impact of intranet resistance (i.e. co-workers affluence, negative prior experience, efficacy experience, poor systems design and loss of power) on manager's performance, which indirectly influences intranet withdrawal in Malaysia maritime industry. The structural equation modelling (SEM) results indicate that all intranet resistance factors negatively influence managers' performance and indirectly influence intranet withdrawal. This is probably the first work that investigate the impact of intranet resistance and withdrawal in Malaysia. The results provide insight on how the Malaysian maritime industry could improve their intranet adoption.

Keywords: co-workers affluence; negative prior experience; efficacy experience; poor systems design and loss of power; intranet withdrawal; Malaysia maritime industry

INTRODUCTION

Most of the key players in the Malaysian port industry such as terminal operators, marine department, port authority, royal customs, excise department and immigration department are using intranet in most of their operation [21, 22]. The organizations started to use intranet in the early 2000s, and so far, intranet had improved the managers' effectiveness and efficiency as well as a return on investment. For instance, Northport (Malaysia) Berhad, major terminal operator in Malaysia introduced Northport Net which operated 24 hours a day, seven days a week to users for queries on vessel sailings, container status, customs clearance status and enquiries on shipping lines, freight forwarders or their agents and port tariff. Northport Net also offers all information on a real-time basis, and also cost-effective and convenient exchanges of operational and trade information [23]. In addition, North Butterworth Container Terminal of Penang Port is using Computerised Cargo and Marine Systems (PELPIN). PELPIN is an on-line real-time system designed to improve productivity and efficiency of the port billing and cargo operations systems. However, after a few years of transformation from manual to intranet systems in maritime industry, there are new issues on surface, for instance intranet resistance and intranet withdrawal.

Resistance is a critical obstacle which prevents organisation from reaping the potential benefits from implementation of an IT [4, 22, 24]; it can undermine its success and is a widespread problem [21]. For instance, when Grubb and Ellis Company introduced its new intranet systems, its professionals yearned for the "old days" of faxing, phoning, and sending letters. Now they have e-mail, but they still wanted to send fax information to clients. They knew it would be faster and easier to send e-mail, but they were not sure they could remember how to add attachments, etc., and they were usually in a hurry, so it was "faster" to just do it the old way [28]. Thus, IT acceptance would lead to its adoption and use in the workplace, which is a necessary condition for effectiveness and competency in the information age [7].

Furthermore, failure to put the IT into implementation process of the proper social context of economic, socio-political, and cultural dimensions could inhibit the success of the process and increase the risks of failure. When there is less IS usage, then, it could diminish individual and organisation performance as well as to lead them to quit from their jobs [15]. As mentioned by Al-Gahtani [1], lack of user acceptance has long been an impediment to the success of the introduction of new technologies. As the goal of most organisationally based IS is to improve performance on the job, unfortunately, performance impact is lost whenever users reject systems and thus acceptance is often the pivotal factor determining the success or failure of introducing new technologies [2, 7]. Thus, to improve productivity of technologies, they have to be accepted and used by employees in organisations. Moreover, the possibility of dysfunctional IT impacts generated by emphasizing that user acceptance is not a universal goal and is actually undesirable in cases where systems fail to provide true performance gains and if users are not willing to accept the IS, it will not bring full benefits to the organisation and propensity

to withdraw from organization is high [4, 5, 15]. Moreover, the more accepting of a new IS the users are, the more willing they are to make changes in their practices, use their time and effort to actually start using the new IS.

While it is widely documented that resistance is a predictor of managerial performance [4, 21, 22, 24], very little information has been made available on the relationships between [1] co-workers affluence and managers' performance; [2] negative prior experience and managers' performance; [3] efficacy expectation and managers' performance [4]; poor systems design [5]; influences of loss of power on managerial performance as well as managers' performance and intranet withdrawal. Also, there is no study that examine indirect effect of intranet resistance and intranet withdrawal [4, 24]. This is due to the limited studies that attempted to relate all possible factors of Intranet usage in one single setting, which reveals a significant gap in knowledge. Further, many of the prior studies outdate and thus newer studies are needed as they might draw different results, looking at the extensive growth rate of technology today and the introduction of newer applications. Moreover, none of the previous studies that analysed constructs of technology resistance by using structural equation modelling (SEM). Based on these grounds the current study is conducted to address the following research questions:

1. Does co-workers affluence influence managers' performance?
2. Does negative prior experience predict managers' performance?
3. Does efficacy expectation influence managers' performance?
4. Does poor systems design predict managers' performance?
5. Does loss of power predict managers' performance?
6. Does managers' performance influence intranet withdrawal?

This study attempts to answer the research questions through the development of a research framework after investigating prior literatures in this context. The next section presents the literature review, then are formulated propositions to be tested in this study.

REVIEW OF LITERATURE

Co-workers affluence

Most of the 50 to 70 percent of IS implementations that failed are not the victims of flawed technology, but rather of organisational and people related issues; the next attributes of user resistance is co-workers influence [4]. This attribute has been well documented that co-workers influence how an individual perceived jobs [3, 5]. The reason is if initially-resistant employees observe that their co-workers are able to easily adjust their work behaviour when they are exposed to a new IT, they are likely to believe that they also have the ability to master new technology [8, 14]. In addition, other studies show co-workers influence technological resistance. For example, Markus [15] found that the expectation of others (co-workers) can influence the degree of technological resistance exhibited by individuals. Naveed [18] indicates that people recognised cues in their environment and may react in accordance with those cues, particularly if these cues come from co-workers held in high esteem. Hence, if co-workers express resistance to the new IT and place specific blame for failure, so the individual might do the same [14]. To substantiate this argument the following hypothesis is proposed:

H1: Co-workers affluence is a predictor of managers' performance

Negative prior experience

According to Martinko et al. [14], reasonably strong empirical support has been found for the notion that negative prior experiences with information technologies are related to the rejection of information technologies. Norzaidi et al [23] conducted a study with several workers at the port authorities in Malaysia. They found that previous attempts at mechanisation had been relatively unsuccessful. Therefore, employees developed negative reactions relating to past experiences with technology, which likely contributed to expectations of future failures with new technology. Norzaidi's study was in line with the study by Norzaidi et al [24]. The findings show that there were a few officers who refused to use Intranet because of their negative experiences of using other similar technologies, such as Internet. These managers believed that if they use Intranet it could fetch negative results. Based on this, prior negative experience on technology is one attribute of user resistance. In other studies, Dishaw and Strong [6], however, have different idea on the issue of experience with technology. They tested the addition of experience with maintenance tools and with the maintenance task to tested task-technology fit (TTF) model for software maintenance tool use. In their research, they tested two hypotheses, for instance, [1] experience with maintenance tools and [2] experience with the maintenance task. They found strong support for the first part of their first hypothesis but could not support the direction of the effect. Also, hypothesis [2] could not be supported at all. According to Dishaw and Strong [6], experience with the task and technology usage ought to be fit and could generate better performance. Hence, experience with the task adds nothing to the fit models either as a main effect or as moderator. In summary, empirical research on negative prior experience of using technology and user resistance is mixed and contradictory. However, it is interesting to uncover whether prior negative experience is one of user resistance components, and how it relates with performance, task-technology fit, perceived usefulness and usage. In line with this argument, the following hypothesis is constructed:

H2: Negative prior experience is a predictor of managers' performance

Efficacy expectation

Efficacy expectation is a negative feeling that users thought about in adopting new technology. Most of the technology resistors strongly believe that when they use technology, e.g. Internet, it could not help him or her to accomplish required tasks. This situation occurs seriously in many departments of corporate companies, which formerly were government agencies that have become private companies where many of their staff are not even ready to explore and adopt new technologies. For example, many middle managers at terminal operator at Port Klang, for instance, have high levels of efficacy expectation on intranet. This situation occurred in the first stage of the introductory level of intranet. According to some IT senior managers, they believed they could excel in their job when they used traditional technologies such as telephones, and fax machines, except for intranet [17, 24]. Sherwood's [28] studies proved that the reason managers resist in using intranet was they are not used to it. Moreover, these technology resistors believed that they could perform better if they used traditional technologies such as fax machines and telephones. Sherwood realised that most of them

do not really know how to handle certain tasks with intranet, and they believed their performance would deteriorate if they used Intranet. There is an argument that efficacy expectation resulted from certain sources. Lawrence and Low [11], for example, believed that efficacy expectation is because of that past failure, which only reinforces anxiety and negative attitudes. Subsequently, this end-user is resistant to the introduction of new computer-based technology (CBT) or changes in existing CBT, regardless of the level of difficulty associated with learning the CBT. The following hypothesis thus ensues:

H3: Efficacy expectation is a predictor of managers' performance

Poor systems' design

Poor systems design is one of people's negative reactions to computer systems [4]. Poor systems could be seen as functionality, interface design, modes of presentation, accessibility of workstation, inadequate response times or others, which do not only amplify negative reactions but also frustrate those individuals who initially exhibit positive reactions [14, 16]. Another study conducted by Gebauer and Shaw [4] indicated that poor systems' documentation has a negative impact on usage. Although systems may be evaluated favourably on every performance measure, the systems may not be used very much because of user dissatisfaction with the systems and its interface. In one study conducted by Neumann and Segev [19] on the usage of computer-based technology (CBT), he found cause of resistance to CBT. From the study, he found that the responses indicated that many professionals believe that end users may blame specific features of CBT for problems which they incur in the workplace. CBT-determined explanations for resistance focus on specific features of the CBT, which the end-user finds difficult to learn or operate. Henry also indicated that the causes of unsuccessful performance, such as difficulty of using CBT, are likely to increase resistance on the part of end-users currently using the CBT and may serve as the initial cause for new end-users. This may be particularly true for those users who expend a great amount of effort with only minimum success. Another study conducted by Norzaidi et al [22], found that poor systems' design is one of the factors why managers resist to technology. The respondents argued that if the technology has a poor system, (i.e. difficult to use, slow-speed operated systems, not compatible to certain technology) it would result in the rejection of the technology. In line with this argument, the following hypothesis is constructed:

H4: Poor systems design is a predictor of managers' performance

Loss of power (Decision-making authority)

A few researchers have discussed the influence of power/authority on IT systems and implementation [4, 23, 24]. Thus, the influence of history and unseen power/authority play leading to conflict and resistance on the outcomes of technologically driven change has been widely recognised and the more social constructivist concepts of technology are stimulating further research and debate. IS is increasingly altering relationships, patterns of communication and perceived influence, authority and control [3, 17]. Thus, much of the research in the area focuses on the balance of power between user and the IS staff and how that balance affects the interplay between the two groups [19]. Tzu and Yin [29] however, defines it as the capacity of one actor to overcome resistance in achieving a desired object or result; force to change the probability of behaviour from what it would have been in the absence of the application of the force. Middle management believed the empowerment enabled through technology of re-engineering communication threatened their position and power within the organisation. In order to maintain their hold on power in the organisation, they need to revolt against the technology of re-engineering imposed on them by senior management. Power is not attributed to individuals, it is in relationships and when it becomes more important than individuals then the relationship breaks down.

The power relationship that had existed previously to support principal manager's introduction of re-engineering communications had broken down as individual managers were threatened by the potential outcome of re-engineering. The power relationship between middle managers and the principal manager broke down and was strained for some time. Many of the internal communication channels had been downgraded or replaced by electronic communications. Management now had to re-establish their power within the confines of the technology [26]. They also predicted that middle managers are carriers of information up and down the organisation, and suggested that management IS/IT, which makes information more widely available, was likely to attack the power/authority of middle managers who previously dominated access to interpretation of a communication of information. Hence, information would directly flow to third layer of management and subordinates rather than through middle managers [2], and their power is eroded relative to these groups. In short, companies have downsized, employees have become empowered, and the middle manager feels that his/her position within the organisation is becoming less and less important. Because of this reason, a few managers were resisting to new technology. The following hypothesis thus ensues:

H5: Loss of power is a predictor of managers' performance

Managers' performance and intranet withdrawal

There are a few studies that investigate the relationship between managers' performance and technology/intranet withdrawal. Technology withdrawal is a pattern of behaviour that refuses to use new technology and opt to relinquish from his or her job. In short, managers will resign because they refuse to accept new technology. Seeing that Intranet resistance will lessen managers' productivity, managers could resign because of psychosomatic problems as well as to execute managerial requisites. In line with this argument, the following hypothesis is constructed:

H6: Managers' performance is a predictor of intranet withdrawal

As summary, Fig. 1 shows the propositions selected for testing in this study.

RESEARCH METHODOLOGY

Sampling

The targeted population consisted of all managers attached to major terminal operators in Malaysia (e.g. Port of Tanjung Pelepas, Northport, Bintulu Port and Kuantan Port etc). About 500 self-reporting questionnaires were distributed to the human resource (HR) departments of the respective terminal operators after identification of the numbers of managers. Guidelines were provided by the researcher. The identification of managers

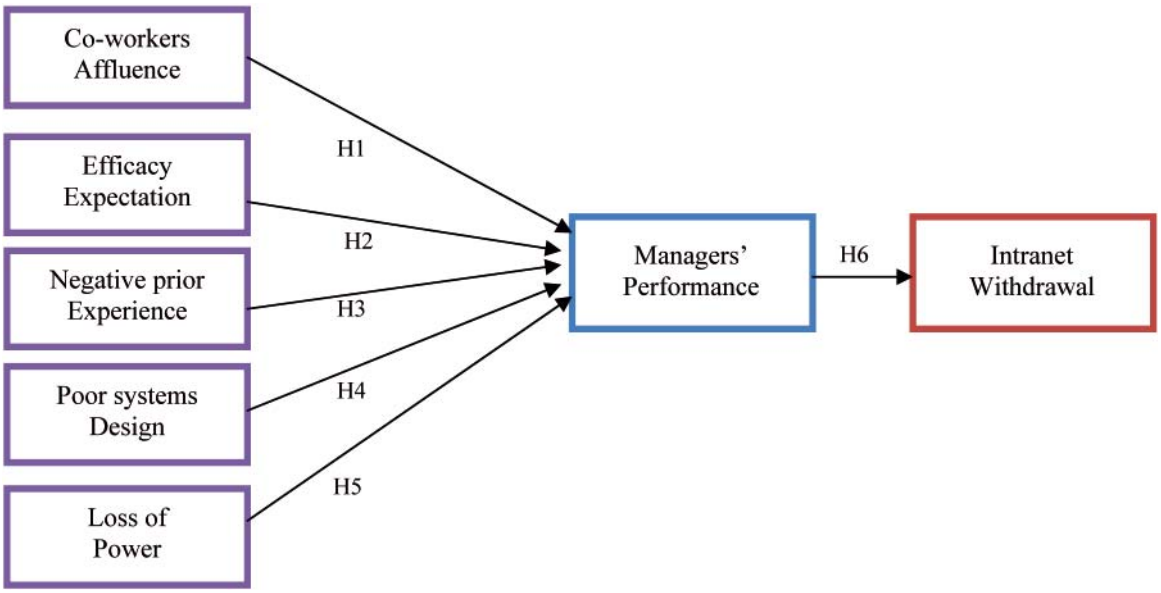

Fig. 1. *Research framework and hypotheses of the study*

is based on the criteria set forth in the literature where they consist of individuals which held positions of general managers, department managers, division heads, directors, department or agency heads, unit chiefs, district managers, division managers and executives [22]. Out of the 500 sent questionnaires, 357 (71 %) responses were obtained. The response rate is noticeably high and representative of the population studied. This enables to generalize the obtained results [27]. The high response rate is due to the recommendation letters provided by the Ministry of Transport and Ministry of Science, Technology and Innovation, Malaysia, to designate that the pertinent authorities supported this study.

The instrument

The questionnaire is divided into five sections to specifically address the six hypotheses formulated in the study. The first section contains five questions capturing the respondents' demographic information such as age, gender, department, highest education qualifications and positions. The remaining sections comprise 3 items measuring the respondents' perception on co-workers affluence [4, 9, 10], 3 items on efficacy expectation [17, 23, 30]; 3 items on negative prior experience [22]; 3 items on poor systems design [4]; 3 items loss on power [4, 23]; 6 items on managers' performance [24], and 3 items on intranet withdrawal. All the items (except demographic section) were measured by using a 7-point Likert scale: from 1 = strongly disagree to 7 = strongly agree.

Analysis of data

Sample characteristics

The majority of the respondents are male (70 %). Most of them fall between the age cohort of 40 to 49 years old (38 %), followed by 30 to 39 years old (29.3 %) and those between 21 to 29 years old (22 %). The majority of them works in a non-IT department (77.3 %) and has a bachelor's degree (60 %). This is followed by the respondents with diploma (16 %) and Master's degree (10.7 %), which indicates that most of the respondents have received tertiary education, including a small percentage of them having a PhD/DBA qualification. This is not surprising because tertiary education is a requirement for an executive position. Further, the education qualification of the respondents corresponds with their age. In terms of position, most of them consist of senior executives/executives (28 %), followed by manager/assistant managers and head of departments.

Assessing validity and reliability

In determining the reliability of the instrument, a general rule is that the indicators should have a Cronbach's Alpha of 0.6 or more [25]. With the range of Alpha scores between 0.72 and 0.95, obtained in this study, we can conclude that the questionnaire is reliable and the data can be applied to the analysis [29] (see Tab. 1).

Descriptive analysis and model fit test

Tab. 1 shows the mean and standard deviation scores of all items. This study suggested that most of managers agreed that they did not resist to intranet because intranet usage could produce better performance.

Tab. 1. *Internal consistency of the constructs*

Construct	Mean	Standard Deviation	Cronbach's Alpha
Co-workers affluences	2.66	0.76	0.87
Efficacy expectation	1.52	0.68	0.84
Negative prior experience	2.96	0.95	0.77
Poor systems design	1.43	0.94	0.95
Loss of power	1.81	0.83	0.72
Managers' performance	6.98	0.74	0.85
Intranet withdrawal	1.14	0.93	0.73

In order to authenticate the instrument, apart from content validity, this study considers construct validation. To achieve construct validity the data was examined by using principal component analysis as the extraction technique and Varimax as the method of rotation. With a cut-off loading of 0.40 and eigenvalues greater than 1.0, none of the attributes was dropped (see Tab. 2). Further, the Kaiser-Meyer-Olkin (KMO) measure of sampling adequacy indicated a practical level of common variance.

Tab. 2. Confirmatory factor analysis (CFA) of results

Construct	Kaiser-Meyer-Olkin Measure of Sampling Adequacy	Eigenvalue	Percent of total variance explained
Co-workers affluence	0.65	1.52	69.12
Efficacy expectation	0.76	2.87	79.72
Negative prior experience	0.68	2.53	59.08
Poor systems design	0.69	1.57	87.53
Loss of power	0.78	2.98	88.41
Manager's performance	0.85	4.44	69.98
Intranet withdrawal	0.77	2.51	58.04

Moreover, the construct validity of the model's scales was also evaluated by using Analysis of Moment Structures (AMOS) with maximum likelihood to analyse the data. AMOS is used because of its simplicity and technically advanced nature [16]. More importantly, it provides more precise assessment of discriminant validity of an instrument than exploratory analysis [24]. While there is no single recommended fit measurement for the structural equation model, varieties of measures are proposed in many research reports [26].

Tab. 3. Goodness-of-fit measures of the research model

Goodness-of-fit-measure	Recommended value	Approximate boundary as a good fit
Relative chi-square	< 3.00	1.995
Ratio of chi-square	p > 0.05	p = 0.195
GFI	Close to 1.0 is better	0.996
IFI Delta 2	Close to 1.0 is better	0.933
TLI rho2	Close to 1.0 is better	0.992
CFI	Close to 1.0 is better	0.956
RMSEA	< 0.08	0.017

The results of the chi-square test indicate that the model fits the obtained data (Chi-square = 268.43; p > 0.05; p = 0.195). As an alternative, we also measured the model by using other multiple fit criteria, such as the model of chi-square (χ^2/DF), relative chi-square, comparative fit index (CFI), the goodness -of -fit index (GFI), the incremental fit index (IFI Delta2), TLI rho2, and the root mean square error of approximation (RMSEA). The value of χ^2/DF is 1.995, which is less than the desired cut-off value of 3.000 suggested by Segars and Grover [26]. Moreover, the GFI (0.996), IFI Delta 2 (0.933), TLI rho2 (0.992) and CFI (0.956) values were considered close to the recommended value. Nonetheless, the RMSEA score (0.017) shows that the model meets a reasonable error of approximation with a cut-off 0.080 [2]. Therefore, it can be concluded that the model used in this study is valid. The results have confirmed that the responses of the managers generally support the theoretical and conceptual distinctions of all the variables proposed in this study. As such, the data can be applied for further analyses. The next section shows the results of the six hypotheses tested in this study.

RESULTS

Tab. 4 shows the results with respect to the seven hypotheses constructed. The Structural Equation Modelling (SEM) analysis indicates that co-workers affluence is significantly predicting managers' performance, thus, hypothesis 1 is not rejected (p = 0.012). Similarly, efficacy expectation significantly predicts managers' performance (p = 0.024), and hypothesis 2 is not rejected. Also, negative prior experience influences managers' performance (p = 0.022), hence, hypothesis 3 is not rejected. Poor systems design significantly predicts managers' performance, and as a result, hypothesis 4 is not rejected (p = 0.002). In addition, loss of power influences managers' performance (p = 0.032), and hence, hypothesis 5 is not rejected. Finally, managers' performance significantly influences intranet withdrawal (p = 0.041), thus, hypothesis 6 is not rejected too.

DISCUSSION AND PRACTICAL IMPLEMENTATIONS

This paper contributes to the existing body of knowledge in terms of narrowing the research gap by examining the causal relationships between dimensions of technology resistance and the managers' performance. The novelty of this study is that it provides a holistic perspective of the critical factors that influence managers' performance, in light of the Intranet technology. The used model is based upon a unified framework combining resistance model with theories related to co-workers affluence, efficacy expectation, negative prior

Tab. 4. Testing the hypotheses

Hypothesis	Causal Relationship		Factor	β	Sig.	Result
H1	Co-workers affluence	→	Managers' performance	-0.664	0.012	Supported
H2	Efficacy expectation	→	Managers' performance	-0.793	0.024	Supported
H3	Negative prior experience	→	Managers' performance	-0.575	0.022	Supported
H4	Poor systems design	→	Managers' performance	-0.799	0.002	Supported
H5	Loss of power	→	Managers' performance	-0.645	0.032	Supported
H6	Managers' performance	→	Intranet withdrawal	-0.219	0.041	Supported

experience, poor systems' design and loss of power, which were identified by means of the extensive review of literature. Moreover, the model is to aid decision makers to understand the relationships between the variables, which have received very little research attention to date. Thus, by combining the variables and testing them in a single setting, this has allowed us to generate a more precise picture of the causal relationships between the variables.

This study suggested that all dimensions of technology resistance negatively influence managers' performance. Most influential dimension is poor systems' design and loss of power has the least influence on managers' performance. The findings suggested that most of managers will resist because of poor systems' design. Thus design of system is important factor that influences managers' performance. In other word, the systems' design must be fitted with the abilities and a given job. Programmer should understand the managers' needs and will design the systems based on the technology and task requirements. As a result, managers could effectively improve their productivity, and finally enhance company's return on investment.

Besides, co-workers affluence is one of the dimensions that predict managers' performance. Typically, managers and their co-workers will work collectively in planning, organising, directing and controlling company's strategies. Therefore, it is potential that co-workers would persuade managers' decision and as well as decision to use intranet. If co-workers defy to intranet, there is great propensity that managers' would also refuse to use intranet. In addition, this study recommended that prior experience could manipulate managers' performance. Let say, managers who have unenthusiastic experience of using technology, will be probably prone to resist intranet. They will think that the functionality of technology is always comparable, and if they use intranet it could yield the similar effect. Also, this study implied that managers' performance is influenced by loss of power. For instance, top manager will correspond directly to his subordinates and does not refer to middle managers. Seeing that subordinates obtain information and direction straight from top managers, middle manager is losing their power on decision making. In short, technology is replacing middle managers functions and their number is decreasing except for MIS department [22, 30]. Finally, this study suggested that managers' performance is a predictor of intranet withdrawal. This indicates that when managers do not perform because of their resistance to intranet, they will resign. As mentioned earlier, managers will become pressured because they could not convene to key productivity indicator and lastly vacate from their jobs.

There are a few practical implications that may help decision makers in achieving the above efforts, such as [1] support and commitment from the top management; [2] ensuring a fit between task requirements and intranet functionalities; and [3] providing users with appropriate training. As far as technology implementation is concerned, there is nothing more important than top management leadership and commitment towards such initiative. A larger portion of technology acceptance is attributed to the cultural factor of an organisation and therefore, top management plays an important role in shaping the organisational culture as well as promoting change in the organisation. Leaders must not only be aware of the benefits from introducing technological changes for the sake of achieving organisational goals, but also become conversant with how middle managers perceive and use technology to enhance managers' performance. It is useless to initiate a system to facilitate managers' tasks assuming the employees are resisting system implementation.

One of the most important considerations is to communicate the rationale of introducing such system to all managers in order to gain their trust and understanding. Another way of communicating the importance of such system is through embedding the system usage and individual's performance in the organisational vision and mission statements. When managers see the commitment from the top management, they will be convinced to use the system. Usage, on the other hand, would improve individual and organisational performance [7, 12]. Besides highlighting the importance of such systems to the organisation, leaders must also inform their managers about how the usage of intranet would benefit them in their daily jobs. Leaders must set good examples in using the system themselves. If the leaders are encouraging managers to use the system, while they continue to issue memos or using the fax machine when they can do so by using the intranet, the trust is diminished and successful implementation of intranet will not be forthcoming. In short, top management support for the spread of intranet usage can be made operational by the communication by top management to organisation's members to use the technology. Further, top management support for infusion of intranet technology can be made operational by the communication offered by top management to incorporate the technology into organisational processes.

Secondly, the importance of adapting the intranet system towards users' needs cannot be overemphasised. Efforts must be undertaken to ensure that there is a match between the task requirements and the functionalities of the intranet. In other words, the system has to be friendly enough to capture all the task requirements. There is a reason to state that task-technology fit is a predictor of individual's performance [7, 13]. It is understandable that managers who have long been working in the same organisation and have used the conventional means of communication and information retrieval, found such systems threatening, and therefore would tend to look for ways to find technical faults in the system. In the case of this study, the managers may repudiate to manipulate their intranet systems if there is no fit between task requirements and technology functionalities. For instance, the Human Resource manager may experience discontentment and decline to use intranet if some important information is not well maintained by his or her organisation.

Thirdly, the training of using intranet is considered a traditional approach of increasing usage and perceived usefulness. It is because the users may also lack in-depth understanding of the capabilities of the intranet resulting in less than optimal usage of functionalities afforded by the systems [7, 10]. Thus, providing training has been linked to the issue of adopting innovative technologies. From a pre-study the authors found that most of managers do not attend any intranet training. This situation occurs mostly at branches of each organization especially to managers at non-IT department. If they have, the training was conducted for only once or twice in the year. Worst, the training that they have attended was not related to technology. Thus, many of them were not competent in using intranet even though usage has been made mandatory. Also, it has been observed that the level of IT literacy among the managers is still not up to expectation. For example, some of the managers interviewed are struggling to even use computers in performing piecemeal tasks, such as producing histogram or to use Microsoft Word. Among the faced problems is shortage of training for the staff. Many training programmes were targeted towards IT personnel while the non-IT staffs are largely ignored. As such, organisations must provide different levels of computer training for its staff; from training for beginners to intermediate and advance users. One cannot expect the

users to know how to use the intranet system when they do not know how to even operate a simple application on computers. And, when such environment is built then the users would feel comfortable in using the intranet system.

CONCLUSION AND FUTURE RESEARCH

Based on the survey findings, it is hoped that the recommendations given in this paper shed some lights to the port organizations to recuperate their intranet implementation. Moreover, it is also hoped that the recommendations would work as a guide to other industries on how to pre-eminently implement a new technology. Nevertheless, given the limited sample size and scope, the interpretation of the survey result has been prepared cautiously. It is recommended for prospective studies to embrace a bigger sample size and take it across different industries. It is also fascinating to survey the non-supervisor/manager level performance as far as the intranet usage is concerned. A cross-cultural study is also viable to distinguish whether the findings are different or similar.

Acknowledgement

The authors extend their appreciation to the Deanship of Scientific Research at King Saud University for funding the work through the research group project No. RGP-VPP-013.

BIBLIOGRAPHY

1. Al-Gahtani S.: *Computer technology acceptance success factors in Saudi Arabia: an exploratory study.* Journal of Global Information Technology Management, 7, 2004.
2. Browne M.W. and Cudek R.: *Alternative Ways of Assessing Model Fit*. in Bollen, K.A., and Long, J.S. Testing Structural Equation Models, Newbury Park, CA, Sage, 1993.
3. Bukhari R.H.: *The relationship between system usage and user satisfaction: A meta-analysis.* The Journal of Entrepreneurship Information Management, 18, 2005.
4. Davis F.D., Bagozzi R.P. and Warshaw P.R.: *User acceptance of computer technology: A comparison of two theoretical models.* Management Science, 35, 1989.
5. DeLone W.H. and McLane E.R.: *Information systems success: The quest for the dependent variable.* Information System Research, 3, 1992.
6. Dishaw M.T. and Strong D.M.: *Assessing software maintenance tool utilisation using task-technology fit and fitness-for-use models.* Journal of Software Maintenance Research & Practice, 10, 1998.
7. Goodhue D.L. and Thompson R.L.: *Task-Technology Fit and individual performance*. MIS Quarterly, 19, 1995.
8. Igbaria M.: *End user computing effectiveness: A structural equation model.* Omega International Journal of Management Science, 18, 1990.
9. Joshi K.: *A causal path model of the overall user attitudes towards the MIS Function: The case of user information satisfaction.* Information & Management, 22, 1992.
10. Joshi K.: *Understanding user resistance and acceptance during the implementation of an order management system: A case study using the Equity Implementation Model.* Information Technology Cases and Application Research, 7, 2005.
11. Lawrence M. and Low G.: *Exploring individual user satisfaction within user-led development.* MIS Quarterly, 17, 1993.
12. Leonard B.D.A. and Deschamps I.: *Managerial influences in the implementation of new technology.* Management Science, 34, 1988.
13. Malhotra Y. and Galletta D.F.: *Extending the technology acceptance model to account for social influence: Theoretical bases and empirical validation.* Proceedings of the 32nd Hawaii International Conference on System Sciences, 6-19, Los Alamitos: IEEE Computer Society Press, 1999.
14. Martinko M.J., Henry J.W. and Zmud R.W.: *An attribute explanation of individual resistance to the introduction of information technologies in the workplace.* Behaviour & Information Technology, 15, 1996.
15. Markus M.L.: *Power, politics and MIS implementation.* Comm. of the ACM. 25 (6), 1993.
16. Miles J.N.V.: *Statistical software for microcomputer: AMOS 4.0.* British Journal of Mathematic and Statistic Psychology, 53, 2000.
17. Moore, G.C. and Benbasat I.: *An empirical examination of a model of the factors affecting utilisation of information technology end users.* Working paper, University of British Columbia, BC, Canada, 1992.
18. Naveed S.: *An empirical test of the contingency approach to user participation in information systems development.* Journal of Management Information System, 13, 1996.
19. Neumann S. and Segev E.: *Evaluate your information system*. Journal of Systems Management, 31, 1980.
20. Norzaidi M.D., and Intan Salwani M.: *Evaluating the post-Intranet usage: empirical study in Malaysian port industry.* Australian Journal Basic and Applied Research, 5, 2011.
21. Norzaidi M.D., Chong S.C. and Intan Salwani M.: *Perceived Resistance, User Resistance and Managers' Performance in the Malaysian port industry.* Aslib Proceedings: New Inform. Perspectives, 60, 2008.
22. Norzaidi M.D., Chong S.C. and Intan Salwani M.: *Intranet usage, managerial satisfaction and performance impact: An empirical analysis.* International Journal of Business Science Research, 3, 2009.
23. Norzaidi M.D., Chong S.C., Intan Salwani M. and Binshan L.: *The indirect effects of intranet functionalities on middle managers' performance: evidence from the maritime industry.* Kybernetes. 40(″), 2011.
24. Norzaidi M.D., Chong S.C., Murali R. and Intan Salwani M.: *Intranet Usage and Managers' Performance in the Port Industry.* Industrial Management and Data System, 107, 2007.
25. Nunnally J.C.: *Psychometric Theory.* McGraw Hill, New York, 1978
26. Segar A.H. and Grover V.: *Re-examining perceived ease of use and usefulness: A confirmatory factor analysis.* MIS Quarterly, 17, 1993.
27. Sekaran U.: *Research Methods for Business*. John Wiley and Son, New York, 2003.
28. Sherwood G.: *Denial managing the human element of technology.* Journal of Property Management, 3, 2001.
29. Tzu T.W. and Yin T.L.: *Key factors for small and medium enterprises in Taiwan to successfully implement information systems*. International Journal of Management and Enterprise Development, 2, 106-121, 2005.
30. Ying L.E., Sheue-L.H. and Eric M.Y.W.: *An integrated framework for continuous improvement on user satisfaction of information systems*. Industrial Management & Data System, 106, 581-595, 2006.

CONTACT WITH THE AUTHORS

Norzaidi Mohd Daud, Assoc. Prof.,
Communities of Research-Humanities and Quality of Life/Arshad Ayub Graduate Business School
Universiti Teknologi MARA
40450 Shah Alam, Selangor, MALAYSIA
e-mail: zaidiuitm2000@yahoo.com

Intan Salwani Mohamed, Ph. D.,
Accounting Research Institute
Universiti Teknologi MARA
40450 Shah Alam, Selangor, MALAYSIA

Saad Alghanim, Ph. D.,
Rashid Alhamali, Ph. D.,
P.O. Box 2454 College of Business Administration
King Saud University
Riyadh, 11451 SAUDI ARABIA

The Ship Handling Research and Training Centre at Ilawa is owned by the Foundation for Safety of Navigation and Environment Protection, which is a joint venture between the Gdynia Maritime University, the Gdansk University of Technology and the City of Ilawa.

Two main fields of activity of the Foundation are:

- Training on ship handling. Since 1980 more than 2500 ship masters and pilots from 35 countries were trained at Iława Centre. The Foundation for Safety of Navigation and Environment Protection, being non-profit organisation is reinvesting all spare funds in new facilities and each year to the existing facilities new models and new training areas were added. Existing training models each year are also modernised, that's why at present the Centre represents a modern facility perfectly capable to perform training on ship handling of shipmasters, pilots and tug masters.

- Research on ship's manoeuvrability. Many experimental and theoretical research programmes covering different problems of manoeuvrability (including human effect, harbour and waterway design) are successfully realised at the Centre.

The Foundation possesses ISO 9001 quality certificate.

Why training on ship handling?

The safe handling of ships depends on many factors - on ship's manoeuvring characteristics, human factor (operator experience and skill, his behaviour in stressed situation, etc.), actual environmental conditions, and degree of water area restriction.

Results of analysis of CRG (collisions, rammings and groundings) casualties show that in one third of all the human error is involved, and the same amount of CRG casualties is attributed to the poor controllability of ships. Training on ship handling is largely recommended by IMO as one of the most effective method for improving the safety at sea. The goal of the above training is to gain theoretical and practical knowledge on ship handling in a wide number of different situations met in practice at sea.

For further information please contact:
The Foundation for Safety of Navigation and Environment Protection

Head office:
36, Chrzanowskiego Street
80-278 GDAŃSK, POLAND
tel./fax: +48 (0) 58 341 59 19

Ship Handling Centre:
14-200 IŁAWA-KAMIONKA, POLAND
tel./fax: +48 (0) 89 648 74 90
e-mail: office@ilawashiphandling.com.pl
e-mail: office@portilawa.com